Deglacial Southern Ocean change: a cold-water coral investigation

Naomi R. A. Pratt

Imperial College London, Grantham Institute for Climate and Environment and the Department of Earth Science and Engineering

A thesis submitted for the degree of Doctor of Philosophy (Ph.D) 2019

Declaration of Originality

I herewith declare that this thesis and the research presented here are of my own work and that any ideas and work from others are fully acknowledged and referenced.

Naomi Pratt

'The copyright of this thesis rests with the author. Unless otherwise indicated, its contents are licensed under a Creative Commons Attribution-Non Commercial 4.0 International Licence (CC BY-NC). Under this licence, you may copy and redistribute the material in any medium or format. You may also create and distribute modified versions of the work. This is on the condition that: you credit the author and do not use it, or any derivative works, for a commercial purpose. When reusing or sharing this work, ensure you make the licence terms clear to others by naming the licence and linking to the licence text. Where a work has been adapted, you should indicate that the work has been changed and describe those changes. Please seek permission from the copyright holder for uses of this work that are not included in this licence or permitted under UK Copyright Law'

To David & Sheila Walker

Acknowledgements

Over the past four years I have had the pleasure of working with generous, supportive and brilliant people, without whom I would have not reached this stage. First and foremost is my supervisor, Tina, who I cannot thank enough for her enthusiasm and help in building my confidence. I am also hugely grateful to Susan, David and Laura for their support and fruitful conversations on proxies and palaeoceanography during this project. Thank you to Nadia for sharing her kindness and coral wisdom, and to Tianyu for his willingness to lend expertise and time in the lab. For collecting the corals, I thank the JC066 cruise members under the leadership of Michelle Taylor and Alex Rogers, who also provided helpful input on my first paper. I'd also like to thank everyone in the MAGIC group, especially Katharina and Barry for their training, advice and problem-solving. Thanks to my elders Rachel and Patric and my PhD twin Alex for being there through all the ups and downs.

The Grantham Institute has been invaluable throughout this process and I thank Sophie, Alyssa, Simon and the team for their support and the many opportunities to broaden my horizons. I am also grateful to Profs. Katharina Pahnke and Mark Rehkamper for agreeing to read this thesis and look forward to our discussion.

These have not been an easy few years and I send love and thanks to everyone who has been there for me, especially to my family. Whether by making me laugh, listening to my rants, or just getting me out of the house you have all helped so much: thank you Mel, Miriam, Roan, Jack, Pete, Alex, Kieran, Jo, Graham, Jonny, Katy, Bella, Christian, Eleanor, Ruth H, Cat, Rocio, Bex, Jay, Cal, Tom, Toby, Rishi, Danielle, Ruth D, Robbie, Dan, Phil, Abi & Paddy.

I also would like to thank everyone who has played a part in the Divest Imperial campaign, and those who are taking it forward, for their contribution and commitment to building a better world.

Abstract

Over the past decades, great progress has been made in understanding the transition of Earth's climate from the last ice age to the present day, in particular the importance of Southern Ocean processes and their impact on transfer of heat and carbon.

This work explores deglacial ocean change through the lens of a new collection of cold-water corals from an understudied region, the southwest Indian Ocean alongside existing palaeo records including two other unpublished cold-water coral collections to form a broader picture of ventilation and structure of the deglacial Southern Ocean.

A compelling peak in abundance of solitary scleractinians in the southwest Indian Ocean, as well as at other sites in the Southern Ocean during the late deglacial hints at widespread oceanic controls on habitat suitability.

Neodymium isotope analysis reveals maintained Atlantic influence at intermediate depths throughout the record, and particularly strong connectivity at the most southerly sampling site, which records rapid fluctuations in seawater chemistry during the Younger Dryas.

Radiocarbon data provides new evidence in support of a Southern Ocean source of atmospheric CO_2 early in Heinrich Stadial 1, and potential transfer of old carbon to the upper cell at the end of the Younger Dryas.

Overall, regional hydrographic changes appear to have played a significant role in the ventilation and water mass history of the southwest Indian Ocean.

Table of Contents

List of Figures 9

List of Tables 10

Glossary of abbreviations 11

Chapter 1: Introduction 12

1.1 Climate evolution of the last deglaciation 12
1.2 Southern Ocean dynamics and role in the global climate system 16
1.3 Cold-water corals and their use as oceanographic archives for seawater neodymium isotopes and radiocarbon 20
1.4 The Southwest Indian Ocean Ridge and regional oceanography 24
1.5 Thesis structure 26

Chapter 2: Methods 28

Chapter summary 28
2.1 Southern Indian Ocean coral sampling 28
2.2 Taxonomic identification 35
2.3 Reconnaissance U-series dating 41
2.4 Sample preparation for U-Th-Nd isotope and ^{14}C analysis 50
2.5 Dissolution and preparation for combined U-Th-Nd extraction 51
2.6 Separation of U, Th and Nd 52
2.7 Isotope dilution U-series dating 53
2.8 Separation of Nd 58
2.9 Neodymium isotope analysis 61
2.9.1 Initial setup and testing of JIM (NP2) 67
2.10 Radiocarbon measurement 73
Statement of contribution 74

Chapter 3: Temporal distribution and diversity of cold-water corals in the southwest Indian Ocean over the past 25,000 years 75

Chapter summary 75
3.1 Introduction 76
3.1.1 Cold-water corals 76
3.1.2 The deglacial Southern Ocean 77
3.2 Materials and methods 79
3.2.1 Sampling location and regional hydrography 79
3.2.2 Taxonomy 82
3.2.3 Laser ablation U-series dating 83
3.2.4 Isotope dilution U-series dating 84
3.3 Results 86
3.3.1 Taxonomy 86
3.3.1.1 Species List 87

3.3.1.2 Taxonomic distribution 93
3.3.2 Ages 96
3.4. Discussion 98
3.4.1 Taxonomy 98
3.4.1.1 Range extensions 98
3.4.1.2 Spatial variability 102
3.4.2 Temporal shifts in CWC populations 104
3.4.2.1 The Last Glacial Maximum 106
3.4.2.2 The early deglacial, Heinrich Stadial 1 108
3.4.2.3 The late deglacial 109
3.4.2.4 The Holocene 114
3.5 Conclusion 118
Statement of contribution 119

Chapter 4: Reconstructing deglacial water mass changes in the southwest Indian Ocean using cold-water coral Nd isotopes 120

Chapter summary 120
4.1 Introduction 120
4.2 Regional setting, samples, and methods 122
4.2.1 Hydrography of the southwest Indian Ocean 122
4.2.2 Materials and methods 128
4.3 Results 129
4.4 Discussion 131
4.4.1 'Modern' Nd isotope distribution in waters and corals of the SWIO 131
4.4.2 Late Holocene CWC Nd isotopic composition 133
4.4.3 Stability of the deglacial Nd isotope record 134
4.4.4 Radiogenic Nd isotope composition at AAIW-depth during HS1 139
4.4.4.1 Local detrital inputs 139
4.4.4.2 Direct influence of surface waters 140
4.4.4.3 AAIW composition change – whole Southern Ocean? 142
4.4.5 Fluctuations in Nd isotope composition at UCDW-depths during the YD 144
4.4.5.1 Sampling resolution 145
4.4.5.2 Shifts in the presence of North Indian Deep Water (NIDW) and UCDW 145
4.4.5.3 Proximal water mass boundary 146
4.4.5.4 Periodic NADW influence at depth 148
4.5 Conclusion 150
Statement of contribution 150

Chapter 5: Deglacial ventilation history of the intermediate southwest Indian Ocean 153

Chapter summary 153
5.1 Introduction 154
5.1.1 Modern ocean radiocarbon distribution 156
5.2 Samples and methods 159

5.2.1 Materials and methods 159
5.3 Results 161
5.3.1 Late Holocene $\Delta^{14}C$ 161
5.3.2 Deglacial to Early Holocene $\Delta^{14}C$ 162
5.4 Discussion 165
5.4.1 Heinrich Stadial 1 (18-14.7 ka) 165
5.4.2 Younger Dryas (12.8-11.7 ka) 174
5.4.3 Early Holocene 176
5.5 Combined ^{14}C and Nd analysis 177
5.5.1 Heinrich Stadial 1 180
5.5.1.1 Possible Northern Indian intermediate water influence 180
5.5.1.2 More radiogenic AAIW in general 181
5.5.1.3 'Gradient' between Pacific and Atlantic sectors 185
5.5.1.4 16.2 ka enrichment 186
5.5.1.5 Late HS1 enrichment 187
5.5.2 Younger Dryas 188
5.5.2.1 High ventilation with periodic unradiogenic excursions 188
5.5.2.2 12.4 ka enrichment 189
5.5.2.3 Decrease in ventilation to 11.4 ka 190
5.5.3 Early Holocene ventilation 191
5.6 Conclusions 193
Statement of contribution 195

Chapter 6: Summary and conclusions 198

Bibliography 201

Appendices 224

A1. Equatorial Atlantic cold-water coral Nd isotope data 224
A1.1 Introduction and methods 224
A1.2 Results and discussion 228

List of Figures

Figure 1.1	Deglacial atmospheric and ice core records	13
Figure 1.2	Proposed mechanisms involved in deglacial carbon release	15
Figure 1.3	Southern Ocean principal fronts and zones	18
Figure 1.4	Schematic of the vertical profile of the Southern Ocean	19
Figure 1.5	Photograph of a deep sea coral garden	21
Figure 1.6	Calibration of cold-water coral and modern seawater Nd isotope data	23
Figure 2.1	Common morphological features of a solitary scleractinian coral	35
Figure 2.2	Photographs of southwest Indian Ocean cold-water coral samples	36
Figure 2.3	SEM images of southwest Indian Ocean cold-water coral samples	38
Figure 2.4	Elution curves for Ln-spec resin column calibration	59
Figure 2.5	Average 2SD for various concentrations of JNDi standard during measurement sessions	64
Figure 2.6	Nd isotope measurements of BCR-2 and in-house coral standards	65
Figure 2.7	Average 2SD for five measured isotope ratios from 'good' runs	67
Figure 2.8	Relationship between source temperature variations and machine conditions	70
Figure 3.1	Modern hydrography proximal to sample locations on the SWIOR	81
Figure 3.2	Morphological variability of CWCs across each transect	92
Figure 3.3	Depth distribution of subfossil CWCs at each seamount	95
Figure 3.4	Frequencies of different coating levels at each level of aragonite preservation	96
Figure 3.5	Relationship of caryophylliid mass and preservation factor to depth and age	97
Figure 3.6	Comparison of LA and ID U-series ages	98
Figure 3.7	Depths and ages of subfossil CWCs at each seamount	106
Figure 3.8	Number of CWCs per 1000-year age bin	114
Figure 3.9	Depths and ages of Late Holocene corals at Coral Seamount	117
Figure 4.1	Map views of modern surface hydrography and ε_{Nd} in the SWIO	123
Figure 4.2	Modern seawater potential temperature and salinity CTD data	126
Figure 4.3	Comparison of late Holocene CWC ε_{Nd} and nearby seawater profiles	127
Figure 4.4	SWIO deglacial and late Holocene ε_{Nd} from cold-water corals	130
Figure 4.5	Deglacial ε_{Nd} records from the SWIO, southeast Atlantic and southeast Pacific Oceans	135
Figure 4.6	Deglacial deep ocean ε_{Nd} records	137
Figure 4.7	Deglacial intermediate water ε_{Nd} records	138
Figure 5.1	Modern seawater $\Delta^{14}C$ distribution in the SWIO and southeast Atlantic	159
Figure 5.2	Late Holocene CWC and modern seawater $\Delta\Delta^{14}C$ from the SWIO	161
Figure 5.3	$\Delta^{14}C$ and $\Delta\Delta^{14}C$ from SWIO CWCs	163
Figure 5.4	B-atm ages of CWCs from the SWIO	164
Figure 5.5	Deglacial ocean B-atm records from the Atlantic and Southern Oceans	168
Figure 5.6	Deglacial ocean ventilation and upwelling records from the southern hemisphere	170
Figure 5.7	Comparisons between ε_{Nd} and ^{14}C data from SWIO CWCs	177
Figure 5.8	ε_{Nd} and $\Delta\Delta^{14}C$ comparison for SWIO CWCs	179
Figure 5.9	Ventilation, water mass and front position data from the Atlantic and Southern Oceans	184
Figure 5.10	Schematic illustrating deglacial water mass and ventilation changes in the SWIO	192
Figure A1	Cold-water coral Nd isotope data from the equatorial Atlantic	227

List of Tables

Table 2.1	Solitary CWC sample locations and ID from cruise JC066	30
Table 2.2	Examples of CWC coating and aragonite preservation	40
Table 2.3	Laser ablation U-series dating of SWIO CWCs	44
Table 2.4	Isotope dilution U-series dating of SWIO CWCs	55
Table 2.5	Sample and whole coral Nd concentrations	61
Table 3.1	Location, bathymetry and number of specimens from SWIO seamounts	93
Table 3.2	Distribution of subtropical and Subantarctic Transition Zone Indian Ocean Scleractinia	101
Table 4.1	Water mass properties in the southern Indian and southeast Atlantic Ocean regions	125
Table 4.2	Cold-water coral Nd isotope data from SWIO seamounts	151
Table 5.1	Calendar age, ^{14}C and Nd isotope data of cold-water corals from the SWIO	196
Table A1	Nd isotope data from equatorial Atlantic cold-water corals	226

Glossary of abbreviations

AABW	Antarctic Bottom Water
AAIW	Antarctic Intermediate Water
ACC	Antarctic Circumpolar Current
ACR	Antarctic Cold Reversal
AMOC	Atlantic Meridonal Overturning Circulation
ARC	Agulhas Return Current
ASF	Antarctic Slope Front
ASH	Aragonite Saturation Horizon
BA	Bølling-Allerød
CSW	Continental Shelf Water
CWC	cold-water coral
HS1	Heinrich Stadial 1
IDW	Indian Deep Water
LGM	Last Glacial Maximum
MoW	Middle of What Seamount
NADW	North Atlantic Deep Water
NIDW	North Indian Deep Water
PDW	Pacific Deep Water
PF	Polar Front
REE	Rare-earth element
ROV	Remotely Operated Vehicle
RSW	Red Sea Water
SACCF	Southern ACC Front
SAF	Subantarctic Front
SAMW	Subantarctic Mode Water
SASW	Subantarctic Surface Water
SAZ	Subantarctic Zone
SB	Southern Boundary (of the ACC)
SEC	South Equatorial Current
STF	Subtropical Front
STSW	Subtropical Surface Water
SWIO	Southwest Indian Ocean
SWIOR	Southwest Indian Ocean Ridge
UCDW	Upper Circumpolar Deep Water
YD	Younger Dryas

Chapter 1: Introduction

1.1 Climate evolution of the last deglaciation

During the last glacial maximum (LGM; ~ 21 ka), temperatures were 3-6 degrees colder than today (Schneider Von Deimling et al., 2006) and atmospheric CO_2 concentrations were 80-90 ppm lower than preindustrial values (Monnin et al., 2001; Fig. 1.1). Stable carbon isotope data (Curry and Oppo, 2005; Ninnemann and Charles, 2002) and dynamical ocean models (e.g. Burke et al., 2015) invoke an expansion in volume of southern-sourced abyssal waters, rich in carbon, at the expense of North Atlantic Deep Water (NADW), during the glacial. Mechanistically, an increased extent of sea ice could have caused the isopycnal separating NADW and Antarctic Bottom Water (AABW), or the upper and lower cell of the overturning circulation, to shoal. This in turn would have moved the boundary between the two cells away from the area of rough bathymetry, which causes intense water mass mixing in the modern ocean (Ferrari et al., 2014; Gersonde et al., 2005). This expansion of southern sourced waters and loss of ocean-atmosphere interaction beneath sea ice, along with changes in the biological and carbonate pumps (e.g. Sigman et al., 2010) are thought to have contributed to the lower atmospheric CO_2 levels.

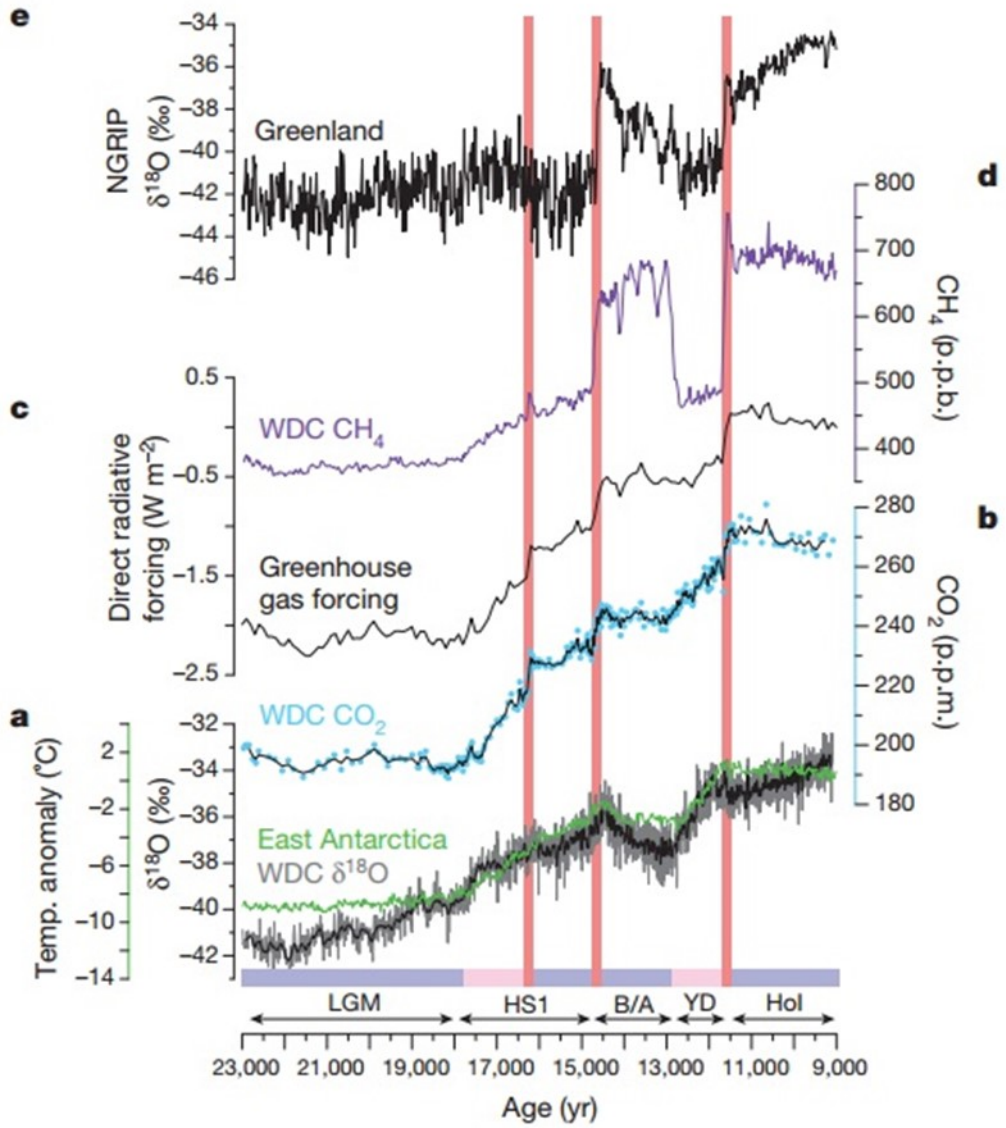

Figure 1.1: From Marcott et al. (2014). Greenhouse gas and water stable isotope measurements from Antarctica and Greenland. **A)** Oxygen isotopes from West Antarctic Ice Sheet Divide core (WAIS Divide Project Members, 2013; grey; black line is 11-point weighted average) and water-isotope-derived temperature composite from East Antarctica (Parrenin et al., 2013; green). **B)** Atmospheric CO_2 concentrations (black line is 5-point weighted average; Marcott et al., 2014). **C)** Direct radiative forcing of CO_2, CH_4 and N_2O (Schilt et al., 2010). **D)** Atmospheric CH_4 concentrations (Marcott et al., 2014; WAIS Divide Project Members 2013). **E)** Oxygen isotope measurements from the North Greenland Ice Project (NGRIP; Andersen et al., 2004). Coloured bands at bottom indicate times when CO_2 is stable (blue), slowly increasing (pink) or rapidly increasing (red). LGM, Last Glacial Maximum; HS1, Heinrich Stadial 1; B/A, Bølling-Allerød; YD, Younger Dryas; Hol, Holocene.

Southern Ocean circulation is a significant player in global climate due to its impact on heat, salt, nutrient and carbon fluxes. The region holds a large potential to drive glacial/interglacial (and millennial-scale) shifts in atmospheric CO_2 levels and high latitude temperatures (e.g. Lüthi et al., 2008; Monnin et al., 2001; Shakun et al., 2012; Sigman and Boyle, 2000; WAIS Divide Project Members, 2015). The size of the deep ocean carbon reservoir is about 25 times that of the combined atmospheric and surface ocean (Sigman and Boyle, 2000), and a number of processes operating in the Southern Ocean can control the partition between this and the atmospheric reservoirs. These include: iron fertilisation and changes in nutrient utilisation (Martin, 1990; Sigman et al., 2010a; Wang et al., 2017; Watson et al., 2000), westerly wind position and strength (Kohfeld et al., 2013; Menviel et al., 2018), changes in geometry of the overturning cells and bathymetry-enhanced vertical mixing (Ferrari et al., 2014), changes in buoyancy fluxes (Watson et al., 2015), surface stratification (Francois et al., 1997), and sea ice formation and retreat (Kohfeld and Chase, 2017; Stephens and Keeling, 2000; Fig. 1.2).

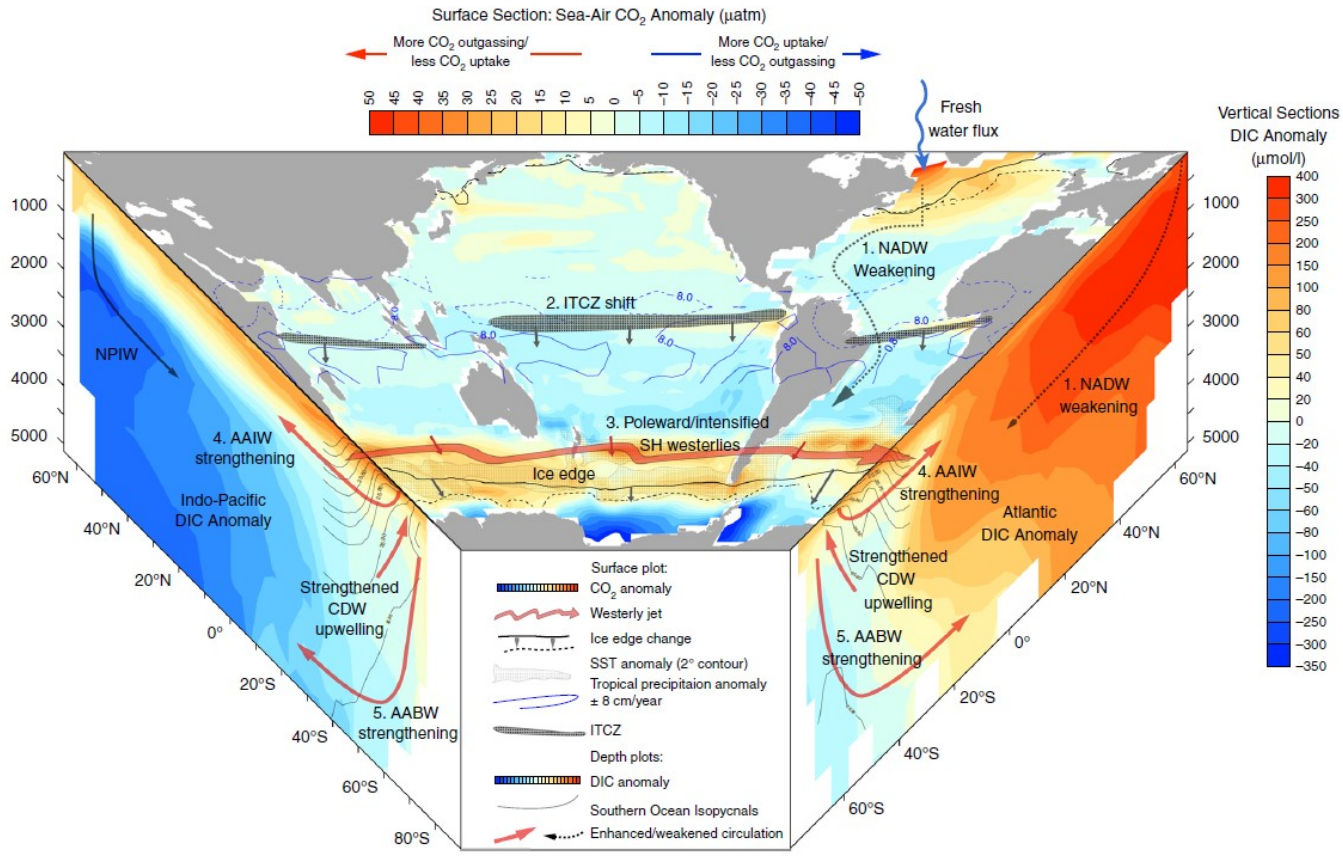

Figure 1.2: Schematic of proposed atmospheric and ocean mechanisms involved in carbon release during the early deglaciation (Menviel et al., 2018).

The subsequent deglaciation (~18 to 11 ka) encompasses the periods of Heinrich Stadial 1, the Bølling-Allerød / Antarctic Cold Reversal, and the Younger Dryas (Fig. 1.1), and is characterised by asynchronous warming between the hemispheres (e.g. Clark et al., 2012), whereby millennial-scale temperature increases in the southern hemisphere correlate with periods of rising atmospheric CO_2 (Monnin et al., 2001; Fig. 1.1). These coincide with peaks in opal production (Anderson et al., 2009) and negative $\delta^{13}C$ signatures consistent with a deep ocean source (Schmitt et al., 2012), and are thought to result from reinvigorated Southern Ocean ventilation. Shifts in westerly winds have been inferred as a mechanism for these physical ocean changes (Marshall and Speer, 2012; Toggweiler et al., 2006), which also

coincide with reduced Atlantic Meridional Overturning Circulation (AMOC) strength (McManus et al., 2004). Conversely, the Antarctic Cold Reversal (ACR; 14.5 – 12.8 ka), a reversal in the warming trend in the Southern Hemisphere characterised by a plateau in CO_2, is thought to have been a return to Southern Ocean stratification (e.g. Weber et al., 2014). In addition, three abrupt increases in CO_2 have been recently revealed from a high-resolution West Antarctic ice core, at 16.2, 14.8 and 11.7 kyr ago (Marcott et al., 2014; Fig. 1.1). Research is currently ongoing to explain these pulses. The latter two shifts, at the start of the ACR and the end of the Younger Dryas (YD) respectively, are thought to have been driven by Atlantic Meridonal Overturning Circulation (AMOC) due to the concomitant abrupt increases in Northern Hemisphere temperature (Buizert et al., 2014) and a ^{14}C-enriched water column in the Eastern Atlantic and Southern Ocean (e.g. Chen et al., 2015). The first deglacial pulse in CO_2 is less well understood. Tracers from new intermediate water sites in the Southern Ocean will help to characterise these proposed deglacial shifts in CO_2 storage and ventilation.

1.2 Southern Ocean dynamics and role in the global climate system

Understanding the relationships between ocean circulation, atmospheric dynamics and the carbon cycle is vital for modelling ocean-atmosphere responses to anthropogenic CO_2 perturbations. The Southern Ocean plays a crucial role in the global thermohaline circulation, by connecting the three main ocean basins in the eastward-flowing Antarctic Circumpolar Current (ACC), and as a locus for upwelling of deep waters from all ocean basins, as well as formation of intermediate and bottom waters (e.g. Kuhlbrodt et al., 2007; Talley, 2013). The wind-driven jets of the ACC cause isopycnals to slope upwards towards the south, raising deep and abyssal waters almost adiabatically to the upper ocean. This closes the Atlantic Meridonal Overturning Circulation (AMOC) loop (which is 'initiated' with deep water formation in the North Atlantic) and enables ventilation of deep ocean waters (e.g. Marshall and Speer, 2012).

Ekman transport then causes upwelled nutrient-rich deep waters to move northwards at intermediate depth, where they supply preformed nutrients for primary producers the southern hemisphere thermocline (Sarmiento et al., 2004). The Southern Ocean is therefore vital to the carbon cycle and climate change, through both the release of abyssal ocean CO_2 to the atmosphere, and the uptake of new atmospheric CO_2 (Talley, 2013).

Most of the transport of the ACC is accomplished through a number of fast flowing jets, or fronts, which separate and merge at various locations due to bathymetric steering (Fig. 1.3; Belkin and Gordon, 1996). To maintain geostrophic balance, isopycnals slope up to the south and cause different water masses to outcrop, resulting in zonation and marked meridonal gradients in surface water properties (Orsi et al., 1995; Fig. 1.4). North of the ACC, the Subtropical Front (STF) separates waters from the subtropical gyres, such as subtropical surface water (STSW) from subantarctic surface and mode waters (SASW, SAMW) of the Subantarctic Zone (SAZ; Orsi et al., 1995). The STF is located between 30 and 45°S, except through the Drake Passage, where it is discontinuous (Fig. 1.3), and is associated with a typical temperature gradient of 4-5°C and a salinity difference of 0.5 (Deacon, 1982).

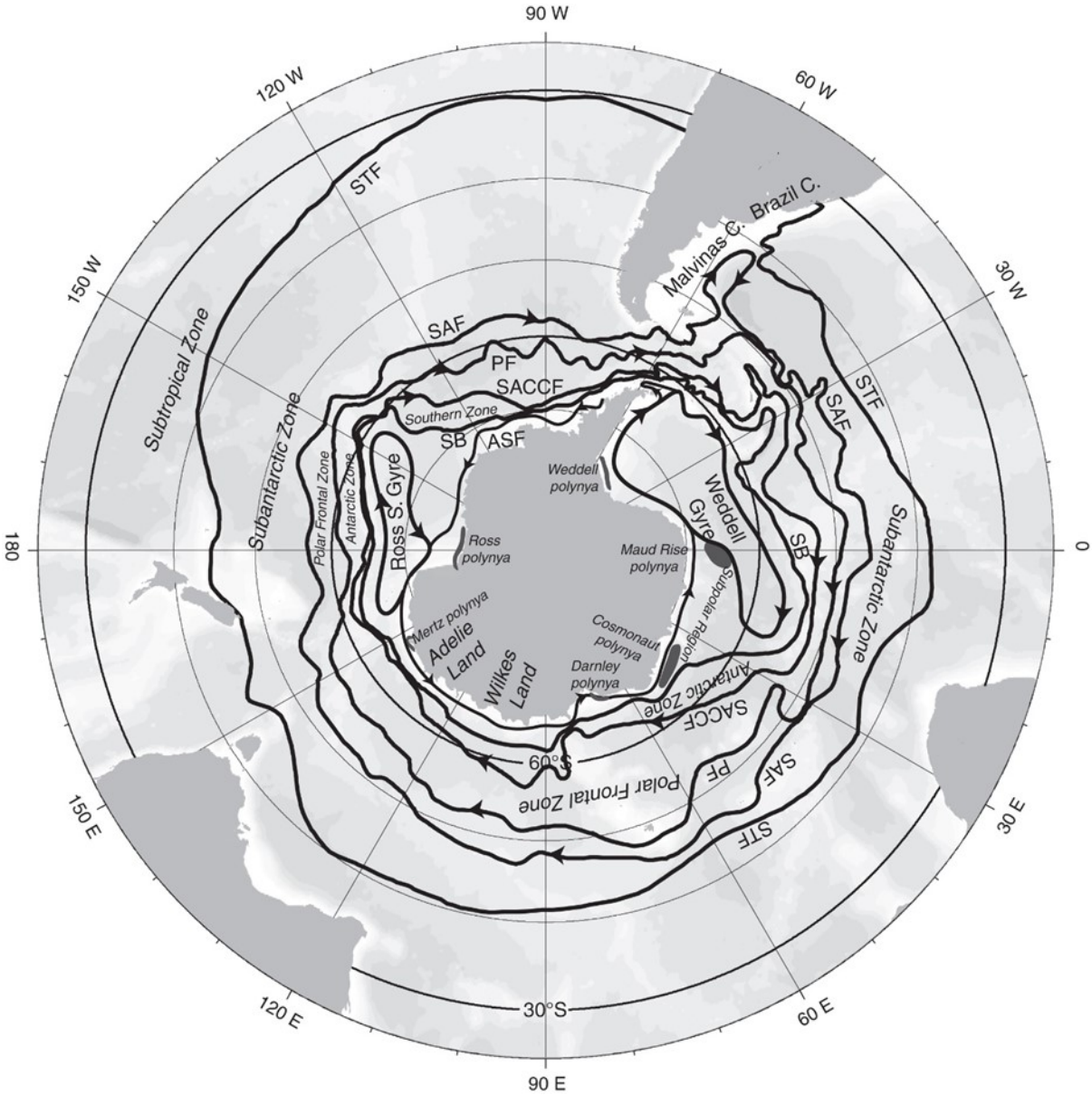

Figure 1.3: Southern Ocean principal fronts and zones (Talley et al., 2011): The eastward flowing Antarctic Circumpolar Current includes the Subantarctic Front (SAF) the Polar Front (PF) and the Southern ACC Front (SACCF). Front locations from Orsi et al. (1995). The dark grey shaded areas represent the positions of polynyas named on the figure.

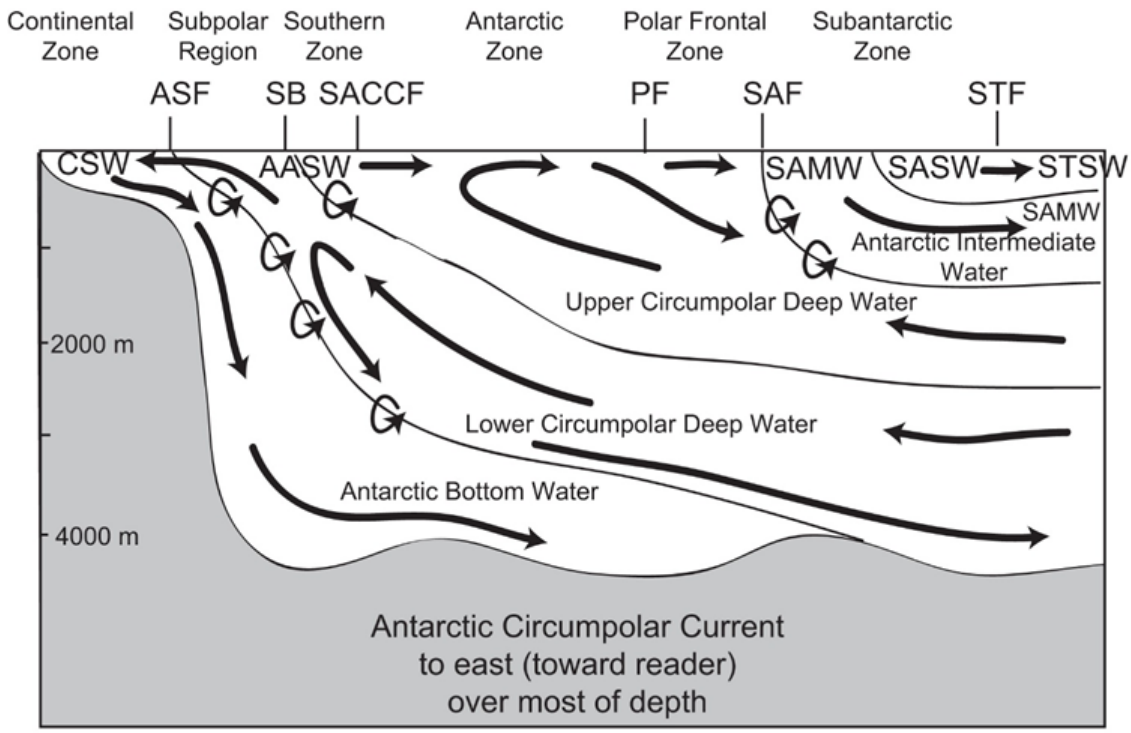

Figure 1.4: Schematic of the vertical profile of the Southern Ocean (Talley et al., 2011)

The SAZ is the main area of Subantarctic Mode Water (SAMW) formation by deep wintertime convection. Antarctic Intermediate Water (AAIW) is the densest variety of lower thermocline waters formed in the SAZ and carries a characteristic salinity minimum. The salinity minimum of AAIW can be seen throughout the Southern Hemisphere subtropical gyres and Atlantic and Pacific tropics at intermediate depths (Fine, 1993). The poleward boundary of the SAZ is the Subantarctic Front (SAF), the northernmost of the circumpolar current cores that make up the ACC. In the Atlantic and Indian sectors it is found between 40° and 50°S (Belkin and Gordon, 1996; Fig. 1.3).

The next ACC jet southward, the Polar Front (PF), marks an area of converging surface waters, separating cold waters from the southern Antarctic Zone from warmer subantarctic waters to the north (i.e. Antarctic convergence). It also separates the areas of intermediate water formation from upwelling of Upper Circumpolar Deep Water (UCDW), which is a mixture of

deep waters from the Indian and Pacific oceans (IDW = Indian Deep Water, PDW = Pacific Deep Water). These old waters are marked by a pronounced oxygen minimum and high nutrient concentrations, especially in phosphate and nitrate (e.g. McDonagh et al., 2008). The most southerly dynamical front of the ACC (the southern ACC front; SACCF) does not separate distinct water masses (Orsi et al. 1995); but sometimes merges with the southern boundary of the ACC defined in terms of water properties (SB; Orsi et al. 1995). The SB divides UCDW outcropping to the north from Lower Circumpolar Deep Water (LCDW) to the south, a mixture of low-salinity NADW and entrained AABW.

1.3 Cold-water corals and their use as oceanographic archives for seawater neodymium isotopes and radiocarbon

The most common archives in palaeoceanography used to investigate biogeochemical and circulation changes are microorganisms such as foraminifera, which can be preserved within sediment cores. In the Southern Ocean, however, these kinds of records are sparse, due to strong ocean currents and limited carbonate preservation. Cold-water corals (CWCs), on the other hand, are found in abundance in the Southern Ocean where their aragonitic skeletons can be preserved on the seafloor or within sediments for thousands of years (e.g. Burke et al., 2010; Margolin et al., 2014; Thiagarajan et al., 2013). This broad polyphyletic grouping comprises cnidarian species from the orders Scleractinia, Octocorallia, Stylasteridae and Antipatharia (Roberts et al., 2009). Unlike their tropical cousins, cold-water corals can inhabit depths outside the reach of sunlight, surviving without the assistance of symbiotic photosynthetic algae (Fig. 1.5). Reef-forming cold-water coral species are a particularly important part of the ocean ecosystem, providing refuge, nursing grounds and food supply for many other species (Freiwald et al., 2004; Roberts et al., 2009). For this reason, they are hotspots of biodiversity

(Roberts et al., 2006), but are also highly vulnerable to human activities such as bottom trawling (e.g. Hall-Spencer et al., 2002) and ocean acidification (Guinotte et al., 2006).

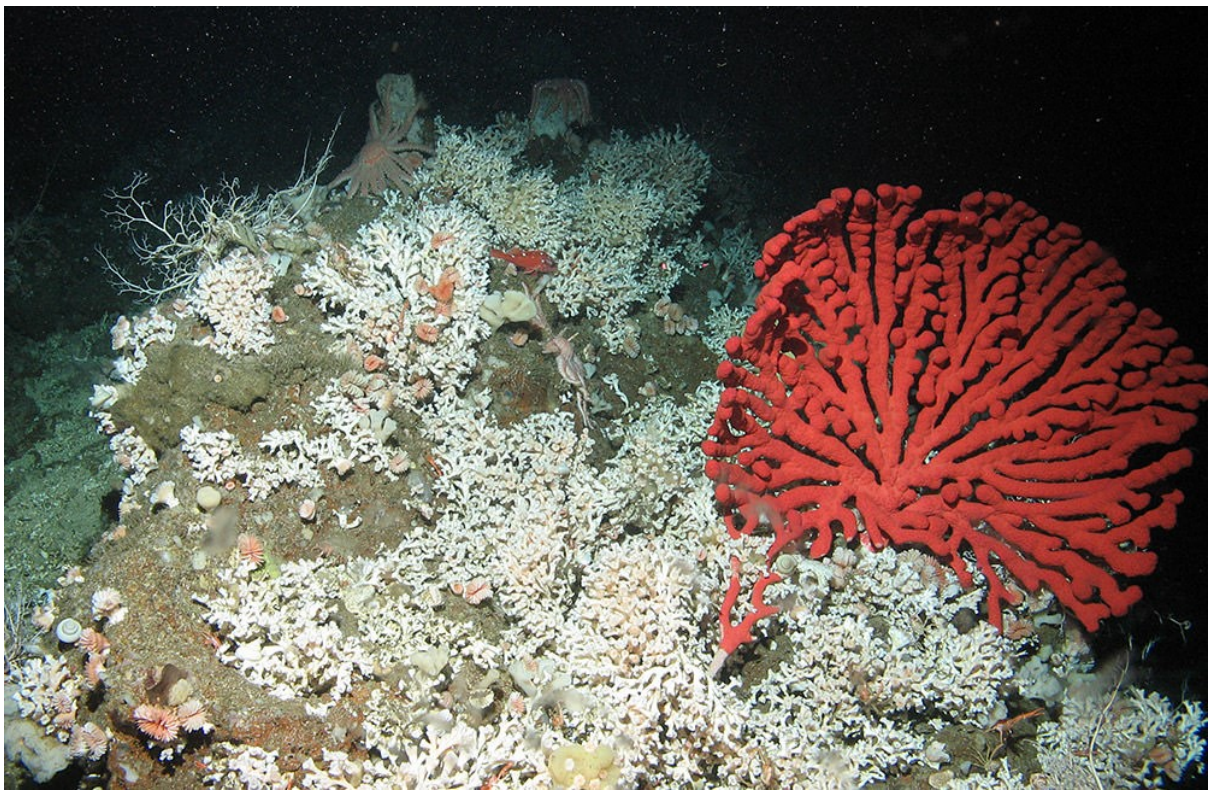

Figure 1.5: A deep sea coral garden consisting of primarily *Lophelia pertusa* off the coast of Southern California (NOAA, 2017).

As the survival and growth of these organisms is dependent, among other factors, on the delivery of food supply and larval dispersal by ocean currents (Dullo et al., 2008; Miller et al., 2011), dissolved oxygen for aerobic function (Dodds et al., 2007), and a high enough carbonate ion concentration to maintain and build their skeletons (Guinotte et al., 2006), their distribution is thought to be sensitive to changes in ocean chemistry and hydrography (Tittensor et al., 2009).

Cold-water corals often grow on seamounts, providing a window into intermediate water depth chemistry, and enabling the construction of vertical transects of mid-depth waters

which proves particularly useful in contrasting the behaviour and geometry of different water masses through time. Their skeletal chemistry enables precise dating using the uranium-thorium decay system (Cheng et al., 2000; Lomitschka and Mangini, 1999) and the utilisation of multiple geochemical tracers of seawater chemistry (Robinson et al., 2014), sometimes measured in the same specimen (e.g. Colin et al., 2019; Wilson et al., 2015). Use of some traditional isotope systems can be complicated by overprinting of external variability by biological activity, so-called 'vital effects' (e.g. oxygen isotopes, carbon isotopes; e.g. Smith et al. 2000; Adkins et al. 2003; Rollion-Bard et al. 2003). Other parameters, such as radiogenic neodymium (Nd) isotopes ($^{143}Nd/^{144}Nd$) and ^{14}C, however, are not significantly affected by biological processes (Adkins et al., 1998; Adkins et al. 2002a; van de Flierdt et al. 2010).

Neodymium isotopes are a useful tracer for water mass provenance and mixing, and coral aragonite has been shown to faithfully recording seawater values in modern calibration experiments (Colin et al., 2010; Struve et al., 2017; van de Flierdt et al., 2010, 2006). The Nd isotopic composition of water masses originates from the geology of proximal continents, which differs depending on age and lithology (Goldstein and Hemming, 2003; Martin, 2002). Once imprinted, the isotopic signature of seawater behaves quasi-conservatively away from ocean margins, and does not become homogenised by global overturning circulation due to the relatively short oceanic residence time of neodymium (Gu et al., 2019; Rempfer et al., 2011; Tachikawa et al., 2003). The $^{143}Nd/^{144}Nd$ ratios of water masses are commonly reported as ε_{Nd}, which describes the deviation of a measured ratio relative to the Chondritic Uniform Reservoir or 'bulk earth value' ($^{143}Nd/^{144}Nd = 0.512638$; Wasserburg et al., 1981) in parts per 10,000. Also measured in ferromanganese crusts, bulk sediment leachates, foraminifera and fish debris (e.g. Abouchami et al., 1997; Gutjahr et al., 2008; Huang et al., 2014; Piotrowski et al., 2012; Roberts et al., 2010), recent cold-water coral applications in the Atlantic, Pacific and Southern

Oceans have produced particularly high resolution records (Colin et al., 2019; Montero-Serrano et al., 2013; Struve, 2016; Wilson et al., 2014).

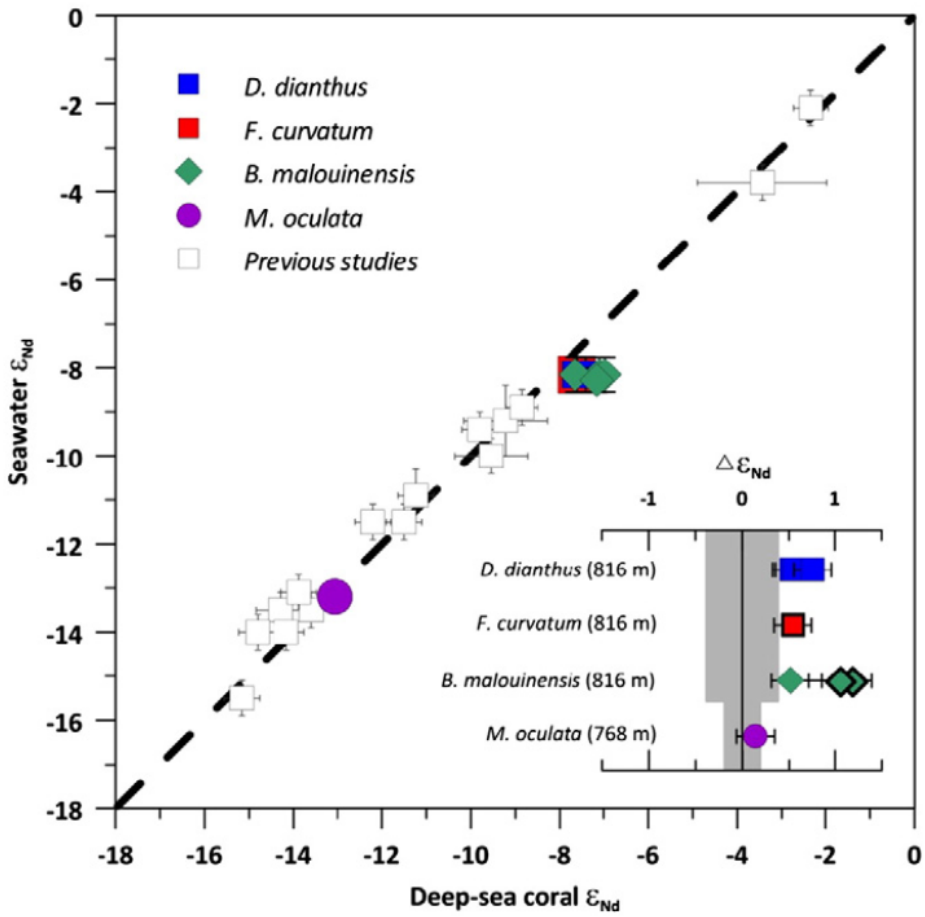

Figure 1.6: Calibration of cold-water coral and modern seawater Nd isotope data from Struve et al (2017), incorporating data from Copard et al. (2010) and van de Flierdt et al. (2010).

Radiocarbon is generated in the atmosphere by cosmic rays and exchanged with the surface ocean. When seawater is taken out of contact with the atmosphere, the ^{14}C it contains decays without being replenished. Traditionally radiocarbon is used as a chronometer, but when applied to marine archives, estimations of this 'reservoir effect' can be a major source of uncertainty. When U-series methods are utilised instead, this drawback can become a powerful tracer of overturning rates and water mass ventilation, as the amount of ^{14}C in the seawater

relative to the contemporaneous atmosphere can be used to calculate ventilation ages. Radiocarbon measurements on deglacial deep-sea corals from the Drake Passage (Burke and Robinson, 2012; Chen et al., 2015) and south of Tasmania (Hines et al., 2015) have been instrumental in understanding glacial carbon storage and the pacing and mechanisms of deglacial release of the 'isolated reservoir'. Due to the sloping isopycnals in the Southern Ocean, localised intermediate water ^{14}C variations can also be caused by latitudinal shifts of fronts in the region (e.g. Hines et al. 2015; Allen et al. 2015), as well as by vertical water mass mixing.

1.4 The Southwest Indian Ocean Ridge and regional oceanography

This investigation utilises a collection of cold-water corals sampled from four seamounts located along the southwest Indian Ocean Ridge (SWIOR). The SWIOR is a major bathymetric feature of the Southern Hemisphere, an ultra-slow spreading ridge connected to the Mid-Atlantic Ridge to the west and the Central Indian and Southeast Indian ridges to the east (Muller et al., 2012). The seamounts of the SWIOR are highly fractured and exhibit a variety of volcanic formations due to spreading of the ridge (Muller et al., 2012; Sauter et al., 2002), including hydrothermal vent fields (e.g. Tao et al., 2004).

The region has been modelled as one of the most suitable and diverse habitats for CWCs (Cairns and Keller, 1993; Tittensor et al., 2009), especially on seamounts (Tittensor et al., 2010). However, due to a lack of modern surveys and dated subfossil corals from the region, their spatial and temporal distribution in the region is poorly known.

The SWIOR intersects the boundary between the South Indian subtropical gyre and the Southern Ocean, and both subtropical waters from the Indian Ocean and subantarctic Southern Ocean waters affect the seamounts studied here. The physical oceanography around the

SWIOR seamounts was extensively surveyed on RV *Fridtjof Nansen* cruise 410 in 2009 (Pollard and Read, 2017; Read and Pollard, 2017). Prior to this, various hydrological and biogeographical surveys have taken place in the region, including a study of SAF steering around the Crozet Plateau (45–47°S, 49–51°E; Pollard et al., 2007), a trans-Indian section at 32°S (McDonagh et al., 2008), extending the section of Toole & Warren (1993), meridonal sections produced from the SWINDEX surveys in 1993 and 1995 (e.g. Pollard and Read, 2001), and older sections compiled in Belkin and Gordon's (1996) analysis between 0° and 150°E.

From these studies it is apparent that the well-known Southern Ocean fronts are not necessarily continuous or discrete in this region, and therefore difficulties arise when constraining their influence over features such as the SWIOR seamounts. In 2009, the STF was marked by a 4°C drop in temperature and a 1.0 drop in salinity around 40°S (Read and Pollard, 2017), at the northern extreme of variation around the average given in Lutjeharms & Valentine (1984). The STF has also previously been described as splitting into a northern and southern front east of southern Africa (Belkin and Gordon, 1996), although evidence for this was not observed in 2009 (Read and Pollard, 2017). Further south, the rough topography of the SWIOR is thought to create eddy 'hotspots' when interacting with jets of the ACC (Tamsitt et al., 2017).

Another prominent hydrological feature of the region is the Aghulas Current, which transports warm Indian surface waters along the African continental margin and releases eddies (Aghulas Rings) into the Atlantic, providing a key source of salt for the overturning circulation (see fig. 3.1; Beal et al., 2011; Gordon et al., 1992; Weijer et al., 2002). Its influence extends to around 2000 m water depth (Bryden et al., 2005). The Agulhas retroflects back into the Indian Ocean and becomes the Agulhas Return Current (ARC) between 16° and 20°E, flowing in close proximity to the STF at ~ 40°S (Belkin and Gordon, 1996; Lutjeharms and Van Ballegooyen, 1988; Read and Pollard, 2017). Due to bathymetric steering around the Crozet

Plateau, the ARC, STF and SAF merge and form the 'Crozet Front' (Belkin and Gordon, 1996; Pollard and Read, 2017; Sultan et al., 2007).

Bathymetry in the region strongly controls the deep and bottom circulation, with deep western boundary currents supported in basins bounded by the N/S trending deep ocean ridges (Donohue and Toole, 2003). North Atlantic Deep Water is transported into the Indian Ocean in complex flow paths around southern Africa and Madagascar before it is mixed and flows northward along the southeast Indian Ocean ridge (van Aken et al., 2004). Northward AABW flow is facilitated through fractures in the SWIOR and the various channels between Del Cano Rise, Crozet Island and Conrad Rise (Boswell et al., 2002).

1.5 Thesis structure

This thesis utilises a new collection of cold-water corals sampled from four seamounts of the southwest Indian Ocean, intersecting the subantarctic Southern Ocean and the subtropical Indian Ocean. Following successful applications of Nd isotopes and ^{14}C on collections from the Drake Passage (Burke and Robinson, 2012; Wilson and Struve, pers. comm.) and south of Tasmania (Hines et al., 2015; Struve, 2016), this study aims to understand how cold-water coral populations may have responded to changing ocean conditions over the past 25,000 years, and utilise tracers of water mass mixing and ventilation age to understand in more detail the role of the Southern Ocean, and specifically the southern Indian sector, in deglacial carbon release.

The thesis is structured as follows:

Chapter 1 (*Introduction*) explains the relevant concepts of the thesis.

Chapter 2 (*Methods*) details the sample collection methodology, taxonomic analysis, cleaning procedure and separation techniques, Nd and ^{14}C analyses and mass spectrometry.

Chapter 3 (*Temporal distribution and diversity of cold-water corals in the southwest Indian Ocean over the past 25,000 years*) contains species descriptions of cold-water corals and investigates possible changes in habitat suitability of the region and Southern Ocean through time.

Chapter 4 (*Reconstructing deglacial water mass changes in the southwest Indian Ocean using cold-water coral Nd isotopes*) discusses the new Nd isotope record in comparison to other Southern Ocean data and deglacial climate changes.

Chapter 5 (*Deglacial ventilation history of the intermediate southwest Indian Ocean*) explores the role of Southern Ocean mechanisms in deglacial carbon release using combined regional ventilation and water mass mixing data.

Chapter 6 (*Summary and conclusions*) summarises the previous chapters, presents general conclusions and considers future avenues of research.

Chapter 2: Methods

Chapter summary

This chapter describes the sampling strategy performed on expedition JC066 for cold-water corals utilised in the thesis. It also explains the strategy used for species identification and full lab procedures and methodologies for rapid and precise U-series dating, Nd isotope and radiocarbon measurements. Setup, testing and behaviour of the Nu Plasma II MC-ICP-MS in the MAGIC laboratories at Imperial College is also described.

2.1 Southern Indian Ocean coral sampling

Opportunistic surveys for subfossil cold-water corals took place during the 2011 *RRS James Cook* expedition JC066, the primary purpose of which was to analyse the depth and spatial variation of benthic communities on seamounts (Rogers and Taylor, 2011). Subfossil corals were collected in situ from four seamounts along the Southwest Indian Ocean Ridge (SWIOR): Coral Seamount (41°21'23" S, 42°50'31" E); Melville Bank (38°31'56" S, 46°45'74" E); Middle of What Seamount (henceforth 'MoW'; 37°56'76" S, 50°22'16" E); and Atlantis Bank (32°42'01" S, 57°17'26" E).

The majority of specimens were collected using the Kiel 6000 Remotely Operated Vehicle (ROV) using manipulator arms, a suction sampler, nets and mini-box corers (Rogers and Taylor, 2011). Dives of the ROV were made along deep to shallow transects at each seamount, with 200m horizontal transects at approximately 1300 m, 1000 m, 700 m and 400 m. Five ROV dives took place at Coral Seamount, four at Melville Bank, two at MoW Seamount, and three at Atlantis Bank. Additional specimens were extracted from a megacore sample (JC066_1116), a boxcore sample (JC066_115), and picked up on a dive of the HYBIS

towed camera system (JC066_4309). The samples cover a water depth range of 172 to 1395 m.

The fossil scleractinian collection provided by Dr Michelle Taylor and Prof Alex Rogers (U Oxford) comprises 149 samples, including 122 solitary specimens (Table 2.1) and over 1.4 kg of fossil colonial scleractinian material.

Table 2.1: Solitary CWC sample locations and ID from cruise JC066.

Cruise	Seamount	Latitude (°N)	Longitude (°E)	Sample number	Depth / m	Family	Genus	Species	Mass / g	Max calicular diameter / cm	Height / cm
JC066	Coral	-41.3628	42.9151	2812D	709.5	Dendrophylliidae	*Balanophyllia*	*gigas*	0.5	7.9	20.2
JC066	Coral	-41.3485	42.9208	1057	1207.2	Dendrophylliidae	*Balanophyllia*	*gigas*	1	10.5	16.3
JC066	Coral	-41.3628	42.9151	2812B	709.5	Dendrophylliidae	*Balanophyllia*	*gigas*	0.6	8.7	23.1
JC066	Coral	-41.3628	42.9151	2810	709.5	Caryophylliidae	*Desmophyllum*	*dianthus*	4.28	21.2	29.3
JC066	Coral	-41.3628	42.9151	2812G	709.5	Dendrophylliidae	*Balanophyllia*	*gigas*	0.4	7.2	17.2
JC066	Coral	-41.3628	42.9149	2808	702	Dendrophylliidae	*Balanophyllia*	*gigas*	0.64	9.4	25.6
JC066	Coral	-41.3628	42.9151	2812K	709.5	Dendrophylliidae	*Balanophyllia*	*gigas*	0.1	8.6	14.7
JC066	Coral	-41.3628	42.9151	2812E	709.5	Dendrophylliidae	*Balanophyllia*	*malouinensis*	0.5	0.7	2.3
JC066	Coral	-41.3628	42.9149	2803	702	Dendrophylliidae	*Balanophyllia*	*gigas*	0.54	7.2	21.3
JC066	Coral	-41.3628	42.9151	2812Q	709.5	Dendrophylliidae	*Balanophyllia*	*gigas*	0.2	5.8	14.6
JC066	Coral	-41.3628	42.9151	2812F	709.5	Caryophylliidae	*Desmophyllum*	*dianthus*	0.5	9.2	22.5
JC066	Coral	-41.3628	42.9151	2811	709.5	Caryophylliidae	*Desmophyllum*	*dianthus*	1.4	13.2	33.8
JC066	Coral	-41.3627	42.9151	2799	710	Dendrophylliidae	*Balanophyllia*	*gigas*	0.29	8	17
JC066	Coral	-41.3628	42.9149	2795	702	Caryophylliidae	*Desmophyllum*	*dianthus*	5.26	20.9	44
JC066	Coral	-41.3628	42.9151	2812L	709.5	Dendrophylliidae	*Balanophyllia*	*gigas*	0.9	5.9	20.7
JC066	Coral	-41.3628	42.9151	2812I	709.5	Dendrophylliidae	*Balanophyllia*	*gigas*	0.5	8	19.7
JC066	Coral	-41.3628	42.9151	2812M	709.5	Dendrophylliidae	*Leptopsammia*	*stokesiana*	0.3	6.8	17.8
JC066	Coral	-41.3628	42.9149	2807	702	Dendrophylliidae	*Balanophyllia*	*gigas*	1.06	8.3	28.4
JC066	Coral	-41.3485	42.9208	0117	1207.2	Caryophylliidae	*Desmophyllum*	*dianthus*	8.7	30.3	18.4
JC066	Coral	-41.3628	42.9151	2812C	709.5	Dendrophylliidae	*Balanophyllia*	*gigas*	0.8	7.6	21.8
JC066	Coral	-41.3628	42.9151	2812J	709.5	Dendrophylliidae	*Balanophyllia*	*malouinensis*	0.3	0.7	2
JC066	Coral	-41.3628	42.9151	2812V	709.5	Dendrophylliidae	*Leptopsammia*	*stokesiana*	0.05	6.6	13.4

JC066	Coral	-41.3627	42.9151	2799B	710	Dendrophylliidae	*Leptopsammia*	*stokesiana*	0.59	8.1	16.6
JC066	Coral	-41.3628	42.9149	2809	702	Dendrophylliidae	*Leptopsammia*	*stokesiana*	0.52	8	22.4
JC066	Coral	-41.3725	42.9107	1116	732	Caryophylliidae	*Desmophyllum*	*dianthus*	8.35	28.5	34.4
JC066	Coral	-41.3724	42.9102	1104B	732	Caryophylliidae	*Trochocyathus*	*gordoni*	0.3	9.2	11.1
JC066	Coral	-41.3724	42.9102	1104A	732	Caryophylliidae	*Trochocyathus*	*gordoni*	0.8	11	10.4
JC066	Coral	-41.3339	42.9188	0486C	1097.2	Flabellidae	*Javania*	*antarctica*	0.7	12.4	19.6
JC066	Coral	-41.3485	42.9208	1062	1207.2	Flabellidae	*Flabellum*	*flexuosum*	0.63	12.3	22.9
JC066	Coral	-41.3485	42.9208	1063	1207.2	Caryophylliidae	*Desmophyllum*	*dianthus*	2.94	16.1	18.6
JC066	Coral	-41.3457	42.9229	0157	1395	Caryophylliidae	*Desmophyllum*	*dianthus*	4.84	20.5	30
JC066	Coral	-41.3485	42.9208	1156	1207.2	Caryophylliidae	*Desmophyllum*	*dianthus*	2.27	15.8	31.6
JC066	Coral	-41.3339	42.9188	1145	1097.2	Caryophylliidae	*Desmophyllum*	*dianthus*	2.86	20.4	28.5
JC066	Coral	-41.3485	42.9208	1069	1207.2	Flabellidae	*Javania*	*antarctica*	0.74	9.2	23.5
JC066	Coral	-41.3485	42.9208	0125	1207.2	Caryophylliidae	*Caryophyllia*	*diomedeae*	3.1	13.5	25
JC066	Coral	-41.3485	42.9208	0124	1207.2	Caryophylliidae	*Caryophyllia*	*diomedeae*	6.33	13.2	35.2
JC066	Coral	-41.3485	42.9208	0128	1207.2	Caryophylliidae	*Desmophyllum*	*dianthus*	3.82	18.3	19.1
JC066	Coral	-41.3485	42.9208	1064	1207.2	Dendrophylliidae	*Balanophyllia*	*gigas*	1.12	8.5	20.8
JC066	Coral	-41.3339	42.9188	0486D	1097.2	Flabellidae	*Javania*	*antarctica*	0.5	13	18.5
JC066	Coral	-41.3485	42.9208	1056	1207.2	Caryophylliidae	*Caryophyllia*	*diomedeae*	7	20.3	44.3
JC066	Coral	-41.3628	42.9151	2812R	709.5	Dendrophylliidae	*Balanophyllia*	*malouinensis*	0.5	1.1	2
JC066	Coral	-41.3485	42.9208	0120	1207.2	Flabellidae	*Flabellum*	*flexuosum*	0.72	11.2	20.2
JC066	Coral	-41.3485	42.9208	1160	1207.2	Caryophylliidae	*Desmophyllum*	*dianthus*	1.64	15.5	22.9
JC066	Coral	-41.3485	42.9208	1059	1207.2	Caryophylliidae	*Desmophyllum*	*dianthus*	1.47	fragmentary	fragmentary
JC066	Coral	-41.3724	42.9102	1072	*624*	Caryophylliidae	*?*	*?*	0.59		
JC066	Coral	-41.3485	42.9208	1155	1207.2	Caryophylliidae	*Caryophyllia*	*diomedeae*	2.2	11	27.5
JC066	Coral	-41.3485	42.9208	1066B	1207.2	Caryophylliidae	*Desmophyllum*	*dianthus*	3.96	17.7	39
JC066	Coral	-41.3485	42.9208	0119	1207.2	Caryophylliidae	*Dasmosmilia*	*lymani*	0.37	8.5	16.1
JC066	Coral	-41.3485	42.9208	0126B	1207.2	Caryophylliidae	*Caryophyllia*	*diomedeae*	1.86	10.7	22.3

JC066	Coral	-41.3485	42.9208	0118	1207.2	Caryophylliidae	*Caryophyllia*	*diomedeae*	5.04	14.5	35.9
JC066	Coral	-41.3560	42.9185	1002	952	Caryophylliidae	*Desmophyllum*	*dianthus*	7.71	24.4	32.5
JC066	Coral	-41.3339	42.9188	1144	1097.2	Caryophylliidae	*Desmophyllum*	*dianthus*	6.53	25.9	26.2
JC066	Coral	-41.3485	42.9208	1157	1207.2	Caryophylliidae	*Caryophyllia*	*diomedeae*	2.59	12.7	31.2
JC066	Coral	-41.3339	42.9188	0107	1097.2	Caryophylliidae	*Caryophyllia*	*diomedeae*	4.04	16.3	31.3
JC066	Coral	-41.3485	42.9208	0135	1207.2	Caryophylliidae	*Caryophyllia*	*diomedeae*	8.36	17.5	34.7
JC066	Coral	-41.3485	42.9208	1159	1207.2	Flabellidae	*Javania*	*antarctica*	0.46	10.2	20
JC066	Coral	-41.3485	42.9208	0123	1207.2	Caryophylliidae	*Desmophyllum*	*dianthus*	9.24	24.5	31
JC066	Coral	-41.3485	42.9208	0127	1207.2	Caryophylliidae	*Desmophyllum*	*dianthus*	12	40.3	36.6
JC066	Coral	-41.3485	42.9208	1061	1207.2	Flabellidae	*Javania*	*antarctica*	0.69	10.7	21.5
JC066	Coral	-41.3485	42.9208	0121	1207.2	Caryophylliidae	*Caryophyllia*	*diomedeae*	31.52	16.4	25
JC066	Coral	-41.3592	42.9176	1046	*922.5*	Caryophylliidae	*Caryophyllia*	*diomedeae*	2	12.9	23.3
JC066	Coral	-41.3485	42.9208	1070	1207.2	Caryophylliidae	*Desmophyllum*	*dianthus*	2.02	16.6	25
JC066	Coral	-41.3485	42.9208	0122	1207.2	Caryophylliidae	*Caryophyllia*	*diomedeae*	7.16	20.7	42.5
JC066	Coral	-41.3339	42.9188	0486Y	1097.2	Caryophylliidae	*Desmophyllum*	*dianthus*	6.33	21.7	25.9
JC066	Coral	-41.3485	42.9208	1158	1207.2	Caryophylliidae	*Desmophyllum*	*dianthus*	1.32	13.9	18.4
JC066	Coral	-41.3485	42.9208	1065	1207.2	Caryophylliidae	*Desmophyllum*	*dianthus*	5.75	22.3	28.4
JC066	Coral	-41.3592	42.9176	1045	*922.5*	Caryophylliidae	*Desmophyllum*	*dianthus*	1.71	13.4	17.2
JC066	Coral	-41.3339	42.9188	1143B	1097.2	Caryophylliidae	*Desmophyllum*	*dianthus*	8.8	3.5	4
JC066	Coral	-41.3339	42.9188	0486E	1097.2	Caryophylliidae	*Desmophyllum*	*dianthus*	0.8	12.4	25.4
JC066	Coral	-41.3592	42.9176	1040	*922.5*	Caryophylliidae	*Desmophyllum*	*dianthus*	4.73	21.9	26.7
JC066	Coral	-41.3339	42.9188	1143A	1097.2	Caryophylliidae	*Desmophyllum*	*dianthus*	14.81	40	45.5
JC066	Coral	-41.3485	42.9208	0115	1207.2	Caryophylliidae	*Desmophyllum*	*dianthus*	2.96	19.7	23.3
JC066	Coral	-41.3485	42.9208	1058	1207.2	Flabellidae	*Javania*	*antarctica*	0.69	14.9	18.7
JC066	Coral	-41.3485	42.9208	1060	1207.2	Caryophylliidae	*Desmophyllum*	*dianthus*	0.65	8	29.4
JC066	Coral	-41.3485	42.9208	1154	1207.2	Dendrophylliidae	*Balanophyllia*	*malouinensis*	0.74	14.2	19.5
JC066	Coral	-41.3627	42.9151	2797	710	Flabellidae	*Flabellum*	*flexuosum*	0.96	10	27

JC066	Coral	-41.3628	42.9151	2812	709.5	Dendrophylliidae	*Balanophyllia*	*gigas*	0.15	5	10.1
JC066	Coral	-41.3339	42.9188	0486B	1097.2	Flabellidae	*Javania*	*antarctica*	0.41	16	18.1
JC066	Coral	-41.3339	42.9188	0486X	1097.2	Caryophylliidae	*Desmophyllum*	*dianthus*	4.83	fragmentary	3.7
JC066	Coral	-41.3485	42.9208	1067B	1207.2	Caryophylliidae	*?*	*?*	0.54	fragmentary	fragmentary
JC066	Coral	-41.3627	42.9151	2794B	710	Dendrophylliidae	*Balanophyllia*	*gigas*	1.59	0.6	1.5
JC066	Coral	-41.3628	42.9151	2812H	709.5	Caryophylliidae	*Desmophyllum*	*dianthus*	0.7	10	16.1
JC066	Coral	-41.3628	42.9151	2812N	709.5	Flabellidae	*Flabellum*	*?*	0.21	8.9	19.1
JC066	Coral	-41.3628	42.9151	2812O	709.5	Dendrophylliidae	*Leptopsammia*	*stokesiana*	0.12	6	11.7
JC066	Coral	-41.3628	42.9151	2812P	709.5	Dendrophylliidae	*Balanophyllia*	*gigas*	0.3	6.4	14.2
JC066	Coral	-41.3628	42.9151	2812S	709.5	Dendrophylliidae	*Balanophyllia*	*gigas*	0.14	4.7	13.7
JC066	Coral	-41.3628	42.9151	2812T	709.5	Dendrophylliidae	*Balanophyllia*	*gigas*	0.17	5.8	11.1
JC066	Coral	-41.3628	42.9151	2812U	709.5	Dendrophylliidae	*Balanophyllia*	*gigas*	0.24	7.2	14.8
JC066	Coral	-41.3628	42.9151	2812W	709.5	Dendrophylliidae	*Balanophyllia*	*gigas*	0.11	4.9	9.8
JC066	Melville	-38.4741	46.7461	3245	171.9	Caryophylliidae	*Caryophyllia*	*profunda*	27.18	30.6	46.6
JC066	Melville	-38.4983	46.7234	2823	897	Caryophylliidae	*?*	*?*	1.02	12.7	23
JC066	Melville	-38.4983	46.7234	3138J	897	Caryophylliidae	*?*	*?*	0.3	1	1.4
JC066	Melville	-38.4983	46.7234	2825	897	Caryophylliidae	*Caryophyllia*	*?*	4.32	14.2	24
JC066	Melville	-38.4983	46.7234	3138M	897	Flabellidae	*Flabellum*	*?*	2.1	20.3	22.3
JC066	Melville	-38.4983	46.7234	2822	897	Caryophylliidae	*Desmophyllum*	*dianthus*	0.17	7.5	9.2
JC066	Melville	-38.4983	46.7234	2824	897	Dendrophylliidae	*Balanophyllia*	*malouinensis*	1.88	1.1	2.1
JC066	Melville	-38.4983	46.7234	3138B	897	Deltocyathidae	*Deltocyathus*	*deltocyathus*	0.06	0.5	0.2
JC066	Melville	-38.4983	46.7234	3138D	897	Flabellidae	*Javania*	*antarctica*	0.18	7.7	13
JC066	MoW	-37.9567	50.4074	3507	1014	Caryophylliidae	*Caryophyllia*	*diomedeae*	2.9	16	26.4
JC066	MoW	-37.9567	50.4074	3508	1014	Caryophylliidae	*Caryophyllia*	*diomedeae*	4.92	15.2	29.2
JC066	MoW	-37.9567	50.4074	3509	1014	Caryophylliidae	*Caryophyllia*	*diomedeae*	4.58	16.5	30
JC066	MoW	-37.9567	50.4074	3506B	1014	Caryophylliidae	*?*	*?*	2.8	1	2.6
JC066	MoW	-37.9567	50.4074	3506A	1014	Caryophylliidae	*Caryophyllia*	*diomedeae*	2.8	14.1	24.1

JC066	MoW	-37.9567	50.4074	2590	1014	Caryophylliidae	*Caryophyllia*	*diomedeae*	10	12.9	32
JC066	MoW	-37.9567	50.4074	3510	1014	Caryophylliidae	*Caryophyllia*	*diomedeae*	7.53	21.6	35.4
JC066	Atlantis	-32.7223	57.2483	2619	922	Caryophylliidae	*Caryophyllia*	*diomedeae*	3.22	18.3	23.5
JC066	Atlantis	-32.7166	57.2451	3718	1035	Caryophylliidae	*Desmophyllum*	*dianthus*	4.42	21.7	23.5
JC066	Atlantis	-32.7222	57.2529	3697	823	Caryophylliidae	*Caryophyllia*	*diomedeae*	9.81	18.8	25
JC066	Atlantis	-32.7166	57.2451	3692	1035	Caryophylliidae	*Desmophyllum*	*dianthus*	4.12	14.7	16.1
JC066	Atlantis	-32.6987	57.2945	3770	763	Caryophylliidae	*Caryophyllia*	*diomedeae*	2.25	15	15.9
JC066	Atlantis	-32.7225	57.2500	3721	870	Caryophylliidae	*Desmophyllum*	*dianthus*	0.48	10.9	12.7
JC066	Atlantis	-32.7223	57.2483	2621	922	Caryophylliidae	*Caryophyllia*	*diomedeae*	1.77	12.5	22.5
JC066	Atlantis	-32.7166	57.2451	3715	1035	Caryophylliidae	*Desmophyllum*	*dianthus*	3.68	16.7	23.9
JC066	Atlantis	-32.6987	57.2945	3741	763	Caryophylliidae	*Caryophyllia*	*diomedeae*	3.14	15.9	20.5
JC066	Atlantis	-32.7223	57.2483	2618	922	Caryophylliidae	*Caryophyllia*	*diomedeae*	6.02	16	31.9
JC066	Atlantis	-32.7122	57.2833	3643	726	Caryophylliidae	*Caryophyllia*	*diomedeae*	8.43	22.4	22.7
JC066	Atlantis	-32.7223	57.2483	2617	922	Caryophylliidae	*Caryophyllia*	*diomedeae*	2.23	12.2	30.2
JC066	Atlantis	-32.7117	57.2758	3661	743	Caryophylliidae	*Caryophyllia*	*diomedeae*	4.45	15.7	30.5
JC066	Atlantis	-32.7223	57.2483	2620	922	Caryophylliidae	*Caryophyllia*	*diomedeae*	3.08	16.5	18.7
JC066	Atlantis	-32.7225	57.2500	3705	870	Caryophylliidae	*Caryophyllia*	*diomedeae*	9.25	20.1	30.2
JC066	Atlantis	-32.7225	57.2500	3712	870	Caryophylliidae	*Caryophyllia*	*diomedeae*	14.52	18.4	25.3
JC066	Atlantis	-32.7222	57.2529	3696	823	Caryophylliidae	*Caryophyllia*	*diomedeae*	5.27	17	36

*Italics indicate depth estimated from incomplete cruise record

2.2 Taxonomic identification

Specimens were identified taxonomically at the Natural History Museum (NHM) under the supervision of Nadiezhda Santodomingo to characterise the past ecology of the seamounts and select appropriate specimens for geochemical analysis.

Firstly, key morphological characteristics were catalogued for each specimen. These were as follows: height; maximum and minimum calicular diameter; corallum shape; pedicel width; septal system, number, exertness and granularity; presence, shape and number of pali; appearance of theca; presence and shape of costae; and presence and shape of columella (Fig. 2.1). Corals were weighed and photographs were taken of each specimen for reference (Figs. 2.2A, B). Images up to 50x magnification were taken for six selected specimen using the LO 1455 SEM at the NHM, and used to identify micro-scale features such as septal granules and thecal porosity (Figs. 2.3A-C).

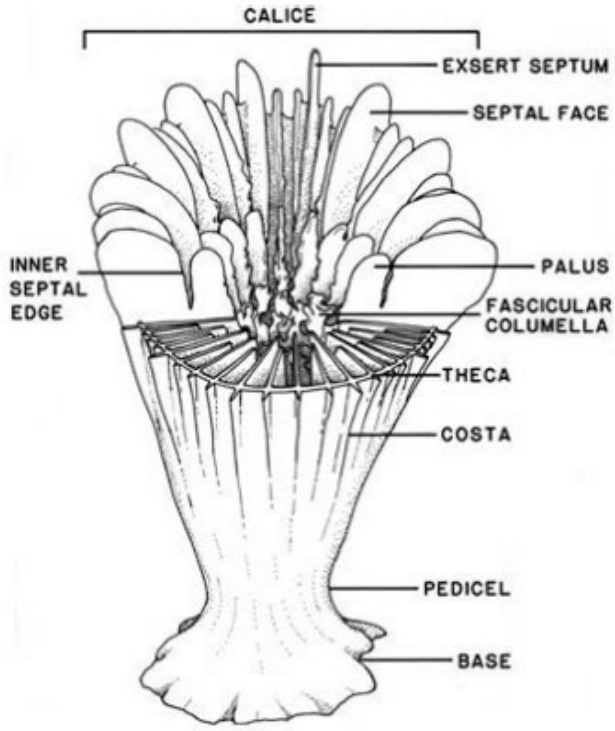

Figure 2.1: Morphological features of a solitary scleractinian coral commonly used for taxonomic identification.

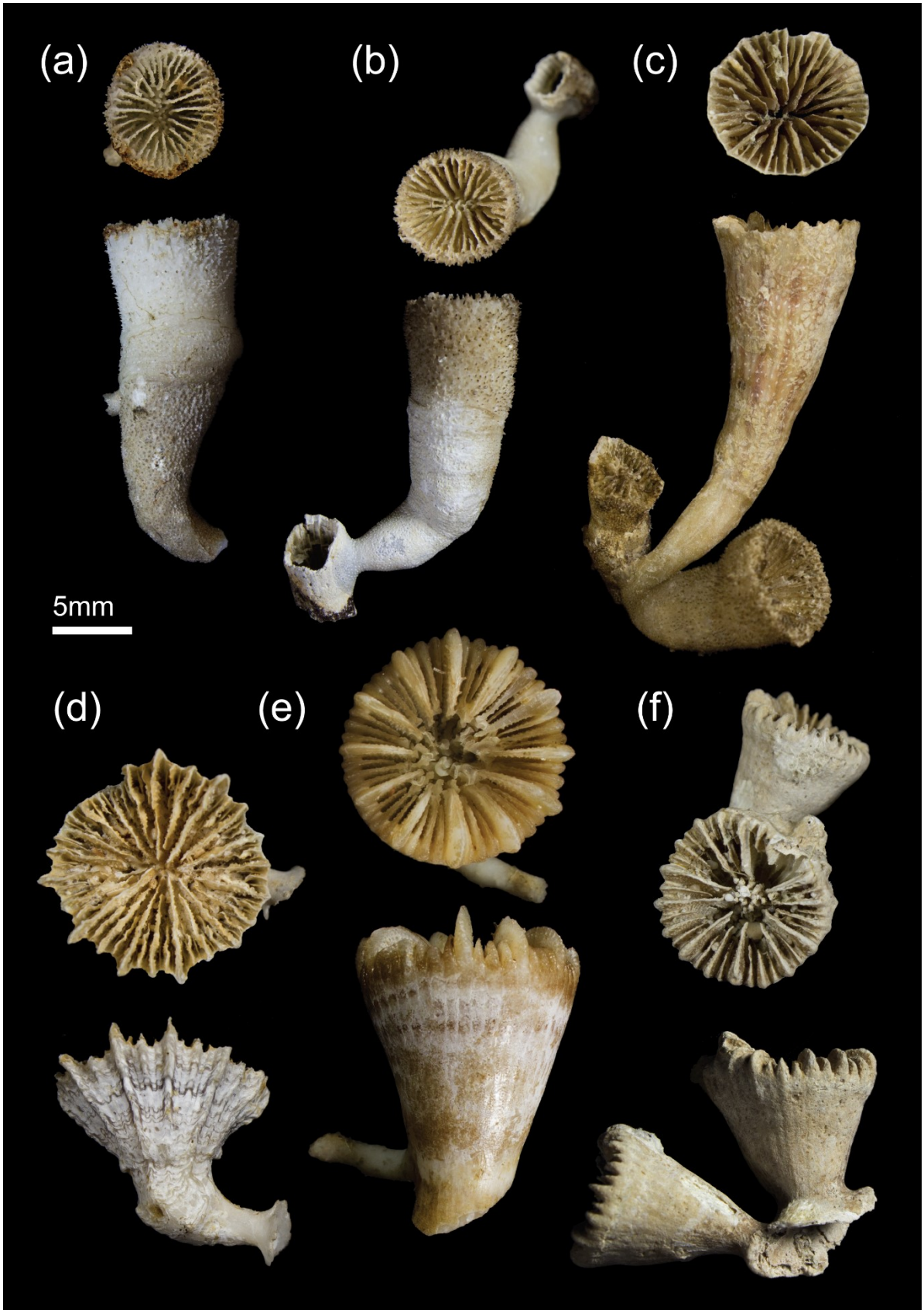

Figure 2.2a: Photographs of cold-water coral samples: **A)** JC066_2812b, *Balanophyllia gigas*; **B)** JC066_2812e *Balanophyllia malouinensis,* **C)** JC066_2797, *Flabellum flexuosum*; **D)** JC066_1058

Javania antarctica; **E)** JC066_3741, *Caryophyllia diomedeae*; **F)** JC066_1104a & JC066_1104b, *Trochocyathus gordoni*.

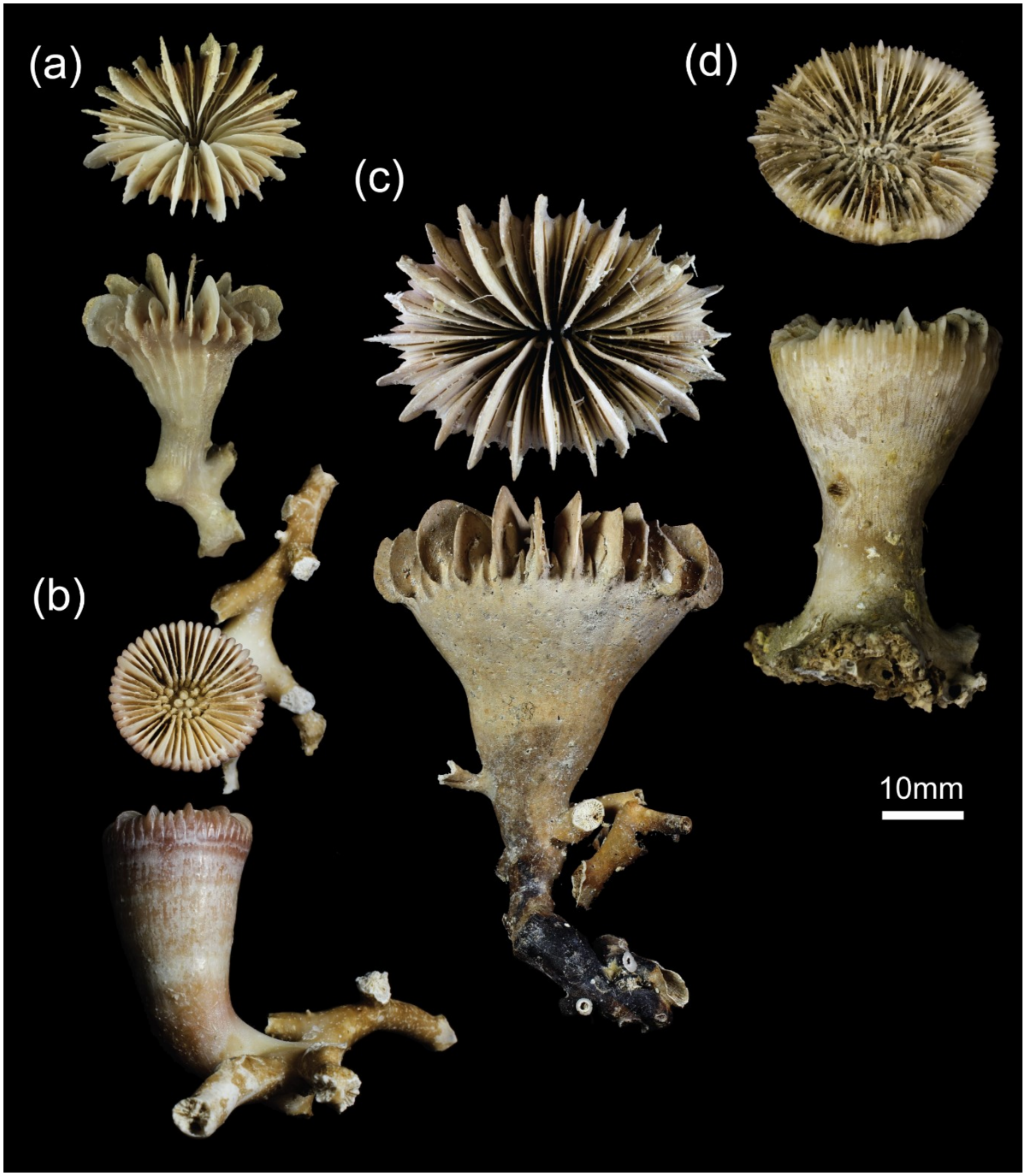

Figure 2.2b: Photographs of cold-water coral samples (clockwise from top left): **A)** JC066_3718, *Desmophyllum dianthus*; **B)** JC066_122, *Caryophyllia diomedeae*; **C)** JC066_127, *Desmophyllum dianthus*; **D)** JC066_3245, *Caryophyllia profunda*.

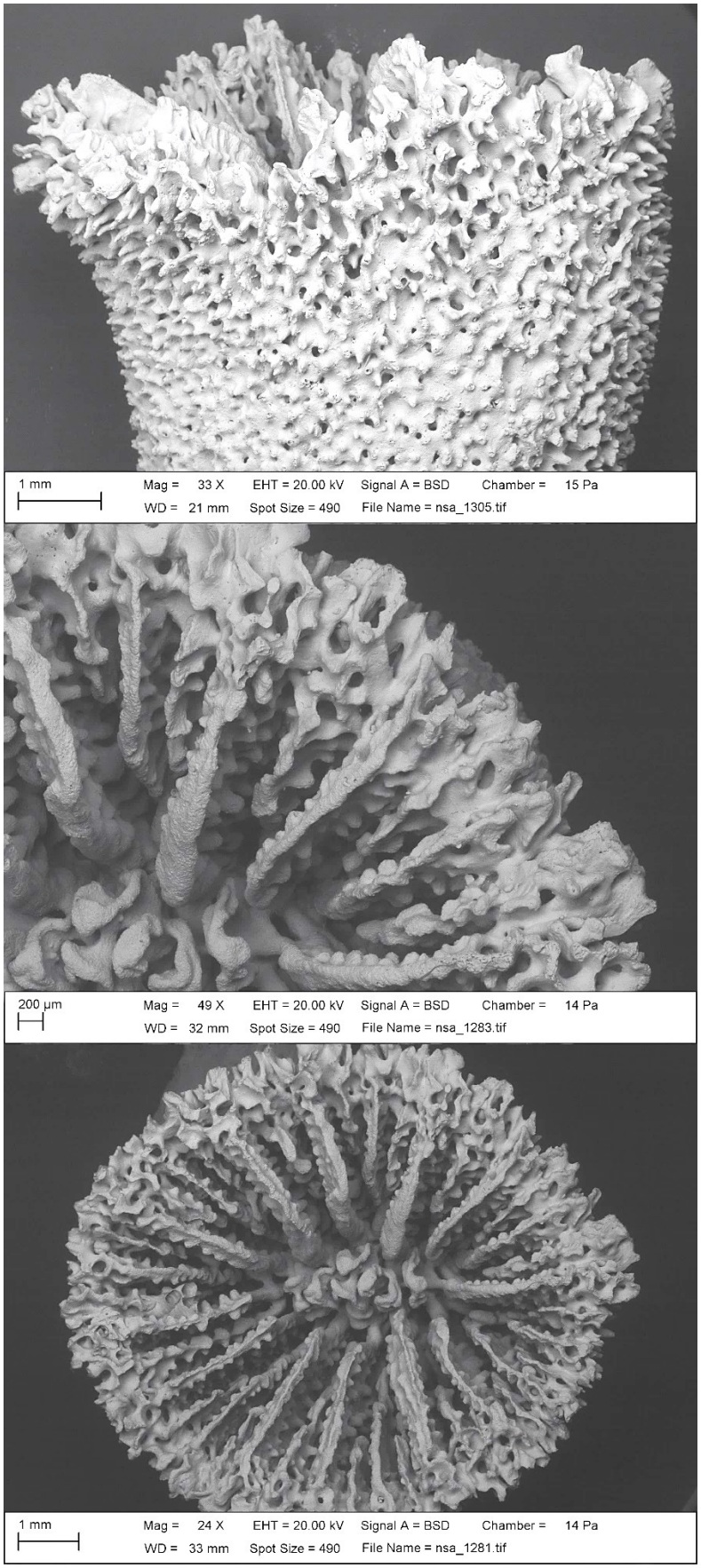

Figure 2.3a: SEM images of JC066_2812r, *Balanophyllia malouinensis*.

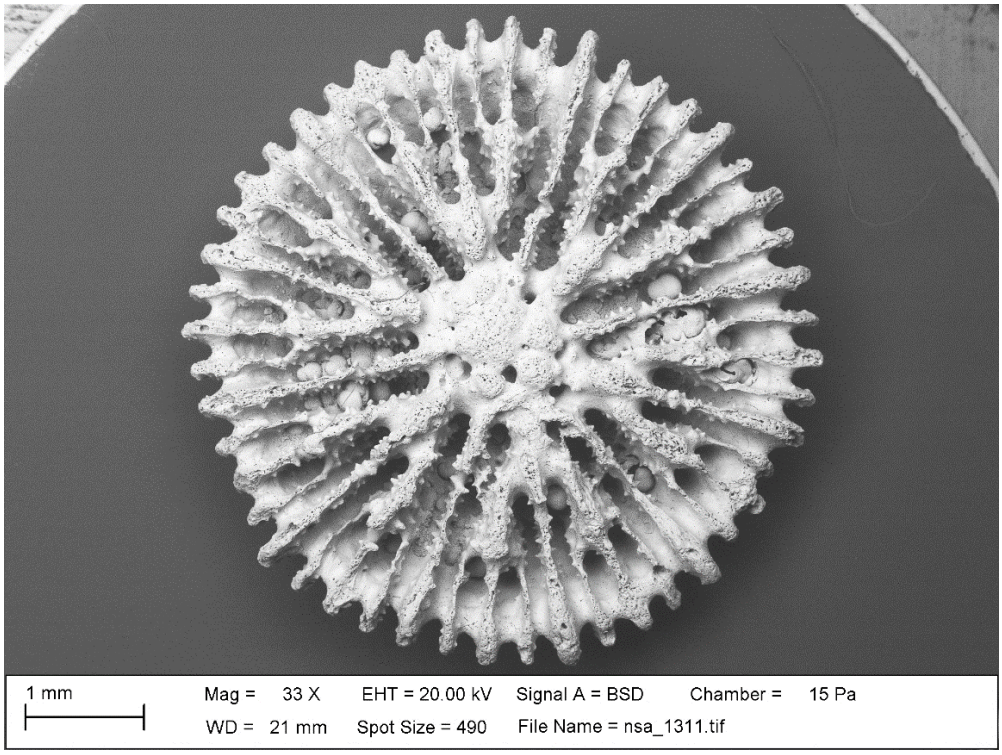

Figure 2.3b: SEM image of JC066_3138b, *Deltocyathus*.

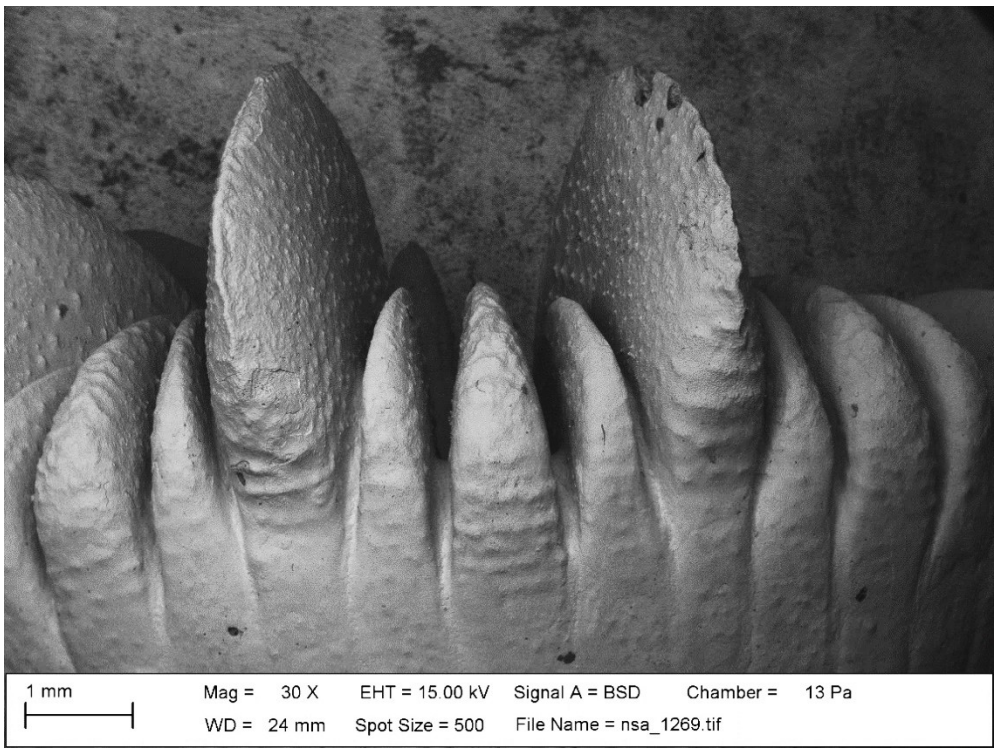

Figure 2.3c: SEM image of JC066_3697, *Caryophyllia diomedeae*.

Specimens were then grouped into 'morphospecies' according to shared morphological features. Descriptions and photographs from monographies representing the most recent, extensive and available documents on azooxanthellate Scleractinia were used to assign these groups to the appropriate taxa. The sources used included Cairns (1982; Antarctic and Subantarctic), Cairns and Keller (1993; SWIO), Cairns (1995; New Zealand), Cairns and Zibrowius (1997; Indonesia), Cairns (2000; Caribbean), Kitahara et al. (2010) and Cairns and Polonio (2013; Indonesia).

During taxonomic analysis, the level of preservation of the specimens was evaluated qualitatively. For each specimen, two values were assigned: one corresponding to the preservation of aragonite, including breakdown by organisms, dissolution and erosion from 1 (highly degraded) to 5 (intact), and one reflecting the level of accumulation of authigenic coating from 0 (no coating) to 3 (fully coated). These metrics were combined into an overall 'preservation factor', by subtracting coating from aragonite preservation (Table 2.2).

Table 2.2: Examples of CWC coating and aragonite preservation.

	'High' aragonite preservation	'Low' aragonite preservation
'Low' coating	JC066_2811; *D. dianthus* (C: 0; A.P: 5)	JC066_1070*; D. dianthus* (C: 0; A.P: 3; no CWCs in collection were described to have low aragonite preservation and low coating)

'High' coating	JC066_1056; *C. diomedeae* (C: 3; A.P: 4)	JC066_0115; *D. dianthus* (C: 3; A.P: 1)

2.3 Reconnaissance U-series dating

A total of 122 solitary scleractinian samples were prepared for rapid uranium-series age screening by laser ablation ICP-MS in the Bristol Isotope Group (BIG) facilities at the University of Bristol, following the method developed by Chen et al. (2015) and Spooner et al. (2016) under the supervision of Dr Tianyu Chen (U Bristol). Twenty-one specimens, predominantly of the genus *Balanophyllia,* were too delicate, small, or poorly preserved to proceed with laser ablation dating. Coral samples of a minimum size of 2 x 1.5 mm were cut using a Dremel® tool with a diamond blade, polished flat on one side using four increasingly fine grades of sandpaper and rinsed with ultrapure water (18.2 MΩ·cm; henceforth MilliQ water). These samples were then mounted in batches of ~ 50 into trough-shaped sample holders, along with an aragonite vein standard from the Salt Wash Graben, Green River, Utah (VS001/1-A).

Auto-focussed and pre-programmed 1.1 mm line scans were ablated automatically using 'Chromium 2.1' software linked to the Photon Machines Analyte G2 193 nm laser, which was coupled to a Thermo Finnigan Neptune MC-ICP-MS.

The low abundance ^{230}Th isotope was measured on a central ion counter whilst ^{238}U was measured simultaneously using Faraday cups. To maximise ^{230}Th intensity, tuning was carried out using NIST 610 glass. The aragonite vein standard (VS001/1-A) was used to bracket every three samples to correct for instrumental, elemental and isotopic fractionation. Measurements consisted of 50 cycles for samples and bracketing standards, and background intensities were measured for 25 cycles following each standard measurement. In the rare case anomalous signal spikes in ^{230}Th were observed, these were removed before calculation of mean isotope intensities, subtraction of the background intensity, and calculation of the isotope ratios.

Activity ratios were used to determine sample age by solving the decay equation (Equation 1) for t:

$$\left(\frac{^{230}\mathrm{Th}}{^{238}\mathrm{U}}\right) - \left(\frac{^{232}\mathrm{Th}}{^{238}\mathrm{U}}\right)\left(\frac{^{230}\mathrm{Th}}{^{232}\mathrm{Th}}\right)_i \left(e^{(-\lambda_{230})t}\right)$$

$$= 1 - e^{-\lambda_{230}t} + \left(\frac{\delta^{234}U_m}{1000}\right)\left(\frac{\lambda_{230}}{\lambda_{230} - \lambda_{234}}\right)\left(1 - e^{(\lambda_{234} - \lambda_{230})t}\right)$$

A fundamental assumption to the reconnaissance dating method is that the total measured ^{230}Th was formed by ^{234}U decay in the sample, and no Th was incorporated during calcification. Although this is unlikely to be true for cold-water corals, previous data indicate that age corrections resulting from corrections for initial ^{230}Th based on ^{232}Th fall within the usual age uncertainties from this method (Robinson et al., 2014b; Spooner et al., 2016). Therefore the equation becomes:

$$\left(\frac{^{230}\mathrm{Th}}{^{238}\mathrm{U}}\right) = 1 - e^{-\lambda_{230}t} + \left(\frac{\delta^{234}U_m}{1000}\right)\left(\frac{\lambda_{230}}{\lambda_{230} - \lambda_{234}}\right)\left(1 - e^{(\lambda_{234} - \lambda_{230})t}\right)$$

Closed system behaviour was also assumed and the term $\delta^{234}U_m$ was calculated using the known modern seawater $\delta^{234}U_i$ (147 ± 7 ‰; Reimer et al., 2009) with the following equation:

$$\delta^{234}U_i = \delta^{234}\mathrm{U}_m e^{\lambda_{234}t}$$

Solving of the age equation was accomplished iteratively using the Newton-Raphson method (Kaufman and Broecker, 1965). Standard errors on the measured ratios, the background measurements, and the errors on the isotope dilution MC-ICP-MS isotope ratios of the standards were combined and propagated through each stage of standard corrections. Final propagation of errors through the age equation was carried out using a Monte Carlo technique. For deglacial age corals these errors range between 500 and 1500 years.

Table 2.3: Laser ablation U-series dating of SWIO CWCs.

Sample number (JC066_)	LA ID	LA Age / y	2σ	^{238}U (V)	2σ	^{230}Th (V)	2σ	measured ^{230}Th/^{238}U	2σ	corrected [^{230}Th/^{238}U]	2σ
0121	In-001	**13453**	**624**	0.2719	0.0080	3.39E-07	1.73E-08	1.24E-06	4.54E-08	0.1325	0.0056
2812B	In-002	**166**	**147**	0.2599	0.0093	1.54E-08	2.81E-09	5.89E-08	1.07E-08	0.0017	0.0015
0123	In-003	**13364**	**769**	0.1720	0.0036	2.17E-07	1.08E-08	1.26E-06	5.81E-08	0.1317	0.0070
2810	In-004	**327**	**277**	0.1375	0.0027	1.30E-08	2.45E-09	9.49E-08	1.80E-08	0.0034	0.0029
2812G	In-005	**329**	**155**	0.2666	0.0071	1.70E-08	2.89E-09	6.40E-08	1.08E-08	0.0034	0.0016
2799B	In-006	**1957**	**245**	0.2467	0.0068	5.43E-08	5.01E-09	2.20E-07	2.02E-08	0.0203	0.0025
2812C	In-007	**1571**	**243**	0.1998	0.0050	3.85E-08	3.92E-09	1.94E-07	2.05E-08	0.0164	0.0025
3696	In-008	**2209**	**397**	0.1079	0.0025	3.12E-08	3.35E-09	2.88E-07	2.97E-08	0.0229	0.0041
3509	In-009	**13555**	**832**	0.1425	0.0056	1.84E-07	9.97E-09	1.30E-06	6.27E-08	0.1335	0.0075
1040	In-010	**17406**	**756**	0.1877	0.0094	3.08E-07	1.53E-08	1.65E-06	5.36E-08	0.1683	0.0065
1144	In-013	**13046**	**755**	0.1413	0.0035	1.82E-07	9.88E-09	1.29E-06	6.11E-08	0.1287	0.0069
1066B	In-014	**12818**	**792**	0.1411	0.0030	1.79E-07	1.01E-08	1.27E-06	6.31E-08	0.1266	0.0072
2618	In-015	**541**	**233**	0.1312	0.0031	1.55E-08	2.39E-09	1.18E-07	1.79E-08	0.0057	0.0024
2795	In-016	**609**	**227**	0.1454	0.0041	1.74E-08	2.52E-09	1.20E-07	1.73E-08	0.0064	0.0024
1056	In-017	**12339**	**615**	0.1789	0.0042	2.19E-07	1.02E-08	1.22E-06	5.00E-08	0.1222	0.0056
3507	In-018	**9435**	**594**	0.1292	0.0039	1.26E-07	6.90E-09	9.79E-07	5.03E-08	0.0947	0.0056
3712	In-019	**1435**	**263**	0.1016	0.0026	1.71E-08	2.43E-09	1.70E-07	2.45E-08	0.0150	0.0027

2812J	In-020	**1579**	**175**	0.2011	0.0063	3.41E-08	3.34E-09	1.70E-07	1.67E-08	0.0164	0.0018
2812I	In-021	**1237**	**186**	0.2123	0.0084	2.87E-08	3.86E-09	1.36E-07	1.76E-08	0.0129	0.0019
0127	In-022	**13405**	**752**	0.1420	0.0029	2.24E-07	1.08E-08	1.57E-06	6.55E-08	0.1321	0.0068
1143B	In-023	**16417**	**709**	0.1602	0.0083	2.96E-07	1.61E-08	1.86E-06	5.88E-08	0.1595	0.0061
1143A	In-024	**17666**	**801**	0.1755	0.0025	3.44E-07	1.35E-08	1.96E-06	6.57E-08	0.1706	0.0069
3510	In-025	**17557**	**866**	0.1417	0.0047	2.89E-07	1.52E-08	2.03E-06	7.09E-08	0.1697	0.0075
0117	In-026	**1476**	**280**	0.1455	0.0039	4.50E-08	4.12E-09	3.09E-07	2.60E-08	0.0154	0.0029
2619	In-027	**negative**	**318**	0.0885	0.0027	1.48E-08	1.90E-09	1.68E-07	2.15E-08	-0.0052	-0.0033
0128	In-028	**12053**	**1090**	0.0552	0.0016	9.80E-08	5.58E-09	1.78E-06	9.88E-08	0.1195	0.0101
2812D	In-029	**negative**	**362**	0.0939	0.0039	2.00E-08	2.35E-09	2.14E-07	2.44E-08	-0.0018	-0.0038
1145	In-030	**10670**	**1010**	0.0670	0.0031	1.04E-07	6.36E-09	1.58E-06	1.02E-07	0.1065	0.0095
0157	In-031	**9777**	**1419**	0.0329	0.0022	5.57E-08	4.97E-09	1.72E-06	1.27E-07	0.0979	0.0135
3506B	In-032	**14157**	**2084**	0.0251	0.0015	5.89E-08	4.84E-09	2.39E-06	2.17E-07	0.1390	0.0191
3506A	In-033	**15863**	**2063**	0.0282	0.0006	6.90E-08	5.44E-09	2.45E-06	1.95E-07	0.1545	0.0186
3245	In-034	**841**	**1585**	0.0209	0.0007	1.68E-08	2.73E-09	8.15E-07	1.35E-07	0.0088	0.0165
2812L	In-035	**1072**	**1291**	0.0302	0.0016	1.85E-08	3.60E-09	6.37E-07	1.29E-07	0.0112	0.0134
2809	In-036	**2796**	**1474**	0.0241	0.0008	2.26E-08	3.04E-09	9.41E-07	1.24E-07	0.0289	0.0151
2620	In-037	**845**	**249**	0.1392	0.0034	2.63E-08	3.44E-09	1.89E-07	2.36E-08	0.0088	0.0026
3508	In-038	**12396**	**695**	0.1515	0.0032	2.08E-07	9.60E-09	1.38E-06	6.21E-08	0.1227	0.0064
1057	In-039	**154**	**111**	0.2444	0.0126	1.76E-08	2.48E-09	7.35E-08	1.01E-08	0.0016	0.0012
2812R	In-040	**12395**	**522**	0.2307	0.0076	2.99E-07	1.32E-08	1.30E-06	4.54E-08	0.1227	0.0047

2812V	In-041	**1689**	**176**	0.2678	0.0086	5.86E-08	5.37E-09	2.16E-07	1.63E-08	0.0176	0.0018
0124	In-042	**12050**	**709**	0.1257	0.0033	1.64E-07	9.21E-09	1.30E-06	6.07E-08	0.1195	0.0065
1064	In-043	**12268**	**592**	0.2382	0.0053	3.00E-07	1.38E-08	1.26E-06	5.04E-08	0.1215	0.0054
2812K	In-044	**460**	**115**	0.2390	0.0098	1.61E-08	2.72E-09	6.67E-08	1.10E-08	0.0048	0.0012
2812E	In-045	**471**	**113**	0.2705	0.0095	1.79E-08	3.04E-09	6.61E-08	1.10E-08	0.0049	0.0012
2808	In-046	**369**	**147**	0.2821	0.0116	2.07E-08	3.74E-09	7.31E-08	1.33E-08	0.0039	0.0015
2812Q	In-047	**511**	**173**	0.2274	0.0088	2.20E-08	3.46E-09	9.66E-08	1.54E-08	0.0054	0.0018
2799	In-048	**567**	**171**	0.2297	0.0101	2.34E-08	3.40E-09	1.03E-07	1.48E-08	0.0059	0.0018
1116	In-049	**4058**	**410**	0.1486	0.0029	7.42E-08	5.53E-09	5.02E-07	3.92E-08	0.0418	0.0041
2803	In-050	**473**	**133**	0.2319	0.0059	2.30E-08	2.55E-09	9.96E-08	1.12E-08	0.0050	0.0014
2807	In-050	**474**	**133**	0.2319	0.0059	2.30E-08	2.55E-09	9.96E-08	1.12E-08	0.0050	0.0014
2812M	In-051	**1332**	**138**	0.2899	0.0074	5.44E-08	4.26E-09	1.87E-07	1.32E-08	0.0139	0.0014
0107	In-052	**1314**	**139**	0.3359	0.0121	6.05E-08	4.56E-09	1.83E-07	1.51E-08	0.0137	0.0014
1002	In-053	**13238**	**635**	0.1922	0.0119	2.77E-07	1.62E-08	1.45E-06	5.78E-08	0.1305	0.0057
1065	In-054	**13045**	**581**	0.2480	0.0050	3.64E-07	1.44E-08	1.47E-06	4.87E-08	0.1287	0.0052
0119	In-055	**14668**	**830**	0.1998	0.0029	3.29E-07	1.53E-08	1.65E-06	7.43E-08	0.1436	0.0074
2823	In-057	**73510**	**3021**	0.2453	0.0040	1.55E-06	3.12E-08	6.32E-06	1.21E-07	0.5537	0.0148
0120	In-058	**6561**	**539**	0.1395	0.0065	1.15E-07	9.36E-09	8.24E-07	5.64E-08	0.0667	0.0053
1069	In-059	**12418**	**622**	0.2060	0.0049	2.96E-07	1.42E-08	1.44E-06	5.75E-08	0.1229	0.0056
0486C	In-060	**10911**	**613**	0.1429	0.0114	1.97E-07	1.56E-08	1.39E-06	5.79E-08	0.1088	0.0057
1058	In-061	**6610**	**809**	0.0690	0.0024	7.04E-08	5.70E-09	1.03E-06	7.95E-08	0.0672	0.0080

3138J	In-063	**15547**	**734**	0.1673	0.0024	2.49E-07	9.39E-09	1.49E-06	5.63E-08	0.1516	0.0065
1061	In-064	**13416**	**689**	0.3066	0.0047	3.91E-07	1.80E-08	1.27E-06	5.36E-08	0.1322	0.0062
1104A	In-065	**5193**	**389**	0.1927	0.0057	1.07E-07	6.91E-09	5.55E-07	3.43E-08	0.0532	0.0038
1104B	In-066	**5013**	**326**	0.2161	0.0069	1.09E-07	6.23E-09	5.05E-07	2.75E-08	0.0514	0.0032
0486D	In-067	**12289**	**600**	0.3077	0.0050	3.51E-07	1.34E-08	1.15E-06	4.58E-08	0.1217	0.0055
1070	In-068	**13747**	**677**	0.2139	0.0032	2.73E-07	1.15E-08	1.28E-06	5.14E-08	0.1352	0.0061
0115	In-069	**24190**	**2176**	0.1832	0.0043	3.81E-07	2.96E-08	2.09E-06	1.56E-07	0.2267	0.0180
2811	In-070	**553**	**134**	0.2729	0.0081	1.86E-08	2.80E-09	6.92E-08	1.07E-08	0.0058	0.0014
0486Y	In-071	**13908**	**656**	0.1903	0.0047	2.40E-07	9.83E-09	1.27E-06	4.74E-08	0.1367	0.0059
1159	In-072	**13319**	**508**	0.3751	0.0063	4.50E-07	1.45E-08	1.20E-06	3.49E-08	0.1313	0.0045
3138M	In-073	**142608**	**7844**	0.2700	0.0137	2.00E-06	9.73E-08	7.42E-06	1.19E-07	0.8128	0.0194
1062	In-074	**6832**	**333**	0.2991	0.0083	1.91E-07	9.54E-09	6.39E-07	2.65E-08	0.0694	0.0032
1158	In-075	**13977**	**728**	0.2116	0.0049	2.72E-07	1.24E-08	1.29E-06	5.61E-08	0.1373	0.0066
3770	In-076	**344**	**221**	0.1540	0.0049	9.20E-09	2.65E-09	5.91E-08	1.68E-08	0.0036	0.0023
2812F	In-077	**527**	**208**	0.1544	0.0038	1.19E-08	2.40E-09	7.67E-08	1.49E-08	0.0055	0.0022
1059	In-078	**12744**	**607**	0.1764	0.0033	2.12E-07	8.84E-09	1.21E-06	4.84E-08	0.1259	0.0055
2825	In-079	**18412**	**931**	0.1311	0.0042	2.22E-07	8.68E-09	1.70E-06	6.66E-08	0.1772	0.0080
3721	In-080	**348**	**158**	0.1342	0.0033	6.45E-09	1.66E-09	4.78E-08	1.22E-08	0.0036	0.0016
3741	In-081	**413**	**146**	0.1238	0.0019	5.46E-09	1.66E-09	4.36E-08	1.32E-08	0.0043	0.0015
0126B	In-082	**12930**	**649**	0.1834	0.0045	2.27E-07	1.26E-08	1.23E-06	5.28E-08	0.1277	0.0059
1072	In-083	**12762**	**665**	0.1375	0.0062	1.68E-07	9.92E-09	1.23E-06	5.58E-08	0.1261	0.0060

1157	In-084	**13049**	**696**	0.1711	0.0060	2.17E-07	1.30E-08	1.26E-06	5.80E-08	0.1288	0.0063
1045	In-085	**15893**	**706**	0.1389	0.0053	2.11E-07	1.14E-08	1.52E-06	5.57E-08	0.1548	0.0062
1063	In-086	**7176**	**491**	0.1438	0.0059	1.04E-07	5.80E-09	7.31E-07	4.44E-08	0.0728	0.0048
3661	In-087	**762**	**212**	0.1126	0.0033	9.43E-09	2.26E-09	8.29E-08	1.90E-08	0.0080	0.0022
486E	In-088	**16892**	**905**	0.1093	0.0032	1.77E-07	9.82E-09	1.62E-06	7.22E-08	0.1637	0.0079
2617	In-089	**607**	**184**	0.0993	0.0034	6.79E-09	1.55E-09	6.81E-08	1.56E-08	0.0063	0.0019
1160	In-090	**12635**	**789**	0.1356	0.0031	1.68E-07	1.01E-08	1.24E-06	6.87E-08	0.1249	0.0072
3643	In-091	**582**	**153**	0.1162	0.0115	7.29E-09	1.86E-09	6.41E-08	1.66E-08	0.0061	0.0016
3692	In-092	**304**	**133**	0.1132	0.0030	3.86E-09	1.46E-09	3.41E-08	1.31E-08	0.0032	0.0014
0125	In-093	**11975**	**705**	0.1280	0.0044	1.50E-07	1.01E-08	1.17E-06	5.92E-08	0.1188	0.0065
3718	In-094	**166**	**201**	0.1032	0.0027	3.84E-09	1.63E-09	3.72E-08	1.59E-08	0.0017	0.0021
2621	In-095	**360**	**155**	0.1164	0.0065	6.37E-09	1.15E-09	5.43E-08	9.76E-09	0.0038	0.0016
1156	In-096	**10521**	**727**	0.1214	0.0023	1.25E-07	7.99E-09	1.03E-06	6.22E-08	0.1051	0.0068
0135	In-097	**13269**	**765**	0.1533	0.0065	1.96E-07	1.28E-08	1.28E-06	6.31E-08	0.1308	0.0069
3715	In-098	**376**	**116**	0.1528	0.0059	6.19E-09	1.64E-09	4.05E-08	1.07E-08	0.0039	0.0012
1155	In-099	**12767**	**629**	0.1390	0.0036	1.70E-07	7.99E-09	1.23E-06	5.13E-08	0.1262	0.0057
0122	In-100	**13782**	**633**	0.1952	0.0050	2.57E-07	1.20E-08	1.32E-06	5.04E-08	0.1355	0.0057
0118	In-101	**12958**	**680**	0.1393	0.0091	1.73E-07	1.60E-08	1.23E-06	5.57E-08	0.1279	0.0062
1046	In-102	**13600**	**735**	0.1603	0.0048	2.14E-07	1.21E-08	1.33E-06	6.19E-08	0.1338	0.0066
3705	In-103	**965**	**187**	0.1519	0.0076	1.67E-08	2.85E-09	1.08E-07	1.72E-08	0.0101	0.0019
3697	In-104	**200**	**127**	0.1676	0.0051	4.96E-09	1.76E-09	2.94E-08	1.02E-08	0.0021	0.0013

2590	In-105	**16060**	**596**	0.1405	0.0067	2.26E-07	1.28E-08	1.61E-06	4.29E-08	0.1563	0.0051

2.4 Sample preparation for U-Th-Nd isotope and ^{14}C analysis

Subsamples for combined U, Th, Nd chemistry (~ 0.6 to 5 g) were cut using a Dremel tool with diamond-coated disc blade attachment in a fume hood to minimise dust inhalation.

Physical and chemical cleaning procedures followed the development and assessment of methods performed before in the MAGIC group at Imperial College on cold-water corals (Crocket et al., 2014; van de Flierdt et al., 2010), building on methods developed by Cheng et al. (2000), Lomitschka and Mangini (1999) and Shen and Boyle (1988).

All samples were rigorously physically cleaned with a Dremel tool with the aim of removing all ferromanganese coatings, detrital material, the surfaces of epibiont boreholes, impurities or discolouration within the skeleton and remineralised or 'powdery' calcite. LED torchlight and magnification proved useful for identifying and assessing successful removal of these features. Between each coral the disc blade was rinsed with ethanol and MilliQ water. Where visible, authigenic coatings were sampled using a scalpel.

In preparation for laser ablation, samples of a minimum size of 2 x 1.5 mm were polished flat on one side using four increasingly fine grades of sandpaper and rinsed with MilliQ water.

Subsamples (~ 0.1 to 2 g) selected for combined U-Th and Nd separations underwent a two-day oxidative-reductive chemical cleaning process. They were transferred to individual acid-cleaned 15mL centrifuge tubes, covered with deionised water, and ultrasonicated for 20 minutes. This process was repeated a minimum of three times, pipetting off the water in between each rinse, until the water ran clear. The rest of the cleaning process consisted of ultrasonication with a series of solutions with MilliQ water rinses in between. These were as follows:

- ‘Oxidising solution’ - 1:1 solution of 30% hydrogen peroxide and 1 M NaOH [FeMn oxide coatings]
- ‘Perchloric wash’ - 1:1 solution of 30% hydrogen peroxide and 1% $HClO_4$ [organics]
- ‘Reducing solution’ – mixture of 20 mL ‘stock’ solution (30 g citric acid powder, 250 g MilliQ water, 250 µL ammonium hydroxide), 20 mL ammonium hydroxide, and 1.5 mL 98% hydrazine [trace metals associated with iron and manganese oxides]

For the ‘pre-clean’ stage, samples were ultrasonicated with oxidising solution for 20 minutes, perchloric wash for 1 minute, oxidising solution for 20 minutes, methanol wash for 20 minutes and perchloric acid wash for 1 minute. After each ultrasonication the cleaning solution was pipetted off, and the samples were rinsed three times in MilliQ water. Radiocarbon subsamples, weighing between 12 and 20mg, were removed following this stage.

The full cleaning stage began with 20 minutes ultrasonication in methanol and 1 minute in 0.2% HNO_3. Samples were then ultrasonicated for 20 minutes in oxidising solution, reducing solution, and oxidising solution again, respectively, in a water bath heated to approximately 60°C. This was followed by a 1 minute ultrasonication in 0.2% HNO_3 and 20 minutes in an EDTA solution (3.7 g EDTA powder and 106.3 g 1M NaOH). Again, samples were rinsed with MilliQ water in between each step. Samples were then transferred into acid-cleaned 30mL teflon vials before a final ultrasonication in 0.2% HNO_3 and water rinse. They were then air-dried and weighed.

2.5 Dissolution and preparation for combined U-Th-Nd extraction

Cleaned coral fragments (~ 0.04 to 1.9 g) were dissolved in the BIG clean room laboratory at the University of Bristol in ~ 2 mL 7.5M HNO_3. Once dissolution was complete,

~ 0.08 g of ^{236}U-^{229}Th mixed spike was added to samples, blanks and standards. This spike has been calibrated to a 4.1‰ (2σ) uncertainty and is described further by Burke and Robinson (Burke and Robinson, 2012).

An iron co-precipitation procedure was utilised to separate trace metals from the carbonate matrix. Samples were taken up in 2M HCl and transferred to acid-cleaned 50mL centrifuge tubes, where 50 µL of $FeCl_2$ solution (97.4 mg Fe/ml) was added. Concentrated ammonium hydroxide was added dropwise until rust precipitate formed and the solution colour changed from yellow to clear. Samples were centrifuged at 4000 rpm for 7-8 minutes and the clear liquid was pipetted off. This was repeated twice more with a slightly alkaline Milli-Q rinse in order to avoid redissolution of Fe-coprecipitated trace metals. The remaining precipitate was transferred to the rinsed original teflon beaker using a small amount of 5% HNO_3, dissolved with 10 drops of concentrated HNO_3 and dried on a hotplate at 180°C. The sample was concentrated in the beaker by the repeated dissolving and drying down with smaller amounts of concentrated HNO_3.

2.6 Separation of U, Th and Nd

Coral U and Th fractions were separated and purified using anion exchange chromatography. Samples were dissolved in 2 mL optima-grade 7.5M HNO_3. Two types of resin were added to acid-cleaned Environmental Express 5.5 mL columns: 0.5 mL Eichrom pre-filter resin followed by 2 mL Biorad analytical grade anion exchange resin 1-X8 (100-200 mesh). Columns were cleaned using analytical-grade 12M HCl, optima-grade 12M HCl and optima-grade 7.5M HNO_3 with alternating MilliQ water rinses. Columns were conditioned with 10 mL 7.5M HNO_3 before sample loading. The matrix, which contains the rare earth elements (REEs), was eluted with 2 x 4 mL 7.5M HNO_3, the Th fraction with 0.5 + 2 + 4 mL 12M HCl,

and the U fraction with 2 x 2mL and 2x 4 mL MilliQ water. All were collected in acid-cleaned teflon vials. One drop (~ 30 μL) of pure ^{236}U spike was added to the Th fraction, and all cuts were dried down, before being refluxed in 200 μL of a 1:1 mix of concentrated HNO_3 and H_2O_2 for 4 hours.

In preparation for isotopic analysis, the U and Th cuts were re-dissolved in 1 mL 5% HNO_3 and 0.75 mL 5% HNO_3 + HF respectively.

2.7 Isotope dilution U-series dating

Uranium and Th isotopes were measured on a Neptune MC-ICP-MS in the BIG laboratories under the supervision of Dr Tianyu Chen and Mr Tao Li. Bracketing standards were used: for U, the international standard U112a, and for Th the in-house standard 'SGS'. A 45ppb U112a standard solution was used to tune the Neptune prior to U measurements, such that sensitivity for ^{238}U was ~ 250 V/ppm with a variation of < 2%, and between 5 and 95% peak height measured 0.1 amu or less. As Th runs always directly followed U runs, only minor tuning was performed using an in-house 'SGS' standard solution. To correct for mass bias, U112a and SGS were used to bracket U and Th samples respectively. Using these bracketing standards, the activity ratios [$^{238}U/^{234}U$], [$^{232}Th/^{230}Th$], [$^{232}Th/^{229}Th$], and [$^{230}Th/^{229}Th$] were corrected for each sample. During U runs, the isotopes ^{238}U, ^{236}U and ^{235}U were analysed in Faraday collectors, and ^{234}U on the secondary electron multiplier (SEM), in measurements of 100 cycles. During Th runs, ^{232}Th was measured in a Faraday collector while the low concentration ^{229}Th and ^{230}Th isotopes were analysed on the SEM by peak jumping in measurements of 50 cycles. The isotope ^{236}U, added as a spike to the Th cut, was measured concurrently in a Faraday collector. It was used to normalise the $^{230}Th/^{229}Th$ ratio for signal instability, by measuring $^{230}Th/^{236}U$ and $^{229}Th/^{236}U$ (Burke and Robinson, 2012; Chen et al.,

2015). The wash solution (i.e. blank) was analysed before every sample run in 10 cycles and subtracted from all absolute values before calculating isotope ratios. Machine accuracy was monitored by measuring Hu84.5 (U) and ThB (Th) standards before each session and every 3-4 samples. A Hu84.5 standard was processed with each batch of column chemistry and yielded a long-term external reproducibility for [^{230}Th/^{238}U] of 0.997 ± 0.003, and for [^{234}Th/^{238}U] of 1.0007 ± 0.0008, within error of secular equilibrium (n=50, 2 S.D.).

Errors including machine uncertainties and procedural blanks were propagated into the isotope ratios of ^{234}U/^{238}U, ^{236}U/^{238}U and ^{229}Th/^{230}Th. A Monte Carlo technique, resolving the U-series age equation 100,000 times for each sample using random numbers generated within the error uncertainty of each variable, was used to propagate the errors of isotope ratios into the final reported uncertainties.

The isotope ^{232}Th was measured in addition to ^{230}Th in order to correct for non-radiogenic sources. Assuming any initial Th incorporated on calcification had a ^{230}Th/^{232}Th ratio equivalent to local modern-day seawater, the measured ^{232}Th can be used to estimate initial ^{230}Th. An initial atomic ^{232}Th/^{230}Th ratio of 12,500 ± 12,500 (2σ) was assumed, corresponding to modern subtropical Atlantic intermediate waters (Chen et al., 2015). This calculation dominates the final error for ages, with measured ^{232}Th correlating with the sample age error due to the greater uncertainty of initial ^{230}Th activity. Measured ^{232}Th ranged from 50 to 3806 ppt, and samples with concentrations greater than 3000 ppt were excluded from further geochemical analyses.

The value $\delta^{234}U_i$ is the deviation (‰) from secular equilibrium of the ^{234}U/^{238}U activity ratio and is used to test for closed-system behaviour of the corals. The $\delta^{234}U_i$ of the SWIO corals ranged from 145.2 to 157.5 ‰. Two of the 53 samples analysed exhibited open-system behaviour with $\delta^{234}U_i$ outside of the modern-day ocean value (147 ± 7 ‰; Reimer et al., 2009).

Table 2.4: Isotope dilution U-series dating of SWIO CWCs. The value $\delta^{234}U_m$ is the present-day deviation (‰) from secular equilibrium of the $^{234}U/^{238}U$ activity ratio in the sample. $\delta^{234}U_i$ is the deviation at the time of carbonate formation, used to test for closed-system behaviour of the corals.

Sample number (JC066_)	Age after ini. ^{230}Th corr. / y	2 σ	Age before ini. ^{230}Th corr. / y	2 σ	$\delta^{234}U_m$	2 σ	$\delta^{234}U_i$	2 σ	^{238}U / ppm	2 σ	^{232}Th / ppt	2 σ	[$^{230}Th/^{238}U$] analytical	2 σ
3718	53	7	60	2	146.9	1.0	146.9	1.0	3.36	0.01	50	0.36	0.0006	1.94E-05
2810	99	17	116	2	146.9	1.0	146.9	1.0	3.42	0.01	124	0.57	0.0012	1.57E-05
3697	105	19	124	2	147.4	1.0	147.4	1.0	3.57	0.01	143	0.72	0.0013	1.87E-05
3245	121	19	140	2	146.9	1.1	146.9	1.1	4.18	0.01	169	0.72	0.0015	1.80E-05
3741	171	26	198	2	146.2	1.0	146.3	1.0	3.21	0.01	184	0.79	0.0021	2.25E-05
3643	296	43	338	4	146.3	1.1	146.4	1.1	3.63	0.01	335	1.47	0.0035	4.36E-05
2620	396	26	421	4	146.9	1.1	147.0	1.1	3.45	0.01	190	0.84	0.0044	3.77E-05
2795	486	128	614	4	146.4	1.0	146.6	1.0	3.84	0.01	1066	4.34	0.0064	4.37E-05
3705	562	81	644	4	146.3	1.0	146.5	1.0	3.14	0.01	554	2.24	0.0067	4.31E-05
3712	926	11	934	6	146.4	1.0	146.8	1.0	3.15	0.01	58	0.33	0.0098	6.64E-05
0117	1782	48	1829	10	146.5	1.1	147.2	1.1	4.64	0.01	473	1.96	0.0191	9.65E-05
3696	1994	47	2040	11	146.0	1.1	146.8	1.1	3.35	0.01	332	1.44	0.0212	1.12E-04
1116	3790	352	4141	21	146.4	1.0	148.0	1.0	4.06	0.01	3088	12.54	0.0427	2.08E-04
3507	9874	204	10064	77	143.0	2.4	147.0	2.5	3.69	0.02	1517	6.29	0.1008	7.03E-04
1156	10568	290	10853	56	145.2	1.0	149.6	1.1	3.76	0.01	2324	9.60	0.1086	5.24E-04
0157	11262	242	11496	57	143.8	1.1	148.5	1.1	3.73	0.01	1895	7.74	0.1145	5.30E-04
0127	11450	79	11468	77	145.1	1.1	149.9	1.1	3.65	0.01	55	0.32	0.1144	7.29E-04
0486x	11579	431	12003	78	147.4	1.2	152.3	1.2	3.51	0.01	1294	5.23	0.1197	7.25E-04
0124	11941	320	12253	76	146.7	1.1	151.7	1.1	3.97	0.01	1071	4.33	0.1220	7.07E-04

0124dup	12097	136	12216	65	145.5	1.0	150.6	1.0	4.49	0.01	1169	4.79	0.1215	6.02E-04
0121	12294	163	12436	82	145.1	1.1	150.2	1.2	4.37	0.01	539	2.22	0.1235	7.58E-04
0135	12300	275	12564	74	143.3	1.2	148.3	1.2	3.71	0.01	851	3.48	0.1245	6.76E-04
1056	12307	985	13285	90	143.0	1.2	148.1	1.3	4.50	0.01	3806	15.33	0.1312	8.26E-04
1002	12373	213	12568	86	144.7	1.1	149.8	1.2	4.21	0.01	715	2.94	0.1247	7.92E-04
1155	12435	134	12554	62	146.5	1.1	151.8	1.1	3.74	0.01	963	3.92	0.1248	5.69E-04
0125	12490	168	12647	63	145.6	1.1	150.8	1.1	3.85	0.01	1306	5.39	0.1256	5.80E-04
3508	12492	117	12572	87	144.0	1.2	149.1	1.2	3.46	0.01	238	1.03	0.1247	8.02E-04
0122	12537	185	12699	89	145.6	1.1	150.9	1.2	4.30	0.01	605	2.51	0.1261	8.22E-04
3509	12574	297	12861	76	145.6	1.1	150.8	1.2	3.83	0.01	959	3.95	0.1276	7.01E-04
0123	12584	237	12805	87	146.5	1.1	151.8	1.2	3.48	0.01	668	2.76	0.1272	8.03E-04
0118	12696	313	13003	63	144.9	1.0	150.2	1.1	4.96	0.01	3316	13.51	0.1288	5.82E-04
0126b	12702	218	12907	73	142.9	1.6	148.1	1.7	4.13	0.01	1836	7.46	0.1277	6.56E-04
1045	12786	125	12894	64	151.9	1.1	157.5	1.1	3.88	0.01	914	3.79	0.1286	5.90E-04
1065	12824	93	12880	75	144.0	1.2	149.4	1.2	4.50	0.01	219	1.00	0.1276	6.83E-04
1157	12832	250	13073	66	143.9	1.1	149.2	1.1	4.86	0.01	2547	10.27	0.1294	6.02E-04
1158	12924	183	13095	65	146.0	1.0	151.5	1.1	4.69	0.01	1742	7.06	0.1298	5.92E-04
1046	12933	202	13125	65	144.7	1.1	150.1	1.1	4.26	0.01	1771	7.18	0.1299	5.96E-04
1066b	12939	185	13101	90	148.8	1.1	154.4	1.1	3.68	0.01	523	2.20	0.1302	8.26E-04
0128	12967	68	12991	63	147.1	1.0	152.6	1.0	4.22	0.01	220	0.94	0.1290	5.83E-04
0107	12967	218	13175	66	147.7	1.1	153.2	1.2	4.03	0.01	1824	7.45	0.1307	6.07E-04
1065dup	12971	81	13018	67	143.7	1.0	149.1	1.1	5.18	0.01	519	2.15	0.1288	6.12E-04
1160	13195	82	13244	65	143.5	1.1	149.0	1.1	4.94	0.01	525	2.20	0.1309	5.97E-04
1144	13697	88	13755	67	144.6	1.0	150.3	1.1	3.54	0.01	441	1.83	0.1358	6.14E-04
1070	14053	131	14163	70	147.9	1.0	153.9	1.0	4.30	0.01	1034	4.23	0.1400	6.43E-04
2590	15038	271	15290	99	141.8	1.1	148.0	1.1	3.70	0.01	808	3.37	0.1496	8.97E-04

3506a	15562	506	16057	99	143.5	1.1	150.0	1.2	3.58	0.01	1530	6.27	0.1568	8.92E-04
3506b	15686	584	16258	113	142.8	1.1	149.3	1.1	4.09	0.01	2033	8.29	0.1585	1.02E-03
3510	16066	368	16418	110	142.9	1.1	149.5	1.1	3.90	0.01	1192	4.87	0.1600	9.77E-04
1040	16310	253	16536	117	143.9	1.1	150.7	1.2	3.92	0.01	768	3.10	0.1612	1.05E-03
1143a	16447	295	16721	104	140.5	1.1	147.2	1.2	3.97	0.01	945	3.86	0.1624	9.25E-04
1143b	16492	431	16911	102	143.6	1.1	150.4	1.2	4.09	0.01	1487	6.09	0.1646	9.03E-04
2825	16670	343	17002	86	138.5	1.1	145.2	1.2	4.58	0.01	3281	13.27	0.1646	7.53E-04

2.8 Separation of Nd

As Nd is collected in the wash fraction of the U-Th chemistry described above (see also Struve et al., 2016), this fraction was utilised for most Nd isotope analyses in this study, performed in the MAGIC laboratories at Imperial College London. If only Nd separation was performed on a coral subsample, e.g. for duplicate samples, Fe co-precipitation was carried out following dissolution, but no spike was added nor anion exchange chromatography performed. Once dried, all samples and Nd cuts were oxidised with aqua regia overnight at 200°C, then with a 1:1 ratio of concentrated HNO_3 and 30% H_2O_2 for ~ 4 hours at 110°C, to remove residual organics. A full procedural blank, BCR-2 rock standard and/or in-house coral standard was processed with each batch of chemistry.

To separate and purify REEs from the matrix, samples were loaded in 1 mL 1M HCl onto 1.4 mL of Biorad AG50 W-X8 resin (200–400 mesh) in Biorad Poly-Prep columns. Prior to loading, the resin was cleaned with 10 mL 6M HCl and conditioned with 2 x 0.5 mL 1M HCl. Samples were rinsed in with 2 x 0.5 mL 1M HCl. Iron was eluted with 0.5 + 2.5 mL 3M HCl, followed by matrix elution with a further 4 mL 3M HCl and 0.5 mL 6M HCl. Rare earth elements were then collected in acid-cleaned teflon vials in 6.5 mL 6M HCl. The resin was subsequently cleaned with 2 mL MilliQ water, 10 mL 4M HNO_3, 2 mL MilliQ water, 10 mL 6M HCl and 10 mL MilliQ water, before columns were stored in weak HCl (0.3-0.5M). Rare earth element cuts were dried down and converted to nitrate form for [Nd] concentration checks by MC-ICP-MS. Concentration checks were carried out at this stage to screen for particularly low [Nd], which were set aside for a different 2nd column in preparation for potential TIMS analysis.

Neodymium was separated from the other REEs using 50-100 μm particle-size Ln-spec resin in 5 mL reservoir savillex columns, cut to ~ 800 μL resin volume. The columns were

calibrated for optimum elution of Nd between 6 and 11.5 mL of 0.189M HCl (for chemistry performed during 2017; Fig. 2.4A) and the same volume for 0.188M HCl (for chemistry performed during 2018; Fig. 2.4B).

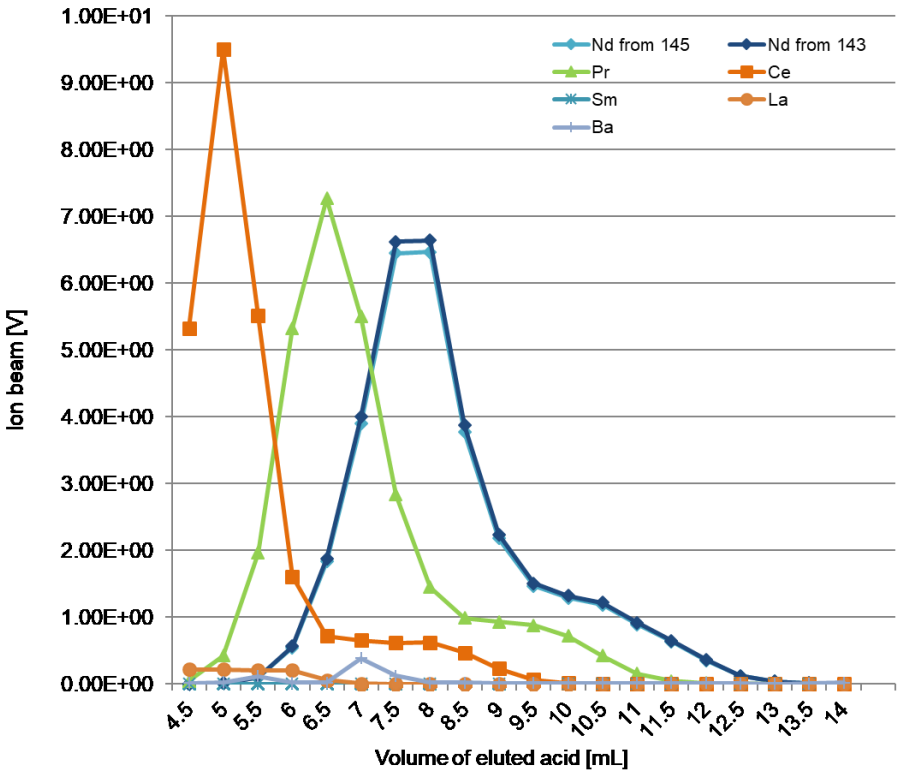

Figure 2.4a: Elution curves from 50-100 µm particle-size Ln-spec resin column calibration in December 2016 using 0.189M HCl.

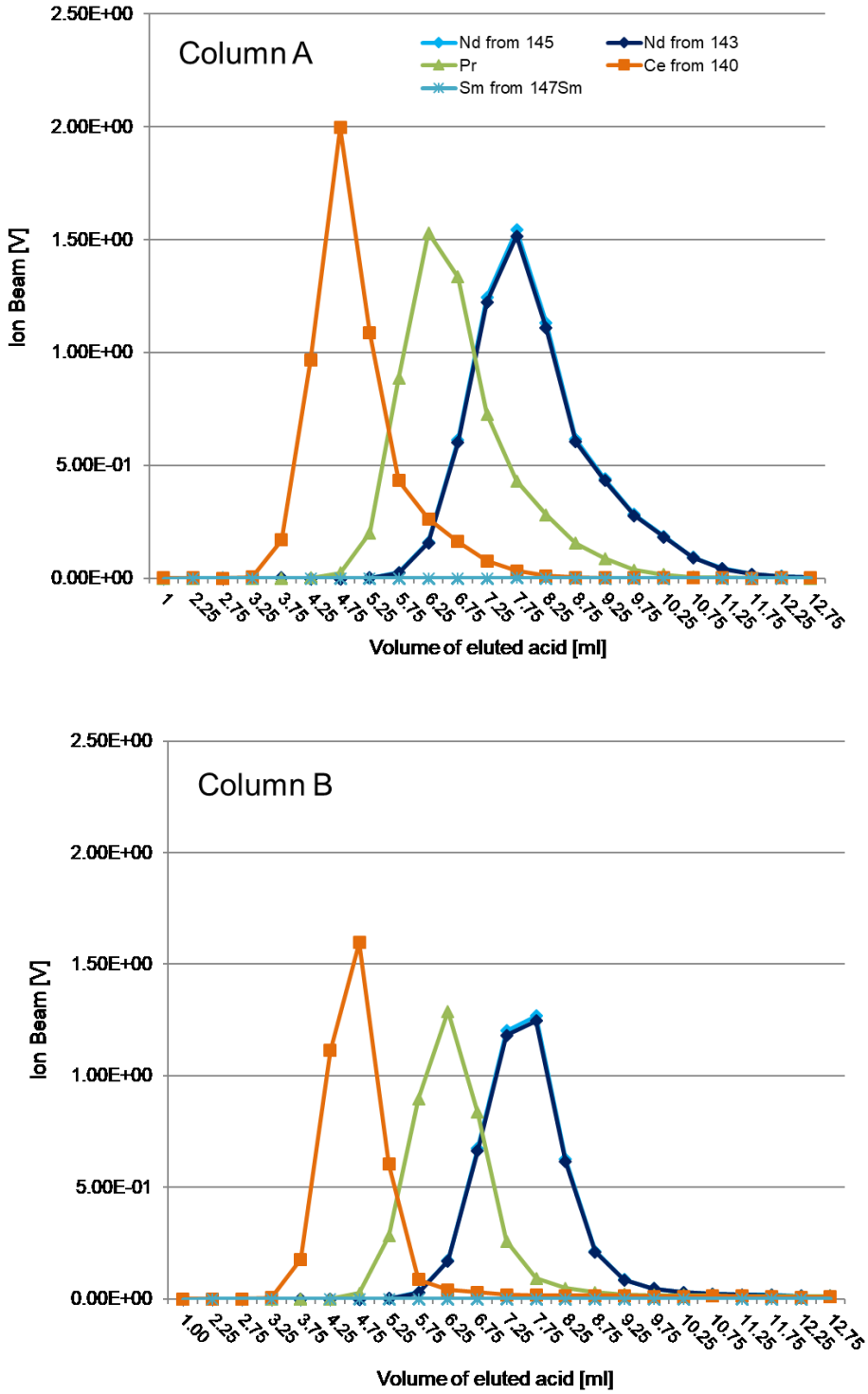

Figure 2.4b: Elution curves from 50-100 µm particle-size Ln-spec resin column calibration in December 2017 using 0.188M HCl.

Columns were stored and the resin was reused for up to 10 sample batches. Before sample loading the resin was back-flushed with MilliQ water using a syringe and rinsed with one reservoir of distilled 6M HCl and 2x 1 mL MilliQ water. Samples were loaded in 200 µL of the 0.188M HCl and the same acid was used to elute the light REEs (4.5 mL) and collect the Nd (5.5 mL). The resin was then cleaned again with a reservoir each of distilled 6M HCl and MilliQ water and stored in MilliQ water. Neodymium cuts were dried down and converted to nitrate form in preparation for measurement.

2.9 Neodymium isotope analysis

Fifty-five samples, including two full duplicates, were screened for Nd concentrations following cation exchange chemistry using a Nu Plasma HR MC-ICP-MS (NP1). The total Nd beam size for 5% aliquots diluted 20 times was measured in cycles of 20 and compared to the beam size for 20 ppb JNdi standards, with a wash time of 6 minutes between samples. Coral samples with [Nd] > ~ 10 ppb, 35 in total, were selected for Ln chemistry and Nd isotope analysis (Table 2.5).

Table 2.5: Sample Nd concentrations and whole coral Nd concentrations. The latter is a minimum estimate as no spike was added nor compensations made for column yield.

Sample ID	SS	Uth, Nd sample ID	Stn	Depth	Age / y	2σ	Sample [Nd] / ng/mL	Sample mass / g	Min coral [Nd] / ppb
107		C5	4	1097.2	12967	218	36.5	0.20889	174.6
117		C15	4	1207.2	1782	48	14.1	0.2931	48.0
118		C10	4	1207.2	12696	313	65.2	0.2442	266.7
121		A2	4	1207.2	12294	163	12.4	0.26924	46.2
122		A8	4	1207.2	12537	185	17.6	0.37729	46.6
123		A7	4	1207.2	12584	237	14.2	0.34682	41.1
124		D12*	4	1207.2	12097	136	14.0	0.1800	78.0
124		A4*	4	1207.2	11941	320	24.5	0.27191	90.0
125		C1	4	1207.2	12490	168	23.9	0.2971	80.4
126	b	C6	4	1207.2	12702	218	1.7	0.25694	6.8
127		A10	4	1207.2	11450	79	2.9	0.39008	7.4

128		D4	4	1207.2	12967	68	8.9	0.3777	23.7
135		A1	4	1207.2	12300	275	9.3	0.18776	49.4
157		C4	4	1395	11262	242	44.2	0.19514	226.7
486	x	A3	4	1097.2	11579	431	34.4	0.2828	121.5
486	y	D7	4	1097.2	13908†	656	17.5	0.0358	487.7
1002		B6	4	952	12373	213	20.0	0.26879	74.3
1040		B7	4	922.5	16310	253	17.6	0.42599	41.3
1045		D9	4	922.5	12786	125	25.0	0.1558	160.5
1046		D10	4	922.5	12933	202	36.8	0.3600	102.2
1056		A6	4	1207.2	12307	985	123.6	0.44952	275.0
1059		D2	4	1207.2	12744†	607	2.1	0.2977	7.1
1065		A5*	4	1207.2	12824	93	3.3	0.21295	15.4
1065		D11*	4	1207.2	12971	81	6.9	0.2760	24.9
1066	b	B10	4	1207.2	12939	185	12.5	0.21956	56.8
1070		D6	4	1207.2	14053	131	32.3	0.2158	149.8
1116		D16	4	732	4058	410	36.1	0.2392	150.8
1143	a	A9	4	1097.2	16447	295	34.3	0.34897	98.4
1143	b	B1	4	1097.2	16492	431	27.2	0.19292	141.2
1144		C2	4	1097.2	13697	88	20.4	0.3452	59.0
1145		D5	4	1097.2	10669†	1010	1.6	0.1950	8.3
1155		C9	4	1207.2	12435	134	24.8	0.26148	94.9
1156		C8	4	1207.2	10568	290	66.3	0.15361	431.4
1157		C7	4	1207.2	12832	250	62.3	0.3809	163.6
1158		D8	4	1207.2	12924	183	30.6	0.2036	150.3
1160		D1	4	1207.2	13195	82	6.6	0.2158	30.7
2590		B2	6	1014	15038	271	9.2	0.2093	44.1
2620		C11	8	922	396	26	5.6	0.26016	21.7
2795		C14	4	702	486	128	10.9	0.2424	45.0
2810		D15	4	709.5	99	17	1.5	0.3024	4.9
2825		D3	5	897	16670	343	40.5	0.3484	116.2
3245		C13	5	171.9	121	19	3.7	0.37407	9.8
3506	a	B9	6	1014	15562	506	14.8	0.28588	51.6
3506	b	B8	6	1014	15686	584	20.0	0.2171	92.1
3507		C3	6	1014	9874	204	0.7	0.16172	4.1
3508		B4	6	1014	12492	117	5.3	0.31131	16.9
3509		B5	6	1014	12574	297	11.2	0.21503	52.1
3510		B3	6	1014	16066	368	15.5	0.31209	49.8
3643		C16	8	726	296	43	2.2	0.2426	9.1
3696		C12	8	823	1994	47	3.6	0.1780	20.4
3697		D17	8	823	105	19	4.5	0.2656	16.9
3705		C17	8	870	562	81	17.5	0.40032	43.7
3712		D18	8	870	926	11	3.7	0.3825	9.6
3718		D14	8	1035	53	7	1.1	0.2608	4.0
3741		D13	8	763	171	26	4.3	0.3096	14.0

*full procedural replicate †dated only with laser-ablation procedure

Coral Nd isotope compositions were measured during seven sessions on the Nu Plasma II MC-ICP-MS (NP2) in the MAGIC laboratories at Imperial College between May 2017 and December 2018. The JNd_i standard (Tanaka et al., 2000) was used to tune the machine for

sensitivity and stability and check peak shape and alignment. Normal sensitivity across all measurement sessions was 500 – 800 V/ppm Nd using a Glass Expansion MicroMist nebuliser (typical uptake rate 0.1-0.14 mL/min) connected to a Nu instruments DSN-100 desolvation nebuliser system for sample introduction. All Nd masses as well as ^{147}Sm ion beams were collected in Faraday cups. Measurements consisted of one block of 50 cycles with a magnet delay time of 3 seconds, measurement of electronic background, peak centring and a wash time of 6 minutes between samples.

Isotope ratios were calculated and corrected for instrumental mass bias online. Firstly, the mass fractionation factor β and a known ^{146}Nd/^{144}Nd ratio of 0.7219 was used to correct all Nd isotope ratios for mass bias (^{142}Nd/^{144}Nd, ^{143}Nd/^{144}Nd, ^{145}Nd/^{144}Nd, ^{148}Nd/^{144}Nd, ^{150}Nd/^{144}Nd). Secondly, isobaric interference from samarium was constrained by measuring ^{147}Sm and calculating the abundance of ^{144}Sm. For all samples the calculated ^{144}Sm interference on the ^{144}Nd signal was significantly below the 0.1% threshold for accurate correction. ^{138}Ba and ^{140}Ce were monitored to test for successful separation during chemistry.

JNdi standard concentrations were adjusted to match coral Nd concentrations and varied between 20, 15 and 10 ppb and were measured before, between and after samples. Sample ^{143}Nd/^{144}Nd ratios for each measurement day were corrected to the recommended JNdi literature ratio of 0.512115 ± 7 (Tanaka et al., 2000). In the rare case that sample measurements occurred during periods of drifting ^{143}Nd/^{144}Nd standard ratios, sample ratios were corrected using the bracketing JNd_i standards.

External reproducibility was based on the two sigma standard deviation of the average ^{143}Nd/^{144}Nd JNdi of each measurement session. Typical values during sample measurement sessions were 20 - 30 ppm and reproducibility was always better than 40 ppm (Fig. 2.5).

Internal errors for standards and samples typically were 3-5 x10^{-6} (1 sigma standard error) for 20 ppb runs, and 5-6 x10^{-6} for 10 and 15 ppb runs.

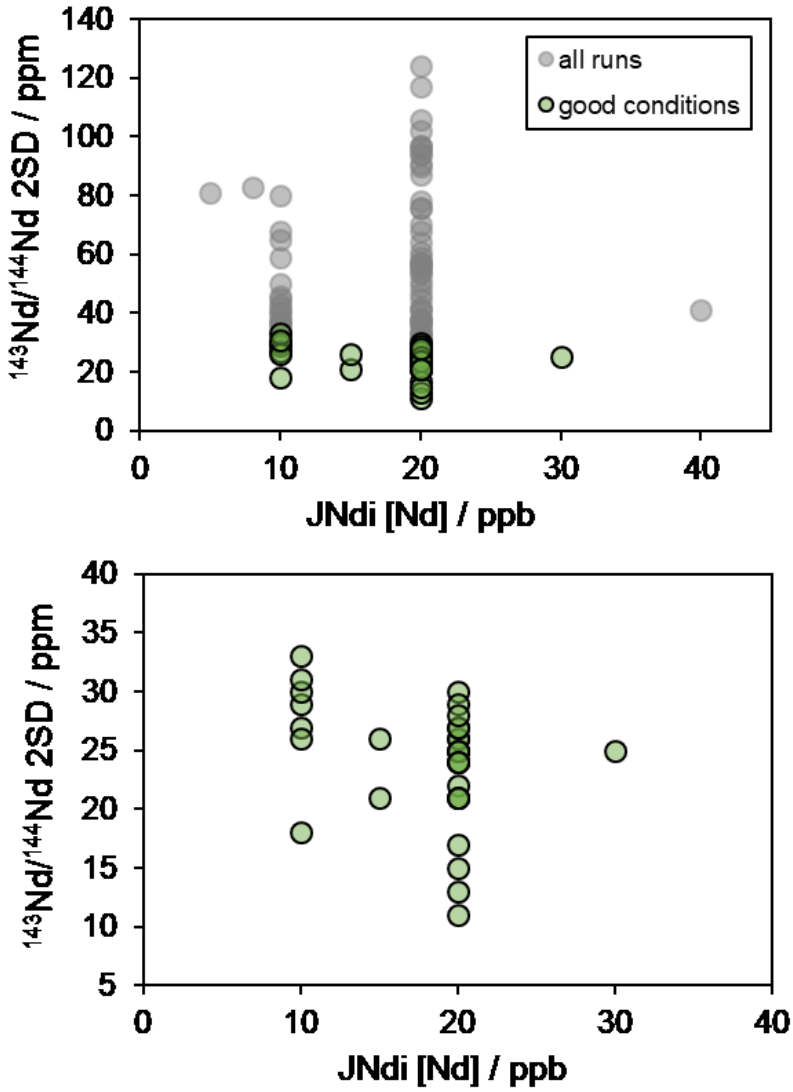

Figure 2.5: Average 2SD for ^{143}Nd/^{144}Nd for various concentrations of JNdi standard during each batch during measurement sessions between January 2017 and December 2018. 'Sub-optimal' batches, in which conditions were not stable enough to measure coral samples, are shown with grey dots. Batches in which coral samples were run, or in which conditions would have been good enough to run samples ('good conditions'), are shown with green dots.

During each session, multiple measurements of the USGS BCR-2 standard were made to assess the long-term external reproducibility of column-processed samples. BCR-2 $^{143}Nd/^{144}Nd$ ratios of 0.512639 ± 21 (2 s.d, n=25) were in excellent agreement with the published value (0.512638 ± 15; Weis et al., 2006; Fig. 2.6A). Additional accuracy and precision tests included measurement of the in-house coral standard, which yielded $^{143}Nd/^{144}Nd$ ratios of 0.512338 ± 15 (2 s.d, n=5), identical to the published TIMS-derived value (0.512338 ± 8; Crocket et al., 2014; Fig. 2.6B).

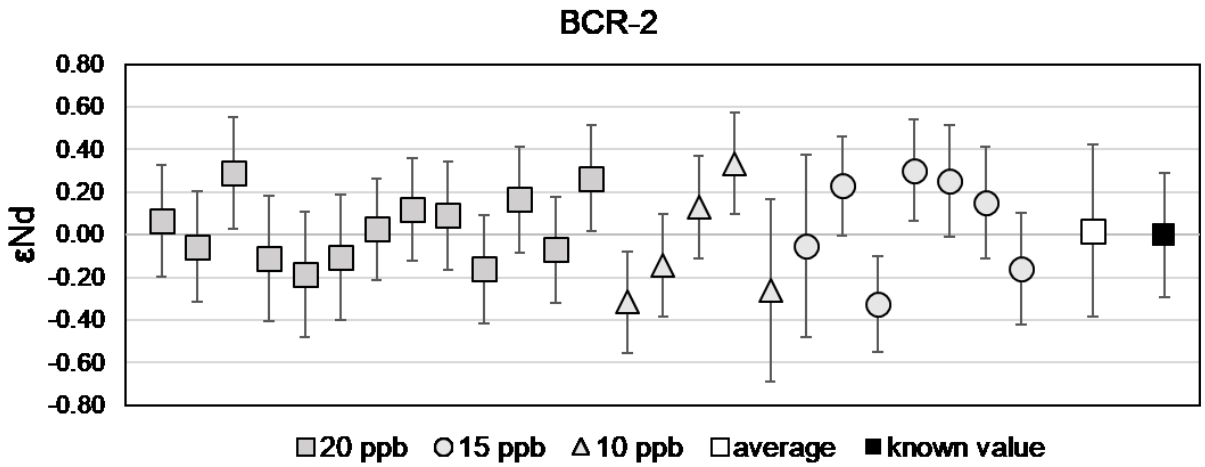

Figure 2.6a: Neodymium isotope measurements of different concentrations of BCR-2 rock standard solutions made between May 2017 and December 2018 during sample run sessions. Error bars for measurements (grey symbols) represent the larger of 2SD or 2SE. The error bars for the average (white square) and for the known value (black square) represent 2SD.

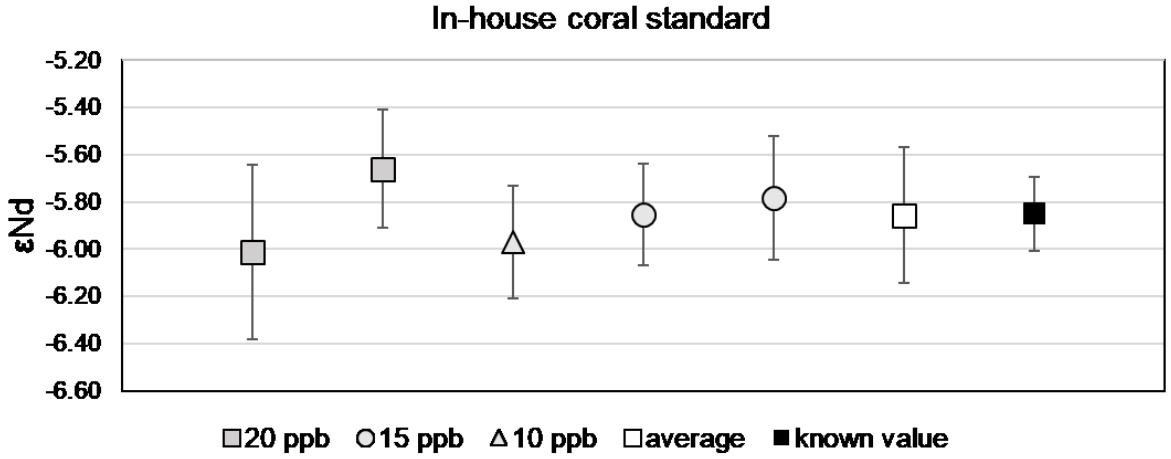

Figure 2.6b: Nd isotope measurements of the in-house coral standard made between August 2017 and December 2018 during sample run sessions. Error bars for all values represent 2SD.

For samples and standards, external reproducibility of $^{145}Nd/^{144}Nd$ ratios was usually similar to that of $^{143}Nd/^{144}Nd$ ratios (Fig. 2.7). $^{148}Nd/^{144}Nd$ and $^{150}Nd/^{144}Nd$ ratios were less precise, as expected, due to their lower isotope abundances, greater mass difference, and normalisation to $^{146}Nd/^{144}Nd$. External errors of $^{148}Nd/^{144}Nd$ were on average double, and $^{150}Nd/^{144}Nd$ triple those of $^{143}Nd/^{144}Nd$ and $^{145}Nd/^{144}Nd$. Due to the incomplete removal of Ce during ion chromatography, $^{142}Nd/^{144}Nd$ ratios for samples were not monitored. For JNdi standards the external errors for $^{142}Nd/^{144}Nd$ ratios were typically 40-50 ppm, intermediate between $^{143}Nd/^{144}Nd$ and $^{148}Nd/^{144}Nd$ uncertainties. ^{138}Ba beams for coral samples and standards were always smaller than 1V, except in the case of four BCRs where the beam size reached up to 6V. $^{143}Nd/^{144}Nd$ ratios were still accurate and precise. The beta fractionation factor, calculated using the exponential law and the known value of $^{146}Nd/^{144}Nd$, typically varied to within 0.05 during batches, similar to the variation observed while using NP1. The absolute value commonly fell between -1.6 and -1.7 during successful measurement sessions.

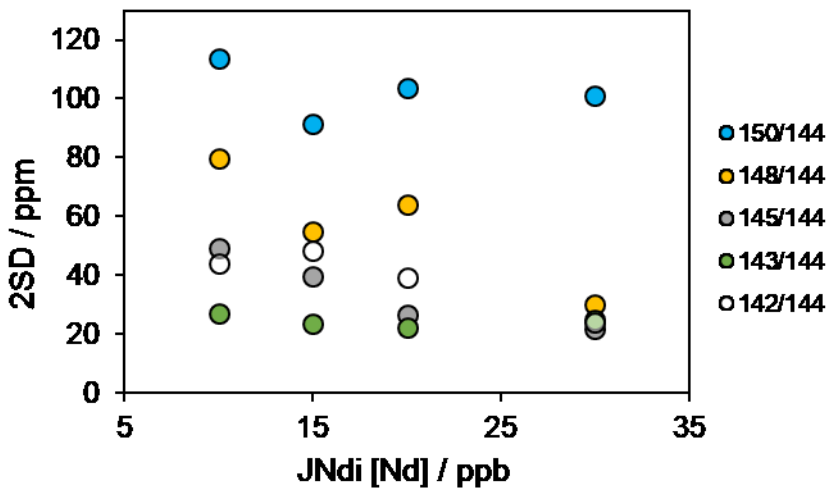

Figure 2.7: Average 2SD for the five measured Nd isotope ratios from batches with 'good conditions' (i.e. where coral samples were, or would have been, measured) using various concentrations of JNdi standard: 10ppb (n=6), 15ppb (n=2), 20ppb (n=27) and 30ppb (n=1).

Blanks for the full U-Th-Nd procedure were 4-49 pg Nd (n = 6) and for the portion of the chemistry performed at Imperial College (Nd separation only) <10 pg Nd (n = 5). One blank which underwent the Fe-separation and Nd chemistry at Imperial College contained 77 pg Nd.

2.9.1 Initial setup and testing of JIM (NP2) – observations from January 2017 to December 2018

Above described results met the expectations for precise and accurate Nd isotope compositions. However, for significant periods of the first two years of operation of JIM (installation in October 2016), measurement conditions were often suboptimal and hence unsuitable for sample analysis. Below some observations and potential solutions are reported.

From August 2017 to October 2017 (sessions 3 to 7), external reproducibilities for $^{143}Nd/^{144}Nd$ ratios were commonly > 50 ppm (2SD), with $^{148}Nd/^{144}Nd$ and $^{150}Nd/^{144}Nd$ ratio reproducibilities > 200 ppm (2SD; Fig. 2.5). During this time the fractionation factor beta increased in absolute value, reaching a high of around -1.2, and became more variable (up to 0.09 units during a batch). Strong correlations between beta and isotope ratios, especially those including ^{148}Nd and ^{150}Nd, were observed, such that even minor beta variability manifested itself in large external errors. Machine sensitivity and internal errors remained within normal boundaries.

These issues arose during a period of increased seismic disturbance caused by nearby construction work. Whilst tempting to blame poor instrument conditions on these external factors, poor reproducibility occurred both during and outside times of heightened disturbance, which was carefully monitored.

Initial ideas that days of worse reproducibility may be linked to increased nebuliser uptake (i.e. ~ 130 uL/min relative to 100 uL/min) were also unsubstantiated, even though earlier experiments in late 2016/early 2017 seemed to indicate that uptake rates of ~ 180 uL/min were too high to obtain reasonable reproducibilities for Nd isotope compositions.

Switching from a cup configuration with ^{142}Nd in the axial cup configuration to one utilising mass 141 or 140 in the same position provided a temporary solution. The external reproducibility for the $^{143}Nd/^{144}Nd$ ratio improved and it was possible to run coral samples at a Nd concentration of 10 ppb. However, beta fluctuations and poor reproducibilities for the $^{148}Nd/^{150}Nd$ and $^{150}Nd/^{144}Nd$ ratios remained a feature.

Several alterations were made to the machine after these sessions, including a replacement of the slits, a software upgrade, and installation of a switchable pre-amplifier bin. In subsequent runs (sessions 8-10, reproducibility returned to normal, with typical $^{143}Nd/^{144}Nd$

external errors of 20-30 ppm for 20 ppb standards, and absolute beta values between -1.6 and -1.7.

During late 2018 (session 9) multiple users on JIM found that poor room temperature regulation caused 45-50 minute cycles in source temperature with a magnitude of ~ 4°C (Fig. 2.8A), which was positively correlated with sensitivity (Fig. 2.8B). Cyclicity of beta values, a feature which had been identified during previous measurement sessions, was of a similar wavelength and appeared to be linked, although a positive correlation could not be confidently identified. After moving the position of the room temperature sensor, temperature regulation of the air-handling unit improved and the range in source temperatures variability dropped to ~ 3°C (Fig. 2.8B). During the same time period, the observation was made that the apparent coupling of instrumental mass bias and temperature stemmed from the interface region and could be reduced by tuning the z-position of the torch. In detail, the most reproducible results were obtained in late 2018 when taking the z-position of the torch as far out as possible before a signal drop was observed, followed by tuning of all other parameters. After doing so, the amplitude of beta variability decreased and the $^{143}Nd/^{144}Nd$ reproducibility improved (20-25 ppm 2SD for 15 ppb; Fig. 2.8C). A correlation between temperature and beam size was still observed (Fig. 2.8D).

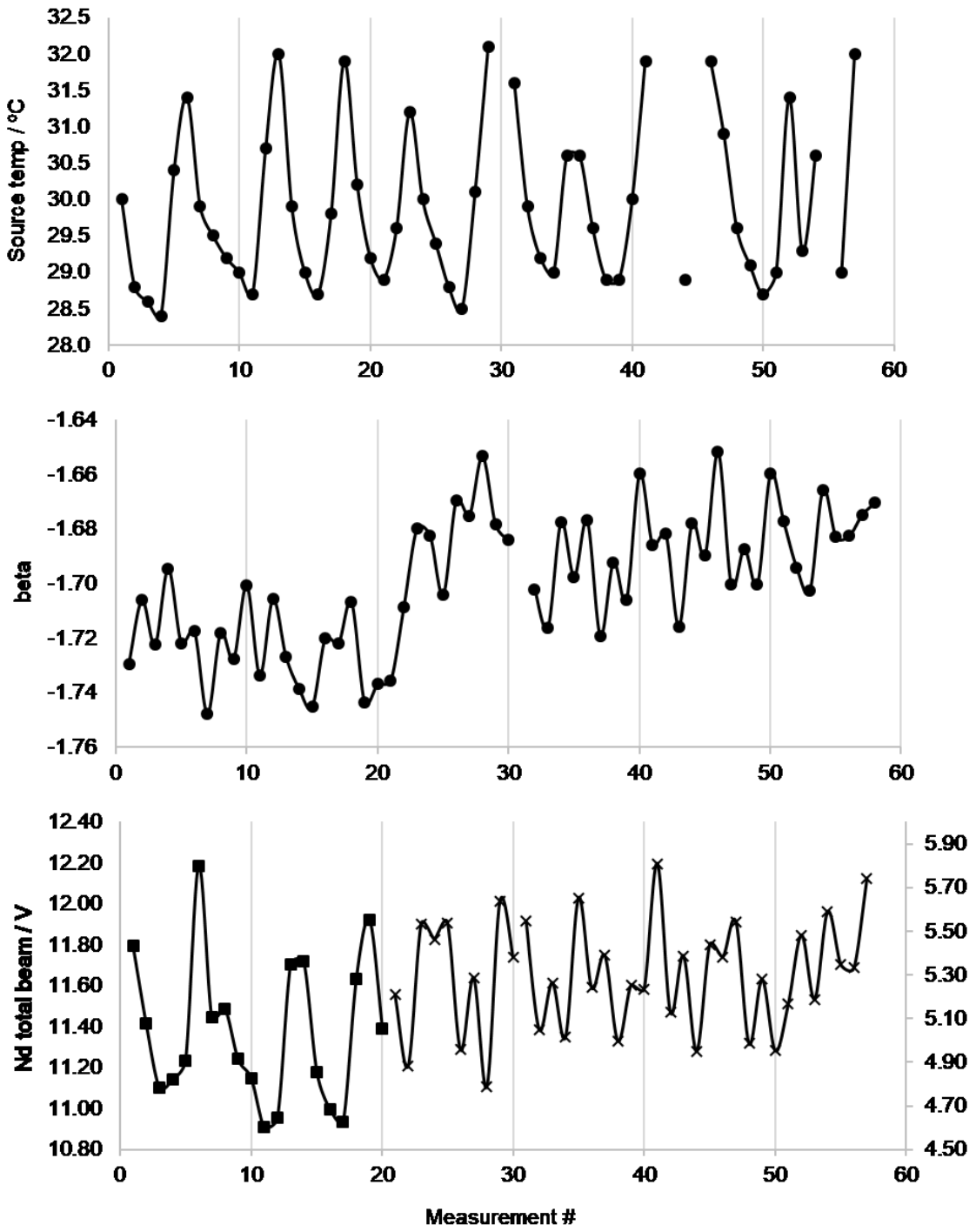

Figure 2.8a: Source temperature variations (top panel), beta variations (middle) and total Nd beam (bottom panel) for consecutive standard runs during session 9, batch c, 1/11/18 (prior to application of temperature solutions). In the bottom panel, JNdi standard run at 20 ppb [Nd] is shown by squares and at 10 ppb [Nd] by crosses.

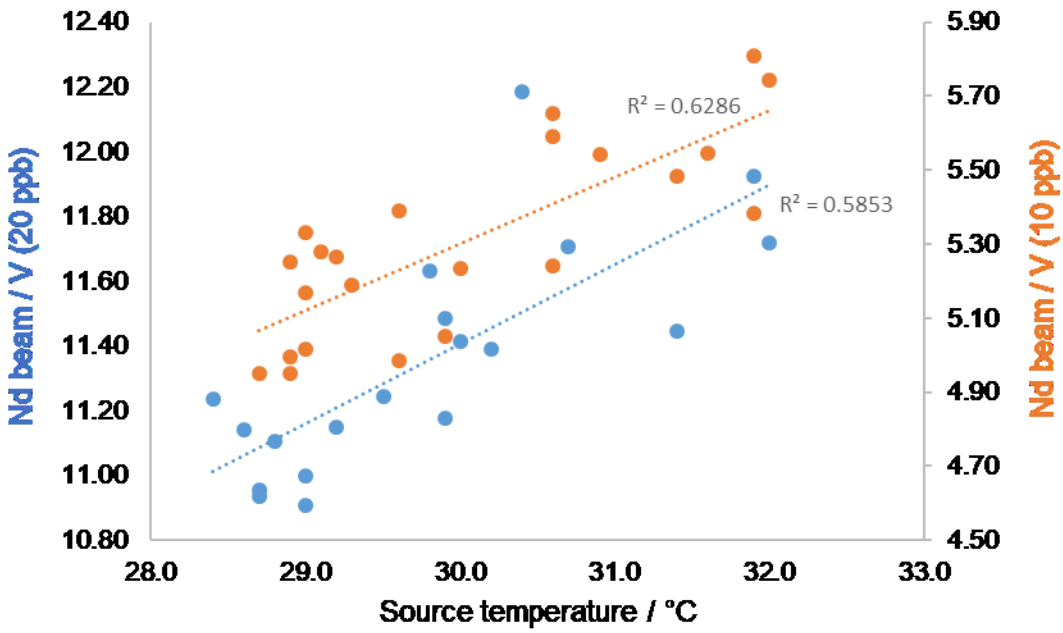

Figure 2.8b: Source temperature and total Nd beam size for 20 ppb (blue) and 10 ppb (orange) JNdi standard measurements during session 9, batch c, 1/11/18.

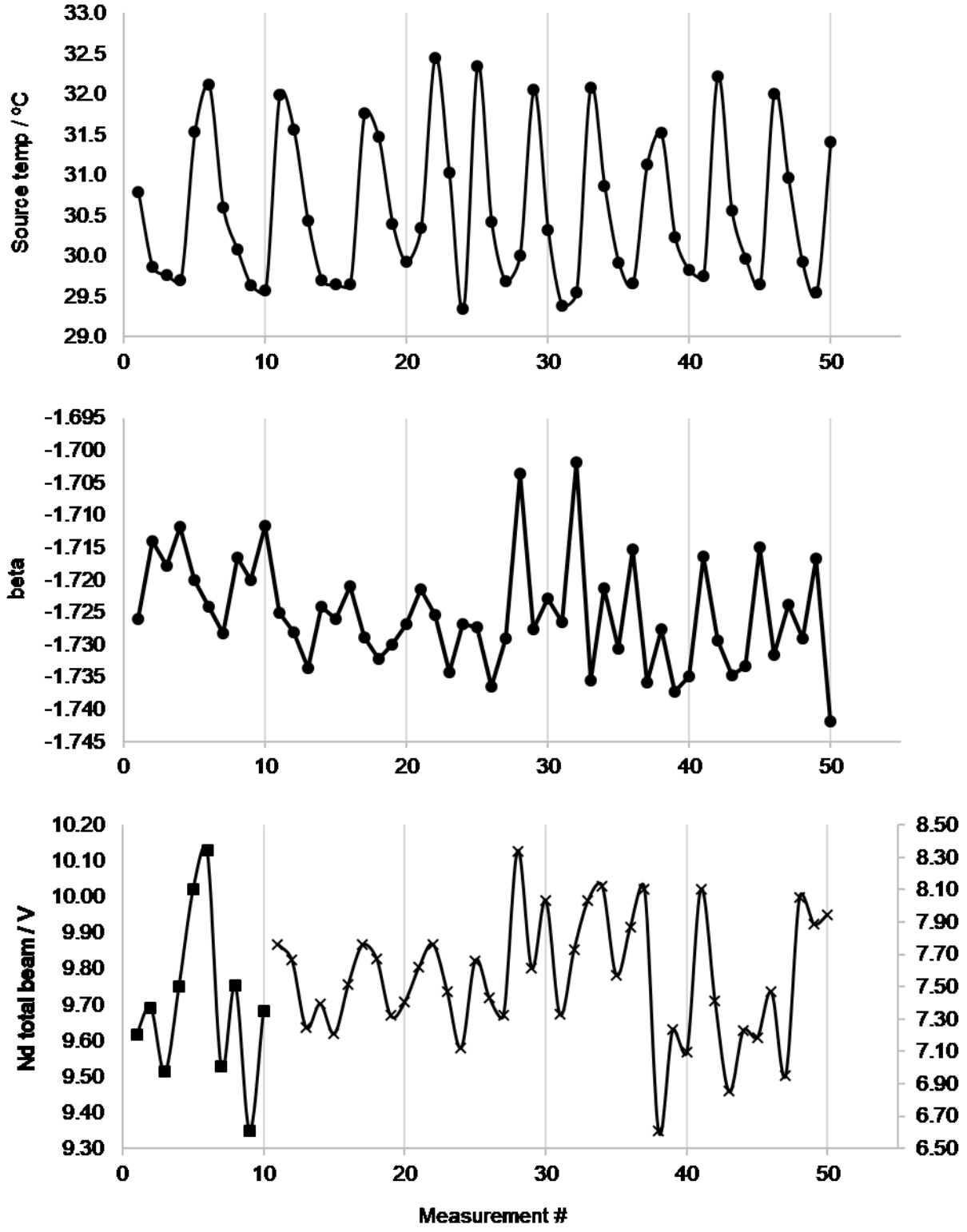

Figure 2.8c: Source temperature variations (top panel), beta variations (middle) and total Nd beam (bottom panel) for consecutive standard runs during session 10, batch a, 17/12/18. In the bottom panel, JNdi standard run at 20 ppb [Nd] is shown by squares and at 10 ppb [Nd] by crosses.

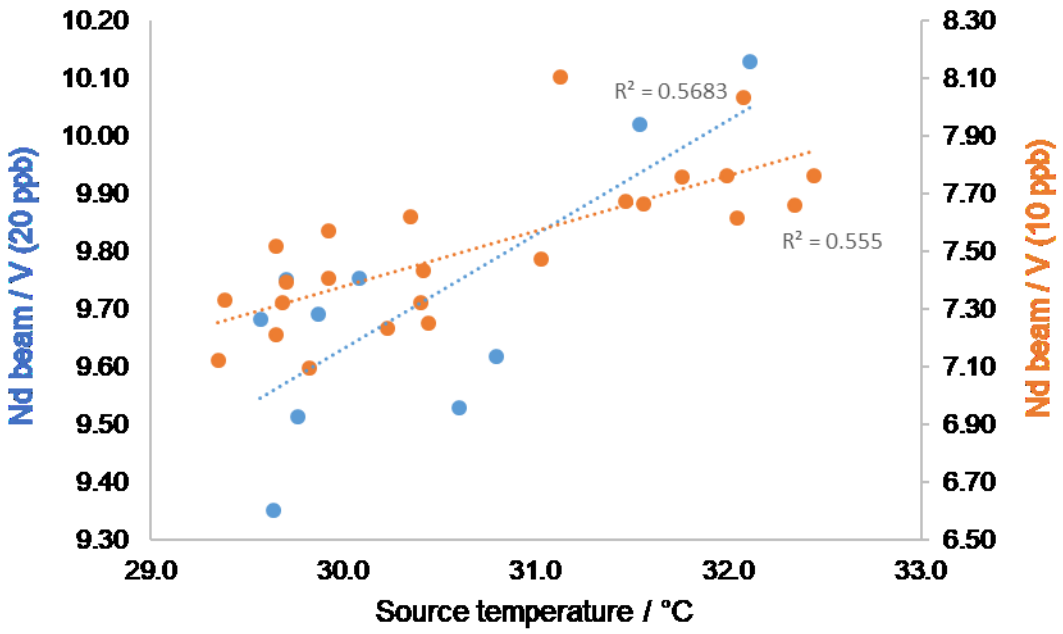

Figure 2.8d: Source temperature and total Nd beam size for 20 ppb (blue) and 10 ppb (orange) JNdi standard measurements during session 10, batch a, 17/12/18.

2.10 Radiocarbon measurement

Twenty-four samples including four full procedural duplicates were processed for radiocarbon measurements and analysed at the Bristol Radiocarbon AMS (BRAMS) facility by Dr. Timothy Knowles, following preparation and analytical methods detailed in Wacker *et al.*, (2010) and Wacker, Christl and Synal (2010). Samples were first crushed and ultrasonicated in MilliQ water, dried and transferred to acid-washed and precombusted exetainers. The exetainers were sealed and the headspace replaced with helium gas using an IonPlus CHS (Wacker et al., 2013). Orthophosphoric acid (1mL 85% *v/v*) was injected through the samples heated at 70°C until CO_2 evolution ceased. The CO_2 generated was transferred to the AGE3 graphitization system in a stream of helium. Graphite samples are pressed into cathodes using an IonPlus PSP.

Analytical approaches for radiocarbon analysis performed on the BrisMICADAS are described in detail in Synal et al. (2007) and Wacker et al. (2010a). Alongside samples, Oxalic acid II targets were used as normalisation standards in addition to an in-house graphitization blank, matrix-matched blanks, a matrix-matched standard and graphitization standards. The matrix-matched standard TIRI sample K (turbidite carbonate, mainly coccolith calcite; Scott, 2003) gave an age of 18127 ± 38 years BP, within error of the consensus value of 18155 ± 34 years BP. Blanks were measured to between 52000 and 55000 years BP. Data reduction was performed using the software package BATS, described in Wacker et al. (2010b). This calculates blank and $\delta^{13}C$ corrected $^{14}C/^{12}C$ ratios for all samples and standards, and then applies a standard normalisation factor. Total analytical uncertainty is calculated within the BATS reduction software and represents the combined uncertainty resulting from counting statistics, isotopic fractionation correction, blank subtraction uncertainty and a sample scatter factor (Wacker et al., 2010b). The average 2σ of coral radiocarbon ages was 55 years (n=24). Of the four duplicates run, two of gave ages within 1σ error, and two within 2σ; it is possible that some of this discrepancy can be accounted for by real age differences of the coral aragonite.

Statement of contribution

Ln column calibration for Nd described in this chapter was performed by Dr. David Wilson.

Chapter 3: Temporal distribution and diversity of cold-water corals in the southwest Indian Ocean over the past 25,000 years

Modified from: Pratt, N., Chen, T., Li. T., Wilson, D. J., van de Flierdt, T., Little, S.H., Taylor, M. L., Robinson, L.F., Rogers, A. D. and Santodomingo, N. (2019) Temporal distribution and diversity of cold-water corals in the southwest Indian Ocean over the past 25,000 years. *Deep Sea Research Part* 1149, 103049.

Chapter summary

Fossil cold-water corals can be used to reconstruct physical, chemical, and biological changes in the ocean because their skeleton often preserves ambient seawater signatures. Furthermore, patterns in the geographic and temporal extent of cold-water corals have changed through time in response to environmental conditions. Here we present taxonomic and dating results from a new collection of subfossil cold-water corals recovered from seamounts of the Southwest Indian Ocean Ridge. The area is a dynamic hydrographic region characterised by eastward flow of the Agulhas Return Current and the northernmost fronts of the Antarctic Circumpolar Current. In total, 122 solitary scleractinian corals and 27 samples of colonial scleractinian material were collected from water depths between 172 and 1395 m, corresponding to subtropical waters, Antarctic Intermediate Water, and Upper Circumpolar Deep Water. Fifteen species were identified, including eight species new to the region. The assemblage reflects the position of the seamounts in a transition zone between Indo-Pacific and Subantarctic biogeographic zones. Morphological variation in caryophyllids and the restriction of dendrophylliids to the southern seamounts could result from genetic isolation or reflect environmental conditions. Uranium-series dating using both rapid laser ablation and precise isotope dilution methods reveals their temporal distribution from the Last Glacial Maximum to the present day. Only one specimen of glacial age was found, while peaks in abundance occur around Heinrich Stadial 1 and the Younger Dryas, times at which ocean chemistry and food

supply were likely to have presented optimal conditions for cold-water corals. A widespread regional preference of cold-water corals for UCDW over AAIW depths during the deglacial, the reverse of the modern situation, could be explained by higher dissolved oxygen concentrations and a temperature inversion that persisted into the early Holocene.

3.1 Introduction

3.1.1 Cold-water corals

Cold-water corals comprise non-symbiotic (azooxanthellate) cnidarian species of the orders Scleractinia, Octocorallia, Stylasteridae, and Antipatharia (Roberts et al., 2009). About half of all species of scleractinian corals are azooxanthellate, some of which can build structural habitats that provide refuge for many other species, although the majority are solitary or free-living (Roberts et al., 2009). Most species of scleractinian CWCs are found in ocean temperatures that range from 1 to 20°C (Stanley and Cairns, 1988) at shallow to lower bathyal depths, with occasional records as deep as 6328 m (Keller, 1976).

Cold-water corals are particularly useful for unravelling changes in ocean biogeochemistry and circulation in the past (Robinson et al., 2014). They are found in abundance in the Southern Ocean, where other proxy archives such as foraminifera are sparse, and they can be preserved on the seafloor or within sediments for thousands of years (e.g. Burke et al. 2010; Margolin et al. 2014; Thiagarajan et al. 2013). Their depth range often covers intermediate and deep water masses, complementing and extending records from abyssal sediment cores. A record of seawater chemistry throughout their lifetime can be preserved in their carbonate skeleton (Robinson et al., 2014), and their high uranium content allows for application of precise uranium-thorium dating methods (Cheng et al., 2000; Douville et al., 2010; Lomitschka and Mangini, 1999; Montero-Serrano et al., 2013; Shen et al., 2012, 2008).

The physiology of CWCs and their response to environmental stressors is understudied in comparison to their shallow-water counterparts. However, research volume has grown in recent years, in part because of concerns about the impact of human activity on CWC ecosystems (Guinotte et al., 2006). Water temperature is thought to be one of the most important controls on their range at a global scale (Davies and Guinotte, 2011), but responses to thermal stress have been shown to vary by species (e.g. Büscher et al., 2017; Gori et al., 2016). Cold-water corals rely on a food supply of zooplankton, algal material and particulate organic matter (Duineveld et al., 2007). Hydrography plays an important role in controlling supply of this nutrition, as well as in the dispersal of larvae (Dullo et al., 2008; Miller et al., 2010). Although dissolved oxygen is crucial for corals to maintain aerobic function, the limit of tolerance is unknown, with colonies of the coral *Desmophyllum pertusum* (formerly known as *Lophelia pertusa*) being found to survive at dissolved oxygen concentrations well below the limit suggested in laboratory experiments (Dodds et al., 2007). The extent to which carbonate ion concentration controls CWC range is also disputed. Although 95% of branching CWCs are found above the aragonite saturation horizon (ASH; Guinotte et al., 2006), recent expeditions have also recovered scleractinians from undersaturated waters (e.g. Baco et al., 2017; Thresher et al., 2011). Regional fluctuations in seawater chemistry, productivity, and water mass structure at times in the past are therefore all likely to have exerted some control on regional habitat suitability for CWCs.

3.1.2 The deglacial Southern Ocean

In this study, we characterise and date a collection of subfossil CWCs from the southern Indian Ocean for the first time and explore the environmental controls on their distribution since the LGM (~ 23-19 ka). At this time, atmospheric CO_2 concentrations were 80-90 ppm lower than preindustrial values (Monnin et al., 2001). Enhanced carbon storage in the deep

ocean resulted from a more effective biological pump (e.g. Wang et al., 2017) and reduced ventilation due to sea ice-induced stratification and/or equatorward wind shifts (Ferrari et al., 2014; Kohfeld and Chase, 2017; Stephens and Keeling, 2000). During the subsequent deglaciation, degassing of CO_2 from the deep ocean is thought to have been responsible for the co-variation in atmospheric CO_2 and Antarctic temperature change (Parrenin et al., 2013), characterised by two 'pulses' of CO_2 release separated by a cooling and stabilisation of atmospheric CO_2 during the ACR (14.5-12.7 ka; Stenni et al., 2011). Radiocarbon records indicate intervals of breakdown in the deep vertical stratification (Burke and Robinson, 2012; Chen et al., 2015; Siani et al., 2013), while changes in pH conditions reflecting outgassing of CO_2 sourced from deep waters have been reconstructed using boron isotopes (Martínez-Botí et al., 2015; Rae et al., 2018).

The Indian sector of the Southern Ocean is an important location in which to study deglacial ocean biogeochemistry. Frontal movements in this region may have led to changes in the 'leakage' of warm, salty eddies from the Agulhas retroflection into the Atlantic Ocean, with implications for Atlantic overturning circulation (e.g. Bard and Rickaby, 2009; Beal et al., 2011; Franzese et al., 2006). In addition, a lag between atmospheric cooling over Antarctica during the ACR (Stenni et al., 2001) and sea surface temperature decline in the southern Indian Ocean (Labracherie et al., 1989) has yet to be fully explained. To date, our understanding of these changes and their global significance has been limited by sparse proxy records from this region, motivating efforts to explore CWCs as a palaeoceanographic archive. By taxonomically cataloguing and dating a new regional sample of intermediate-water CWCs, this study provides a first step towards investigating these processes.

3.2 Materials and methods

3.2.1 Sampling location and regional hydrography

Subfossil corals were collected from four seamounts along the SWIOR, which were surveyed in 2011 during expedition JC066 of the *RV James Cook*. From south to north these were: Coral Seamount (41°21'23" S, 42°50'31" E); Melville Bank (38°31'56" S, 46°45'74" E); Middle of What Seamount (henceforth 'MoW Seamount'; 37°56'76" S, 50°22'16" E); and Atlantis Bank (32°42'01" S, 57°17'26" E; Fig. 3.1A; Table 3.1).

The modern SWIO is dominated by two major hydrographic features, the ACC and the Agulhas Current system. The SAF, the northernmost front of the ACC, is strongly steered by bathymetry in the SWIO (e.g. Pollard et al., 2007), resulting in a latitude range of 48-43°S (Sokolov and Rintoul, 2009a; Fig. 3.1A). Further north, a 4°C increase in temperature and a sharp increase in salinity (Fig. 3.1B) marks the position of the STF, the boundary between subantarctic and subtropical surface waters, at around 40°S (Read and Pollard, 2017). The Agulhas Current overshoots the southern tip of the African continent and is retroflected by westerly winds, forming the Agulhas Return Current (ARC); this is found in close proximity to the STF in the SWIO (Belkin and Gordon, 1996; Lutjeharms and Van Ballegooyen, 1988; Read and Pollard, 2017; Fig. 3.1B). Peak chlorophyll concentrations are found at the ARC/STF, but the highest surface particulate organic carbon concentrations and microorganism abundances are found between the two fronts, in the SAZ (Djurhuus et al., 2017b).

Density surfaces rise upwards to the south, in geostrophic balance with the eastward flow of the ACC, affecting the depth at which specific water masses are present across the SWIO transect (Fig. 3.1B, C). The subsurface salinity minimum of AAIW is found between 500m (Coral) and 1500m (Atlantis) in the southern Indian Ocean and was sampled at all

seamounts (Fig. 3.1B, C). Upper Circumpolar Deep Water, a high-nutrient water mass consisting of a combination of Indian and Pacific deep waters, with its upper bound defined by the 27.5 kg m^{-3} neutral density surface (Plancherel, 2012), intersected with sampling at Coral (~ 900 m) and MoW (~ 1050 m) seamounts. Lower Circumpolar Deep Water is found in the SWIO at depths of 2 to 3 km (van Aken et al., 2004; Fig. 3.1C), but such depths were not sampled during this study.

Sampling was opportunistic and not all fossil CWCs seen were collected. All but three of the specimens described here were collected during dives of the *Kiel 6000* Remotely Operated Vehicle (ROV), using manipulator arms, a suction sampler, nets and mini-box corers (Rogers and Taylor, 2011). The remaining specimens were extracted from a megacore sample (JC066_1116), a boxcore sample (JC066_115), and picked up on a dive of the HYBIS towed camera system (JC066_4309). On each seamount, ROV dives were made along deep to shallow transects to analyse the depth and spatial variation of benthic communities. Five ROV dives took place at Coral Seamount, four at Melville Bank, two at MoW Seamount, and three at Atlantis Bank. The 149 scleractinian samples in the collection, of which 122 were solitary, cover a depth range of 172 to 1395 m.

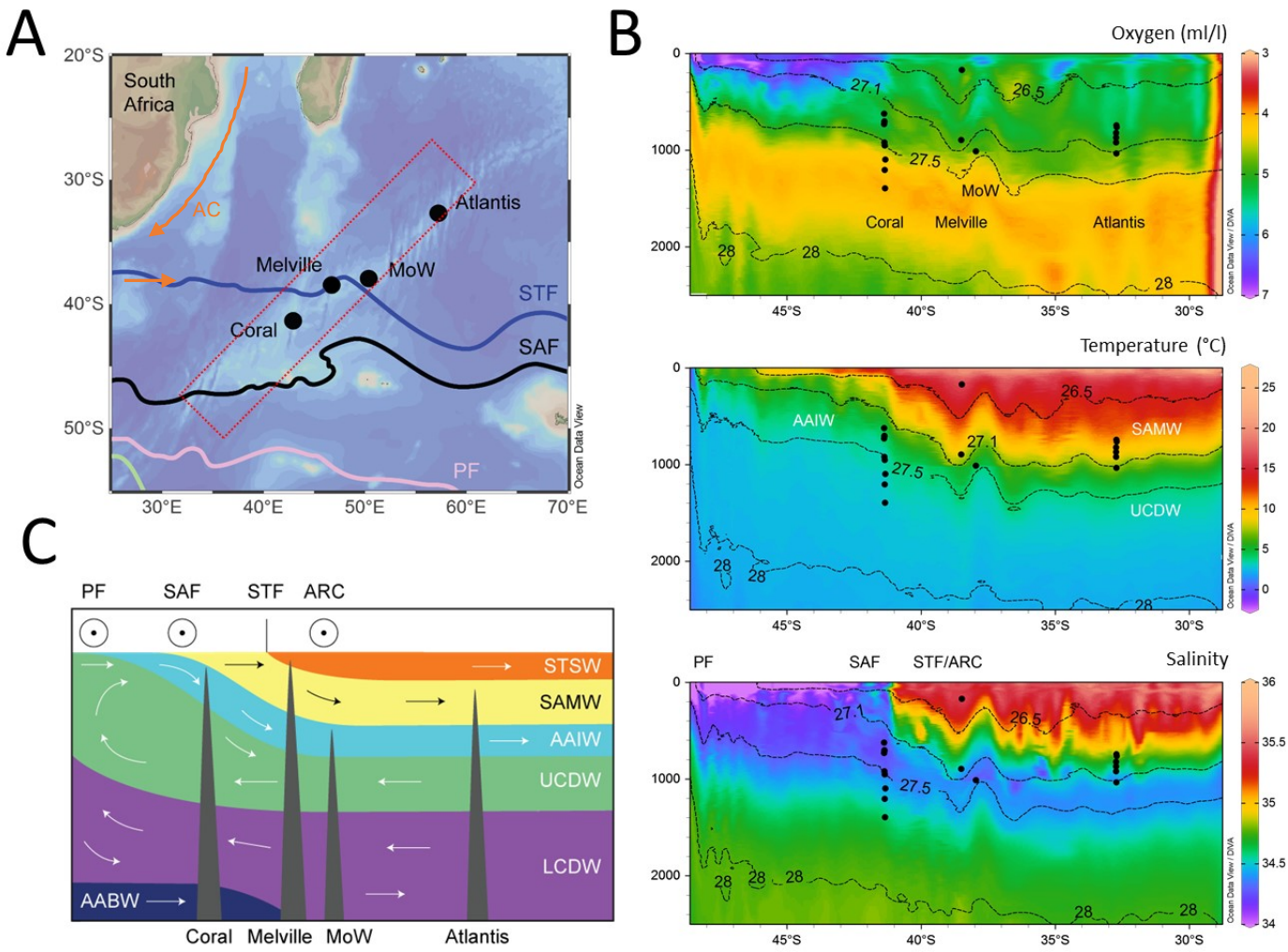

Figure 3.1: Modern day hydrography proximal to sample locations on the Southwest Indian Ocean Ridge (SWIOR). **A)** bathymetric map of the sampling region in the Southwest Indian Ocean with positions of fronts marked from north to south: Subtropical Front (STF), Subantarctic Front (SAF), Polar Front, (PF), Southern Antarctic Circumpolar Current Front (green), from Sokolov and Rintoul, (2009). Sample locations are shown with black dots, and the red box highlights the transect along which sections are plotted. **B)** Vertical sections with sampling locations shown with black dots. CTD data accessed from the World Ocean Database, plotted with Ocean Data View (Schlitzer, 2017). From top to bottom are plotted oxygen, labelled with seamount names; temperature, labelled with water masses Subantarctic Mode Water (SAMW), Antarctic Intermediate Water (AAIW) and Upper Circumpolar Deep Water (UCDW); and salinity, labelled with the three regional fronts. The path of the Agulhas Return Current (ARC) combines with the STF as it crosses the SWIOR. Contours of neutral density

surfaces (kg m^{-3}) corresponding to water mass boundaries are shown on all three sections. **C)** Schematic section of present-day circulation and positions of frontal jets of the Antarctic Circumpolar Current in the Indian sector of the Southern Ocean. Water masses depicted in addition to SAMW, AAIW and UCDW are subtropical surface waters (STSW); Lower Circumpolar Deep Water (LCDW) and Antarctic Bottom Water (AABW).

3.2.2 Taxonomy

Taxonomic identifications of the scleractinian coral specimens were based on monographs which represent the most recent, extensive, and available documents on azooxanthellate Scleractinia. These include Cairns (1982; Antarctic and Subantarctic), Cairns and Keller (1993; SWIO), Cairns (1995; New Zealand), Cairns and Zibrowius (1997; Indonesia), Cairns (2000; Caribbean), Kitahara et al. (2010) and Cairns and Polonio (2013; Indonesia).

Discrepancies in the boundaries and number of biogeographical realms exist between studies of azooxanthellate Scleractinia (see Cairns, 2007) and more recent classifications using benthic marine species and oceanographic proxies (most recently Watling et al., 2013). For the purposes of this study, we use a combination of the two. Atlantis Bank, Melville Bank and MoW Seamount fall within the Indian Lower Bathyal Province proposed by Watling et al. (2013) and the southwest Indian Ocean (SWIO) region following the terminology of Cairns (Cairns, 2007). The STF is designated as the northern boundary for the Subantarctic realm in Cairns (Cairns, 2007), whereas Watling et al. (2013) use the Polar Front. Therefore, Coral Seamount is located in the Subantarctic according to Cairns (Cairns, 2007), but in the Indian Province following Watling et al. (2013). To acknowledge this difference, along with the likelihood that the boundary is transitional, we place Coral Seamount in the 'Subantarctic Transition Zone'.

During taxonomic analysis, specimens were evaluated for preservation of aragonite (1 – highly degraded to 5 – intact) and the relative accumulation of authigenic coating (0 – no coating to 3 – fully coated). These qualitative metrics were combined into a 'preservation factor', by subtracting coating from aragonite preservation (Table 2.2).

3.2.3 Laser ablation U-series dating

A total of 122 solitary scleractinian samples were prepared for laser ablation uranium-series age screening in the Bristol Isotope Group (BIG) facilities, following the method developed by Chen et al. (2015) and Spooner et al. (2016). Twenty-one specimens, predominantly of the genus *Balanophyllia,* were too delicate, small, or poorly preserved to proceed with laser ablation dating. Coral samples of a minimum size of 2 x 1.5 mm were cut using a Dremel® tool with a diamond blade, polished flat on one side using four increasingly fine grades of sandpaper, and rinsed with deionised water (18.2 MΩ. cm). Visibly altered or discoloured sections of aragonite were avoided. The samples were then mounted in batches of ~ 50 into trough-shaped sample holders.

Auto-focussed and pre-programmed 1.1 mm line scans were ablated automatically using 'Chromium 2.1' software linked to the Photon Machines Analyte G2 193 nm laser, which was coupled to a Thermo Finnigan Neptune MC-ICP-MS. The low abundance isotope ^{230}Th was measured in sequence on a central ion counter, with ^{238}U measured simultaneously using Faraday cups (Spooner et al., 2016). Tuning was carried out using NIST 610 glass in order to maximise ^{230}Th signal intensity. An aragonite vein standard from the Salt Wash Graben, Green River, Utah (VS001/1-A) was used to bracket every three samples. Measurements consisted of 50 cycles for samples and bracketing standards, and background intensities were measured for 25 cycles following each standard measurement. Anomalous signal spikes in ^{230}Th were

removed before calculation of mean isotope intensities, subtraction of the background intensity, and calculation of the isotope ratios; however, such spikes were rarely observed. Corrections for instrumental, elemental, and isotopic fractionation were applied using bracketing standards. Ratios were used to determine sample age by iteratively solving the age equation using the Newton-Raphson method (Kaufman and Broecker, 1965). Closed system behaviour was assumed, and the known modern seawater $\delta^{234}U_i$ value of 147 ± 7 ‰ (Reimer et al., 2009) was used in the calculation. Previous data indicates age corrections for initial ^{230}Th based on ^{232}Th fall within the usual age uncertainties for this method (Robinson et al., 2014; Spooner et al., 2016), and therefore no correction was made for detrital or seawater Th contribution. Standard errors on the measured ratios, the background measurements, and the errors on the isotope dilution MC-ICPMS isotope ratios of the standards were combined and propagated through each stage of standard corrections (Spooner et al., 2016). Final propagation of errors through the age equation was carried out using a Monte Carlo technique, whereby random Gaussian distributions for each ratio are generated and used to calculate a distribution of possible ages from which the final sample ages and errors are determined. For deglacial age corals these errors range between 500 and 1500 years. The background level was typically 1 count per second, with deglacial corals recording 10-20 cps.

3.2.4 Isotope dilution U-series dating

Fifty-two subsamples including two full procedural duplicates for combined U, Th, Nd chemistry (~ 0.6 to 5 g) were taken for precise isotope dilution U-series analysis. Physical and chemical cleaning procedures followed the development and assessment of methods performed before in the MAGIC group at Imperial College on cold-water corals (Crocket et al., 2014; van de Flierdt et al., 2010), building on methods developed by Cheng et al. (2000), Lomitschka and Mangini (1999) and Shen and Boyle (1988). All samples were rigorously physically cleaned

with a Dremel tool, before undergoing a two-day oxidative-reductive chemical cleaning process. In the BIG laboratory facilities at the University of Bristol, cleaned coral fragments (~ 0.04 to 1.9g) were then dissolved and spiked with a ^{236}U-^{229}Th mixed spike calibrated to a 4.1‰ (2σ) uncertainty, described further by Burke and Robinson (2012). An iron co-precipitation procedure was utilised to separate trace metals from the carbonate matrix, before U and Th fractions were separated and purified using anion exchange chromatography using columns filled with an Eichrom pre-filter resin and 2 mL Biorad analytical grade anion exchange resin 1-X8 (100-200 mesh).

Uranium and Th isotopes were measured on a Neptune MC-ICP-MS in the BIG laboratories. Bracketing standards were used: for U, the international standard U112a, and for Th the in-house standard 'SGS'. A 45 ppb U112a standard solution was used to tune the Neptune prior to U measurement, such that sensitivity for ^{238}U was ~ 250 V/ppm with a variation of < 2%, and between 5 and 95% peak height measured 0.1 amu or less. To correct for mass bias, U112a and SGS were used to bracket U and Th samples respectively. Using these bracketing standards, the activity ratios $^{238}U/^{234}U$, $^{232}Th/^{230}Th$, $^{232}Th/^{229}Th$, and $^{230}Th/^{229}Th$ were corrected for each sample. The isotopes ^{238}U, ^{236}U and ^{235}U were analysed in Faraday collectors, and ^{234}U on the secondary electron multiplier (SEM), in measurements of 100 cycles. The low concentration ^{229}Th and ^{230}Th isotopes were analysed on the SEM by peak jumping in measurements of 50 cycles. ^{236}U, added as a spike to the Th cut, was measured concurrently on a Faraday cup. The latter was used to normalise the $^{230}Th/^{229}Th$ ratio for signal instability, by measuring $^{230}Th/^{236}U$ and $^{229}Th/^{236}U$ (Burke and Robinson, 2012; Chen et al., 2015). The wash solution (i.e. blank) was analysed before every sample run in 10 cycles and subtracted from all absolute values before calculating isotope ratios. Machine accuracy was monitored by measuring Hu84.5 (U) and ThB (Th) standards before each session and every 3-4 samples. An HU84.5 standard was processed with each batch of column chemistry and

yielded a long-term external reproducibility for [^{230}Th/^{238}U] of 0.997 ± 0.003, and for [^{234}Th/^{238}U] of 1.0007 ± 0.0008, within error of secular equilibrium (n=50). Errors including machine uncertainties and procedural blanks were propagated into the isotope ratios of ^{234}U/^{238}U, ^{236}U/^{238}U and ^{229}Th/^{230}Th. A Monte Carlo technique was used to propagate the errors of isotope ratios into the final reported uncertainties.

The isotope ^{232}Th was measured in addition to ^{230}Th in order to correct for non-radiogenic sources. Assuming any initial Th incorporated on calcification had a ^{230}Th/^{232}Th ratio equivalent to local modern-day seawater, the measured ^{232}Th can be used to estimate initial ^{230}Th. An initial atomic ^{232}Th/^{230}Th ratio of 12,500 ± 12,500 (2σ) was assumed, corresponding to modern subtropical Atlantic intermediate waters (Chen et al., 2015). This calculation dominates the final error for ages, with measured ^{232}Th correlating with the sample age error due to the greater uncertainty of initial ^{230}Th activity. Measured ^{232}Th ranged from 50 to 3806 ppt, and was the main factor determining the age errors, which ranged from 68 to 985 years for deglacial age corals.

The value $\delta^{234}U_i$ is the deviation (‰) from secular equilibrium of the ^{234}U/^{238}U activity ratio and is used to test for closed-system behaviour of the corals. The $\delta^{234}U_i$ of the SWIO corals ranged from 145.2 to 157.5 ‰. Two of the 50 corals analysed exhibited open-system behaviour with $\delta^{234}U_i$ outside of the modern-day ocean (147 ± 7 ‰; Reimer et al., 2009). Ages of the full procedural duplicates were within error.

3.3 Results

3.3.1 Taxonomy

Material from colonial species accounts for 27 of the 149 scleractinian samples, including *Solenosmilia variabilis*, *Madrepora oculata*, *Goniocorella dumosa*, and

Enallopsammia rostrata. *Solenosmilia variabilis* appears to be the most common species represented among the colonial specimens. However, it is difficult to evaluate the relative abundance of these species as the number of samples cannot be considered representative of the communities found at each seamount.

Of the 122 solitary specimens, the majority represent the family Caryophylliidae, which includes *Desmophyllum dianthus* (*n* = 36), and *Caryophyllia diomedeae* (*n* = 32). Dendrophylliids are also common, including *Balanophyllia gigas*, *Balanophyllia malouinensis*, and *Leptopsammia stokesiana* (*n* = 31). The remaining solitary specimens comprise 13 flabellids (*Flabellum flexuosum* and *Javania antarctica*), two attached *Trochocyathus gordoni*, and free-living specimens of *Deltocyathus sp.* and *Dasmosmilia lymani*. Five solitary and four colonial samples were not identified to genus level due to poor preservation.

An annotated list detailing the 15 scleractinian taxa represented within the new collection is presented below.

3.3.1.1 Species List

Order SCLERACTINIA

Family **OCULINIDAE** Gray, 1847

1. *Madrepora oculata* Linnaeus, 1758. Four fragments of this colonial coral, characterised by sympodial budding and anastomosed branches, were collected from patches of coral rubble at Melville Bank and MoW Seamount.

Family **CARYOPHYLLIIDAE** Dana, 1846

2. *Caryophyllia diomedeae* Marenzeller, 1904. Thirty specimens found at Coral Seamount, MoW Seamount and Atlantis Bank shared a hexameral S1=S2>S3≥S4 septal

pattern, low, evenly spaced costae, sinuous pali on S3, and a columella formed of fascicular elements (Cairns, 1995; Cairns and Zibrowius, 1997; Kitahara et al., 2010). Two specimens displayed an irregular septal pattern, with 43 and 44 septa in total; similar variations have been described previously from the Atlantic (Zibrowius, 1980) and New Zealand (Stephen D. Cairns, 1995). At least eight specimens had fewer than three columella elements. A few specimens from Atlantis Bank and one from MoW Seamount have highly exert S1-2, up to 5mm (Fig. 2.2A); however, in most specimens from Coral Seamount and Melville Bank S1-2 were only moderately exert (Fig. 2.2B). This character arguably places the latter group closer to the range of *Caryophyllia laevigata*, a species described by Kitahara et al. (2010). In this case, the differences amongst specimens was not consistent enough to identify them as separate species, rather than considering a wide range of morphological variation of *C. diomedeae*. Another diagnostic feature, colour banding, was variably expressed and did not necessarily correlate with septal exertness. Finally, it is worth mentioning that most of the Atlantis Bank specimens exhibit fused costal granules near the calicular margin.

3. *Caryophyllia profunda* Moseley, 1881. One specimen of this taxa was collected, from Melville Bank (Fig. 2.1B). Unlike specimens described by Cairns (1995, 1982), all septal edges are straight.

4. *Trochocyathus (T.)* cf. *gordoni* Cairns, 1995. One specimen composed of two budded coralla found at Coral Seamount was assigned to *T.* cf. *gordoni*, although poor preservation, especially of the pali, hampers conclusive identification (Fig. 2.1A). As in the New Zealand specimens (Stephen D. Cairns, 1995), deep intercostal striae are present near calicular edge, becoming less defined towards the pedicel. Both specimens have an irregular septal arrangement approaching decameral.

5. *Solenosmilia variabilis* Duncan, 1873. Fragments of *S. variabilis* were collected from Coral Seamount and Melville Bank.

6. *Goniocorella dumosa* (Alcock, 1902). Fragments were found at Coral Seamount only. Specimens display straight, cylindrical branches and right-angled budding as described in Cairns (1982).

7. *Dasmosmilia lymani* (Pourtalès, 1871). One specimen was found at Coral Seamount, having fewer columella components than described in Cairns (1995), but a similar septal arrangement, budding pattern, and serrate calicular edge.

8. *Desmophyllum dianthus* (Esper, 1794). The most common species with a total of 36 specimens collected from Coral Seamount, Melville Bank, and Atlantis Bank. They exhibit a wide range of variation within the species, from small juvenile to large adult specimens, straight to slightly bent corallum, and low to highly exert septa. A few specimens from Atlantis Bank are distinct in that they most clearly bear the characteristic features of *D. dianthus*: clear, ridged costae; highly exert, flared septa and finely granular theca (Fig. 3.2C; Cairns, 1982).

Family **DELTOCYATHIDAE** Kitahara et al., 2012

9. *Deltocyathus* sp. Milne Edwards and Haime, 1848. A single, small, free living specimen was found at Melville Bank. The specimen exhibits diagnostic characters of the genus *Deltocyathus*, having pali before septa of all but first cycle and axial edges of higher septa (S4) joining to faces of adjacent septa (S3). However, the poor preservation of the specimen hampers its identification to species level.

Family **FLABELLIDAE** Bourne, 1905

10. *Flabellum flexuosum* Cairns, 1982. Three specimens were collected at Coral Seamount. They exhibit a thin, porcellaneous theca, and sinuous, wrinkled edges of the inner septa (Cairns, 1982, Fig. 2.1A). However, none have a fifth septal cycle.

11. *Javania antarctica* (Gravier, 1914). Seven specimens from Coral Seamount and one from Melville Bank were collected. Although similar in morphology to *F. flexuosum*, these specimens were distinguished by their distinctive chevron growth lines peaking at intersections with 'costae', as described in Cairns (1982; Fig 2.1A). Only one specimen displayed a rudimentary fifth septal cycle.

Family **DENDROPHYLLIIDAE** Gray, 1847

12. *Balanophyllia gigas* Moseley, 1881. Twenty-one specimens representing this species were found at Coral Seamount. It is likely that all specimens are juvenile, as none express a full Pourtalès plan septal arrangement and they are much smaller than specimens described from New Zealand (Stephen D. Cairns, 1995). The presence of banded epitheca above the synapticulotheca (Cairns and Zibrowius, 1997) is variable. They all have in common a deep, narrow fossa and relatively narrow septa (Fig 2.1A).

13. *Balanophyllia malouinensis* Squires, 1961. A total of five specimens were recovered from Coral Seamount and Melville Bank. They were distinguished from *B. gigas* by having a thick, spinose synapticulotheca and a shallower fossa with a larger columella (Cairns, 1982; Fig 2.1A). Like the *B. gigas* specimens, the septa are arranged only in a rudimentary Pourtalès plan.

14. *Leptopsammia stokesiana* Milne Edwards and Haime, 1848. Five specimens were found at Coral Seamount. Although similar in size and morphology to the other solitary dendrophylliids in the collection, these do not have a Pourtalès plan septal arrangement (Cairns and Zibrowius, 1997).

15. *Enallopsammia rostrata* (Pourtalès, 1878). In total four fragments of this robust, uniplanar colonial coral were found at Melville Bank and Atlantis Bank.

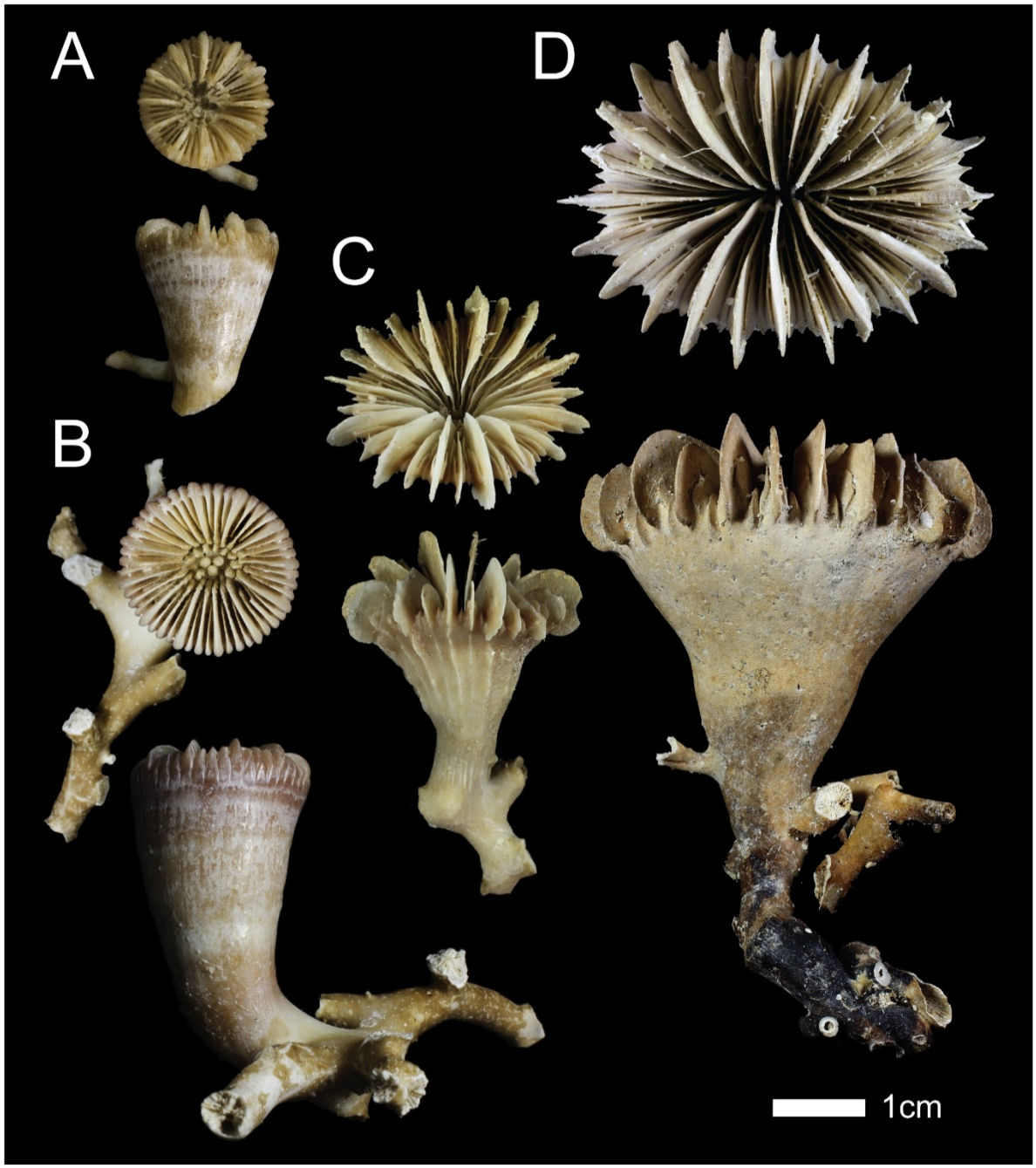

Figure 3.2: Morphological variability of CWCs across seamount transect. Calice and corallum of *Caryophyllia diomedeae* from **A)** Atlantis Bank (JC066_3741) and **B)** Coral Seamount (JC066_122); and calice and corallum of *Desmophyllum dianthus* from C, Atlantis Bank (JC066_3718) and D, Coral Seamount (JC066_127).

3.3.1.2 Taxonomic distribution

All solitary CWCs except the *C. profunda*, which was collected at the summit of Melville Bank at 172 m water depth, were found between 600 and 1400 m (Figs. 3.1, 3.3), covering modern SAMW, AAIW, and UCDW depths, although the latter was only represented by specimens from Coral Seamount. This depth range is in part constrained by the position of the seamount summits, particularly at MoW Seamount (1100 m) and Atlantis Bank (750 m), and the maximum depth of the ROV surveys (see Table 3.1 and Fig. 3.3).

Table 3.1: Location, bathymetry, and number of specimens from SWIO seamounts

Seamount	**Latitude (°S)**	**Longitude (°E)**	**Summit (m)**	**Max survey depth (m)**	**Solitary CWC specimens**	**CWC specimens dated**
Coral	41°21’23” S	42°50’31” E	175	1395	89	72
Melville	38°31’56” S	46°45’74” E	91	1276	9	5
MoW	37°56’76” S	50°22’16” E	876	1414	7	7
Atlantis	32°42’01” S	57°17’26” E	690	1117	17	17

At Coral Seamount, the greatest number (n = 89) and diversity of CWCs was found, with 9 out of 11 solitary species represented (Fig. 3.3). Samples were collected between 624 and 1395 m, intersecting the boundary between AAIW and UCDW at ~ 900 m. Most corals of this collection were recovered at ~ 700 m, where 27 of the 30 Dendrophylliidae specimens are found, and ~ 1200 m, dominated by Caryophylliidae.

At Melville Bank and MoW Seamount, solitary CWC specimens were found near to the modern-day SAMW/AAIW and AAIW/UCDW boundaries, respectively (Fig. 3.1B). Nine specimens from Melville Bank represent a minimum of five species (Fig. 3.3). All seven CWCs

from MoW Seamount are *C. diomedeae*. At both seamounts the ROV transect extended a few hundred metres below where the deepest CWCs were found.

The 17 CWC specimens from Atlantis Bank span the full depth range surveyed from 700 to 1100 m. *Desmophyllum dianthus* and *C. diomedeae* were the only solitary species collected in this locality (Fig. 3.3).

A range of preservation of the skeletal aragonite was observed, from near-perfect to heavily bored and/or dissolved. Corals were often found coated with grey-brown authigenic deposits. On the whole, coating levels and aragonite degradation appear to be positively correlated, i.e. poor aragonite preservation was linked to high coating levels (Fig. 3.4). No significant correlation was found between water depth and individual coral mass or preservation factor (Fig. 3.5A).

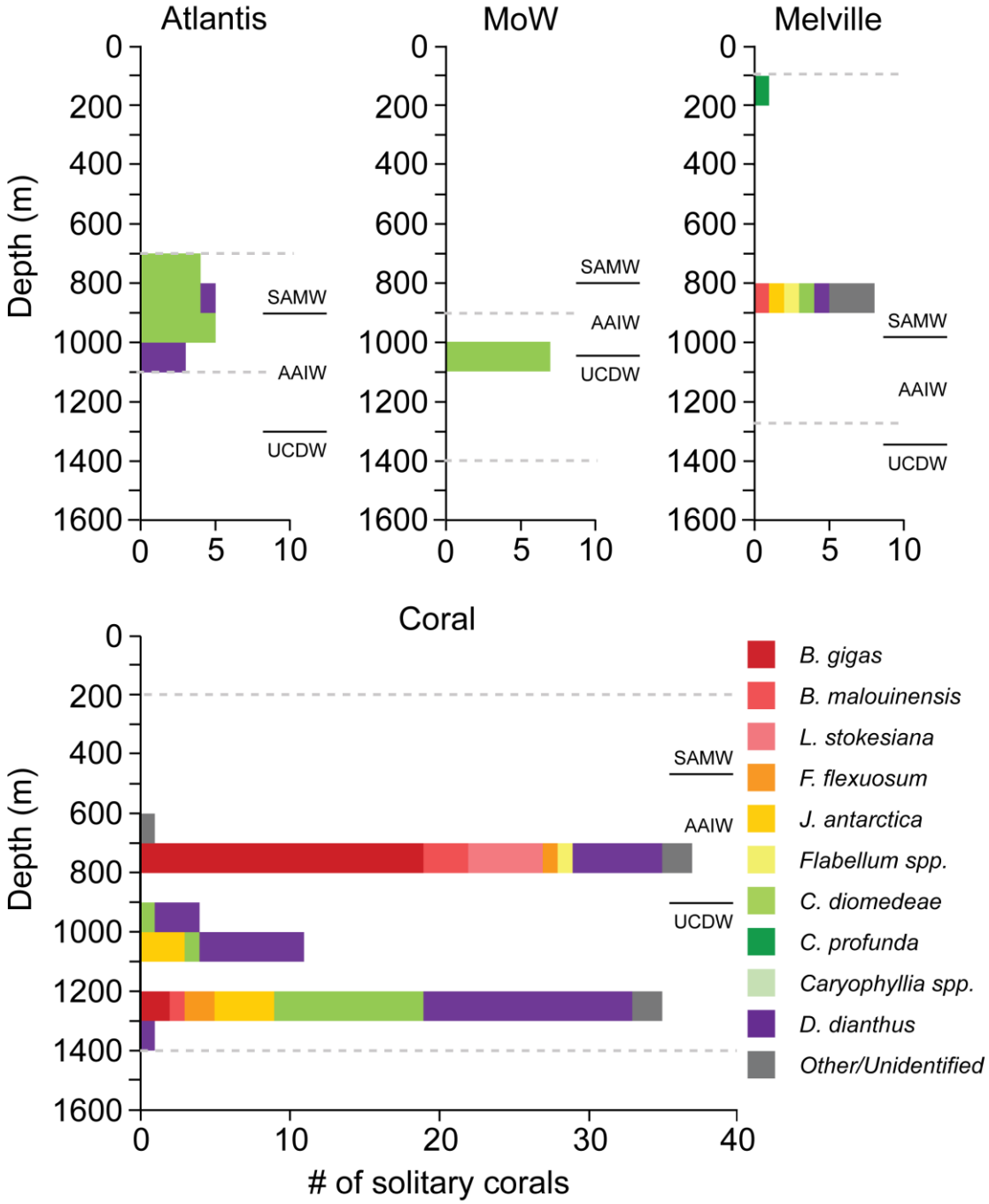

Figure 3.3: Depth distribution of subfossil CWCs at each seamount, colour coded by species. Seamount summits and the deepest vertical extent of ROV surveying are represented by dashed grey lines. Modern day water mass boundaries between Subantarctic Mode Water (SAMW), Antarctic Intermediate Water (AAIW) and Upper Circumpolar Deep Water (UCDW) are defined using the depths of neutral density for AAIW ($27.1 < \gamma_n < 27.5$; Plancherel, 2012) at each seamount, from World Ocean Database CTD data.

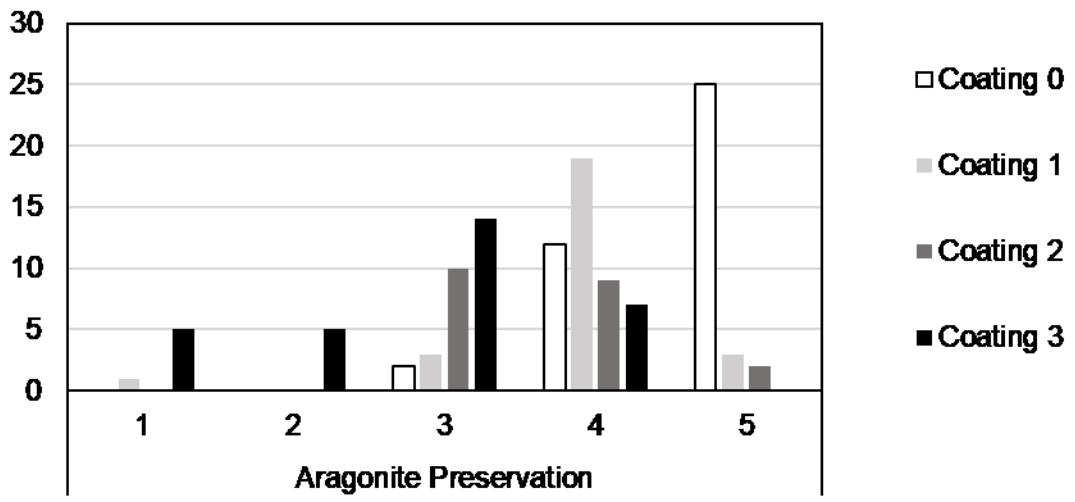

Figure 3.4: The frequency of specimens at each aragonite preservation category (A.P: 1 low, 5 high) at different coating levels (C: 0 low, 3 high).

3.3.2 Ages

The 101 dated CWCs range in age from the LGM to the modern day (Fig. 3.7), except for a single 140 ka specimen from Melville Bank. Isotope dilution U-series dating of 50 of the samples demonstrated the accuracy of the laser ablation technique, with a close correlation and 33 samples giving ages within error of the laser ablation dates (Fig. 3.6). Only late Holocene CWCs were found at Atlantis Bank, whereas both Holocene and deglacial specimens were found at Coral Seamount, Melville Bank and MoW Seamount. There are relatively few samples from the mid-Holocene (~ 5 ka) and the Last Glacial Maximum (19 – 25 ka). The most well preserved CWCs, and those with the greatest mass, date from periods of greatest abundance. Conversely, the few corals found during the LGM and early- to mid-Holocene are poorly preserved (Fig. 3.5B).

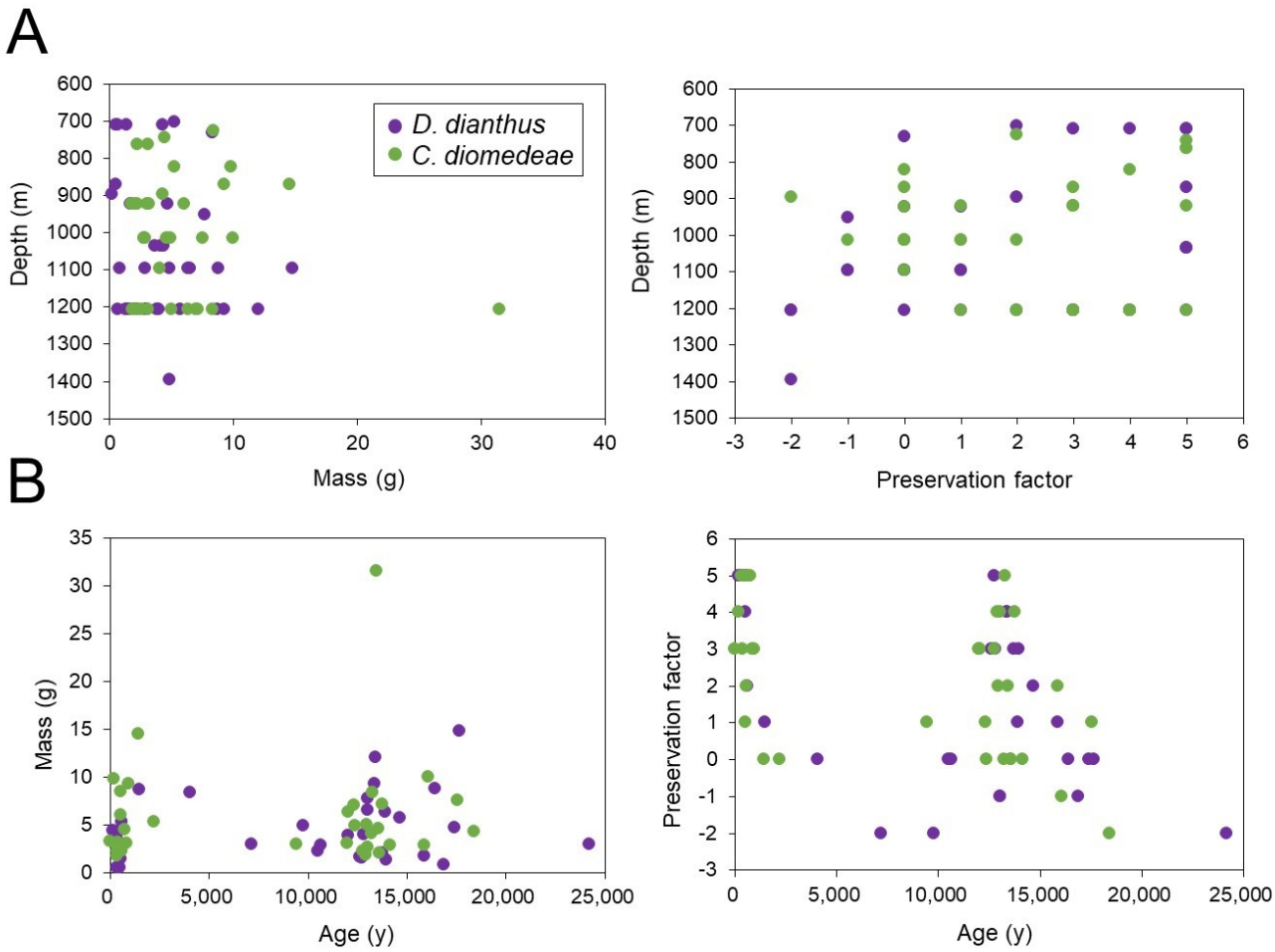

Figure 3.5: Relationship of caryophylliid mass and preservation factor to **A)** depth and **B)** age, at all seamounts for the two most prevalent species (colour coded). Preservation factor is a qualitative metric that takes into account the amount of ferromanganese coating and aragonite dissolution, and ranges from -2 (least well preserved) to 5 (intact).

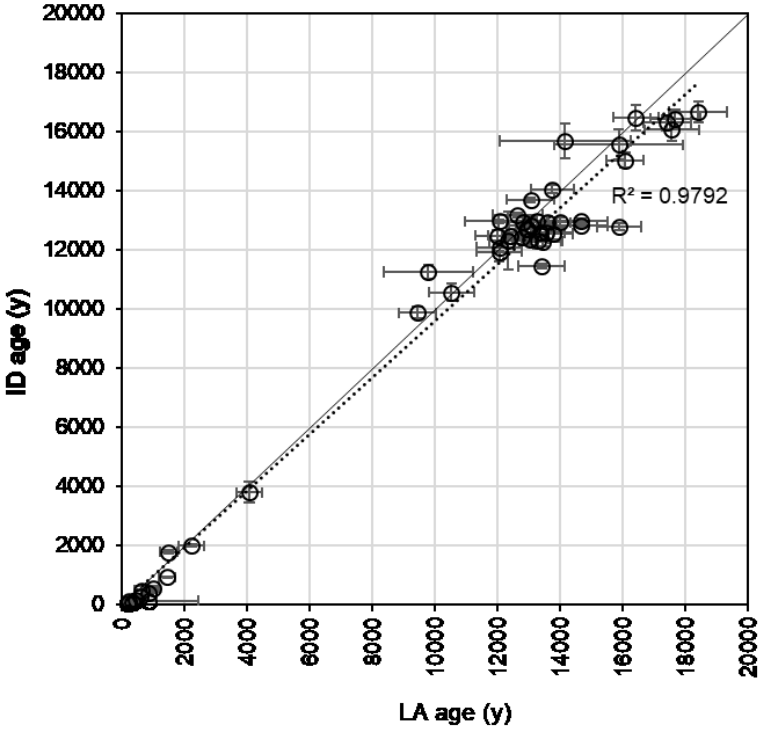

Figure 3.6: Comparison of laser ablation (LA) and isotope dilution (ID) U-series ages for 50 cold-water corals from southwest Indian Ocean seamounts. The 1:1 line (solid) and trendline (dashed) are shown.

3.4. Discussion

3.4.1 Taxonomy

3.4.1.1 Range extensions

Previous surveys of CWC diversity in the region include the works of Cairns and Keller (1993) for southern Africa and Madagascar, and Cairns (1982) for the Antarctic and Subantarctic. In the former, the scleractinian fauna is described as having influence from Pacific, and to a lesser extent, Atlantic faunas, in addition to species endemic to the Indian Ocean. The distribution of the species in this collection and their proposed latitudinal and/or vertical range extensions are shown in Table 3.2. Of the 15 scleractinian deep-water coral species found in this study, six have already been recorded from the SWIO and/or Subantarctic

regions: the cosmopolitan species *C. profunda, D. dianthus*, *M. oculata, E. rostrata* and *S. variabilis,* in addition to *G. dumosa*, which has only been found in the Indian and West Pacific oceans (Cairns and Keller, 1993; Cairns, 1982). The genus *Deltocyathus* is also widely distributed in all oceans; although as we were not able to identify the specimen to species level, future explorations and collection of well-preserved specimens from these localities will be needed to allow a better knowledge of this genus in the region. The remaining eight species represent extensions to their previously documented geographical ranges (Table 3.2), increasing the known scleractinian diversity of the SWIO and Subantarctic Transition Zone. Surprisingly, none of the Dendrophylliidae or Flabellidae species described previously from the SWIO (Cairns and Keller, 1993) were observed in this collection.

The connectivity of Indian and Pacific surface waters through the Indonesian throughflow led Cairns and Keller (1993) to predict that representation of the 'Indo-West Pacific' fauna would increase with further exploration in the SWIO. The first record of three species in the Indian Ocean supports that prediction: *T. gordoni* (known only from the Kermadec Islands, New Zealand / Kerguelen province; Cairns, 1995), *B. gigas* (West Pacific and New Zealand / Kerguelen; Cairns and Zibrowius, 1997), and *D. lymani* (warm temperate Pacific and Atlantic; Cairns, 2000). Connectivity of the Southern Ocean through the ACC could also have contributed to the spread of these species. All three species were found at depths (700-1200 m) which extend their distribution to deeper waters (Table 3.2).

The seamounts cover a transitional biogeographic zone between the Indian and Subantarctic regions, which is reflected both by the extension of species from the south into the Indian province, and from temperate regions into the Subantarctic. Known previously only from waters close to the Antarctic continent (Cairns, 1982), *F. flexuosum* was found north of the SAF at Coral Seamount. There is evidence that genetic dispersal of CWCs follows ocean density gradients and is less likely to occur vertically (Dullo et al., 2008; Miller et al., 2011).

It is possible that *F. flexuosum* extend their distribution up to the SWIO thanks to northwards transport via intermediate waters, as it is found below its previously known depth range between 700 and 1200 m. *Javania antarctica* and *Balanophyllia malouinensis*, whose ranges were recently extended from the Antarctic / Subantarctic (Cairns, 1982) to the southwest Atlantic (Cairns and Polonio, 2013), were also found at Coral Seamount as well as Melville Bank. Water temperature at Atlantis Bank may be above the tolerance of these Antarctic species. It is also possible that the ARC acts as a dispersal barrier to the Indian Ocean for CWC larvae, in a similar manner to the ACC (e.g. Dueñas et al., 2016); although to our knowledge this has not yet been modelled or evaluated.

Neither *C. diomedeae* nor *L. stokesiana* were listed in Cairns and Keller's (1993) SWIO monograph, but both have been found previously in the Indian and West Pacific provinces (Cairns and Zibrowius, 1997; Kitahara et al., 2010). As they were collected from Coral Seamount, their geographical ranges are extended into the Subantarctic Transition Zone. This find also extends the depth range of *L. stokesiana* from shallow to bathyal waters.

Table 3.2: Distribution of subtropical and Subantarctic Transition Zone (TZ) southwest Indian Ocean (SWIO) and Indian Ocean (IO) Bathyal Province azooxanthellate Scleractinia discussed in this study. Crosses under the TZ/SWIO seamount names represent specimens described in this study. Depth range in bold signifies a proposed bathymetric extension. References are given for previously known latitudinal ranges. MoW: Middle of What seamount.

Species	**Antarctic** (Cairns 1982)	**Subantarctic** (Cairns 1982)	TZ	SWIO			**SWIO** (Cairns and Keller, 1993)	**Indian** (Cairns and Keller, 1993)	**West Pacific** (Cairns and Zibrowius, 1997)	**New Zealand / Kermadec** (Cairns 1995)	**Atlantic** (Cairns 2000; Cairns and Polonio, 2013)	**Cosmopolitan**	Depth (m) (worldwide)	New record in region		
			Coral Seamount	**Melville Bank**	**MoW seamount**	**Atlantis Bank**								SWIO *sensu* Cairns (1982)	IO Bathyal Province *sensu* Watling et al. (2013)	Subantarctic Transition Zone
Madrepora oculata		x		x	x		x	x	x	x	x	x	55-1950			
Caryophyllia diomedeae			x		x	x		x	x	x	x		225-2200	x		x
Caryophyllia profunda	x	x		x			x	x		x		x	35-1116			
Trochocyathus (T). gordoni			x							x			**398-732**	x	x	x
Solenosmilia variabilis	x	x	x	x			x	x	x		x	x	220-2165			
Goniocorella dumosa		x	x				x	x	x	x			88-1488			
Dasmosmylia lymani			x						x	x	x		**37-1207**	x	x	x
Desmophyllum dianthus	x	x	x	x		x	x	x	x	x	x	x	8-2460			
Deltocyathus sp.				x			x	x	x				44-5080			
Flabellum flexuosum	x		x										**101-1207**	x	x	x
Javania antarctica	x		x	x							x		53-1280	x	x	x
Balanophyllia gigas			x						x	x			**90-1200**	x	x	x
Balanophyllia malouinensis	x	x	x	x							x		**75-1207**		x	
Leptopsammia stokesiana			x					x	x				**46-710**	x		x
Enallopsammia rostrata		x		x		x	x	x			x	x	110-2165			

3.4.1.2 Spatial variability

The seamounts in the SWIO form a transect across contrasting hydrographic and productivity regimes, with peak chlorophyll concentrations nearest to the ARC/STF frontal zone (Melville and MoW seamounts; Read et al., 2000). During the JC066 cruise, surface nutrient and particulate organic carbon (POC) concentrations were found to be highest at Coral Seamount (Djurhuus et al., 2017b), as was microorganism abundance (Djurhuus et al., 2017a). These features, along with the systematic variability in microbial community structure, led Djurhuus et al. (2017a) to separate the region into three biogeographic zones – south (Coral Seamount), convergence zone (Melville Bank and MoW Seamount), and north (Atlantis Bank). At depth, water masses were considered more influential, with similar taxa occurring below 200 m across the seamounts (Djurhuus et al., 2017a). The limited sample size and opportunistic nature of the sampling in this study makes a quantitative assessment of spatial variability patterns in CWCs difficult. Because of the differing seamount heights, the maximum depth of the ROV, and cruise time constraints (i.e. opportunistic sampling of subfossil CWCs), the full depth range of CWCs may not have been surveyed (Table 3.1). Nevertheless, notable variations in coral diversity are present in the dataset and warrant exploration.

Firstly, a larger number of samples and greater species diversity in subfossil Scleractinia was found at Coral Seamount relative to the other seamounts (Fig. 3.3). This could be explained by sampling bias, as ROV bottom time was approximately 35 hours at Coral, longer than at Melville (~ 29 hrs), Atlantis (~ 26 hrs) and MoW (~11 hrs); at MoW sampling was severely hampered by turbulent conditions. However, a wide variety of habitats was noted from video footage at Coral Seamount (Rogers and Taylor, 2011), and video surveys suggest it hosts the greatest diversity and number of species for corals and sponges (Frinault, 2017). It was also found to host the largest microbial community (Djurhuus et al., 2017a) and the highest surface chlorophyll concentrations of the four seamounts (Djurhuus et al., 2017b). There are

several factors which could contribute to the favourability of Coral Seamount as a habitat for CWCs. As a result of its position south of the STF, water temperatures at Coral were ~ 3°C to 5°C at the depths of coral collection (~ 600 – 1400 m; Fig. 3.1B). In contrast, at the three more northerly seamounts, temperatures above 12°C occur down to ~ 600 m and only fall below 5°C at ~ 1100 m. As scleractinian CWCs are most commonly found in waters of 4-12°C (Roberts et al., 2006), Coral Seamount may provide more suitable thermal conditions over a wider depth range. The location of Coral Seamount south of the STF, in the transition between two biogeographic provinces, could also contribute to its high diversity. In contrast, at the subtropical site of Atlantis Bank no flabellids or dendrophylliids were collected. The temperature profile at Atlantis Bank below 200 m is similar to Melville Bank, where dendrophylliids were present, but additional factors such as low POC concentration could reduce the viability of certain species at Atlantis Bank, even those known from temperate locations such as *B. gigas* and *L. stokesiana* (Stephen D. Cairns, 1995; Cairns and Zibrowius, 1997).

We also find some evidence of within-species variations between the four seamounts. A 'robust' morph of *C. diomedeae*, with exert, transversally ridged and laterally protruding septa was dominant at Atlantis Bank (Fig. 3.2A), whereas most specimens at Coral Seamount had less exert septa (Fig. 3.2B). It is worth noting that the Atlantis specimens are dated to the late Holocene, whereas all *C. diomedeae* from Coral Seamount are deglacial in age. A few specimens at Melville Bank and MoW Seamount share features of these two end members. To some extent a similar pattern is seen in *D. dianthus;* three specimens at Atlantis Bank have particularly flared septa and well-defined costae (Fig. 3.2C), whilst specimens to the south display a smoother corallum with less exert septa (Fig. 3.2D). These discrepancies exist between specimens of the same age at Atlantis Bank and Coral Seamount. Wide intraspecific variability is a characteristic of both of these species (Addamo et al., 2015; Kitahara et al.,

2010), and could be due to phenotypic flexibility in different environmental conditions, or genetic isolation and divergence (Miller et al., 2011). Either explanation could apply here, but since the variation could best be described as a spectrum across the seamounts, it seems more likely to be a response to environmental conditions such as temperature and/or food availability.

Overall, the variations in the subfossil CWC collection north and south of the STF give some support to the idea of biogeographic zonation. But there are also similarities in the species found, which may result from the water mass connectivity at depth. Without surveys and phylogenetic analyses on modern CWCs, the importance of these two factors cannot be quantified. The rarity of expeditions to the area and the disturbance of organisms and substrate because of trawling in the SWIO (Rogers and Taylor, 2011) are likely to inhibit these more robust investigations.

3.4.2 Temporal shifts in CWC populations

Uranium-series dating of the SWIO collection reveals variability in the distribution and diversity of CWCs over the past 25,000 years. Here we discuss patterns of coral abundance in relation to deglacial climate and regional oceanographic changes (Figs. 3.6-3.8).

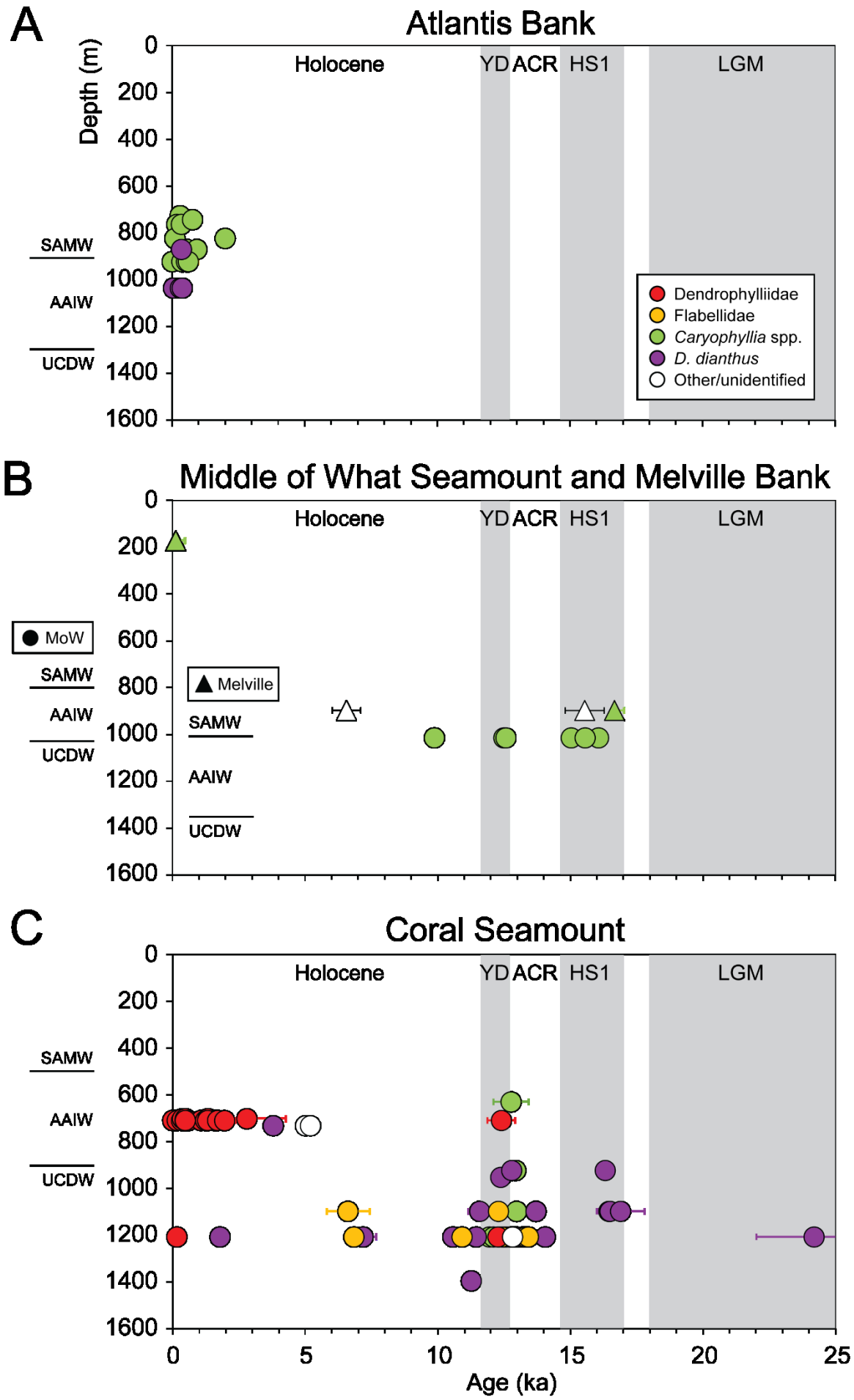
A
Atlantis Bank
Depth (m)
Holocene
YD
ACR
HS1
LGM
SAMW
AAIW
UCDW
Dendrophylliidae
Flabellidae
Caryophyllia spp.
D. dianthus
Other/unidentified
B
Middle of What Seamount and Melville Bank
MoW
Melville
C
Coral Seamount
Age (ka)

Figure 3.7: Depths and ages of subfossil CWCs at **A)** Atlantis Bank; **B)** Melville Bank (triangles) and Middle of What Seamount (dots) and **C)** Coral Seamount, colour coded by taxonomic category. Precise ages are given for samples which underwent isotope dilution U-series dating, and laser ablation ages are used for all other samples (see Appendices 1-3). Grey and white bars indicate the timings of the Holocene, Younger Dryas (YD), Antarctic Cold Reversal (ACR), Heinrich Stadial 1 (HS1), and the Last Glacial Maximum (LGM). The depths of boundaries between Subantarctic Mode Water (SAMW), Antarctic Intermediate Water (AAIW) and Upper Circumpolar Deep Water (UCDW) at each seamount are indicated by black lines.

3.4.2.1 The Last Glacial Maximum

One of the most notable aspects of the SWIO coral record is the absence, bar one *D. dianthus* specimen, of samples dating to the LGM (Figs. 3.5, 3.6). Preservation bias cannot be ruled out, though an older specimen, dated from MIS 6 (142 ± 8 ka) was found, and much older *D. dianthus* specimens from the subpolar region have previously been recorded (Burke and Robinson, 2012). It is unlikely that food supply was limiting; opal and organic carbon flux increases point to higher export production in the SAZ of both the Atlantic (Martínez-García et al., 2014) and Indian oceans (Dezileau et al., 2003) during the glacial. In general, coral recruitment will not occur unless there is a consistent supply of larvae to the region in question. Hence, the LGM absence of CWCs could indicate the existence of a barrier to larval dispersal into the SWIO at that time, for example, the ACC. In the Drake Passage, glacial age CWCs were found almost exclusively in the Antarctic Zone, leading Margolin et al. (2014) to suggest that the Polar Front posed a barrier to larval transport further north. As samples south of the Polar Front were not sampled in the SWIO, it is difficult to make direct comparisons. If larval dispersal to the SWIO seamounts from south of the ACC was inhibited during the glacial, a subsequent expansion of CWCs would require either a weakening of the ACC flow, or a

northward shift of the Southern Ocean fronts. Reconstructions of glacial flow speeds suggest a similar current speed (Mastumoto et al., 2001; McCave et al., 2014) or lower flow speed (Roberts et al., 2017) compared to the Holocene. In terms of frontal position, it is likely that the Polar Front occupied its most northerly position during the LGM, moving poleward during the early deglacial (Barker et al., 2009; De Deckker et al., 2012). Therefore, evidence for the Polar Front and ACC posing a greater barrier to CWC distribution in the subantarctic and subtropical Southern Ocean during the LGM is unconvincing. If the deglacial appearance of CWCs resulted from enhanced larval transport from lower latitudes, we would perhaps expect to see earlier occurrences at Atlantis Bank. The circumpolar transport of the ACC, the influence of the ARC, and the overturning circulation (Henry et al., 2014) could all have provided routes for widespread larval dispersal throughout the glacial and in the modern day.

Given the likelihood of an adequate food supply and open routes for larval dispersal northwards, we suggest that environmental boundary conditions limited CWC growth in the SWIO during the LGM. A broad consensus exists that a large proportion of glacial CO_2 was stored in the deep ocean as a result of a more effective biological pump and reduced deep ocean ventilation (Kohfeld and Chase, 2017). The resulting decrease in carbonate ion concentration and shoaling of the ASH (Sigman et al., 2010; Yu et al., 2010) may therefore have reduced the ability of CWCs to calcify, especially in deep waters. This environment may also have caused dissolution of existing subfossil CWCs, explaining the absence, bar one, of corals dating to earlier periods of more favourable climate conditions. Trace metal evidence also suggests intermediate waters were depleted in dissolved oxygen (Durand et al., 2018; Jaccard et al., 2016), likely resulting from stratification and increased isolation from the atmosphere (Burke et al., 2015). In addition, temperatures in intermediate waters are estimated to have been 3-5°C lower at this time compared to the Holocene, and deep waters ~ 3°C cooler than the deglacial maxima (Fig. 3.8E; Elmore et al., 2015; Roberts et al., 2016). We therefore suggest that a

shoaled ASH and cool, deoxygenated intermediate waters contributed to unfavourable conditions for CWC growth during the glacial, outcompeting any possible benefits of enhanced food supply. Glacial subfossil coral abundance is also low south of Tasmania (Fig. 3.8B; Thiagarajan et al., 2013) and in the subantarctic Drake Passage (Fig. 3.8C; Margolin et al., 2014), supporting a consistent circumpolar response of CWCs to the glacial boundary conditions.

3.4.2.2 The early deglacial, Heinrich Stadial 1

The early deglacial appearance of CWCs at the three seamounts south of the STF (Coral, Melville and MoW; Fig. 3.7) is concurrent with the onset of Antarctic warming and HS1 (18-14.7 ka; Fig. 3.8A) ~ 18 ka ago. During this time interval, release of a deep inorganic carbon pool through processes in the Southern Ocean is thought to have contributed to the atmospheric CO_2 rise (Marcott et al., 2014). Increases in benthic $\delta^{13}C$ (Ninnemann and Charles, 2002; Roberts et al., 2016), reductions in deep water ventilation age (Burke and Robinson, 2012; Skinner et al., 2010), and increases in abyssal carbonate ion concentrations (Yu et al., 2010) all support the deep ocean ventilation hypothesis. These processes may have resulted in a deepening of the ASH and improved conditions for CWC calcification. However, such changes in the deep and abyssal oceans may not have reached depths less than 1400 m at which CWCs were found; on the contrary, depletions in intermediate water radiocarbon have been reported (Bryan et al., 2010; Romahn et al., 2014), likely reflecting transient transport of the deep stored carbon into shallower levels before its release to the atmosphere.

During HS1, increased oxygenation is recorded in the deep Southern Ocean (Jaccard et al., 2016) and the intermediate northern Indian Ocean (Jaccard and Galbraith, 2012), which would have contributed to improving conditions for CWC growth. It is also possible that coral population growth was boosted by increased food supply in the form of sinking particulate organic matter, given the increase in opal flux in the Pacific and Atlantic sectors of the Southern

Ocean at this time (Anderson et al., 2009; Fig. 3.8D). We therefore suggest that the simultaneous appearance of subfossil corals in the SWIO, Tasmania (Thiagarajan et al., 2013), and the subantarctic Drake Passage (Margolin et al., 2014) during HS1 could have been facilitated by increasing oxygen concentrations and food supply, but was still limited by carbonate chemistry at mid-depths, particularly in the Indian and Pacific sectors of the Southern Ocean. Cold-water coral growth also seems to have been enhanced off the coast of Brazil during this time, potentially as a result of increased upwelling and food supply (Mangini et al., 2010).

3.4.2.3 The late deglacial

The greatest abundance of subfossil CWCs in the SWIO occurs in the late deglacial (33 specimens; Figs. 3.6, 3.7A), predominantly within the Younger Dryas (YD), between 13.5 and 11.5 ka. During this period, Coral Seamount supported a diverse community of at least seven solitary scleractinian species including *C. diomedeae*, *F. flexuosum* and *J. antarctica*. Notably, this peak in abundance is located at UCDW depths (~ 900-1400 m at Coral Seamount), with only four specimens found at modern-day AAIW depths. Late deglacial abundance peaks also occur at modern UCDW depths in the Tasmanian (Fig. 3.8B; Thiagarajan et al., 2013) and Drake Passage collections (Fig. 3.8C; Margolin et al., 2014).

As AAIW depths appear to be preferable for CWCs in the late Holocene, it is tempting to explain their presence deeper in the water column during the deglaciation by a deepening of AAIW and displacement of the lower-oxygen UCDW. Water mass boundaries will have occupied deeper positions in the water column as a result of lower sea level; however this effect can only account for ~ 60 m displacement between the YD and Holocene, rather than the observed 200 – 500 m depth shift observed at Coral Seamount. Because of the sloping isopycnals in this region (Fig. 3.1), a more southerly position of the SAF would effectively deepen AAIW at the SWIO and seamounts and around Tasmania. However, reconstructions

suggest the SAF occupied a similar position to the present day during the late deglacial (De Deckker et al., 2012; Roberts et al., 2017). A deepening of AAIW would also not explain the relative lack of corals from < 900 m. Hence, we consider other possible controls on the CWC distribution.

Oxygen concentrations below ~ 145 µmol/kg have been shown to limit respiration of certain *D. pertusum* (=*L. pertusa*) specimens in laboratory experiments (Dodds et al., 2007). An early- to mid-Holocene decline of CWC populations in the Mediterranean has been linked to a fall in oxygenation below ~ 180 µmol/kg (Fink et al., 2012), and low oxygen also appears to affect the distribution of CWCs in the late Holocene south of Tasmania (Thiagarajan et al., 2013). Elevated oxygen concentrations recorded in the intermediate northern Indian Ocean (Jaccard and Galbraith, 2012) and the deep Southern Ocean (Jaccard et al., 2016) during the period of relative CWC abundance in the SWIO, suggest a plausible role for oxygenation. Intermediate water pH in the Drake Passage also peaked during this time (Rae et al., 2018). Although these ocean chemistry reconstructions cover density intervals below the corals in this collection, chemical changes could feasibly have been communicated to UCDW depths.

Increased food availability is also an important driver of CWC fitness (Naumann et al., 2011), and for cold-water corals this consists of particulate organic carbon and microorganisms (Roberts et al., 2009). There is clear evidence for higher export production in the Antarctic Zone of the Atlantic Southern Ocean at 13-11.5 ka, coeval with the CWC abundance peak (Anderson et al., 2009; Fig. 3.8D). Enhanced export production could have resulted in higher POC concentrations at depth, supplying CWCs with nutrition in the SAZ. However, the most likely path for northward transport of this food supply would be in surface currents and AAIW via Ekman pumping (Marshall and Speer, 2012). In the SWIO, UCDW flows northward above 1500 m (McCave et al., 2005), so could also have advected POC northwards towards Coral Seamount, but it seems unlikely that it would have been the main conduit. Productivity peaks

and an associated increase in food availability may explain the overall increase in abundance of CWCs during the late deglacial period, but do not explain the apparent preference for UCDW depths.

Global scale modelling of CWC distribution shows a strong correlation with temperature (Davies and Guinotte, 2011), and although a lower limit has not been tested in laboratory experiments (to our knowledge), CWCs are rarely found below temperatures of 1°C (Stanley and Cairns, 1988). *Desmophyllum dianthus* has been found in waters as cold as 1°C in the Drake Passage (Margolin et al., 2014), and in the late Holocene SWIO we find specimens at depths corresponding to modern temperatures of between ~ 16°C and 3°C. In the subantarctic South Atlantic, Mg/Ca-derived temperature reconstructions suggest that intermediate waters were colder than deep waters for much of the deglacial interval, initially at -1 to -2°C and remaining below 1°C until the early Holocene (Roberts et al., 2016; Fig. 3.8E). Deep waters were warmer at around 0-2 °C during the early deglacial and reached a peak of 4°C between 13 and 11ka, with a stable vertical density stratification being conserved because of higher salinities at depth (Adkins et al., 2002b; Roberts et al., 2016). Therefore, we propose that low temperatures may have been an important factor in the relative paucity of CWCs from AAIW depths during the deglacial. In addition, we note that deep waters in the Indian, Pacific, and Atlantic oceans reached a peak in carbonate ion concentration between 15 and 10 ka (Yu et al., 2010). Such globally enhanced carbonate ion concentrations would have deepened the ASH, and possibly enabled the expansion of CWCs into CDW, which by that time had reached a warmer and more optimal temperature.

In summary, we propose that increased oxygenation, a deepened ASH, warmer temperatures, and a peak in regional food supply created suitable conditions for CWC growth in UCDW depths during the YD. In contrast, CWCs may have been unable to survive at AAIW

depths until the salinity-controlled stratification broke down and temperatures increased in the Holocene.

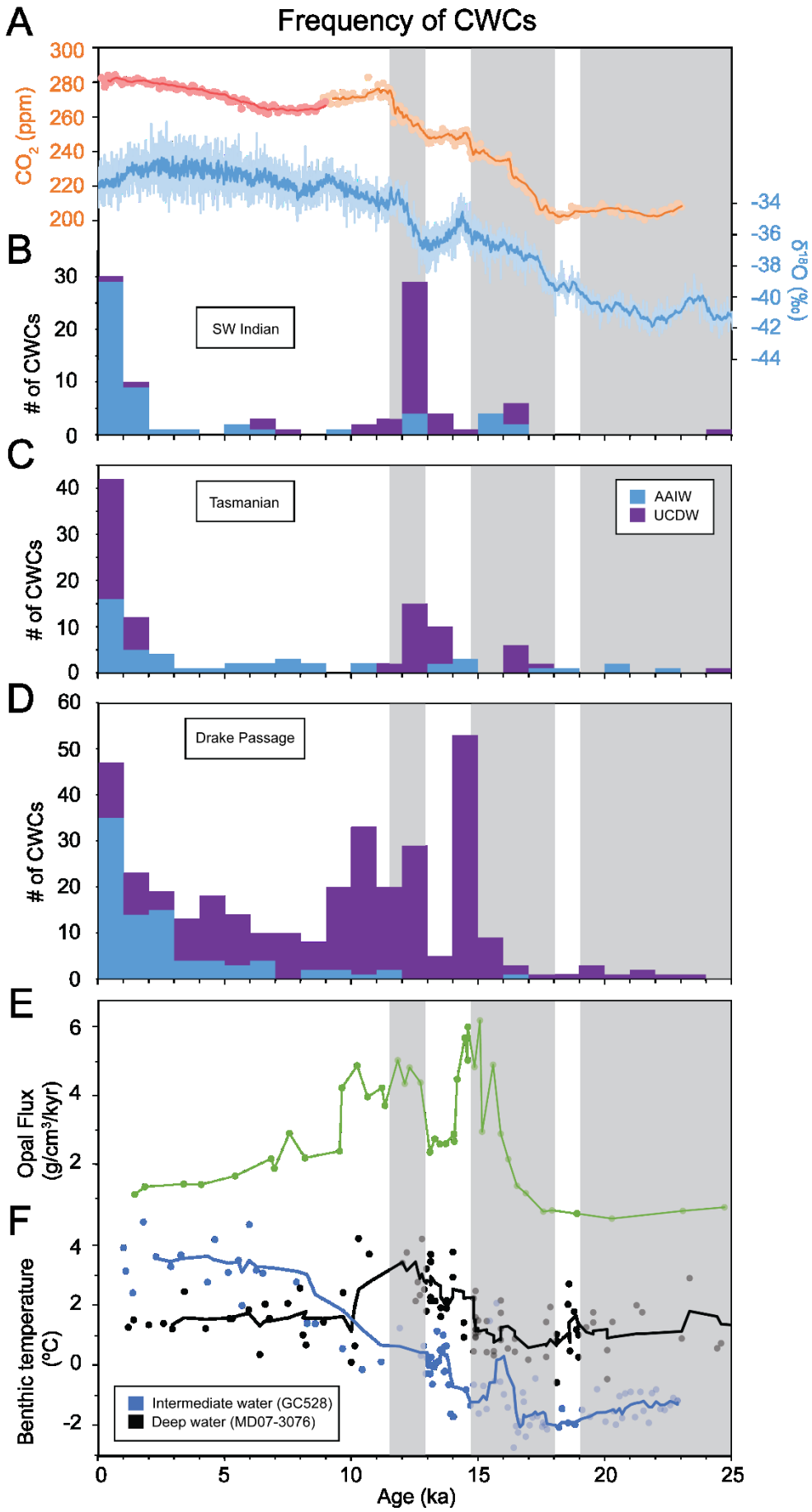
A
Frequency of CWCs
CO2 (ppm)
300
280
260
240
220
200
-34
-36
-38
-40
-42
-44
δ18O (‰)
B
# of CWCs
30
20
10
0
SW Indian
C
# of CWCs
40
30
20
10
0
Tasmanian
AAIW
UCDW
D
# of CWCs
60
50
40
30
20
10
0
Drake Passage
E
Opal Flux (g/cm3/kyr)
6
4
2
F
Benthic temperature (ºC)
4
2
0
-2
Intermediate water (GC528)
Deep water (MD07-3076)
0
5
10
15
20
25
Age (ka)

Figure 3.8: Number of cold-water corals (CWCs) per 1000-year age bin at three Southern Ocean locations, coded by water mass, with Antarctic Intermediate Water (AAIW) in blue and Upper Circumpolar Deep Water (UCDW) in purple. Precise ages are given for samples which underwent isotope dilution U-series dating, and laser ablation ages are used for all other samples (see Appendices 1-3). **A)** SW Indian CWCs (this study), overlain with the West Antarctic Ice Sheet (WAIS) Divide Core $\delta^{18}O$ record and 11-point moving average (WAIS Divide Project Members, 2015), and composite CO_2 record with 5-point moving averages from WDC (orange, Marcott et al., 2014) and EPICA (red, Monnin et al., 2001). **B)** Tasmanian *D. dianthus* abundances (Thiagarajan et al, 2013), assigned to water mass following Hines et al. (2015; AAIW 500-1500 m). **C)** Drake Passage *D. dianthus* abundances, using water mass designations from Margolin et al. (2014). **D)** Opal flux record from South Atlantic core TN057-13-4PC (53.1728°S, 5.1275°E, 2848 m; Anderson et al., 2009). **E)** Mg/Ca-derived benthic temperatures for intermediate (GC528, 598 m; blue) and deep waters (MD07-3076, 3770 m; black) from the subantarctic South Atlantic (Roberts et al., 2016).

3.4.2.4 The Holocene

Specimens from the early- to mid-Holocene are notably scarce in the SWIO collection, with only seven specimens dating to between 5 and 10 ka, all collected from south of the STF (Figs. 3.5, 3.6A). Those that were found are poorly preserved (Fig. 3.5), possibly indicating greater susceptibility to degradation. During this time interval, deep water carbonate ion concentrations reached their lowest values (Yu et al., 2010). It is possible that a shoaled ASH reduced the suitability of UCDW, whilst the temperature of AAIW was still sub-optimal for coral growth (Fig. 3.8E; Roberts et al., 2016). Corals are present throughout this period in the Tasmanian and Drake Passage collections (Fig. 3.8B, C), but at much lower abundances than during the ACR (Margolin et al., 2014; Thiagarajan et al., 2013).

After this decrease in abundance, the number of CWC specimens increases at Coral and Atlantis (Fig. 3.7). Late Holocene CWC specimens are found at shallower depths compared to the deglacial period, with 95 % of CWC dated to < 6 ka being found in SAMW or AAIW (Fig. 3.8A). Only two specimens dated to < 6 ka are found below 750 m at Coral Seamount, within UCDW depths, and no live corals were seen below 700 m during ROV surveys (Rogers and Taylor, 2011). In the southeast Pacific (Cape Horn) and Drake Passage (Burdwood Bank), Late Holocene corals are also more common above 1000 m (Margolin et al., 2014; Fig. 3.8C). South of Tasmania, the CWCs undergo a depth expansion from 2000 to 2400 m in CDW depths, with abundant corals also at shallower AAIW depths, but with a 'hiatus' at depths of 1500-1800 m influenced by lower dissolved oxygen values (170-180 µmol/kg; Thiagarajan et al., 2013).

In the modern subantarctic SWIO, 900-1000 m marks the upper boundary of UCDW, a water mass which brings in old, nutrient-rich deep waters from the northern Indian Ocean and which is associated with a similar dissolved oxygen minimum (< 180 µmol O_2 /kg from 1000 – 1500 m; Figs. 3.1B, 7) to the Tasmanian coral hiatus (Thiagarajan et al., 2013). The depth of the ASH, controlled mainly by temperature and pressure, is also approximately coincident with UCDW in the region of Coral Seamount (~ 1400 m; Sabine et al., 2002; Fig. 3.9). Because sampling did not take place below the ASH or oxygen minimum, it is difficult to evaluate their relative influence. However, the coincidence of most late Holocene CWCs between 600 and 800 m with the oxygen peak within AAIW (~ 220 µmol/kg) is striking.

The absence of CWCs from Atlantis Bank before the late Holocene (Fig. 3.7A) is difficult to explain in terms of any of the above discussed environmental factors, and may instead be an artefact of the limited depth survey performed there. Today, surface waters at Atlantis Bank have the lowest chlorophyll fluorescence of the four seamounts (Djurhuus et al., 2017b), indicating low productivity and a limited food source, although modern corals there may benefit from organic matter export via SAMW. If anything, food supply at Atlantis Bank

is likely to have been higher in the past as a result of increased iron fertilisation (Kohfeld et al., 2005) and a northward-shifted STF (De Deckker et al., 2012; Sikes et al., 2009), making food supply an unlikely factor in controlling their absence. Similarly, temperatures were likely no warmer and oxygen concentrations similar throughout the Holocene at these depths. However, it could perhaps be the case that favourable calcification conditions arose only in the late Holocene, because the ASH shoals to the north in the modern day SWIO (Sabine et al., 2002), making this location particularly sensitive to changes in ocean carbonate chemistry.

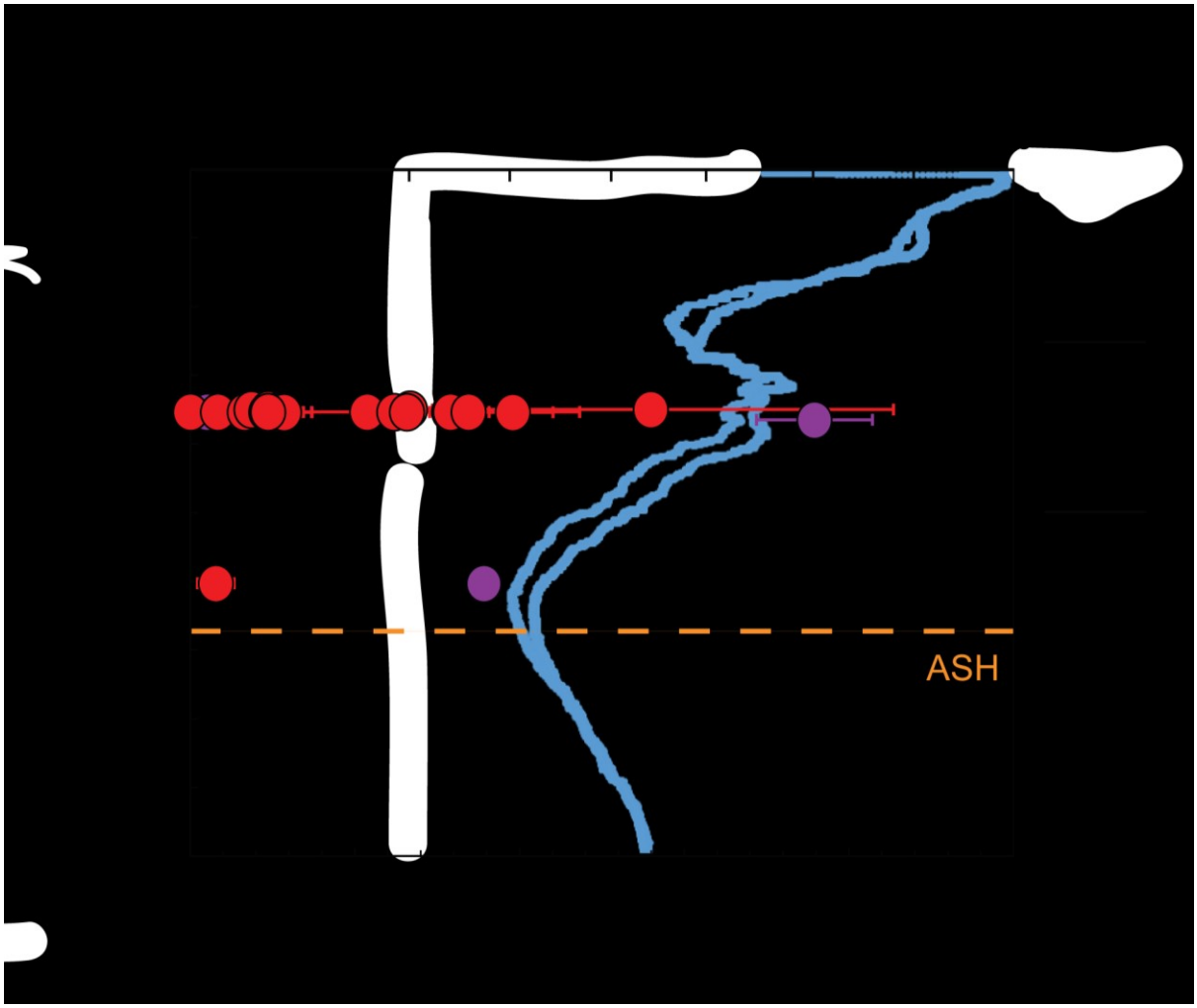

Figure 3.9: Depths and ages (lower axis) of Late Holocene corals at Coral Seamount, colour coded by taxonomic grouping where red dots are Dendrophylliidae and purple dots are *Desmophyllum dianthus*. Precise ages are given for samples which underwent isotope dilution U-series dating, and laser ablation ages are used for all other samples (see Appendices 1-3). Blue curves show seawater oxygen concentration from CTD data at Coral Seamount (upper axis) and the approximate depth of the aragonite saturation horizon (ASH; Sabine et al., 2002) is indicated in orange. Modern day boundaries between Subantarctic Mode Water (SAMW), Antarctic Intermediate Water (AAIW) and Upper Circumpolar Deep Water (UCDW) are indicated with black lines.

3.5 Conclusion

The species assemblage of subfossil scleractinian corals recovered from SWIO seamounts indicates influences from the Indian, Pacific, and Antarctic biogeographic zones. Particular diversity and abundance of CWCs at Coral Seamount may be a result of its location in the SAZ, between the Antarctic and Indian biogeographic zones, and higher food availability. We also find indications of biogeographic controls on morphology across the seamount transect, with a more robust *D. dianthus* and *C. diomedeae* morphology occurring more commonly north of the STF, compared to specimens from intermediate and deep waters in the SAZ.

Striking similarities in the temporal distribution of CWCs from the SWIO with other Southern Ocean CWC collections hint at widespread impacts on coral habitats from deglacial changes in ocean stratification and biogeochemistry. As observed elsewhere in the subpolar Southern Ocean, solitary coral growth seems to have been limited during the LGM. Unfavourable carbonate, temperature, and oxygen conditions may have outweighed higher productivity in the SAZ. Although CWCs begin to appear during HS1, we argue that carbonate and oxygen conditions did not become optimal until the late deglacial (14 -11.5 ka), when a peak in abundance is seen in solitary CWC records from the SWIO, Tasmania, and the Drake Passage. This abundance peak is coincident with increased productivity in the Antarctic Zone, which could have provided enhanced supply of POC to the SAZ sites via advection. Water temperatures within AAIW may have been below the habitable range, a possible explanation for the relative lack of solitary CWCs at intermediate depths at this time. In contrast, warmer temperatures within UCDW, combined with greater oxygenation, higher deep-water carbonate ion concentrations and a deeper ASH than during the LGM, could have facilitated colonisation at UCDW depths.

In the late Holocene SAZ, the mid-depth oxygen minimum associated with the inflow of old deep waters from the Indian and Pacific Oceans appears to have been a less favourable habitat for solitary CWCs in the SWIO and Tasmania than well-oxygenated AAIW depths. This observation suggests that their survival here requires higher oxygen concentrations than cold-water coral reefs elsewhere. Future investigations on larger numbers of CWCs, collected in a systematic survey of this region, combined with a greater understanding of the responses of solitary CWC to environmental conditions, would likely provide stronger constraints on the patterns we describe, and on future responses of CWCs to environmental change.

Statement of contribution

This project was a collaborative effort involving all authors of the publication. Samples were supplied by Tina van de Flierdt, following collection on cruise JC066 by Alex Rogers and Michelle Taylor. I carried out sample identifications, prepared samples for dating and interpreted the data. Laser ablation and isotope dilution U-series dating and data processing was led by Tianyu Chen, with Tao Li carrying out part of the isotope dilution U-series analyses, under the supervision of Laura Robinson at the University of Bristol. Nadia Santodomingo provided training and guidance on taxonomic analysis of the specimens at the Natural History Museum. David Wilson and Susan Little aided discussions on data interpretation, and along with all others mentioned edited the manuscript prior to publication.

Chapter 4: Reconstructing deglacial water mass changes in the southwest Indian Ocean using cold-water coral Nd isotopes

Chapter summary

The history of water mass changes in the Southern Ocean is integral to our understanding of the role of the region in deglacial climate change pacing and mechanisms. In this study the new collection of fossil cold-water corals from the southwest Indian Ocean was utilised to reconstruct intermediate water mass variations using neodymium isotopes. The samples date from HS1 to the modern day, with particularly high sample resolution during the YD. Apart from slightly more radiogenic values found at Middle of What Seamount in the early deglacial, the neodymium isotopic compositions of samples fall consistently within the modern seawater range, indicating consistent supply of Atlantic sourced waters to the intermediate Southern Ocean, in contrast to records from the deep ocean. During HS1, samples at Coral Seamount are slightly less radiogenic than corals at Middle of What and the other Southern Ocean sites, possibly resulting from the influence of shoaled NADW flowing directly into the Indian Ocean. This mechanism may also be responsible for the rapid variations observed at Coral Seamount during the YD between ε_{Nd} values of ~ -8, similar to the Drake Passage record, and ~ -9, closer to Cape Basin values.

4.1 Introduction

Variability in ocean circulation and ventilation is thought to have been instrumental in the warming and millennial-scale climate changes that took place during the most recent deglaciation (19 - 10 ka; Broecker and Barker, 2007; Burke and Robinson, 2012; Rae et al., 2018; Sigman et al., 2010). Deep water records have provided a crucial insight into these

dynamics (e.g. McManus et al., 2004; Piotrowski et al., 2012; Roberts et al., 2010), but data from mid-depths, especially in the Indian Ocean, are sparse.

To understand past ocean circulation, it is useful to employ tracers of water mass provenance and mixing which are not affected by biological activity; neodymium (Nd) isotopes can be utilised in this manner. Water masses acquire different Nd isotopic compositions at the interface with continents, which show a large range in isotopic composition due to differences in age and lithology (Frank, 2002; Goldstein and Hemming, 2003). The relatively short oceanic residence time of neodymium (500 - 785 years; Gu et al., 2019; Rempfer et al., 2011; Tachikawa et al., 2003) in turn means it is removed before it becomes homogenised by global overturning circulation. The Nd isotope composition of seawater, expressed as ε_{Nd} (the deviation of the sample $^{143}Nd/^{144}Nd$ ratio relative to the Chondritic Uniform Reservoir value in parts per 10,000), appears to behave conservatively away from ocean margins in large parts of the oceans, enabling it to be used as a water mass tracer.

Cold-water corals have been shown to accurately record the Nd isotopic composition of the waters in which they grew (Colin et al., 2010; Struve et al., 2017; van de Flierdt et al., 2010, 2006), and they can be dated using precise U-series methods, making them a powerful palaeoceanographic archive. There is currently a growing database of Nd isotope records from deep sea corals, especially in the North Atlantic and Southern Ocean regions and at intermediate depths (see Robinson et al., 2014 for a recent review), complementing deep and bottom water records from sediment cores (e.g. Piotrowski et al., 2005; Roberts et al., 2010; Skinner et al., 2013) and ferromanganese crusts (e.g. Foster et al., 2007).

In this study we aim to reconstruct the deglacial water mass history of the southwest Indian Ocean using precisely dated cold-water corals. As waters from the Pacific and Atlantic are mixed in the circumpolar Southern Ocean before they reach the region as intermediate and

deep water masses (Talley, 2013), changes in the nature of the overturning circulation and water mass mixing may be recorded here. Evidence of shifts in the fronts of the ACC and corresponding vertical movement of water mass boundaries could be found in this region (Ferrari et al., 2014), with implications for carbon outgassing (Marcott et al., 2014; Toggweiler et al., 2006). Due to the proximity of the ARC, this study may also provide insights into the history of Agulhas leakage, a mechanism by which warm, salty water is released from the Indian Ocean into the Atlantic, playing an important role in the global overturning circulation (e.g. (Bard and Rickaby, 2009; Beal et al., 2011; Martinez-Mendez et al., 2010; Peeters et al., 2004a).

4.2 Regional setting, samples, and methods

The subfossil coral samples discussed in this chapter were collected in 2011 during expedition JC066 of the *RV James Cook* from four seamounts along the southwest Indian Ocean Ridge (SWIOR). From south to north, these are Coral Seamount (41°21'23" S, 42°50'31" E), Melville Bank (38°31'56" S, 46°45'74" E), Middle of What Seamount (37°56'76" S, 50°22'16" E), and Atlantis Bank (32°42'01" S, 57°17'26" E).

4.2.1 Hydrography of the southwest Indian Ocean

The SWIOR intersects the boundary between the South Indian subtropical gyre and the Southern Ocean, in a particularly dynamic region of the world ocean (Fig. 4.1). To the south, the ACC flows eastward, uninterrupted by continental land masses. Its flow, which is taken up along three main fronts (the SAF, PF and SACCF), causes isopycnals to slope upward to the south, allowing deep waters to rise to the surface. The Agulhas Current transports warm, salty water along the western boundary of the Indian Ocean, overshooting south of Africa and

retroflecting to the east, where it is found close to the STF. These features are found at around 40°S in the vicinity of the SWIOR (Deacon, 1982; Sokolov and Rintoul, 2009; Wong, 2005), at approximately the same latitude as Middle of What Seamount and Melville Bank.

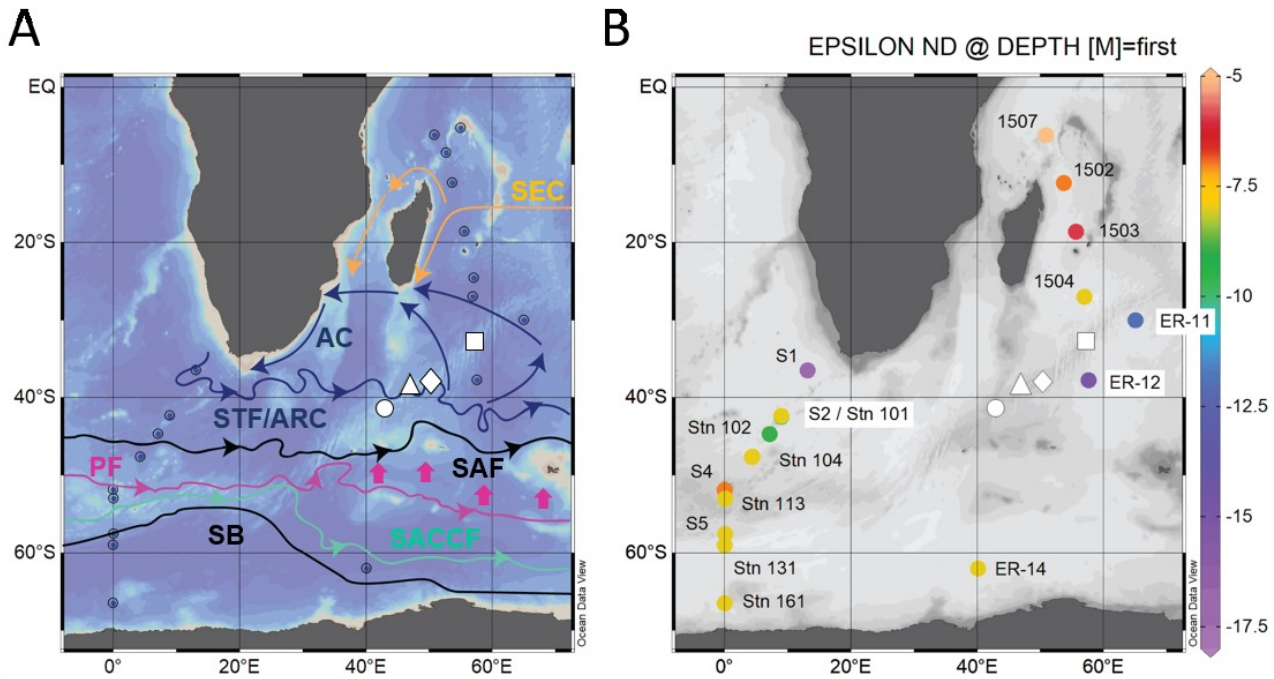

Figure 4.1: Map views of **A)** modern surface hydrography and **B)** modern surface water εNd in the southwest Indian Ocean, southeast Atlantic Ocean and Indian sector of the Southern Ocean. Seamount locations from this study are shown by white filled symbols, from south to north: Coral Seamount (circle), Melville Bank (triangle), Middle of What Seamount (diamond), and Atlantis Bank (square). Frontal positions and surface current paths are indicated by solid lines, from north to south: the South Equatorial Current (SEC; orange) and Agulhas Current (AC; blue; Tomczak and Godfrey, 2003); Subtropical Front (STF) and Agulhas Return Current (ARC; blue; Sokolov and Rintoul, 2009); the fronts of the Antarctic Circumpolar Current, the Subantarctic Front (SAF; black), the Polar Front (PF; magenta), and the Southern ACC front (SACCF; teal), and the southern boundary of the ACC (SB; black; Sokolov and Rintoul, 2009). The area of AAIW formation north of the PF is marked with magenta arrows (Fine, 1993; Wong, 2005). Blue dots mark the positions of modern seawater εNd measurements. In (B), the colour of each dot represents the εNd value of the shallowest seawater sample

(0 - 500 m) at stations from Charles Darwin cruise 15 (1502, 1503, 1504 and 1507; Bertram and Elderfield, 1993), and GEOTRACES transects GI04 (ER-11, -12 and -14; Amakawa et al., 2019), GIPY04 (S1, S2, S4 and S5; Garcia-Solsona et al., 2014) and GIPY05_e (Stn 101, Stn 102, Stn 104, Stn 113, Stn 131 and Stn 161; Stichel et al., 2012).

At intermediate depths, the two main masses in the region are SAMW and AAIW, advected northwards into the Indian Ocean north of the SAF and PF respectively. The primary site for AAIW formation in the Southern Ocean is thought to be the southwest Atlantic and southeast Pacific sectors (Talley, 1996), but there is also evidence of recently formed AAIW injection in the south Indian ocean west of 72°E (Fine, 1993; Wong, 2005). Near the African continent, AAIW recirculates as part of the Agulhas Current, flowing south and mixing with Red Sea Water and Indonesian Intermediate Waters (Donohue and Toole, 2003; You, 2002). Due to the sloping isopycnals in the ACC, water mass boundaries cross the SWIO seamounts at shallower depths at Coral Seamount than at the three northerly seamounts. Antarctic Intermediate Water is found between ~ 500 - 1020 m at Coral Seamount, where it is slightly fresher, whereas at Melville Bank it is seen at 1015 – 1335 m, at Middle of What Seamount 950 – 1400 m, and 900 – 1315 m at Atlantis Bank.

Underlying AAIW, UCDW is found down to depths of ~ 2000 m at Coral Seamount and ~ 2400 m at the other seamounts, marked by an oxygen minimum. Comprised of Indian and Pacific Deep Waters, as well a fraction of NADW (Tomczak and Godfrey, 2003), UCDW flows northwards through fracture zones in the SWIOR (McCave et al., 2005).

The hydrography in the vicinity of Coral Seamount differs from the other coral collection locations, in that surface waters above it are subantarctic rather than subtropical (Read and Pollard, 2017; Fig. 4.2). The AAIW found there is also slightly fresher, and the

salinity maximum of NADW is more apparent at ~ 2000 m water depth (Fig. 4.2). In these respects, it shares a similar hydrography to stations in the Subantarctic Zone of the southeast Atlantic (e.g. S2; Garcia-Solsona et al., 2014). The three other seamounts have very similar hydrographic profiles to each other and to nearby profiles ER-11 and ER-12 (Amakawa et al., 2019), with STSW overlying SAMW, AAIW, and circumpolar deep waters. The properties of the water masses found in the region are detailed in Table 4.1.

Table 4.1: Water mass properties in the southern Indian and southeast Atlantic Ocean regions

water mass	**salinity**	**potential temperature (^{o}C)**	**neutral density (kg m^{-3})**	**citation**
SASW	33.5-34	4.0-14	<27.0	Lambelet et al. (2018)
STSW	35.5-35.6	15-24		Read and Pollard (1993)
SAMW	34.5-35.3	7.1-13.7	26.5-27.13	Lee et al. (2015); Plancherel (2012)
AAIW	34.4-34.6	2.9-5.4	27.13-27.55	Lee et al. (2015); Stichel et al. (2012)
UCDW / IDW	34.54-34.7	1.6-2.5	27.55-28	Rintoul et al. (2001); Garcia-Solsona et al. (2014a); Lambelet et al. (2018)
NADW	~ 34.8	1.9-2.5	27.7-28.27	Stichel et al. (2012)

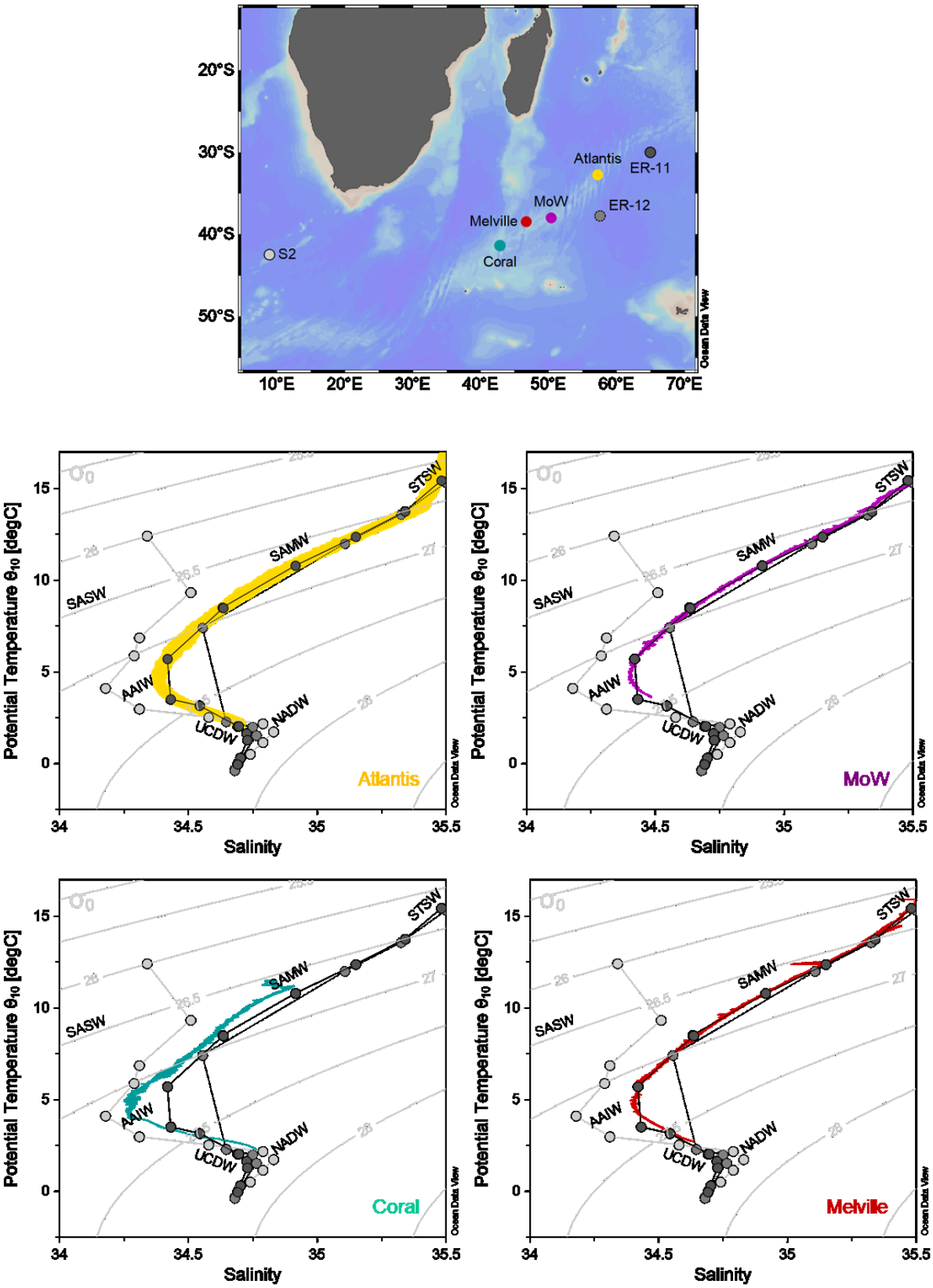

Figure 4.2: Seawater potential temperature and salinity CTD data from ERIDANUS Expedition (KH-09-5) stations (ER-11; dark grey; ER-12; medium grey; Amakawa et al., 2019), BONUS GoodHope

(BGH) IPY-GEOTRACES cruise stations (S2; light grey; Garcia-Solsona et al., 2014) and JC066 seamounts (Djurhuus, pers. comm.). Water mass temperature and salinity values are indicated by annotations (citations in Table 4.1).

As the mid-depth water masses are well mixed in the Southern Ocean before reaching the SWIO, there is not much discrepancy between their neodymium isotope compositions; both AAIW and UCDW have an ε_{Nd} range of ~ -8.4 to -7.9 (Stichel et al., 2012; Garcia-Solsona et al., 2014; Amakawa et al., 2019). The exceptions to this relative homogeneity are the Agulhas Current (ε_{Nd} ~ -12 to -15; Amakawa et al., 2019; Fig. 4.3) and NADW, which enters the basin south of South Africa at ~ 2000 m (ε_{Nd} ~ -9.3; Amakawa et al., 2019; McCave et al., 2005).

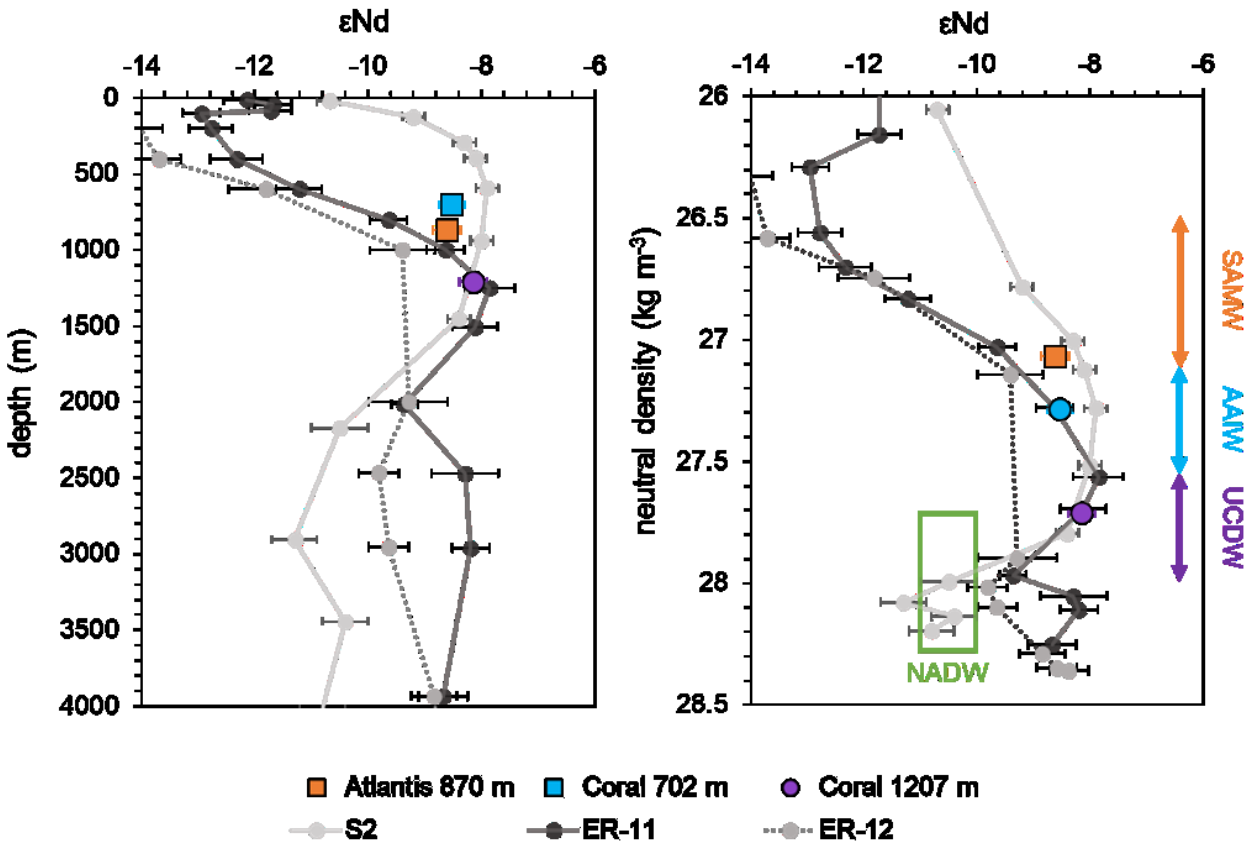

Figure 4.3: Neodymium isotope composition of direct seawater analyses illustrated with depth (left panel) and neutral density (right panel) from selected stations. Dark grey dots illustrate station ER-11

and medium grey dots and dotted line are from station ER-12 (Amakawa et al., 2019). Pale grey dots are from the southeast Atlantic (S2; Garcia-Solsona et al., 2014). Large coloured symbols show Nd isotope compositions of late Holocene cold-water corals in the SWIO (this study). Water mass neutral density ranges for Subantarctic Mode Water (SAMW; Plancherel, 2012), Antarctic Intermediate Water (AAIW; Stichel et al., 2012; Lambelet et al., 2018) and Upper Circumpolar Deep Water (UCDW; Lambelet et al., 2018; Rintoul et al., 2001) are indicated by coloured arrows. The neutral density and εNd range of modified North Atlantic Deep Water in the southeast Atlantic Ocean is indicated by the green box (Stichel et al., 2012).

4.2.2 Materials and methods

A total of 161 fossil scleractinian coral skeletons were sampled opportunistically during dives of the Kiel 6000 ROV (Rogers and Taylor, 2011). Following age screening using a rapid laser ablation method, 55 samples were selected for precise dating including 2 duplicates. These were all from the species *Desmophyllum dianthus* or genus *Caryophyllia*, as these were robust enough to withstand the cleaning procedures and have been calibrated to modern seawater for Nd isotopes most successfully (Copard et al., 2010; Struve et al., 2017; van de Flierdt et al., 2010). All dated samples were then screened for their Nd concentrations. Of these, 34 coral samples containing > ~ 10 ng Nd were selected for Nd isotope analysis (Table 4.2).

Two samples had $\delta^{234}U_i$ values outside of the modern-day ocean values, and four had concentrations of ^{232}Th above 3000 ppt; these were omitted retrospectively from interpretations (Table 4.2). The remaining 28 samples comprise three corals from the late Holocene (Coral Seamount and Atlantic Bank) and 25 from the deglacial period (Coral Seamount and Middle of What Seamount), spanning 10.6 – 16.5 ka. Due to the nature of sampling, many corals were collected from the same depths: ~ 950 m (n = 3), 1097.2 m (n = 5) and 1207.2 m (n = 12) at Coral Seamount and 1014 m at MoW Seamount (n = 5). The sample set covers each water mass

in the late Holocene, and provides the best possible coverage for the deglacial period, both temporally and in terms of inferred water mass sampling.

Full details of the sample preparation, dating, neodymium separation and measurement methodology can be found in Chapter 2.

4.3 Results

Over the period 16.0 to 0.4 ka the Nd isotopic composition of 34 cold-water corals from 700 to 1395 m depth in the southwest Indian Ocean ranges from -9.2 to -6.7 (Fig. 4.4).

Samples from 702 m to 1395 m water depth at Coral Seamount span the full range of ages in the record and their Nd isotopic composition encompasses values from -9.2 ± 0.2 to -7.2 ± 0.2 (Fig. 4.1). The oldest deglacial sample at this location dates to 16. 4 ka and records an ε_{Nd} value of ~ -7.9 ± 0.3. Most samples at Coral Seamount date to between 14 and 10 ka (n = 22). Corals in this age range were recovered from between 922 and 1395 m water depths and fluctuate in their Nd isotopic composition between ε_{Nd} = -8 and ε_{Nd} = -9 on sub-centennial timescales. It is notable that only samples from the deepest depths at Coral Seamount, 1200-1400 m, reach the most unradiogenic values below -9. Two late Holocene samples record ε_{Nd} values of -8.1 ± 0.2 (1207.2 m water depth, 1713 ± 48 years BP) and -8.5 ± 0.2 (702 m water depth, 417 ± 128 years BP; Fig. 4.3).

The five samples analysed from Middle of What Seamount were all deglacial in age and from 1014 m depth. They have the most radiogenic Nd isotope values in the collection, decreasing with time from -6.7 ± 0.4 at 15.5 ka, which is distinct from contemporaneous Coral Seamount samples, to -8.0 ± 0.2 at 12.4 ka (Fig. 4.4).

The only sample measured from Atlantis Bank was late Holocene in age (493 ± 81 years BP) and records an ε_{Nd} of -8.6 ± 0.2 (Figs. 4.3, 4.4). This sample was recovered from 870 m water depth, equivalent to modern SAMW.

The single sample measured from Melville Bank (897 m water depth, 16.7 ± 0.3 ka) gave a more radiogenic Nd isotope composition than the samples from similar depths at Coral Seamount (-7.3 ± 0.3), but had a Th concentration of 3281 ppt and will hence be omitted in the discussion.

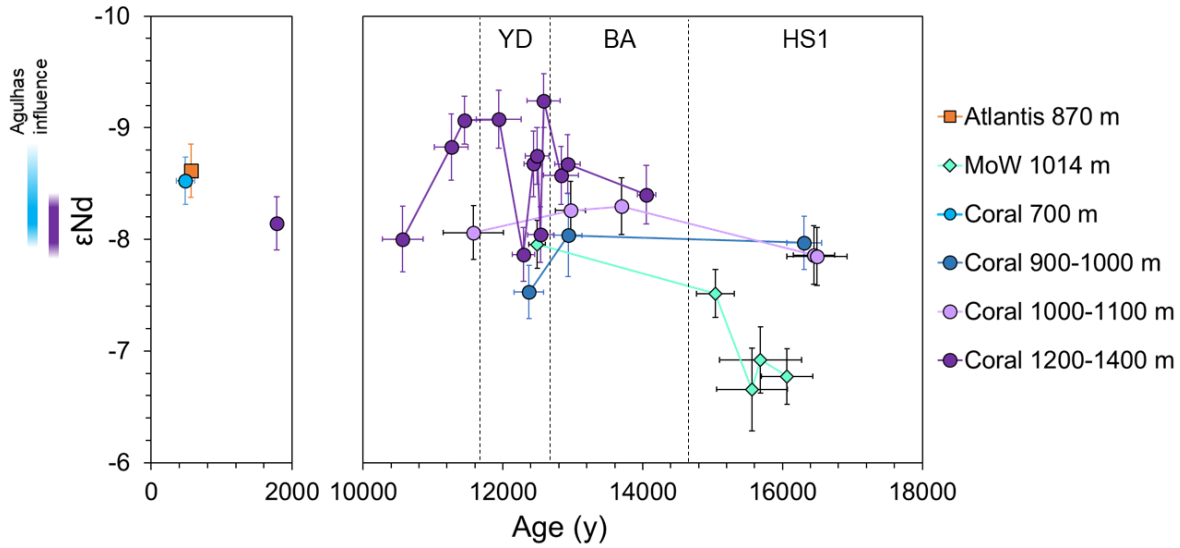

Figure 4.4: Southwest Indian Ocean deglacial and late Holocene εNd data from cold-water corals collected from Atlantis Bank (orange square), Middle of What (MoW) Seamount (turquoise diamonds) and Coral Seamount (blue and purple circles). Data from Coral Seamount are split into depth boundaries corresponding to modern AAIW (blue) and UCDW (purple) depths. The modern εNd range of these water masses in the region (Amakawa et al., 2019, stations ER-11 and ER-12; Garcia-Solsona et al., 2014, station S2) are indicated by blue and purple bars to the left of the figure. Northern Hemisphere deglacial time periods are separated by dashed lines: Heinrich Stadial 1 (HS1); Bølling-Allerød (BA) and Younger Dryas (YD).

4.4 Discussion

4.4.1 'Modern' Nd isotope distribution in waters and corals of the SWIO

The Indian Ocean is the least studied of all the ocean basins with regard to its modern dissolved Nd isotope distribution (van de Flierdt et al., 2016). In the vicinity of the SWIO ridge, four depth profiles exist, two recently published from GEOTRACES transect GI04 (cruise KH-09-5, stations ER-11 and ER-12; Amakawa et al., 2019) and two from the Madagascar Basin (Fig. 4.1, 1504 and 1505, Bertram and Elderfield, 1993). Further afield, there are seawater profiles from the Mascarene and Somali Basins (Fig. 4.1, 1502, 1503, 1507; Bertram and Elderfield, 1993), and one from the Indian sector of the Southern Ocean (Fig. 4.1, ER-14; Amakawa et al., 2019). Being upstream of the region, it is also useful to refer to data from the southeast Atlantic, a more comprehensively studied region covered by two transects (Fig. 4.1, Stn 101, 102, 104, 113, 131 and 161; Stichel et al., 2012; S1, 2, 4 and 5; Garcia-Solsona et al., 2014).

The influence of Agulhas waters can be clearly seen in unradiogenic surface water ε_{Nd} values at S1 (-17.1 ± 0.2; Garcia-Solsona et al., 2014), ER-12 (-15.27 ± 0.4) and ER-11 (-12.15 ± 0.4; Amakawa et al., 2019; Fig. 4.1). Stations S2 and 102 also appear to record some Agulhas influence (Stichel et al., 2012; Garcia-Solsona et al., 2014). The more radiogenic surface waters recorded at stations 1503, 1502 in the Mascarene Basin and 1507 in the Somali Basin (ε_{Nd} = -7.0 ± 0.7; -7.0 ± 0.5 and -6.0 ± 0.7, respectively; Bertram and Elderfield, 1993), could be influenced by the South Equatorial Current (SEC) or local volcanic sources of the Mascarene Plateau (ε_{Nd} = 6.3 ± 1.6; White et al., 1990) and Reunion Island (ε_{Nd} = 3.1-4.5; Bosch et al., 2008). Outside of these areas, surface waters in the region fall between Nd isotope compositions of -7.5 and -9 (Amakawa et al., 2019; Stichel et al., 2012; Garcia-Solsona et al., 2014).

To understand the Nd isotopic composition at depth we utilise water profiles S2 (Garcia-Solsona et al., 2014), ER-11 and ER-12 (Amakawa et al., 2019), which show the closest resemblance in their hydrography at the point of sampling to the hydrography observed during the coral collection at the SWIO seamounts (Fig. 4.2). Although the Madagascar Basin profiles of Bertram and Elderfield (1993) are close by, no measurements are reported between 400 and 3100 m water depth.

Fairly unradiogenic ε_{Nd} values are recorded in the SWIO at AAIW depths (500 – 1500 m): -9.4 ± 0.6 at 1000 m at ER-12, and -9.6 ± 0.3 at 803 m at ER-11 (Amakawa et al., 2019). However, these measurements appear to be affected by presence of the Agulhas Rings (Figs. 4.1, 4.3). Outside of the influence of the Agulhas Current, AAIW has an average ε_{Nd} of -8.1 in the region (n = 3; Garcia-Solsona et al., 2014, station S2; Amakawa et al., 2019, station ER-11). This composition is shared with UCDW, found between 1000 – 2000 m, which has an average ε_{Nd} of -8.1 (n = 3; Garcia-Solsona et al., 2014; Amakawa et al., 2019).

In the SWIO, ER-11 and ER-12 appear to diverge at ~ 1500 m with ER-11, the more northerly station, exhibiting more radiogenic ε_{Nd} values (Fig. 4.3). However, when the data is plotted by neutral density it becomes apparent that this 'excursion' could simply be a result of lower sampling resolution at ER-12 (Fig. 4.3).

Unradiogenic values at the base of UCDW (ε_{Nd} ~ 9.3; Amakawa et al., 2019; γ_n ~ 28 and ~ 2000 m water depth) are found at both stations (~ 9.3; Amakawa et al., 2019). This signature results from NADW flowing into the basin from the South Atlantic (van Aken et al., 2004), where it is seen as ε_{Nd} values around -11 between 2000 and 4000 m (station S2, Fig. 4.3, Garcia-Solsona et al., 2014). The NADW signal appears more pronounced at ER-12, the more southerly station, where unradiogenic values persist to ~ 3000 m.

4.4.2 Late Holocene CWC Nd isotopic composition

The modern CWC collected from 870 m at Atlantis Bank (493 ± 81 y BP), most likely sampling SAMW, recorded an ε_{Nd} of -8.6 ± 0.2 (Fig. 4.4). This value is slightly more radiogenic than waters at equivalent neutral density levels at the closest site, ER-11, but within error of that at ER-12, S2 (Fig. 4.3; Amakawa et al., 2019; Garcia-Solsona et al., 2014) and CD-1504 in the Madagascar Basin (-8.8 ± 0.4; Bertram and Elderfield, 1993). The upper ~ 1000 m of ER-11 seem strongly influenced by waters of the Agulhas Return Current, a feature which may, over the lifetime of a coral, be too transient to be recorded. We consider the similarity of the coral ε_{Nd} to most seawater measurements from SAMW depths in the region as evidence of effective recording of seawater Nd isotopic composition.

The late Holocene coral sample measured from AAIW depths at Coral Seamount records an ε_{Nd} of -8.5 ± 0.2 and hence falls between the modern seawater measurements from the BGH cruise southwest of Africa (Garcia-Solsona et al., 2014) and the Indian Ocean measurements from ER-11 and ER-12 (Amakawa et al., 2019, Fig. 4.3).

A late Holocene coral sample from 1207.2 m at Coral Seamount plots within the modern UCDW range (-8.1 ± 0.2; Figs. 4.3, 4.4; Lambelet et al., 2018). It records an almost identical ε_{Nd} value as the modern seawater measurement from roughly the same depth and neutral density at ER-11 (1253 m; γ_n = ~ 27.7; Amakawa et al., 2019). Although station ER-12 is more proximal to Coral Seamount, the lack of seawater samples between ~ 1000 and 2000 m at this station means it is less suitable for comparison. It is worth noting that at UCDW depths modern seawater ε_{Nd} appears to be very similar in the Cape Basin and SWIO. The corals in this study are too shallow to have encountered direct flow of NADW, which is at ~ 2000 m and below (γ_n = 27.7-28.27; Stichel et al., 2012; Amakawa et al., 2019).

In summary, the three late Holocene corals faithfully record the Nd isotopic composition of ambient seawater. The fact they plot within error of each other, despite occupying different water masses, is a similar observation to Nd isotope data from the Drake Passage (Stichel et al., 2012; Struve et al., 2017) and south of Australia (Lambelet et al., 2018). This suggests that the modern ACC effectively mixes and to a certain extent homogenises the properties of intermediate circumpolar waters (Carter et al., 2012; Stichel et al., 2012). The samples show no sign of local boundary exchange with either radiogenic rocks of the SWIO ridge (ε_{Nd} = 8.6 ± 3.05; 2SD; n = 155; PetDB database), or unradiogenic sediments from the proximal continental crust of Madagascar (ε_{Nd} = -28.2 ± 8.0, -22.1 ± 8.0; Kroner et al., 2000; Paquette et al., 1994) or South Africa (ε_{Nd} = ~ -15; Franzese et al., 2006; Noble et al., 2012 and references therein).

4.4.3 Stability of the deglacial Nd isotope record

Samples from Coral Seamount record ε_{Nd} values between -7.5 and -9.2 throughout the deglacial. There is no discernible first-order trend; the oldest HS1-age corals record modern day seawater values of ~ -7.8 and the most unradiogenic values occurred during the YD. Samples from north of the STF at Middle of What Seamount record an increase of ~ 1 ε_{Nd} between HS1 and the YD (Figs. 4.4, 4.5).

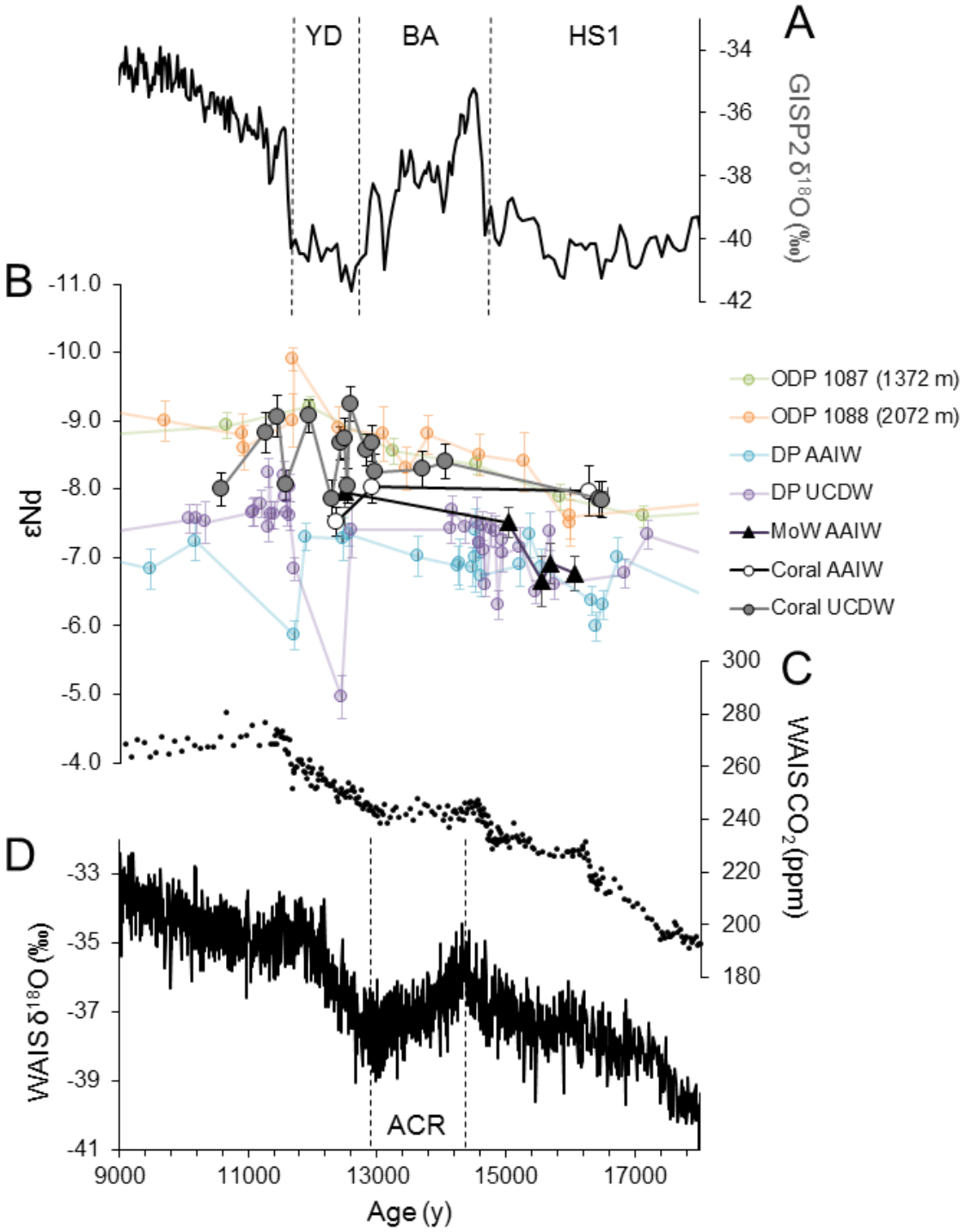

Figure 4.5: Deglacial εNd records from the southwest Indian, southeast Atlantic and southeast Pacific Oceans. **A)** Greenland oxygen isotope record from GISP2 (Stuiver et al., 1995). **B)** εNd values derived from cold-water corals at modern Antarctic Intermediate Water (AAIW) depths at Coral Seamount (<1000 m; white circles) and Middle of What Seamount (black triangles) and from modern UCDW

depths at Coral Seamount (>1000 m; grey circles); uncleaned foraminifera from cores ODP 1087 (1372 m; green circles) and 1088 (2082 m; orange circles) from the Cape Basin (Hu et al., 2016) and cold-water corals from AAIW (726-816 m at Burdwood Bank and 648-1012 m at Cape Horn; blue circles) and UCDW depths (695-1323 m at Sars Seamount and 1516 m at Burdwood Bank; purple circles) in the Drake Passage (Wilson and Struve, pers. comm.). **C)** CO_2 record (Marcott et al., 2014) and **D)** oxygen isotope record from the WAIS Divide Core (WAIS Divide Project Members, 2015). Time intervals for the Younger Dryas (YD); Bølling-Allerød interstadial (BA) and Heinrich Stadial 1 (HS1; top panel) and the Antarctic Cold Reversal (ACR; bottom panel) are delineated by dashed lines.

The boundary between AAIW and UCDW ($\gamma_n = 27.55$) is found at ~ 1020 m at Coral Seamount in the modern day; if the same water mass structure existed during the deglacial, both water masses are sampled. The ε_{Nd} values of these water masses reflect mixing between unradiogenic Atlantic waters (-13.5; Piepgras and Wasserburg, 1987) and radiogenic Pacific waters (PDW; -4; Piepgras and Jacobsen, 1988) in the Southern Ocean (Carter et al., 2012). Therefore, a stable ε_{Nd} within error of modern-day seawater suggests that, at least by HS1, the relative contribution of Atlantic and Pacific sources to circumpolar waters was either similar to today, or end-member composition changes balanced any differences in fluxes.

A number of deep Nd isotope records from the Atlantic Basin indicate a reduced contribution from northern-sourced waters to the deep ocean during the LGM, and a deglacial increase in NADW export to the Southern Ocean (Fig. 4.6; Gutjahr et al., 2008; Howe et al., 2016a; Piotrowski et al., 2012, 2005; Roberts et al., 2010). Further along the flow path of deep waters increasing influence of NADW from the LGM onwards also appears to be recorded at 3800 m water depth in the equatorial Indian Ocean (Fig. 4.6; Piotrowski et al., 2009).

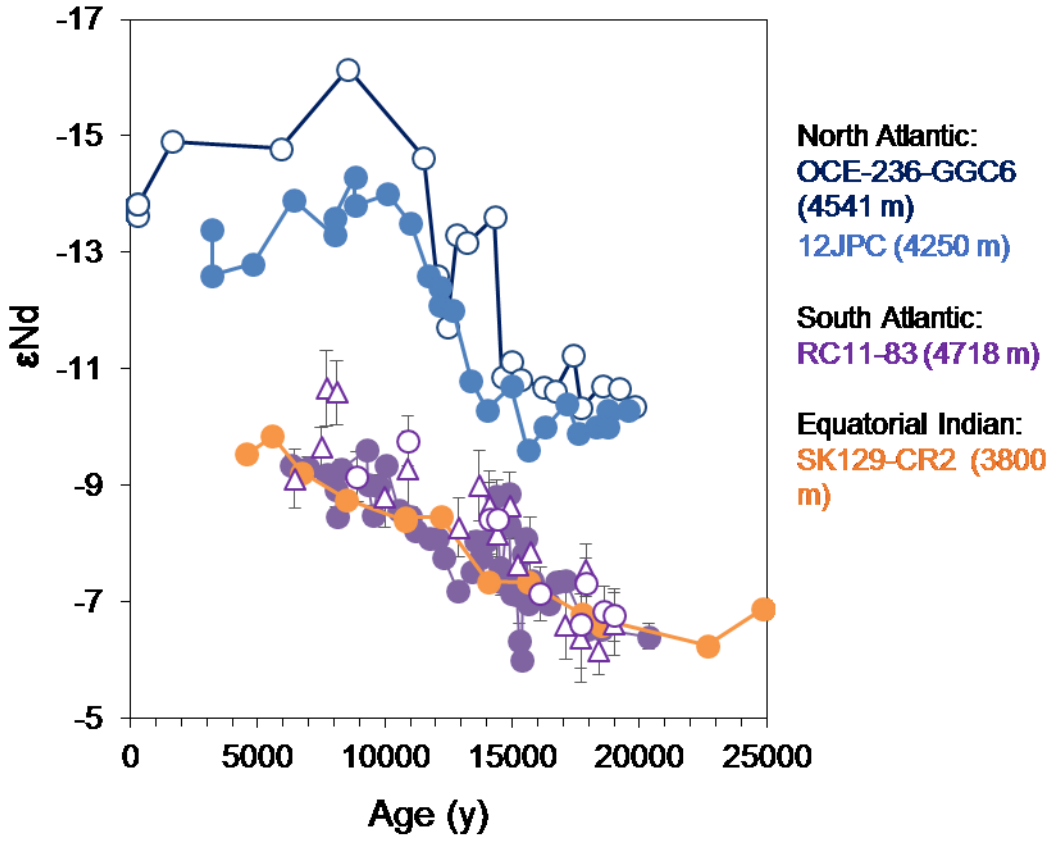

Figure 4.6: Deglacial deep ocean εNd records. Uncleaned foraminifera from the Bermuda Rise core OCE-236-GGC6 (navy circles; Roberts et al., 2010), bulk sediment leachates from Blake Ridge core 12JPC (blue dots; Gutjahr et al., 2008); leachates (purple dots), cleaned (purple triangles) and uncleaned (purple circles) foraminifera from core RC11-83 (Piotrowski et al., 2005; Piotrowski et al., 2012); and leachates from equatorial Indian Ocean core SK129-CR2 (orange dots; Piotrowski et al., 2009).

However, a signature of reduced NADW contribution during the LGM is not as pronounced in intermediate depth Nd isotope records (Fig. 4.7; Howe et al., 2016a; Huang et al., 2014; Noble et al., 2013; Wilson and Struve, pers. comm.). This observation is consistent with a maintained supply of northern-sourced Atlantic waters to the upper overturning cell of the ocean during the LGM and subsequent deglaciation. There is evidence for compositional changes in the northern end-member (Gutjahr et al., 2008; Wilson et al., 2014), but these

changes in chemical composition likely represent changes near the water mass source regions, which do not appear to be transferred downstream to the area of the SWIO.

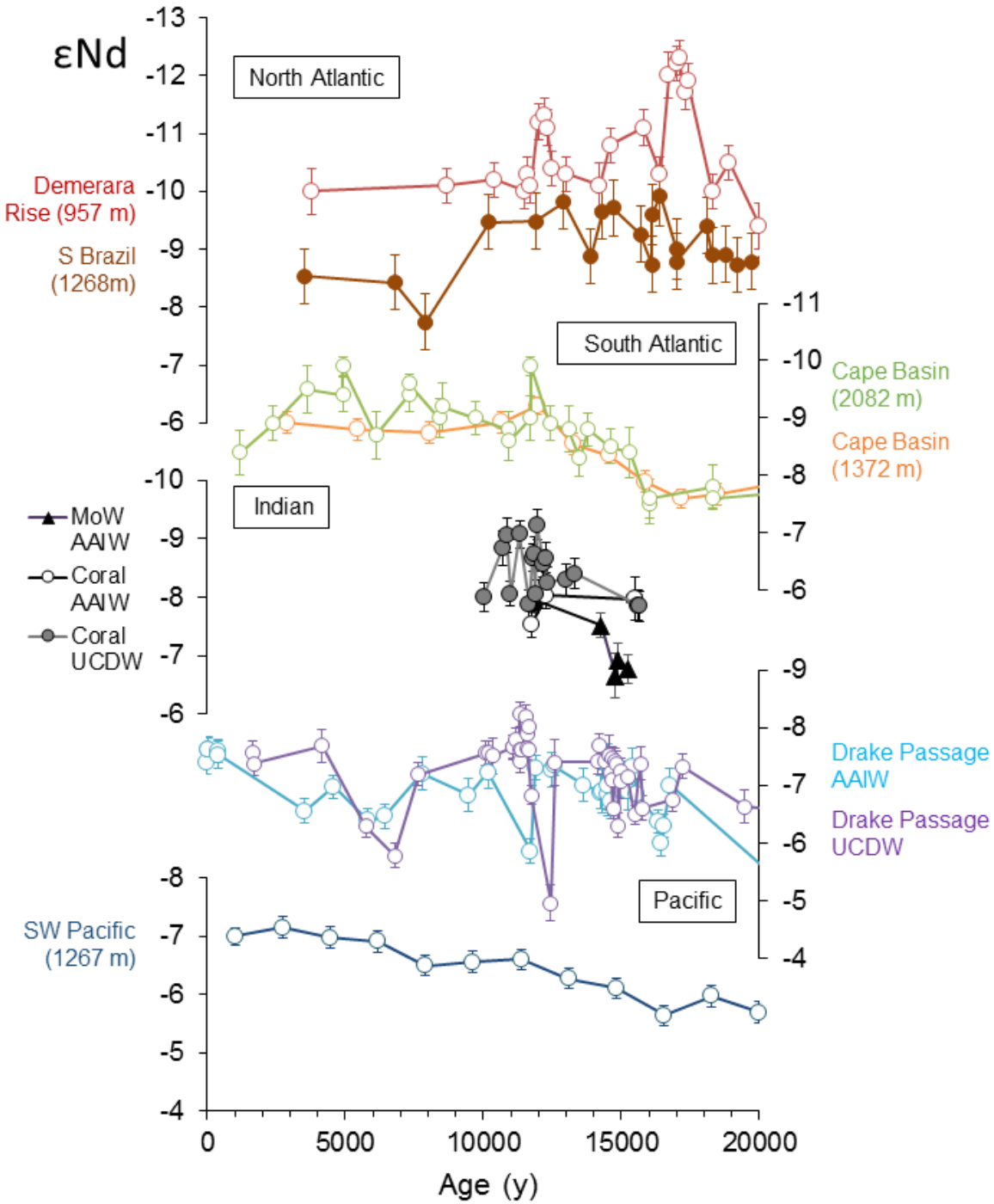

Figure 4.7: Deglacial intermediate water ε_{Nd} records. From top to bottom: uncleaned foraminifera from cores KNR197-3-46CDH (red circles; Huang et al., 2014), KNR159-5-36GGC (brown dots; Howe et al., 2016b), ODP 1087 and 1088 (orange and green circles; Hu et al., 2016); cold-water corals from

AAIW depths at Middle of What Seamount (black triangles), Coral Seamount (white circles) and UCDW depths at Coral Seamount (grey circles; this study), from AAIW (726-816 m at Burdwood Bank and 648-1012 m at Cape Horn; blue circles) and UCDW depths (695-1323 m at Sars Seamount and 1516 m at Burdwood Bank; purple circles) in the Drake Passage (Wilson and Struve, pers. comm.), and uncleaned foraminifera from core Y9 (navy circles; Hu et al., 2016).

4.4.4 Radiogenic Nd isotope composition at AAIW-depth during HS1

During Heinrich Stadial 1 (18 – 14.7 ka; Buizert et al., 2014), samples from Middle of What Seamount at 1014 m are distinctly radiogenic ($\varepsilon_{Nd} \sim -7$, n = 3; Fig. 4.4, 4.5, 4.7). Although there are no measured late Holocene analogues or seawater Nd isotope data from Middle of What Seamount, the hydrography appears very similar to that at Atlantis Bank and modern seawater profiles ER-11 and ER-12 (Fig. 4.1). Seawater measurements at similar neutral density surfaces to these corals gave ε_{Nd} values of -9.4 ± 0.6 (ER-12; 37°S, 57°E; 1000 m) and -8.6 ± 0.3 (ER-11; 30°S, 65°E; 999 m) respectively (Amakawa et al., 2019). Therefore ε_{Nd} values of ~ -7 fall outside of the range of modern seawater at intermediate depths around SWIOR. Below we discuss the potential role of changes in local detrital inputs, surface waters, and AAIW in setting this isotopic composition.

4.4.4.1 Local detrital inputs

There are a few sources of radiogenic Nd that have the potential to influence seawater in the region. Firstly, the geology of the SWIO ridge itself is radiogenic, with an average ε_{Nd} of 8.6 ± 3.1 (2SD; n=155; PetDB database). However, there is no evidence for this source influencing modern seawater; deep and bottom water compositions near the ridge are similar to intermediate waters, with values around -8.5 recorded at stations ER-11 and ER-12 (Amakawa et al., 2019). Furthermore, Nd incorporation into seawater occurs largely through continental drainage (Elderfield et al., 1990) and dissolution of sediments (Lacan and Jeandel,

2005; Rousseau et al., 2015; Wilson et al., 2013). If boundary exchange occurred, one would expect the samples to exhibit lower ε_{Nd} values, as terrigenous sediments in the region are mostly derived from the unradiogenic cratonic crust of Madagascar (-28.2 ± 8.0; Paquette et al., 1994; -22.1 ± 8.0; Kroner et al., 2000) and South Africa (-12.8 ± 0.4; Noble et al., 2012).

Secondly, southern Africa is a potential proximal source of radiogenic dust to the region (ε_{Nd} of -3.8 and -5.2; Grousset et al., 1992; Li et al., 2008). However, the supply and deposition of dust is much lower in the Southern Hemisphere than in the Northern Hemisphere (Prospero et al., 2002), and particularly low in the southern Indian Ocean (Li et al., 2008). There also does not appear to be any evidence for the incorporation of such a signal in surface waters in the modern day in the region (Fig. 4.3). It is thought that there was an increased supply of dust to the region during the LGM, particularly from South America (Kumar et al., 1995), evidence of which can be seen in cores from the Cape Basin (Rutberg et al., 2005). The Nd isotopic composition of these sediments is also likely to be radiogenic; Franzese et al. (2006) identifies 'South Atlantic' derived sediments with an ε_{Nd} of ~ -5. However, if a radiogenic signal was imparted to AAIW waters via dust, one would expect to also see this in AAIW closer to its source at Coral Seamount (see section below). Furthermore, it is thought that the large Nd budget of the ACC reduces its susceptibility to modification by terrigenous inputs relative to other parts of the ocean (Carter et al., 2012).

For these reasons, we turn to explanations of water mass provenance and mixing to interpret the ε_{Nd} distribution seen during HS1.

4.4.4.2 Direct influence of surface waters

Surface waters in the modern day SWIO at stations northeast and southeast of Middle of What Seamount show clear influence from the unradiogenic waters of the Agulhas Current (Fig. 4.1; Amakawa et al., 2019), a signal that appears to mix into intermediate waters (Fig.

4.3). Therefore, it seems possible that a shift in latitude of the ARC away from MoW in the past could result in more radiogenic surface and intermediate waters. This could plausibly occur with an altered position of the westerly winds and fronts of the Southern Ocean, or a change in strength of the Agulhas Current.

During the LGM, evidence from numerous studies suggests 'leakage' of Agulhas waters into the Cape Basin and wider Atlantic was reduced, interpreted to result from a more equatorward position of the westerly winds and STF (Flores et al., 1999; Franzese et al., 2006; Peeters et al., 2004). During HS1, sea surface temperature reconstructions and microfossil assemblages suggest that the STF had migrated further south (De Deckker et al., 2012; Sikes et al., 2009), potentially even poleward of its modern location (Barker et al., 2009). If this was the case, the ARC may have been closer to Coral Seamount than Middle of What. In the modern day, the influence of the unradiogenic Agulhas can be seen to intermediate depths (Fig. 4.3). Therefore, such a frontal shift could cause samples at AAIW depths at the southerly seamount to record more unradiogenic ε_{Nd} values than those at Middle of What during HS1 (Fig. 4.4).

However, even if the influence of the ARC was reduced at MoW, intermediate water values with an ε_{Nd} above -7 are uncommon in the modern SWIO. The only comparable sites are surface and intermediate waters in the Mascarene Basin (1503, 1502; Fig. 4.1; Bertram and Elderfield, 1993), where the more radiogenic Nd isotopic compositions could result from a greater influence of the South Equatorial Current (SEC) or Red Sea Waters (RSW; Bertram and Elderfield, 1993; Amakawa et al., 2019), or contributions from boundary exchange with nearby volcanic provinces (Bosch et al., 2008; White et al., 1990; Wilson et al., 2012).

Although the Nd isotopic composition of SEC waters has not been directly measured to date, they originate from the eastern equatorial Indian Ocean where the ε_{Nd} values of intermediate and thermocline waters range from -5.3 ± 0.2 to -2.9 ± 0.4 (Jeandel et al., 1998).

At 799 m in the Mascarene Basin, seawater was recorded as having an ε_{Nd} of -7.2 ± 0.4 (Bertram and Elderfield, 1993), potentially recording RSW influence.

The modern hydrography in the Mascarene Basin appears to be quite different from that at MoW seamount today. At MoW there is little indication of RSW influence, the T-S profile being almost identical to sites in the Crozet Basin (ER-11; ER-12; Fig. 4.1; Amakawa et al., 2019). At present, RSW and AAIW are thought to meet at around 0-10° S near the Amirante Passage (McCave et al., 2005). Therefore, a significant reorganisation of hydrography would be required for RSW incursion to sites near the STF/ARC.

In conclusion, a more poleward positioning of the westerly winds a during HS1 is plausible and may have contributed to more radiogenic intermediate waters at MoW in comparison to Coral Seamount. Even assuming reduced influence of the ARC, however, ε_{Nd} values of ~ -7 are still more radiogenic than one would expect for this region.

4.4.4.3 AAIW composition change – whole Southern Ocean change?

In the modern SWIO, at intermediate depths outside of the influence of the Agulhas Current, the Nd isotopic composition is similar to that in the eastern Pacific and eastern Atlantic sectors of the Southern Ocean (ε_{Nd} ~ -8 to -9; Stichel et al., 2012; Carter et al., 2012). This suggests a well-mixed modern ACC combining unradiogenic Atlantic (NADW; -13.5; Piepgras and Wasserburg, 1987) and radiogenic Pacific waters (PDW; -4; Piepgras and Jacobsen, 1988). If this was maintained during HS1, more radiogenic values in AAIW would suggest either a relative increase in the volume of Pacific waters relative to Atlantic waters, or a radiogenic shift in the end-member composition of either source.

Characterisation of the isotopic composition of NADW during HS1 remains inconclusive at present. The shallower glacial NADW analogue GNAIW may have been 3-4 ε_{Nd} units more radiogenic, due to a shift in formation region (Gutjahr et al., 2008); this water

mass is suggested to have also been more dominant in the Atlantic Ocean during HS1 (Xie et al., 2014). Corals from intermediate waters in the North Atlantic do record a maximum in ε_{Nd} in the latter stages of HS1 (-11.3) but deeper samples (at a higher-resolution part of the record) indicate an extremely variable Nd isotopic composition (-14.5 to -11.0; Wilson et al., 2014). Reconstructions from intermediate waters further south in the Atlantic exhibit more unradiogenic values than the modern day (~ -12; Huang et al., 2014; Fig. 4.7), which would not be possible without the presence of a northern end-member of similar composition to NADW during HS1, unless local sources imprinted on the signal (see Martin et al., 2012).

Although the end-member composition of NADW is difficult to tie down, there is evidence its overall transport was reduced (McManus et al., 2004). This mechanism has been invoked to explain more radiogenic Nd isotope compositions of deep waters during HS1 in the North Atlantic (~ -11; Roberts et al., 2010), South Atlantic (~ -7; Piotrowski et al., 2005), and equatorial Indian Oceans (~ -7; Piotrowski et al., 2009; Fig. 4.6). There is also disagreement over whether northward AAIW extension into the Atlantic increased (Pahnke et al., 2008) or decreased (Huang et al., 2014; Xie et al., 2014, 2012) in response to reduced NADW flux.

If the circumpolar ocean was more radiogenic during HS1, we would expect to see the same radiogenic AAIW signal in the other sectors of the Southern Ocean. This is broadly the case, with reconstructions from mid-depth waters of the Drake Passage recording ε_{Nd} values of ~ -6 to -7 (Fig. 4.5; Wilson and Struve, pers. comm.), -7.6 to -7.9 at UCDW depths in the Cape Basin, and ~ -6 in southwest Pacific AAIW (Hu et al., 2016). The similarity between ε_{Nd} values at MoW seamount with those in the Pacific sector suggest that a well-mixed circumpolar ocean existed at the time.

But why do contemporaneous Heinrich Stadial 1 samples from similar depths at Coral Seamount (i.e. modern UCDW) record more unradiogenic values? Both water masses are part

of the upper cell of the overturning circulation, formed from upwelled IDW and PDW. However, UCDW presently incorporates some NADW directly into its lower reaches in the SWIO (van Aken et al., 2004). If NADW shoaled during HS1 and was incorporated south of Africa via the 'shortcut', mid-depth waters in the Cape Basin and SWIO could have maintained ε_{Nd} values of ~ - 8, while AAIW ε_{Nd} in the Southern Ocean responded to an overall decrease in NADW export. The unradiogenic waters from the Atlantic may not have been incorporated into the circumpolar flow, and not reached the SW Pacific and Drake Passage, where UCDW was similar in Nd isotopic composition to AAIW (Wilson and Struve, pers. comm.).

In summary, it seems most likely that the more radiogenic values in AAIW at MoW Seamount during HS1 are the response to a decrease in the export of Atlantic-sourced waters to the Southern Ocean. The more unradiogenic samples at UCDW-level at Coral Seamount of comparable age may have been influenced either by an Agulhas Current positioned south of the modern day, or a shallower NADW 'shortcut' entering the SWIO south of Africa.

4.4.5 Fluctuations in Nd isotope composition at UCDW-depths during YD

Between 12.9 and 10.6 ka the deepest samples from Coral Seamount (1200 – 1400 m) record the lowest Nd isotope compositions of the record ($\varepsilon_{Nd} < -9$) and resolvable fluctuations of ~ 1 ε_{Nd} units (Fig. 4.4). These fluctuations occur on hundred-year timescales, within error of the dating method. Slightly shallower samples (~ 1100 m) at the same seamount record values at the upper end of the range during this time (ε_{Nd} between -8.1 and -8.3). The two shallowest samples from Coral Seamount (900 - 1000 m), situated above the modern AAIW/UCDW boundary, include the most radiogenic value for the time period, -7.5 ± 0.2 (Fig. 4.4).

4.4.5.1 Sampling resolution

Due to the apparent preference for CWC growth in this location during the YD (see Chapter 3), the 'noisy' nature of the signal may be due to the higher sample density and hence resolution during these times in comparison to other parts of the record. It is interesting to note that similar centennial-scale fluctuations in CWC records have been documented from the Drake Passage and North Atlantic (Wilson et al., 2014; Fig. 4.5). In each of these cases, the fluctuations are observed during times of preferred coral growth and high sampling resolution. As it seems unlikely that changes in end-member Nd isotope compositions would manifest themselves in such rapid variations in ε_{Nd} at locations distal from the water mass sources, we explore other potential mechanisms (i.e. physical ocean changes) to explain the fluctuations.

4.4.5.2 Shifts in the presence of North Indian Deep Water (NIDW) and UCDW

In the modern day, UCDW enters the SWIO from the south, flowing through fracture zones in the ridge, whilst, at similar depths, North Indian Deep Water (NIDW) flows poleward from the north into the Somali and Mascarene Basins (McCave et al., 2005; You, 2000). One could imagine a scenario whereby the reach of southward NIDW flow extended periodically into the region presently occupied by northward flowing UCDW. If NIDW was more radiogenic, which would be expected given that it lacks recently incorporated NADW, this could potentially account for the fluctuations seen at Coral Seamount.

Few modern measurements of the Nd isotopic composition of NIDW exist, but in the eastern Indian Ocean it has been recorded as having an ε_{Nd} of -6.1 ± 0.2 (Jeandel et al., 1998). Wilson et al. (2012) speculate that core-top foraminifera from the Mascarene Basin WIND 30-35B cores record southward-flowing NIDW rather than CDW, with ε_{Nd} values of -7.9 to -7.3. However, as ~ -8 is the modern day value of UCDW and was recorded consistently at Coral Seamount throughout the deglacial, it seems unnecessary to invoke a new water mass to explain these values, especially as NIDW is likely to be more radiogenic than this. There is also no

apparent mechanism for periodic increased NIDW export to reach the modern day subantarctic during the YD. A more likely explanation would be that the values close to -8 indicate circulation patterns similar to the modern day.

4.4.5.3 Proximal water mass boundary

An alternative idea is that during the YD, the deepest samples at Coral Seamount could have been growing close to a shifting AAIW/UCDW water mass boundary, resulting in short-term fluctuations in the Nd isotopic composition of waters bathing them. The two water masses in question are indistinguishable in their Nd isotope composition in the modern day SWIO (Fig. 4.3; Amakawa et al., 2019; Garcia-Solsona et al., 2014). For shifts in the water mass boundary to be responsible for the late deglacial fluctuations therefore, a different scenario must have existed whereby one water mass exhibited ε_{Nd} values of ~ -9 and the other one of ~ -8. As only the deepest samples at Coral Seamount record Nd isotopic compositions at the lower end of the range, UCDW is the best candidate for the water mass with a more unradiogenic signature. The first evidence of the 'divergence' is at ~ 12.5 ka, with a 1207 m sample recording an ε_{Nd} of -9.2 ± 0.2. Samples at this depth at Coral Seamount record similarly unradiogenic values until ~ 11.3 ka, with the exception of single samples at 12.5 ka (-8.0 ± 0.3) and 12.2 ka (-7.9 ± 0.2). These values are within error of contemporaneous samples at 952 m at Coral Seamount (-7.5 ± 0.2) and at 1014 m at Middle of What Seamount (-8.0 ± 0.2), depths which correspond in the modern day to AAIW. In this scenario, only the samples at ~ 1200 m at Coral Seamount are bathed in UCDW, and, in the short intervals that the water mass boundary deepens (or shifts south if the slope of the isopycnals is preserved), AAIW.

A more unradiogenic UCDW could have been brought about by a smaller relative contribution of PDW than Atlantic waters. One would expect such a change in water mass balance would be recorded across the Southern Ocean. Samples from the Cape Basin record values ~ -9 during the YD at UCDW depths, which is more unradiogenic than the same depths

during HS1 (Hu et al., 2016). However, in the Drake Passage, UCDW-depth corals record a range of values ~ -6.8 to -8.2, at the more radiogenic end of the modern range, with similar AAIW values of ~ -7 (Wilson and Struve, pers. comm., Fig. 4.5). As waters tend to be more well-mixed in the narrow Drake Passage (Stichel et al., 2012), this does not necessarily eliminate the possibility that in the SWIO there could have been a gradient between AAIW and UCDW.

For this gradient in Nd isotopic composition to exist, a change in the formation mechanism for AAIW and UCDW is required. It is interesting to note that deeper records in the Cape Basin show an excursion to more radiogenic values during the YD (Piotrowski et al., 2005) while UCDW expresses the opposite trend (Hu et al., 2016). This has been suggested to be the result of a shoaling of NADW, reducing the input of unradiogenic waters at depth but increasing their influence higher in the water column. A less dense version of NADW could have been exported into the Southern Ocean and incorporated directly into UCDW, leading to less radiogenic Nd isotope compositions in the Atlantic and western Indian sectors, but without affecting AAIW.

The modern 27.55 kg m^{-3} neutral density surface marks the AAIW/UCDW boundary (Stichel et al., 2012; Lambelet et al., 2018) and sits at ~ 1020 m at Coral Seamount (Djurhuus, pers. comm). Therefore, a situation in which the samples at ~ 1200 m are bathed in AAIW requires a considerable deepening of the water mass boundary, even considering ~ 60 m lower sea level (Carlson and Clark, 2012). As the slope of isopycnals in the Southern Ocean is set by the balance between upwelling and eddies and is approximately constant (Marshall and Speer, 2012), lateral (north-south) shifts in the position of fronts of the ACC can cause an apparent shoaling or deepening of water masses in a given location. At Middle of What Seamount, 3° of latitude further north, the modern AAIW/UCDW boundary is found at ~ 1400 m (Djurhuus, pers. comm). Gersonde et al. (2005) reported a northward LGM position of the PF and the SAF

of 5-10°, and of 5° for the STF. This suggests that there is precedent in this region for the magnitude of frontal shifts required, but there is little evidence of fronts being positioned south of their modern location during the YD, which is the direction required for a deepening AAIW/UCDW boundary at Coral Seamount. During the ACR (14.5-12.9 ka; WAIS Divide Core members, 2015), Antarctic sea ice expanded (Lowry et al., 2019), and there is evidence that fronts responded with a northward migration (Barker et al., 2009; De Deckker et al., 2012). Although this situation is thought to have reversed after the ACR, it seems unlikely that by 12.5 ka the PF and SAF would have been south of their present position.

4.4.5.4 Periodic NADW influence at depth

If the Southern Ocean fronts were slightly north of their modern position during the YD, and/or if NADW was shoaled, the deepest samples at Coral Seamount could have been more easily exposed to unradiogenic Atlantic waters entering the Cape Basin south of Africa. This scenario would explain why unradiogenic values at AAIW depths are not observed, as well as the similarity in values between the SWIO and the Cape Basin (Hu et al., 2016), and why ε_{Nd} values of ~ -9 appear not to be transmitted to the Drake Passage (Fig. 4.5; Wilson and Struve, pers. comm.).

In the modern SWIO, NADW is observed at around 2000 m depth (Donohue and Toole, 2003; Thomas et al., 2006), indicated by ε_{Nd} values of -9.3 ± 0.7 and -9.4 ± 0.2 recorded at ER-11 and ER-12 respectively (Amakawa et al., 2019). For the 1200 m corals to be affected by NADW without any changes in water mass structure, fronts would need to have been considerably further north until as late as 11.3 ka, when the youngest sample is found with an ε_{Nd} of ~ -9 (Fig. 4.1, 4.4, 4.5). However, sea surface temperature estimates and microfossil assemblages do not support this scenario. In the SW Pacific, high SSTs south of Australia are recorded at the time (De Deckker et al., 2012). In the Drake Passage, the SAF is thought to have shifted south to its present-day position at ~ 15-14 ka (Roberts et al., 2017), and in the

Cape Basin SSTs and the relative abundance of polar foraminifera species are similar to the Holocene (Barker et al., 2009).

The unradiogenic coral skeleton Nd isotope ratios could result from periodic incursions of less modified NADW at shallower depths than the modern day. Atlantic Meridonal Overturning Circulation is thought to have been weaker during the Younger Dryas (McManus et al., 2004) with more radiogenic values in bottom waters in the Atlantic indicating reduced NADW transport at depth (Roberts et al., 2010; Piotrowski et al., 2005). Conversely, intermediate depth cores in the tropical Atlantic record an unradiogenic excursion during the YD (~ -11; Huang et al., 2014; Fig. 4.7), and on the Brazil margin modern AAIW values are not recorded until after the YD (Hu et al., 2016). Initially interpreted as a change in the isotopic signature of AAIW, it seems more likely that these data record a shoaling of the AAIW/NADW boundary, which would provide additional support for an increased influence of NADW at ~ 1000 -1200 m in the SWIO at this time. If this is the case, the possible controls on this local, relatively shallow NADW incursion could be an interesting area of future research, and may be related to the history of Agulhas rings (see van Sebille et al., 2012).

In summary, the most likely explanation for rapid fluctuations to an ε_{Nd} of ~ -9 during the YD at Coral Seamount is a periodic influence of NADW affecting the deepest coral samples via the direct route south of the African continent. This hypothesis is supported by the similarity of Nd isotopic compositions at UCDW depths in the Cape Basin and at 1000 - 1200 m at Coral Seamount. In addition, unradiogenic excursions in intermediate waters in the tropical Atlantic hint at a shoaling of NADW during the YD. The explanation based on proximity to a fluctuating water mass boundary between AAIW with an ε_{Nd} of ~ -8 and UCDW with an ε_{Nd} of ~ -9 is considered less likely. This is because it would require a deeper AAIW/UCDW water mass boundary and therefore more poleward ACC fronts than today.

4.5 Conclusion

In this study we report new mid-depth neodymium isotope records from cold-water corals in the southwest Indian Ocean. Using uranium-series methods, samples were dated to between 16.5 ka and modern, and represent depths equating to SAMW, AAIW and UCDW. During the late Holocene, samples record typical modern-day seawater ε_{Nd} values of ~ -8, but none record more unradiogenic values typical of the Agulhas Current. The overall variation in Nd isotopic composition during the deglaciation is low with the majority of samples falling within modern-day values for circumpolar waters. This finding differs from deep and bottom water records from the Atlantic and Indian Oceans, which show decreases in ε_{Nd} during the deglaciation, thought to result from a gradual recovery of the export of NADW after the LGM. Therefore, our data suggests that the overall supply of Atlantic-sourced waters to the SWIO was similar to today. During HS1, slightly more radiogenic values of ~ -7 are recorded at AAIW depths at Middle of What Seamount. This shift is also seen in the Drake Passage (Wilson and Struve, pers. comm.), suggesting the change was circumpolar. However, Coral Seamount maintains an ε_{Nd} signature of ~ -8, similar to modern seawater and within error of contemporaneous UCDW depth Nd isotope reconstructions from the Cape Basin (Hu et al., 2016). We suggest that NADW export to the Southern Ocean was reduced and shoaled during HS1, such that the circumpolar signal was more radiogenic but NADW was incorporated into UCDW south of Africa. Centennial fluctuations in ε_{Nd} between ~ -9 and -8 at Coral Seamount during the YD also hint at periodic incursions of NADW into the SWIO. However, the mechanism for the pacing of these changes is as yet unclear.

Statement of contribution

I conducted all sample preparations, REE separations and Nd isotope measurements. I also assisted with isotope dilution U-series dating and data processing, which was led by Tianyu Chen and carried out in part by Tao Li, under the supervision of Laura Robinson at the University of Bristol. Tina van de Flierdt, David Wilson and Susan Little contributed to discussions of data interpretation.

Table 4.2: Cold-water coral Nd isotope data from seamounts of the southwest Indian Ocean

JC066 ID	Sample ID	Species	Site	Age / y BP	2σ	Depth / m	error	Sample mass / g	Coral [Nd] ppb	Coral /[Th] ppt	/δ^{234}U$_i$	^{143}Nd/^{144}Nd	SE	εNd	2σ*
0127	A10	*D. dianthus*	Coral	11381	79	1207.2		1.874	9	55	149.9	0.512173	0.000006	-9.07	0.21
0121	A2	*C. diomedeae*	Coral	12225	163	1207.2		0.269	45	539	150.2	0.512235	0.000005	-7.87	0.24
0486X	A3	*D. dianthus*	Coral	11510	431	1097.2		0.283	95	1294	152.3	0.512225	0.000003	-8.06	0.24
0124	A4	*C. diomedeae*	Coral	11872	320	1207.2		0.272	86	1071	151.7	0.512173	0.000006	-9.08	0.26
1056	*A6*	*C. diomedeae*	*Coral*	*12238*	*985*	*1207.2*		*0.450*	*295*	*3806*	*148.1*	*0.512176*	*0.000006*	*-9.00*	*0.26*
0123	A7	*D. dianthus*	Coral	12515	237	1207.2		0.347	34	668	151.8	0.512164	0.000005	-9.24	0.24
0122	A8	*C. diomedeae*	Coral	12468	185	1207.2		0.377	39	605	150.9	0.512226	0.000005	-8.04	0.25
1143A	A9	*D. dianthus*	Coral	16378	295	1097		0.349	89	945	147.2	0.512235	0.000005	-7.86	0.26
1143B	B1	*D. dianthus*	Coral	16423	431	1097		0.193	132	1487	150.4	0.512236	0.000005	-7.85	0.26
1066B	*B10*	*D. dianthus*	*Coral*	*12870*	*185*	*1207.2*		*0.220*	*55*	*523*	*154.4*	*0.512180*	*0.000006*	*-8.92*	*0.24*
2590	B2	*C. diomedeae*	MoW	14969	271	1014		0.327	60	808	148.0	0.512253	0.000004	-7.51	0.21
3510	B3	*C. diomedeae*	MoW	15997	368	1014		0.312	46	1192	149.5	0.512291	0.000004	-6.77	0.25
3508	B4	*C. diomedeae*	MoW	12423	117	1014		0.909	28	238	149.1	0.512230	0.000005	-7.96	0.21
1002	B6	*D. dianthus*	Coral	12304	213	952		0.269	56	715	149.8	0.512252	0.000005	-7.53	0.24
1040	B7	*D. dianthus*	Coral	16241	253	922.5	59.5	0.426	32	768	150.7	0.512229	0.000004	-7.97	0.24
3506B	B8	*C. diomedeae*	MoW	15617	584	1014		0.217	89	2033	149.3	0.512283	0.000003	-6.92	0.30
3506A	B9	*C. diomedeae*	MoW	15493	506	1014		0.286	52	1530	150.0	0.512297	0.000004	-6.66	0.37
0125	C1	*C. diomedeae*	Coral	12421	168	1207.2		0.297	57	1306	150.8	0.512190	0.000004	-8.75	0.25

0118	*C10*	*C. diomedeae*	*Coral*	*12627*	*313*	*1207.2*		*0.244*	*211*	*3316*	*150.2*	*0.512200*	*0.000006*	*-8.54*	*0.26*
2795	C14	*D. dianthus*	Coral	417	128	702		0.360	41	1066	146.6	0.512201	0.000005	-8.52	0.21
0117	C15	*D. dianthus*	Coral	1713	48	1207.2		0.293	35	473	147.2	0.512221	0.000006	-8.14	0.24
3705	C17	*C. diomedeae*	Atlantis	493	81	870		0.400	34	554	146.5	0.512196	0.000005	-8.61	0.24
1144	C2	*D. dianthus*	Coral	13628	88	1097.2		0.345	50	441	150.3	0.512213	0.000003	-8.30	0.25
0157	C4	*D. dianthus*	Coral	11193	242	1395		0.195	187	1895	148.5	0.512185	0.000004	-8.83	0.30
0107	C5	*C. diomedeae*	Coral	12898	218	1097.2		0.209	133	1824	153.2	0.512215	0.000005	-8.26	0.26
1157	C7	*C. diomedeae*	Coral	12763	250	1207.2		0.381	143	2547	149.2	0.512198	0.000004	-8.57	0.26
1156	C8	*D. dianthus*	Coral	10499	290	1207.2		0.154	401	2324	149.6	0.512228	0.000004	-8.00	0.30
1155	C9	*C. diomedeae*	Coral	12366	134	1207.2		0.261	77	963	151.8	0.512193	0.000004	-8.68	0.30
1046	D10	*C. diomedeae*	Coral	12864	202	922.5	59.5	0.360	69	1771	150.1	0.512226	0.000004	-8.04	0.37
2825	*D3*	*C. diomedeae*	*Melville*	*16601*	*343*	*897*		*0.348*	*112*	*3281*	*145.2*	*0.512262*	*0.000004*	*-7.34*	*0.30*
1070	D6	*D. dianthus*	Coral	13984	131	1207.2		0.216	140	1034	153.9	0.512207	0.000005	-8.40	0.26
486y	*D7*	*D. dianthus*	*Coral*	*13839*	*656*	*1097.2*		*0.036*	*452*			*0.512219*	*0.000004*	*-8.17*	*0.25*
1158	D8	*D. dianthus*	Coral	12855	183	1207.2		0.204	139	1742	151.5	0.512193	0.000004	-8.68	0.26
1045	*D9*	*D. dianthus*	*Coral*	*12717*	*125*	*922.5*	*59.5*	*0.156*	*82*	*914*	*157.5*	*0.512239*	*0.000005*	*-7.79*	*0.24*

*2σ is the higher value between a) 2 x the average standard error of JNdi standards measured around the samples or b) 2 x the internal standard error of the measurement

Grey italics signify that the sample was screened out due to non-seawater $\delta^{234}U_i$ values, [Th] > 3000 pt, or no measurement of these parameters being made due to unsuccessful precise U-series dating

Chapter 5: Deglacial ventilation history of the intermediate southwest Indian Ocean

Chapter summary

This chapter describes radiocarbon measurements from fifteen cold-water coral samples from the southwest Indian Ocean. Analysis alongside Nd isotope data described in the previous chapter allows the observed changes in ventilation between HS1 and the early Holocene to be linked to water mass influence. The range of radiocarbon offsets from the contemporaneous atmosphere is broadly equivalent to modern seawater in the region, highlighting the relative consistency of the contribution of relatively well-ventilated NADW to intermediate waters, in addition to the dynamism of regional hydrography in the SWIO. Periods of 'enrichment' are noted at 16.2, 12.4 and 9 ka, where ^{14}C values closer to atmospheric levels are recorded briefly by one or more corals. The first event is timed concurrently with an atmospheric CO_2 increase recorded in ice cores, and could represent of a release of carbon from Southern Ocean intermediate waters. The latter two events are more likely related to local surface current influence and/or deepening of the mixed layer. Samples in the SWIO record with the highest ventilation ages recorded by ^{14}C are also the most radiogenic with respect to Nd, and are from Middle of What Seamount during HS1. This is likely the result of a lower flux of NADW to the Southern Ocean; subsequent shifts to more modern-like ε_{Nd} and ^{14}C between 15.5 and 15 ka, recorded across the Southern Ocean, points to a gradual increase in NADW and deep ocean ventilation. Although there is a lack of samples covering the end-HS1 atmospheric CO_2 'pulse', a similar event at the end of the YD is recorded by an 11.4 ka depletion in ^{14}C in the mid-depth SWIO, signifying the transfer of old carbon from the depths triggered by rapidly increased export of NADW.

5.1 Introduction

The most recent glacial to interglacial transition, though initiated by orbital factors, was characterised in large part by increasing atmospheric CO_2 concentrations, which occurred non-linearly (Marcott et al., 2014). A broad consensus has formed over the past decades that carbon storage and release from the deep ocean was a major control on the pacing of atmospheric CO_2 increases. Meridional overturning circulation, and the dynamics of the Southern Ocean, were instrumental in carbon release and the anti-phase relationship between northern and southern hemisphere temperature changes (Blunier et al., 1998; Broecker, 1998). The synchronicity of warming in Antarctica from ~18 to 14.5 ka, and ~ 13 to 11.5 ka with the two major millennial-scale CO_2 increases (Parrenin et al., 2013) hints at the importance of the Southern Ocean, in addition to its unique ability to bring deep waters into direct contact with the sea surface (Marshall and Speer, 2012). Factors which are thought to have controlled the rate and timing of carbon release in the Southern Ocean, often in concert with each other, include sea ice expansion and retreat (Stephens and Keeling, 2000), westerly wind position and strength (Anderson et al., 2009; Toggweiler, 2009), surface ocean stratification (Francois et al., 1997), changes in the geometry of overturning cells in relation to sea ice coverage (Ferrari et al., 2014), reorganisation of surface buoyancy fluxes (Watson et al., 2015), and nutrient delivery and utilisation (Martin, 1990; Sigman et al., 2010).

The history of carbon storage and degassing in the ocean can be explored with a number of tracers, with radiocarbon proving particularly useful in directly reconstructing the ventilation age of seawater. When ^{14}C is transferred from the atmosphere (where it is continuously produced) to the ocean interior, it decays with a 5370 year half-life, allowing calculation of the time the ocean reservoir has been isolated. This technique relies on knowledge of atmospheric ^{14}C through time, which has been constructed using terrestrial records (Reimer et al., 2013), and precise dating of the seawater archive material. Cold-water corals are especially useful for

these reconstructions as their aragonite skeleton can be dated independently using U-Th methods (see Cheng et al., 2000). A dual approach utilising both ^{14}C and Nd isotope composition can give a more complete picture of carbon sources and the circulation changes potentially contributing to their release (e.g. Skinner et al., 2013; Wilson et al., 2014).

Radiocarbon records from cores and cold-water corals from the Atlantic, Drake Passage and Tasmania have been instrumental in building a picture of carbon release from the deep ocean (Barker et al., 2010; Burke and Robinson, 2012; Chen et al., 2015; Hines et al., 2015; Skinner et al., 2010). There is now strong evidence that, during two rapid atmospheric CO_2 increases at ~14.7 ka and ~ 11.6 ka, ^{14}C gradients were eroded between deep and shallow waters (Burke and Robinson, 2012; Chen et al., 2015; Skinner et al., 2010). Concomitant increases in AMOC overturning strength (McManus et al., 2004) and low-pH excursions in upper cell waters of the Drake Passage (Rae et al., 2018) suggests a Northern Hemisphere driver and Southern Ocean release for stored carbon. The first rapid deglacial CO_2 increase at 16.2 ka is less well explained, however. Antarctic Intermediate Water was considered a candidate for transporting a depleted signature to the eastern North Pacific and northern Indian Ocean during this time (Bryan et al., 2010; Marchitto et al., 2007), but the absence of a depleted signal from sites further upstream along the modern pathway of AAIW (Burke and Robinson, 2012; De Pol-Holz et al., 2010) has led to suggestions that these ^{14}C signals arose from local controls, rather than reflecting Southern Ocean processes.

In this study we present cold-water coral ^{14}C data from a new region, the southwest Indian Ocean. This site not only crucially bridges a gap in data between sites in the Atlantic and Pacific Oceans but should also provide insights into changes in flux of North Atlantic-sourced water close to its pathway into the Southern Ocean, and in the impact of shifts of the Agulhas Current and potentially the northern ACC fronts on local and regional ventilation. This new data may also shed light on the origins and routes of carbon released during deglacial

atmospheric CO_2 increases, especially for the first centennial-scale pulse during Heinrich Stadial 1.

Throughout this chapter, the terms 'enrichment' and 'depletion' refer to instances where the ^{14}C content of seawater is respectively higher or lower relative to the contemporaneous atmosphere. This is equivalent to a reduction or increase in the ^{14}C age offset between seawater and the atmosphere - the 'B-atm age' of the CWC samples. When discussing Nd isotope data, the terms 'radiogenic' and 'unradiogenic' will be used to refer to samples or seawater that have respectively higher or lower ε_{Nd} values, as in Chapter 4.

5.1.1 Modern ocean radiocarbon distribution

The distribution of ^{14}C in the deep ocean broadly follows the pattern of overturning circulation. The most enriched waters with highest $\Delta^{14}C$ values (deviation from the preindustrial modern atmosphere in parts per mil) are found in North Atlantic Deep Water (~ -70 ‰; Broecker et al., 1960) and the most depleted in the deep Pacific (~ -240 ‰), with deep Indian (~ -190 ‰) and circumpolar waters (~ -160 ‰) falling in between (Stuiver et al., 1983). In the southwest Indian Ocean, as well as the wider Southern Ocean, there is a steep gradient in surface $\Delta^{14}C$ as progressively older waters outcrop towards the south (Stuiver and Östlund, 1980; 1983; Fig. 5.1). Bomb-enriched ^{14}C can be seen down to ~ 800 m between 30 - 40°S from samples collected in the 1970's (Stuiver and Östlund, 1983), potentially mixed in by the turbulence of the Agulhas Return Current. At the depths of AAIW, $\Delta\,^{14}C$ ranges from ~ 20 ‰ to -120 ‰ (Fig. 5.1). Upper Circumpolar Deep Water is less enriched, between ~ -70 and -150 ‰. Below this, waters are close to uniform at ~ -150 to -160 ‰ (Östlund and Stuiver, 1980; Stuiver and Östlund, 1983), with the exception of one profile close to the southern tip of South

Africa which records an enrichment to ~ -100 ‰ seen between ~ 2000 - 3500 m (Östlund and Stuiver, 1980), likely caused by inflow of NADW.

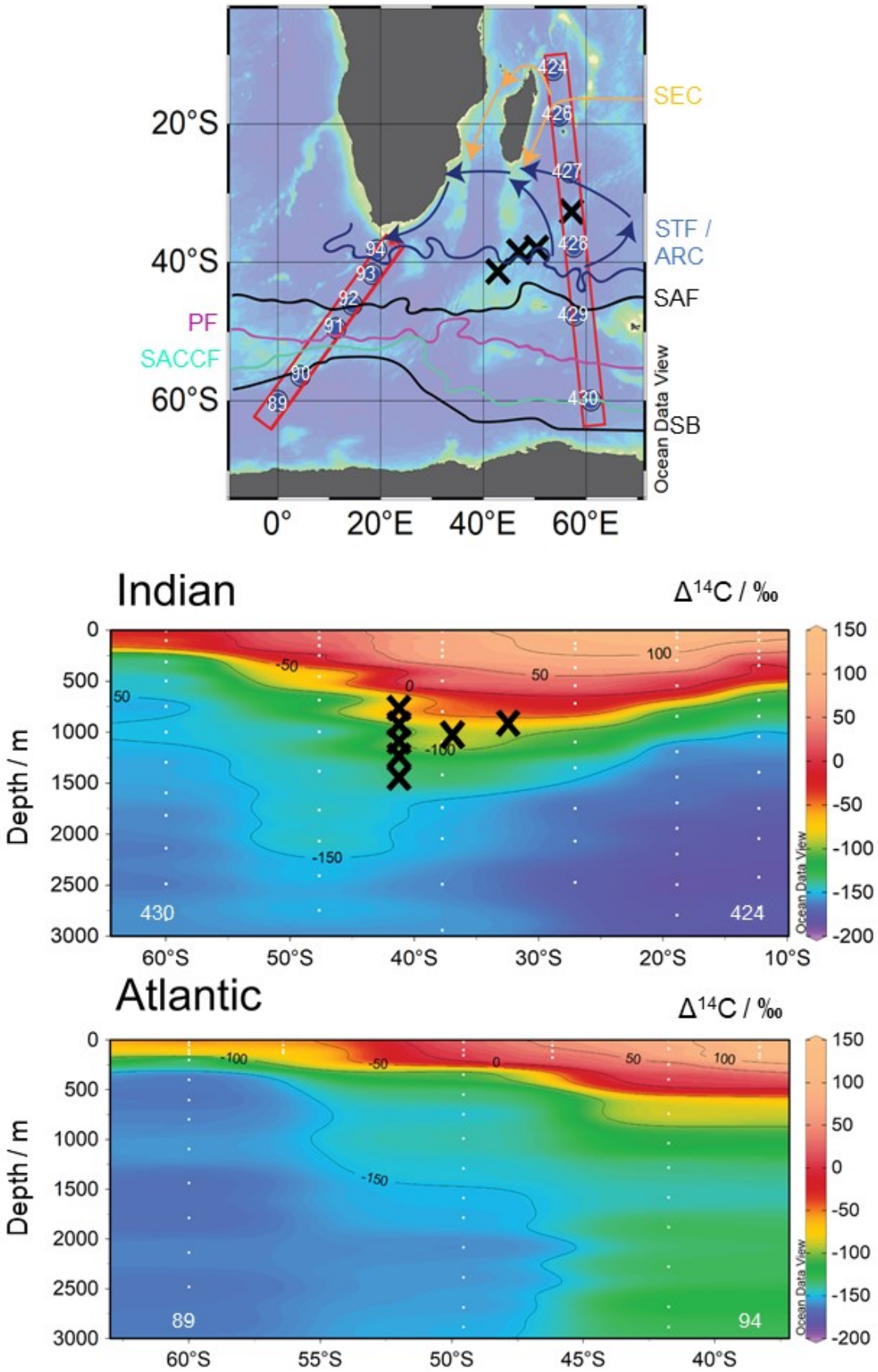
20°S
40°S
60°S
0°
20°E
40°E
60°E
SEC
STF /
ARC
SAF
PF
SACCF
SB
Ocean Data View
424
426
427
428
429
430
94
93
92
91
90
89
Indian
Δ14C / ‰
Depth / m
430
424
Atlantic
Δ14C / ‰
Depth / m
89
94
60°S
55°S
50°S
45°S
40°S
30°S
20°S
10°S

Figure 5.1: Modern seawater $\Delta^{14}C$ distribution in the southwest Indian and southeast Atlantic sectors of the Southern Ocean. GEOSECS stations 89-94 (Stuiver and Östlund, 1980) and 424-430 (Stuiver and Östlund, 1983) are indicated with white dots. Regional surface currents and front locations are, from south to north, the Southern Boundary of the ACC (SB; black), the southern ACC front (SACCF; turquoise), the Polar Front (PF; magenta), the Subantarctic Front (SAF; black), the Subtropical Front / Agulhas Return Current (STF / ARC; navy) and the South Equatorial Current (SEC; orange; Amakawa et al., 2019; Sokolov and Rintoul, 2009). The locations of cold-water corals in this study are shown with black crosses. Sections were plotted using weighted-average gridding in Ocean Data View (Schlitzer, 2017).

5.2 Samples and methods

The subfossil coral samples discussed in this chapter were collected in 2011 during expedition JC066 of the *RV James Cook* from four seamounts along the southwest Indian Ocean Ridge (SWIOR). From south to north, these are Coral Seamount (41°21'23" S, 42°50'31" E), Melville Bank (38°31'56" S, 46°45'74" E), Middle of What Seamount (37°56'76" S, 50°22'16" E), and Atlantis Bank (32°42'01" S, 57°17'26" E; see Chapters 3 and 4).

5.2.1 Materials and methods

A total of 161 fossil scleractinian coral skeletons were sampled opportunistically during dives of the Kiel 6000 ROV (Rogers and Taylor, 2011). Following age screening using a rapid laser ablation method, 55 samples were selected for precise dating including 2 duplicates. These were all from the species *Desmophyllum dianthus* or genus *Caryophyllia*, as these were robust enough to withstand the cleaning procedures and have been calibrated to modern seawater for Nd isotopes most successfully (Copard et al., 2010; Struve et al., 2017; van de

Flierdt et al., 2010). The methodologies for isotope dilution U-series dating and Nd isotope analysis are detailed in Chapters 2 and 4 of this thesis.

Twenty-four samples (including four procedural duplicates) were selected for radiocarbon analysis. Three Late Holocene samples were chosen in order to assess the accuracy of seawater ^{14}C reconstruction, forming a vertical transect through SAMW, AAIW and UCDW. Samples that were measured successfully are from both north (Middle of What Seamount, n = 5) and south (Coral Seamount, n = 10) of the modern day STF, at depths corresponding to modern-day positions of AAIW and UCDW. This spread enabled a multi-dimensional assessment of deglacial ventilation changes.

Full details of the sample preparation, dating and radiocarbon measurement methodology can be found in Chapter 2. The fraction modern (Fm; the sample $^{14}C/^{12}C$ over the modern atmospheric $^{14}C/^{12}C$, corrected for fractionation) and calendar ages of the samples (derived from the precise U-Th ages) were used to calculate a number of other parameters. The deviation of the sample ^{14}C activity from the preindustrial modern atmosphere in parts per mil is calculated using the equation: $\Delta^{14}C = (Fm \times e^{(\text{calendar age}/8267)} - 1) \times 1000$ (see Chen et al., 2015; Senstrom et al., 2011). This value includes corrections for both isotope fractionation and the decay of ^{14}C that takes place between coral death and measurement, providing an estimate for seawater $\Delta^{14}C$ at the time the coral was alive. The offset between the $\Delta^{14}C$ of the seawater and the contemporaneous atmosphere from IntCal13 (Reimer et al., 2013), $\Delta\Delta^{14}C$, was also calculated. The difference in ^{14}C age between the sample and atmosphere, B-atm, was the most useful tool for comparison across the record as it accounts for changes in the overall ^{14}C inventory (Burke and Robinson, 2012; Chen et al., 2015; Cook and Keigwin, 2015). All measured and calculated values are reported in Table 5.1.

5.3 Results

5.3.1 Late Holocene $\Delta^{14}C$

Three late Holocene corals all have $\Delta\Delta\ ^{14}C$ values within modern seawater range in the region (Fig. 5.2). At -67‰, the sample from Atlantis Bank at SAMW depths is almost identical in value to seawater measured at the same depth at GEOSECS site 93 (Stuiver and Östlund, 1980). This sample is the most enriched of the three, which is to be expected given its lower latitude. Although it was recovered from shallower water depth, the sample from AAIW depths at Coral Seamount is slightly more depleted, with a $\Delta\Delta\ ^{14}C$ of -93 ‰, part-way between seawater at sites 91 and 93 (Stuiver and Östlund, 1980; Fig. 5.2). The sample from UCDW depths at Coral Seamount has the most depleted $\Delta\Delta\ ^{14}C$ of the three at -108 ‰, again very close to the nearby seawater profiles.

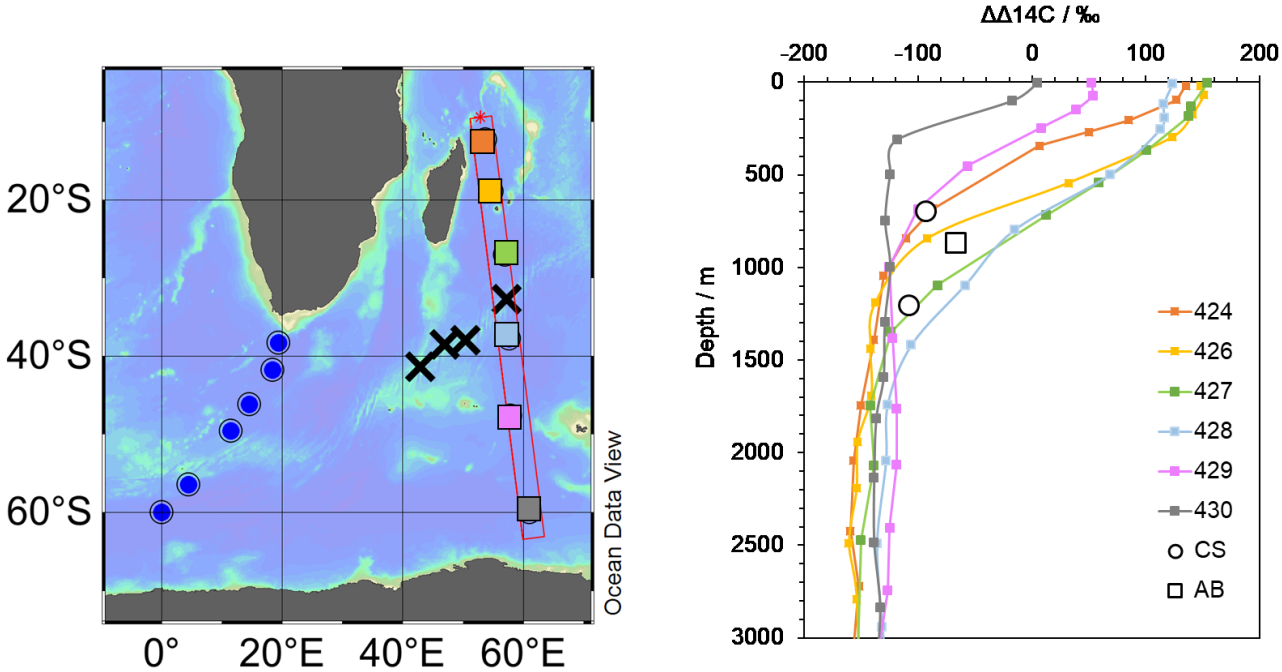

Figure 5.2: Late Holocene coral $\Delta\Delta^{14}C$ from Coral Seamount (circles) and Atlantis Bank (square), and modern seawater $\Delta\Delta^{14}C$ from GEOSECS stations 424 and 426-430; Stuiver and Östlund, 1983) in the southwest Indian Ocean. Blue dots show the positions of GEOSECS stations 89-94 (Stuiver and Östlund, 1980) used to construct the Atlantic section in in Fig 5.1.

5.3.2 Deglacial to Early Holocene $\Delta^{14}C$

Over the period 400 - 16,400 years BP, the $\Delta^{14}C$ values of 15 cold-water corals from 700 to 1395 m water depth in the southwest Indian Ocean show a range of 369 ‰ (Table 5.1). A maximum value of 246 ‰ is reached in the early deglacial, and the minimum value of -123 ‰ is observed in the Late Holocene (Fig. 5.3A). The overall trajectory of coral $\Delta^{14}C$ values follows the decreasing trend of atmospheric $\Delta^{14}C$, with the largest offset ($\Delta\Delta^{14}C$ = -156 ‰) occurring during Heinrich Stadial 1 (18 – 14.7 ka; Buizert et al., 2014) and the smallest offset ($\Delta\Delta^{14}C$ = -29 ‰) occurring during the early Holocene (Fig. 5.3B). Throughout the deglacial, the $\Delta\Delta^{14}C$ of SWIO cold-water corals (-29 to -156 ‰) remains within range of modern mid-depth waters in the region (~ -20 to -160 %, Stuiver and Östlund, 1983, 1980). There does not seem to be an appreciable difference between the UCDW samples and AAIW in terms of ventilation age overall (Fig. 5.4).

Duplicate samples were taken from different parts of the skeletons of four corals and underwent the full measurement procedure. Two of these were within 1σ standard deviation of the ^{14}C age of their duplicate, and two were within 2σ. Five samples from corals between 12.9 and 13.6 kyrs BP were excluded from further analysis, as their $\Delta^{14}C$ values were more enriched than, or close in value to, the contemporaneous atmospheric $\Delta^{14}C$ (Fig. 5.3A; Table 5.1). This may have arisen due to incomplete cleaning of the aragonite skeleton, as those specimens exhibited considerable alteration.

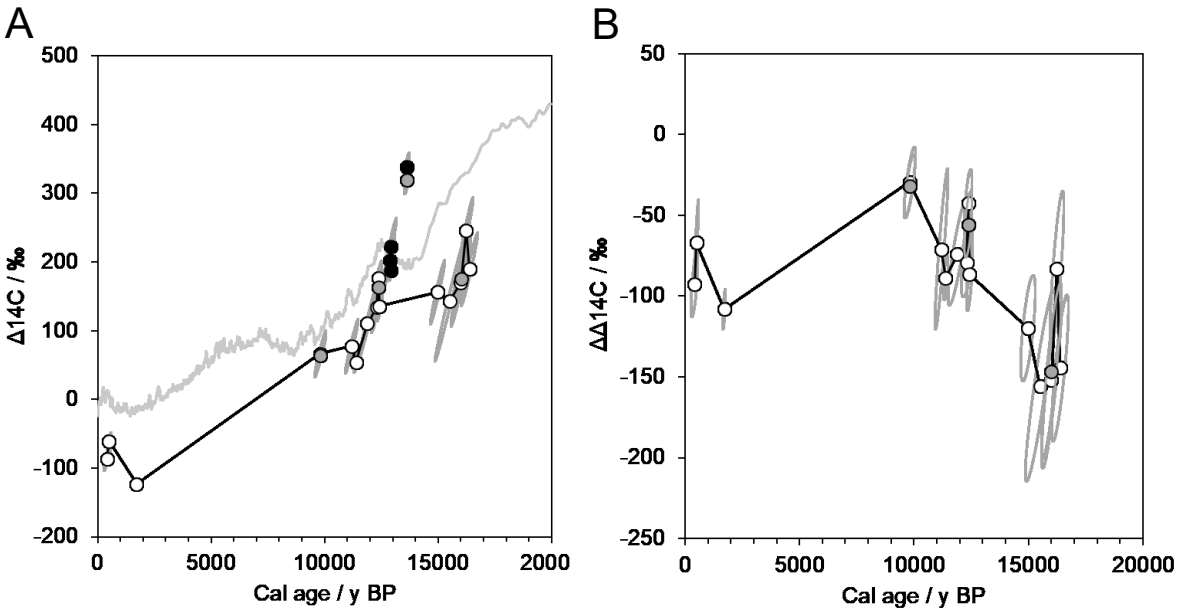

Figure 5.3: **A)** $\Delta^{14}C$ and **B)** $\Delta^{14}C$ offset from the contemporaneous atmosphere, $\Delta\Delta^{14}C$, reconstructed from southwest Indian Ocean cold-water corals, with uncertainties represented by 2σ error ellipses. Atmospheric radiocarbon (IntCal13; Reimer et al., 2013) is shown with a grey line. Duplicate samples are represented by grey filled circles and samples removed due to high $\Delta^{14}C$ values are shown by black dots.

In order to account for the changing $\Delta^{14}C$ inventory and approximate more closely the ventilation age of the seawater through time, 'B-atm' was calculated for the samples (also known as $t_{B\text{-}Atm}$; Cook and Keigwin, 2015; Fig. 5.4). This is the difference between the ^{14}C age of the sample and the contemporaneous atmosphere. In the SWIO samples B-atm ages range from 1028 years during the early deglaciation to 220 years during the early Holocene. The only reversal of this trend towards younger ages takes place between ~12 and 11 kyrs BP, where there is high sampling resolution. Late Holocene B-atm ages range from 933 to 539 years.

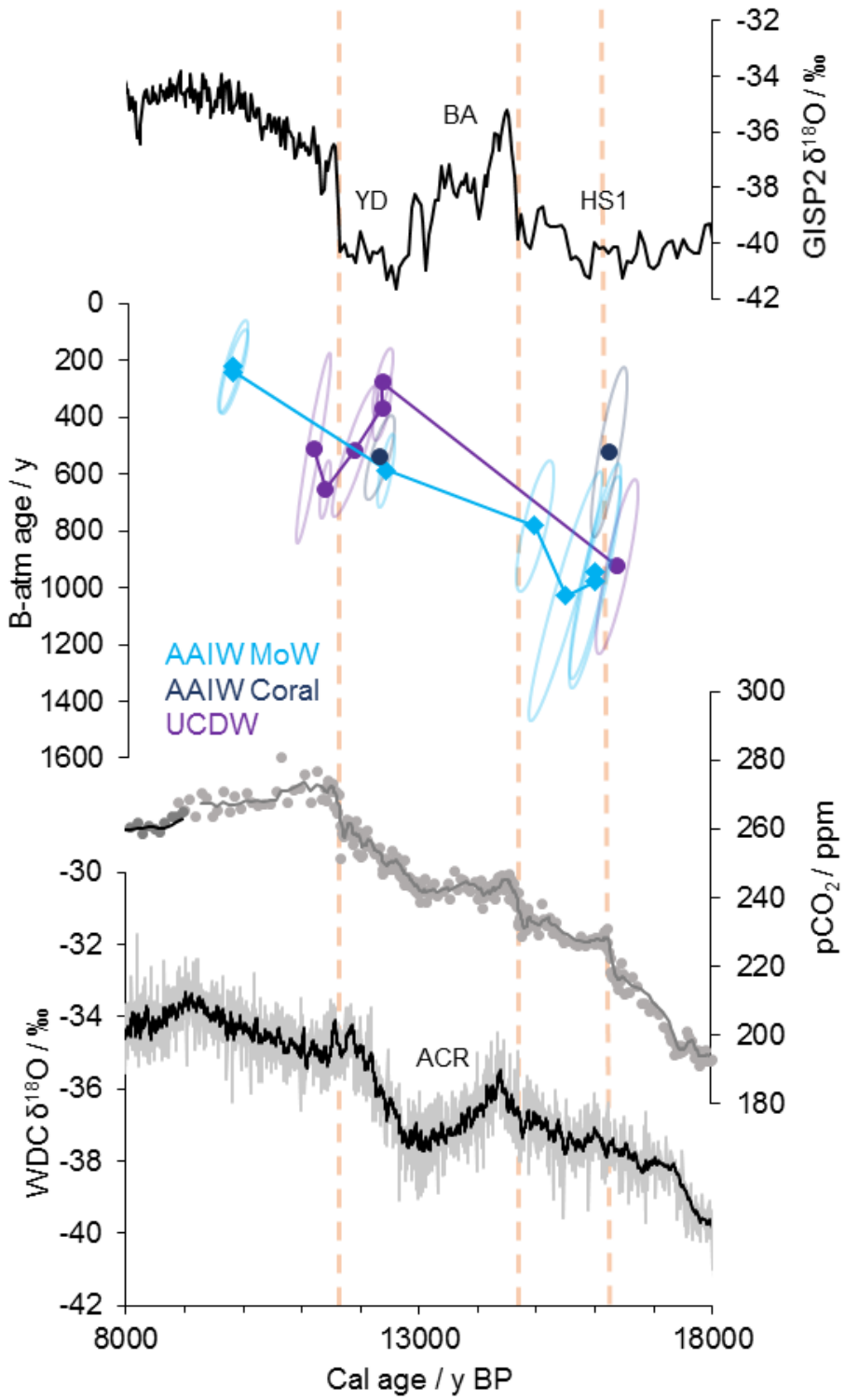

Figure 5.4: B-atm ages of cold-water corals from the southwest Indian Ocean, split into Antarctic Intermediate Water (AAIW, blue) and Upper Circumpolar Deep Water (UCDW, purple) depth samples from Coral Seamount (dots) and Middle of What Seamount (diamonds), with uncertainties represented by 2σ error ellipses. Heinrich Stadial 1 (HS1), the Bølling-Allerød (BA), the Antarctic Cold Reversal

(ACR) and the Younger Dryas (YD) are annotated. The top panel displays the Greenland oxygen isotope record from GISP2 (Stuiver et al., 1995); the bottom panel shows the WAIS Divide Core (WDC) atmospheric CO_2 (Marcott et al., 2014) and oxygen isotope records (WAIS Divide Project Members, 2015). Vertical dashed orange lines mark three most pronounced centennial-scale atmospheric CO_2 increases during the deglacial.

5.4 Discussion

The new SWIO cold-water coral radiocarbon record shows clear variability throughout the deglacial, which is discussed below in the context of other radiocarbon and climate records.

5.4.1 Heinrich Stadial 1 (18-14.7 ka)

Samples between 15 and 16 ka in age from Middle of What and Coral Seamount record the most depleted $\Delta\Delta^{14}C$ values of the deglacial (~ -150‰; Fig. 5.3B), with B-atm ages ~ 1000 years (Fig. 5.4), placing them at the lower end of the modern seawater range (Fig. 5.2). In the absence of data for earlier parts of HS1, or the LGM, these late HS1 data points describe the least ventilated waters throughout the record. Samples from both AAIW depths at Middle of What Seamount and UCDW depths at Coral Seamount are equally depleted at this time.

A ^{14}C depletion in mid-depth waters in the SWIO could have resulted from a more northerly position of the Subtropical and Subantarctic fronts than the modern day, due to the pronounced meridional gradient in $\Delta^{14}C$ (Figs. 5.1, 5.2). Deglacial reconstructions of front positions around the Southern Ocean are inconclusive and at times contradictory (e.g. De Deckker et al., 2012). Abundances of warm-water foraminiferal species at Site TNO57-21 in the Southeast Atlantic Ocean suggest that the latter part of HS1 was the warmest of the deglacial period (Barker et al., 2009). Therefore, it is more likely that the corals were bathed

in waters more enriched than they would have been under modern surface hydrography, under a scenario with southward-shifted fronts.

Across the mid-depth Southern Ocean during HS1 there appears to be a greater disparity in ventilation ages compared to the modern day, where seawater $\Delta^{14}C$ profiles are relatively similar across the Atlantic, Indian and Pacific sectors (Östlund and Stuiver, 1980; Stuiver and Östlund, 1983, 1980). The oldest B-atm ages are found in the SW Pacific (Hines et al., 2015), followed by the Drake Passage at UCDW depths (Burke and Robinson, 2012) and finally the youngest values in the SWIO and AAIW depths in the Drake Passage (Figs 5.5, 5.6). This suggests that either (i) differently aged water masses were bathing the sites, (ii) there was greater stratification between AAIW and UCDW and/or (iii) the ACC was less effective at delivering ^{14}C enriched, Atlantic-sourced waters to the circumpolar ocean. The latter hypothesis could explain the discrepancy between the Pacific sites and the SWIO if overturning circulation was potentially weaker. Although transport of NADW at depth may have been reduced at this time (McManus et al., 2004; Fig. 5.6), a shoaled Atlantic-sourced water mass could have delivered relatively enriched carbon to the SWIO (Huang et al., 2014). Indeed, the SWIO samples share similar B-atm ages to those from intermediate waters in the Equatorial Atlantic (~ 1000 y; Chen et al., 2015; Fig. 5.5).

This theory does not explain why the Tasmanian corals record older ventilation ages than the Drake Passage, however. The highest B-atm ages in the Southern Ocean during HS1 were found in the deep South Atlantic and southwest Pacific (Barker et al., 2010; Skinner et al., 2015, 2010; Fig. 5.5). As the ACC shifted southwards after the LGM (Barker et al., 2009), some of this old carbon may have begun to mix into UCDW as deep currents encountered major topographic features upstream or in the vicinity of Tasmania such as the Kerguelen Plateau and Macquarie Ridge (Tamsitt et al., 2017). One would expect a signal of this old carbon to also be seen near the SWIOR, but there is the possibility that only AAIW was

sampled at Coral Seamount due to lower sea levels (Carlson and Clark, 2012). Deeper samples in the SWIO during HS1 would help to explore this idea further. Another possibility is that the Tasman corals experienced greater PDW influence during HS1, a water mass which could have transmitted old carbon to the Southern Ocean from the north Pacific.

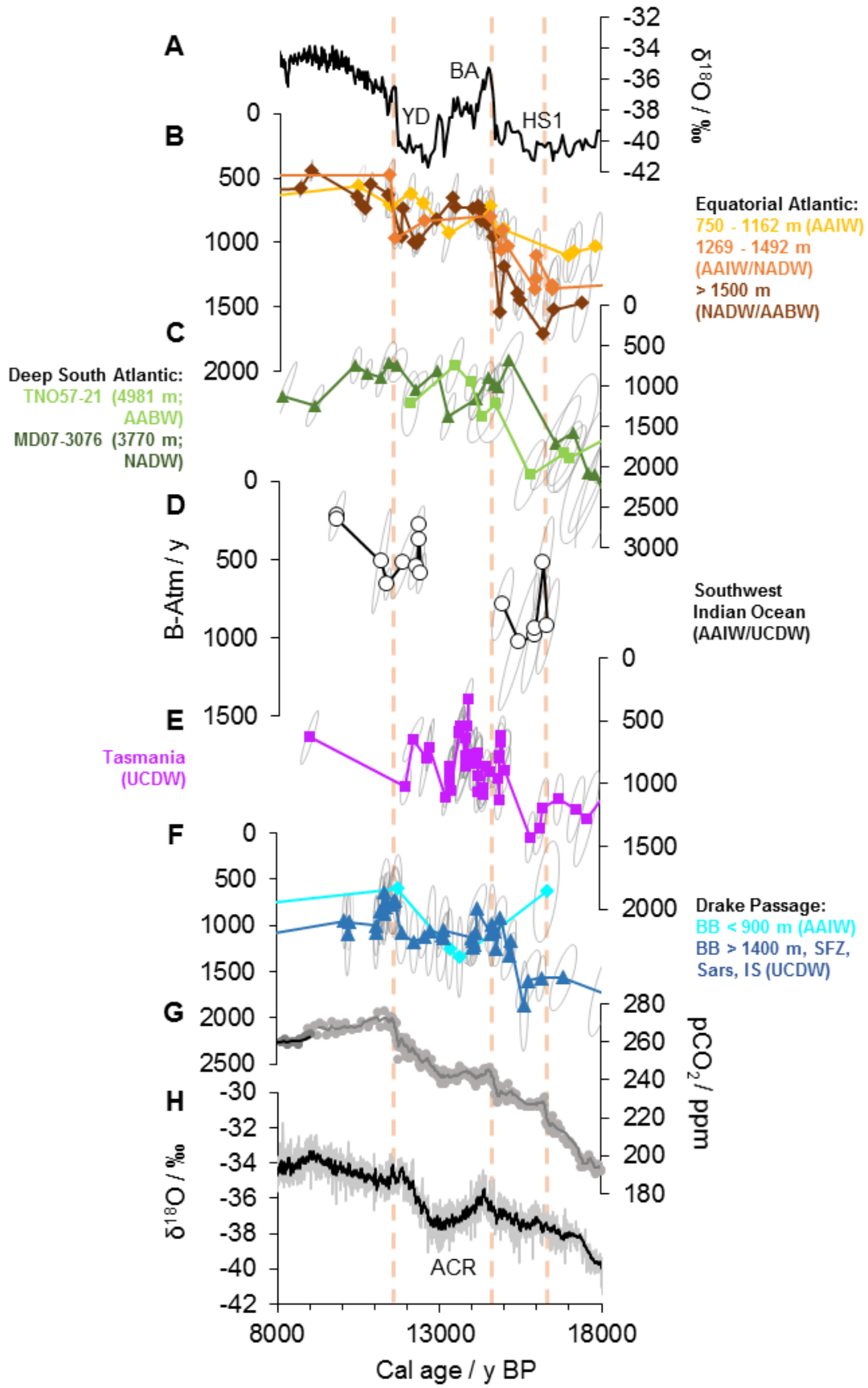
A
B
C
D
E
F
G
H
BA
YD
HS1
ACR
δ18O / ‰
Equatorial Atlantic:
750 - 1162 m (AAIW)
1269 - 1492 m (AAIW/NADW)
> 1500 m (NADW/AABW)
Deep South Atlantic:
TNO57-21 (4981 m; AABW)
MD07-3076 (3770 m; NADW)
B-Atm / y
Southwest Indian Ocean (AAIW/UCDW)
Tasmania (UCDW)
Drake Passage:
BB < 900 m (AAIW)
BB > 1400 m, SFZ, Sars, IS (UCDW)
pCO2 / ppm
Cal age / y BP

Figure 5.5: Deglacial ocean B-atm records from the Atlantic and Southern Oceans. **A)** Greenland oxygen isotope record from GISP2 (Stuiver et al., 1995); **B)** Cold-water coral (CWC) B-atm ages from the equatorial Atlantic, separated by depth range (Chen et al., 2015), **C)** sedimentary B-atm ages from cores TN057-21 (Barker et al., 2010) and MD07-3076 (Skinner et al., 2010) in the deep South Atlantic, **D)** CWC B-atm ages from the southwest Indian Ocean (white circles, this study), **E)** south of Tasmania (magenta triangles; Hines et al., 2015), **F)** and at AAIW (turquoise diamonds) and UCDW (blue triangles) depths in the Drake Passage (Burke and Robinson 2012; Chen et al., 2015); **G)** West Antarctic Ice Sheet Divide Core atmospheric CO_2 (Marcott et al., 2014) and **H)** oxygen isotope record (WAIS Divide Project Members, 2015). Dashed orange lines represent periods of centennial-scale atmospheric CO_2 increase. Timings of Heinrich Stadial 1 (HS1), the Bølling-Allerød (BA), the Antarctic Cold Reversal (ACR) and the Younger Dryas (YD) are indicated.

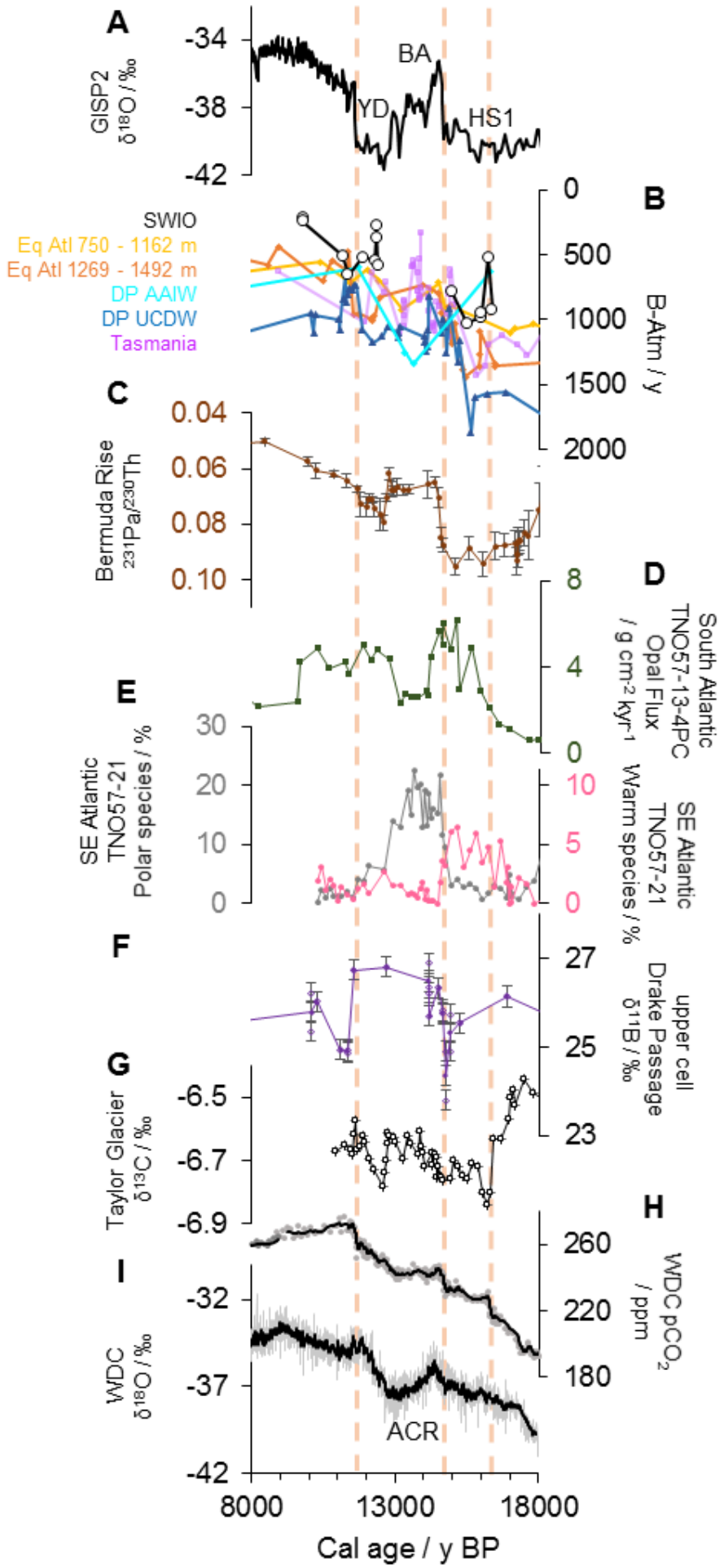
A
GISP2
δ18O / ‰
-34
-38
-42
BA
YD
HS1
B
SWIO
Eq Atl 750 - 1162 m
Eq Atl 1269 - 1492 m
DP AAIW
DP UCDW
Tasmania
B-Atm / y
0
500
1000
1500
2000
C
Bermuda Rise
231Pa/230Th
0.04
0.06
0.08
0.10
D
South Atlantic
TNO57-13-4PC
Opal Flux
/ g cm-2 kyr-1
8
4
0
E
SE Atlantic
TNO57-21
Polar species / %
30
20
10
0
SE Atlantic
TNO57-21
Warm species / %
10
5
0
F
upper cell
Drake Passage
δ11B / ‰
27
25
23
G
Taylor Glacier
δ13C / ‰
-6.5
-6.7
-6.9
H
WDC pCO2
/ ppm
260
220
180
I
WDC
δ18O / ‰
-32
-37
-42
ACR
8000
13000
18000
Cal age / y BP

Figure 5.6: Deglacial ocean ventilation and upwelling records from the southern hemisphere. **A)** Greenland oxygen isotope record from GISP2 (Stuiver et al., 1995); **B)** cold-water coral B-atm ages (refer to Figure 5.5 caption for details and references); **C)** sedimentary Pa/Th from the Bermuda Rise (McManus et al., 2004); **D)** opal flux from core TN057-13-4PC in the Atlantic sector of the Southern Ocean (Anderson et al., 2009); **E)** percentage abundance of 'polar' (grey) and 'warm' (pink) foraminiferal species from core TN057-21 in the Southeast Atlantic (note different scales; Barker et al., 2009); **F)** Upper cell cold-water coral $\delta^{11}B$ data with individual measurements (averages) in open (filled) diamonds from the Drake Passage (Rae et al., 2018); **G)** Taylor Glacier $\delta^{13}C$ record (Bakusa et al., 2016); **H)** WAIS Divide Core (WDC) atmospheric CO_2 record (Marcott et al., 2014) and **I)** oxygen isotope record (WAIS Divide Project Members, 2015). Shaded bars represent periods of millennial- (pale orange) and centennial-scale (green) atmospheric CO_2 increase. Timings of Heinrich Stadial 1 (HS1), the Bølling-Allerød (BA), the Antarctic Cold Reversal (ACR) and the Younger Dryas (YD) are indicated.

A very short-lived excursion is recorded at 16.2 ka by one sample from ~ 900 m at Coral Seamount, to a B-atm of 525 y (Fig. 5.4). Due to its transience, it is tempting to link the event to frontal movement, which could have briefly situated the sample site in a more ventilated part of the water column. In the modern ocean, surface ^{14}C ages can vary by ~ 500 years between fronts (Stuiver and Östlund, 1980); and therefore a shift of 5° could produce an excursion of the magnitude seen in the record. As discussed earlier, it is likely that the STF was poleward of its modern position during late HS1 (Barker et al., 2009; Fig. 5.6), which would make enriched $\Delta^{14}C$ values at Coral Seamount more likely. However, samples within calendar age error from further north at Middle of What seamount have considerably older B-atm ages (980 y and 1028 y; Fig. 5.4). We should expect to see B-atm ages at least as young at MoW, if not younger, unless the presence of a particularly strong Agulhas Return Current over Coral Seamount enriched the signal locally due to vigorous mixing, as is the case further north

in the modern ocean (Fig. 5.1). Interestingly, an equally enriched signal occurs in the Drake Passage almost simultaneously (B-atm = 586 y; Burke and Robinson, 2012; Fig. 5.5). Furthermore, ventilation ages are similar to those observed at intermediate water depths in the subtropical southeast Pacific (B-atm ~ 530 y; De Pol-Holz et al., 2010).

Given that North Atlantic Deep Water is the most radiocarbon-enriched water mass below the thermocline in the Southern Ocean (Broecker et al., 1960), it is also worth exploring as a cause of the enrichment. Some NADW is known in the modern day to enter the SWIO directly at around the latitude of Coral Seamount (van Aken et al., 2004). Reconstructions close to the source of NADW from the New England Seamounts in the northwest Atlantic at 16.3 ka give $\Delta^{14}C$ values of between 200 and 250 ‰ at mid-depths, with a minimum of ~ 175 ‰ at 16.2 ka (Robinson et al., 2005). These values are very similar to the enrichment of corals in the SWIO and Drake Passage, which record $\Delta^{14}C$ values of 246 and 242 ‰ respectively. There is no indication of an increase in the rate of MOC from the deep ocean at this time (McManus et al., 2004; Fig. 5.6), but transport of northern-sourced waters could have taken place at shallower depths than the modern day (Bradtmiller et al., 2014; Huang et al., 2014).

The peak in $\Delta^{14}C$ in the SWIO coincides with a rapid increase in atmospheric CO_2 of 12 ppm, a spike in CH_4 and a decrease in atmospheric $\delta^{13}C$ at around 16.2 ka (Bauska et al., 2016; Marcott et al., 2014; Rhodes et al., 2015; Figs. 5.4 – 5.6). We therefore explore the idea that the signal could be evidence of a rapid release of aged carbon occurring close to the latitude of the Drake Passage and SWIO sites. Some depleted carbon from the deep ocean may have been transported to the upper cell earlier in HS1, recorded by a gradual enrichment of samples from the deep South Atlantic (Skinner et al., 2010; Fig. 5.5). Then, an ice rafting event in the North Atlantic (Stern and Lisiecki, 2013) may have triggered warming in the South Atlantic, a migration of the ITCZ, and southern hemisphere westerlies reaching a threshold latitude which enhanced air-sea gas exchange over the Southern Ocean (Menviel et al., 2018). This series of

events could be responsible for the peak in ventilation age we see in the Southwest Indian Ocean and Drake Passage intermediate waters (Figs. 5.5, 5.6). Following this carbon release and/or entrainment of atmospheric carbon, vertical mixing and horizontal transport from deeper water masses may have re-supplied depleted carbon, causing the signal to be short-lived. More AAIW samples from the locations in question would be useful to constrain the duration of this event.

Between 15.5 and 15.0 ka, a radiocarbon enrichment occurs in the southwest Indian Ocean from ~ 1000 to 800 B-atm years (Fig. 5.4). Almost simultaneously, a decrease in B-atm from 1400 – 900 y occurs in the Southwest Pacific (Hines et al., 2015) and from 1600 to 1000 y in the Drake Passage (Burke and Robinson, 2012; Chen et al., 2015; Figs. 5.5, 5.6). Therefore, we can infer a widespread enrichment in upper-cell waters in the Southern Ocean at this time, albeit of a smaller magnitude than that seen in the lower cell (Burke and Robinson, 2012; Skinner et al., 2010; Fig. 5.5). Some aged carbon could have been released directly to the atmosphere from deep waters south of the ACC, with progressively more enriched carbon transported northwards via surface and intermediate waters. The gradual increase in atmospheric $\delta^{13}C$ seen at this time suggests that some of the carbon release may have also occurred due to rising sea surface temperatures (Bauska et al., 2016; Fig. 5.6). There may have been an additional role for frontal positions: during this period the STF is thought to have reached a poleward maximum, which may have decreased the B-atm age of waters bathing the seamounts (Barker et al., 2009; Fig. 5.6).

The rapid warming in the Northern Hemisphere and atmospheric CO_2 increase at the end of HS1 has recently been attributed to an 'AMOC overshoot', whereby old carbon is flushed out of the deep ocean by enhanced deep water formation in the North Atlantic (Chen et al., 2015; Rae et al., 2018). In the upper cell of the Southern Ocean there is evidence of this event from a low-pH excursion at around 14.7 ka (Rae et al., 2018; Fig. 5.6) and a 'degassing'

of intermediate waters in the SW Pacific (Allen et al., 2015). One might expect the fingerprint from this event to be seen in other upper cell records, such as the SWIO. Unfortunately, there is a paucity of coral samples at this interval (Fig. 5.4). No notable ^{14}C depletion can be seen at this time in the higher-resolution Tasmanian record (Hines et al., 2015; Fig. 5.5), which might suggest that the old carbon was rapidly released from the upper cell after being incorporated from below, before a depleted ^{14}C signal could reach lower latitudes, or that the Tasmanian samples were bathed in waters sourced from the deep Pacific, rather than the Southern Ocean.

5.4.2 Younger Dryas (12.8-11.7 ka)

No radiocarbon results were obtained from the Antarctic Cold Reversal (Table 5.1). During the Younger Dryas, at ~ 12.4 ka, samples from the SWIO have the lowest ventilation ages of the deglacial (B-atm = ~ 300 years; Fig. 5.4). This feature includes both UCDW- and AAIW-depth samples from both seamounts. Like HS1, this was a period of low northern hemisphere temperatures (Andersen et al., 2004), low AMOC strength (McManus et al., 2004) and increased upwelling in the Southern Ocean (Anderson et al., 2009; Fig. 5.6). Therefore, it seems plausible that increased air-sea gas exchange in the circumpolar ocean, due to an optimal poleward position of SH westerlies, is responsible for the apparent ventilation in mid-depth waters. The two AAIW–depth corals from the YD have very similar ventilation ages, despite being from different seamounts (Fig. 5.4), which could indicate they occupy a similar position with respect to the fronts, possibly north of the STF. A small peak in warm foraminiferal species at core TNO57-21 in the SE Atlantic supports this idea, though it is not as pronounced as the 16.2 ka peak during HS1 (Barker et al., 2009; Fig. 5.6). A ventilation increase is also recorded at this time south of Tasmania, but only to ~ 650 B-atm years (Hines et al., 2015; Figs. 5.5, 5.6). The extremely low B-atm ages of the SWIO samples at this time may not be circumpolar, instead reflecting the positioning of the STF and ARC over the seamounts. Earlier

in the YD, at 13.9 ka, a brief enrichment event of a similar magnitude is seen at the Tasmanian site (Hines et al., 2015; Figs. 5.5, 5.6); taken together these two events may be evidence of a progressive migration of the STF.

In contrast, many of the deeper ocean records show a peak in ventilation ages between 12.4 and 12.1 ka, with B-atm ages of > 1000 years recorded at UCDW depths in the Drake Passage (Burke and Robinson, 2012; Figs. 5.5, 5.6), and the lower cell in the southeast Atlantic (Skinner et al., 2010; Barker et al., 2010) and equatorial Atlantic (Chen et al., 2015; Fig. 5.5). This could be due to a reduction in the delivery of enriched NADW to the deep ocean, as indicated by high sedimentary PaTh ratios in the deep Northwest Atlantic Ocean (Bermuda Rise; McManus et al., 2004; Fig. 5.6) and highly depleted deep waters bathing the New England seamounts in the Northwest Atlantic (Robinson et al., 2005). In the first part of the YD, the vertical gradient in $\Delta^{14}C$ between the upper and lower cells seems to have increased, due to a combination of this reduced Atlantic export and intermediate water ventilation in the Southern Ocean.

An older ventilation age of ~ 650 B-atm years is recorded in the mid depth Southwest Indian Ocean at 11.4 ka (Fig. 5.4). This could represent a final transfer of old carbon, flushed out by a re-invigorated AMOC (McManus et al., 2004; Fig. 5.6), from the lower to upper cells, depleting mid-depth waters at the SWIOR. Corals from UCDW depths in the Drake Passage and deep sediments from the South Atlantic both record a concurrent enrichment, reaching almost identical B-atm values to the SWIO (Burke and Robinson, 2012; Chen et al., 2015; Figs. 5.5, 5.6). In deep waters of the Equatorial Atlantic, the most enriched values are found (< 500 B-atm years; Chen et al., 2015; Fig. 5.5). Taken together, this picture seems to indicate a release of carbon from the deep ocean and a rapid transfer to intermediate waters and the atmosphere as indicated by the final rapid rise in atmospheric CO_2 concentration during the deglaciation (Marcott et al., 2014; Figs. 5.4 – 5.6). Deep sea coral $\delta^{11}B$ data from the Drake Passage support

this hypothesis, with a pronounced minimum in upper cell pH at 11.7 ka (Rae et al., 2018; Fig. 5.6).

5.4.3 Early Holocene

The youngest ventilation age in the record is found in the early Holocene at ~ 9 ka (B-atm = 220 y; Fig. 5.4). Relatively low values are also seen in the intermediate Drake Passage, Tasmania and the equatorial Atlantic at the time, but none as enriched as the SWIO (Fig. 5.5). Therefore, it is likely that this is a local signal, representing vigorous transport of CO_2 from the surface ocean to deeper waters as a result of close proximity of the STF/ARC to Middle of What Seamount. Close to this location in the modern ocean, GEOSECS station 428 recorded seawater offsets from atmospheric $\Delta^{14}C$ of -15.4 ‰ at 797 m and -59 ‰ at 1096 m (Stuiver and Östlund, 1983; Fig. 5.2), meaning the $\Delta\Delta^{14}C$ value of -27 ‰ of the 1014 m coral sample sits at the enriched end of the modern range. The early Holocene is described as a thermal optimum in the Southern Hemisphere (Masson et al., 2000), with high SST in the subantarctic southern Indian Ocean (Labracherie et al., 1989). Under these conditions it seems likely that the STF and ARC would have been south of their present-day location, rather than close to Middle of What Seamount, and indeed there is evidence from the southwest Pacific that this was the case (Sikes et al., 2009). Therefore, the ventilation in the early Holocene may be due to a deeper mixed layer in the subtropical gyre. Subsequently, during the mid-Holocene, there is evidence that southern hemisphere westerlies moved equatorward, and wind stress weakened (Lamy et al., 2010), potentially altering the structure of the Drake Passage water column (Struve et al., under revision).

In summary, radiocarbon data at the SWIO seem to reflect three distinct processes during the deglaciation: (i) release of old carbon upstream in the Southern Ocean following ice sheet retreat and/or more optimal westerly wind position between 15.5 and 15 ka; (ii) flushing out of old radiocarbon due to resumption of NADW export from the North Atlantic at 11.4 ka,

and (iii) unusually young radiocarbon ages at 16.2, 12.4 and 9 ka, probably related to the exact position of the fronts and/or a deep ventilation of the water column.

5.5 Combined ^{14}C and Nd analysis

Fourteen of the 15 samples successfully measured for ^{14}C also have Nd isotope composition data. Direct comparison reveals correlations between ε_{Nd} and both $\Delta\Delta^{14}C$ (R^2 = 0.6) and B-atm ages (R^2 = 0.4), such that more radiogenic samples on average have higher $\Delta^{14}C$ and ^{14}C-age offsets from the contemporaneous atmosphere (Fig. 5.7).

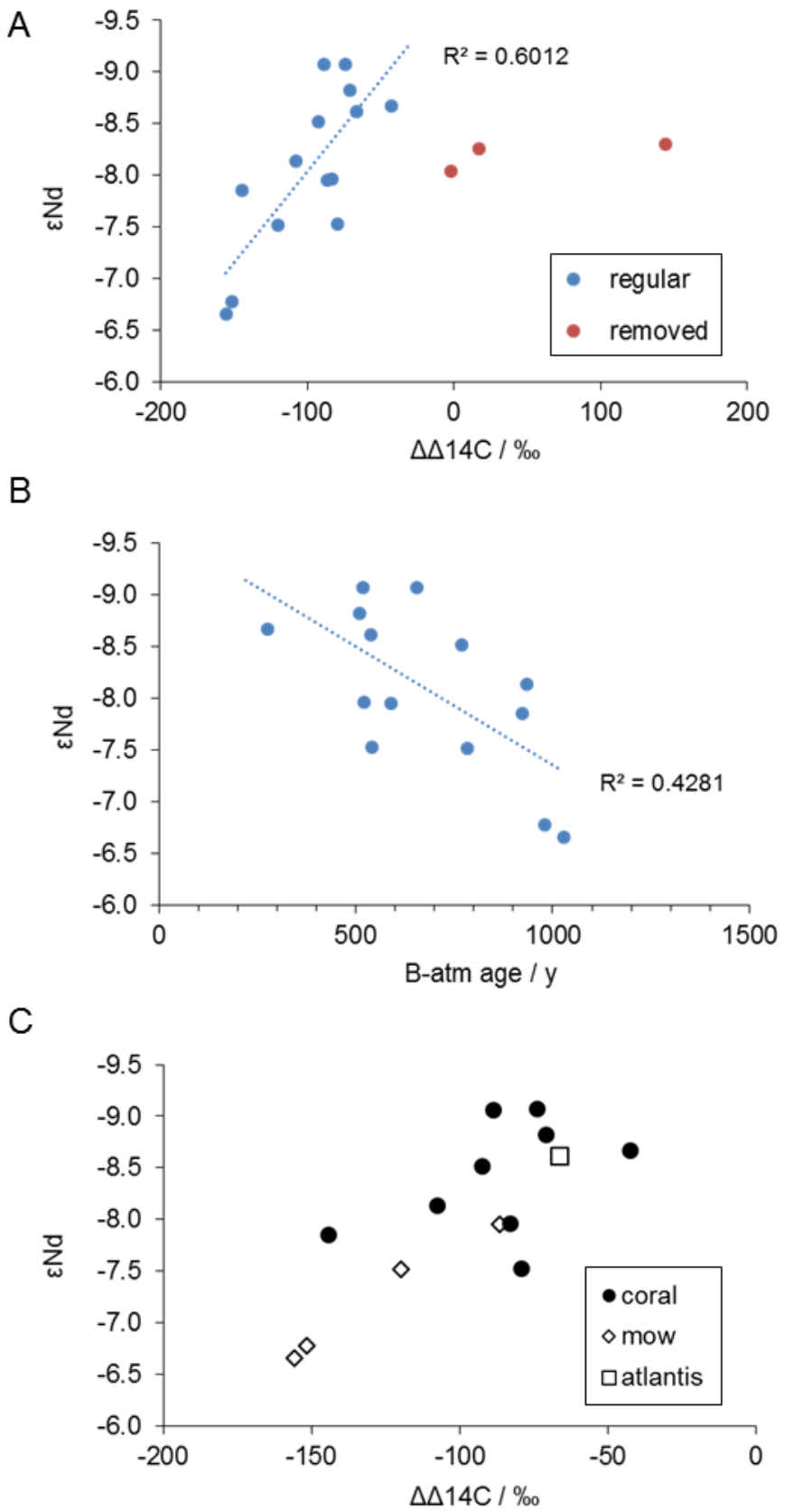
A
-9.5
-9.0
-8.5
-8.0
-7.5
-7.0
-6.5
-6.0
εNd
R² = 0.6012
regular
removed
-200
-100
0
100
200
ΔΔ14C / ‰
B
-9.5
-9.0
-8.5
-8.0
-7.5
-7.0
-6.5
-6.0
εNd
R² = 0.4281
0
500
1000
1500
B-atm age / y
C
-9.5
-9.0
-8.5
-8.0
-7.5
-7.0
-6.5
-6.0
εNd
coral
mow
atlantis
-200
-150
-100
-50
0
ΔΔ14C / ‰

Figure 5.7: Comparisons between ε_{Nd} and ^{14}C data from southwest Indian cold-water coral samples. Nd isotope composition plotted against A, $\Delta\Delta^{14}C$ in samples used for interpretations (blue dots) and those removed due to unfeasible ^{14}C values (red dots); B, B-atm age; and C, $\Delta\Delta^{14}C$ with samples from Coral Seamount indicated with black dots, Middle of What Seamount with open diamonds, and Atlantis Bank with open squares.

The correlation suggests that the changes seen in εNd through the deglacial have physical oceanographic drivers, as opposed to chemical inputs. These could be changes in the degree of mixing between radiogenic/poorly-ventilated and unradiogenic/well-ventilated end-members, or independent responses of the two parameters to changes such as breakdown in stratification and shifts in wind belt.

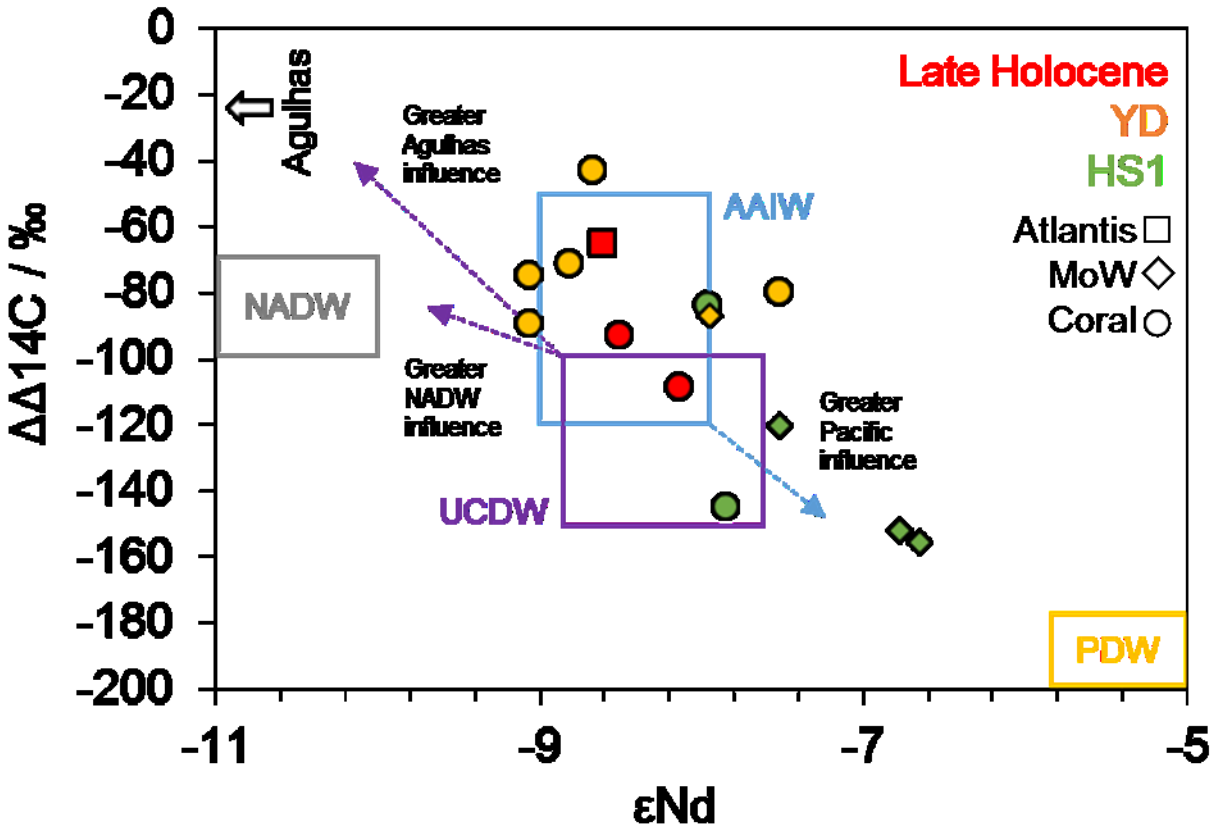

Figure 5.8: ε_{Nd} and $\Delta\Delta^{14}C$ from cold-water coral samples from Coral Seamount (circles), Middle of What Seamount (diamonds) and Atlantis Bank (squares) dating to the Late Holocene (red), the Younger Dryas (yellow; YD) and Heinrich Stadial 1 (green; HS1). Boxes indicate estimates for the modern-day ε_{Nd} (Amakawa et al., 2019; Garcia-Solsona et al., 2014b; Lambelet et al., 2018; Stichel et al., 2012a) and $\Delta\Delta^{14}C$ ranges (Stuiver and Östlund, 1983, 1980) of regionally influential water masses: North Atlantic Deep Water (NADW; grey), Antarctic Intermediate Water (AAIW; blue), Upper Circumpolar Deep Water (UCDW; purple), and Pacific Deep Water (PDW; yellow). As ε_{Nd} values as low as -15 have been recorded surface waters of the Agulhas Current (Amakawa et al., 2019) it is indicated by an arrow. Dashed arrows signify the potential influence of different end members at the depths of the corals.

5.5.1 Heinrich Stadial 1

Of the samples which exhibit relatively depleted ^{14}C values during HS1, those from Middle of What Seamount are also the most radiogenic of the record (ε_{Nd} ~ -6.7), whilst the sample from Coral Seamount has an ε_{Nd} of -7.9, within the range of mid-depth waters in the modern SWIO (Fig. 5.8). The Coral Seamount sample with a very young B-atm age dated to 16.2 ka has an ε_{Nd} of -8.0.

5.5.1.1 Possible Northern Indian intermediate water influence

The resolvable difference in Nd isotope composition between the two sites, despite their proximity, opens the possibility that intermediate waters sourced from the northern Indian Ocean were more influential at Middle of What Seamount during HS1. As far south as 20°S, Red Sea Water (RSW) is known to occupy similar densities as AAIW (Beal et al., 2000; Fine, 1993), and is visible in profiles from the Somali and Mascarene Basins (Bertram and Elderfield, 1993). Traces of this water mass have even been observed in the Agulhas overshoot region south of South Africa (Gordon et al., 1987) and in AAIW in the southwest Pacific (Lynch-

Stieglitz et al., 1994). Away from the path of the Agulhas Current its extension further south is thought to be prevented by the northward spread of AAIW (Wyrtki, 1971).

At depths in the western Indian Ocean where the influence of high-salinity RSW can be observed, intermediate waters exhibit ε_{Nd} values of -6.7 to -7.3 (Bertram and Elderfield, 1993), notably more radiogenic than AAIW in the region of the SWIOR (~ 8.2; Amakawa et al., 2019). Radiocarbon values appear to be similar to AAIW, however, with $\Delta^{14}C$ values at these depths of ~ -110 to -155 (Stuiver and Östlund, 1983; Fig. 5.8). Therefore, perhaps only a small amount of radiogenic RSW is required to shift the ε_{Nd} of intermediate waters, whilst retaining the $\Delta^{14}C$ signature of AAIW. In this case, enhanced RSW incursion could be a plausible hypothesis for shared ventilation ages and different Nd isotopic compositions of mid-depth corals at Middle of What and Coral seamounts. However, as the route for intermediate waters out of the Red Sea is through a shallow strait only ~137 m deep, it is difficult to imagine RSW being stronger during HS1 when sea level was ~ 100 m lower than the present day (Carlson and Clark, 2012).

5.5.1.2 More radiogenic AAIW in general

Given evidence that export of NADW to the Southern Ocean was reduced during HS1 (McManus et al., 2004; Piotrowski et al., 2012; Roberts et al., 2010), that PDW production increased (Okazaki et al., 2010) and export extended polewards (Struve, 2016; Fig. 5.9) it seems likely that early deglacial AAIW was more radiogenic and radiocarbon-depleted than today. Neodymium isotope compositions within error of those at Middle of What Seamount were also recorded during this period in intermediate waters in both the Drake Passage (Wilson and Struve, pers. comm.) and the Bay of Bengal (Yu et al., 2018; Fig. 5.9). This seems to suggest that the samples from Middle of What Seamount, rather than Coral Seamount, are more typical of AAIW characteristics during HS1.

The similarity between the intermediate SWIO and northern Bay of Bengal sites could be taken as further evidence that AAIW reached a more northerly extent than the modern day in the Indian Ocean (Yu et al., 2018). This water mass does not appear to provide a conduit for the extremely depleted $\Delta^{14}C$ values described by Bryan et al. (2010), however; in the intermediate SWIO B-atm ages are ~ 1500 years younger than those recorded in the northern Indian Ocean during HS1. The old ventilation ages recorded in both the northern Indian Ocean and the eastern Pacific (Marchitto et al., 2007) are thought to have been the result of local releases of depleted carbon, mixing from Antarctic Bottom Waters, or isolation and in-situ decay of radiocarbon at intermediate depths (see Chen et al., 2015); this study provides more evidence in support of this hypothesis.

In this proposed scenario where AAIW is radiogenic and more latitudinally extensive, a shallower direct inflow of NADW at ~ 40°S could be responsible for the less radiogenic ε_{Nd} at Coral Seamount, with such a signal being diluted further downstream along the ACC (i.e., in the Drake Passage) by PDW. Upper cell waters in the Cape Basin just west of Coral Seamount also record ε_{Nd} values around -8 at this time (Hu et al., 2016; Fig. 5.9); complementary radiocarbon records from the intermediate South Atlantic would help to test this idea. The relative enrichment of the mid-depth SWIO in comparison to UCDW in the Drake Passage (Burke and Robinson, 2012), and similarity of the B-atm ages between the SWIO and AAIW-depths in the intermediate Atlantic (Chen et al., 2015) suggests that both ^{14}C samples at Coral Seamount were bathed by AAIW. This is not unfeasible, as the deeper sample is only ~ 100m below the modern AAIW/UCDW boundary, sea level was considerably lower (Carlson and Clark, 2012), and the STF/ARC may have been in a more southerly position (Barker et al., 2009; Fig. 5.9), possibly close to or south of Coral Seamount. The ~ 500-year ventilation age gap between AAIW in the SWIO and UCDW in the Drake Passage indicates that greater stratification than the modern day existed at mid-depths during HS1, before the

breakdown in stratification recorded at 14.7 ka (Barker et al., 2010; Burke and Robinson, 2012; Chen et al., 2015). It appears in fact that, during most of HS1, AAIW was better ventilated than contemporaneous NADW in the equatorial Atlantic (Chen et al., 2015).

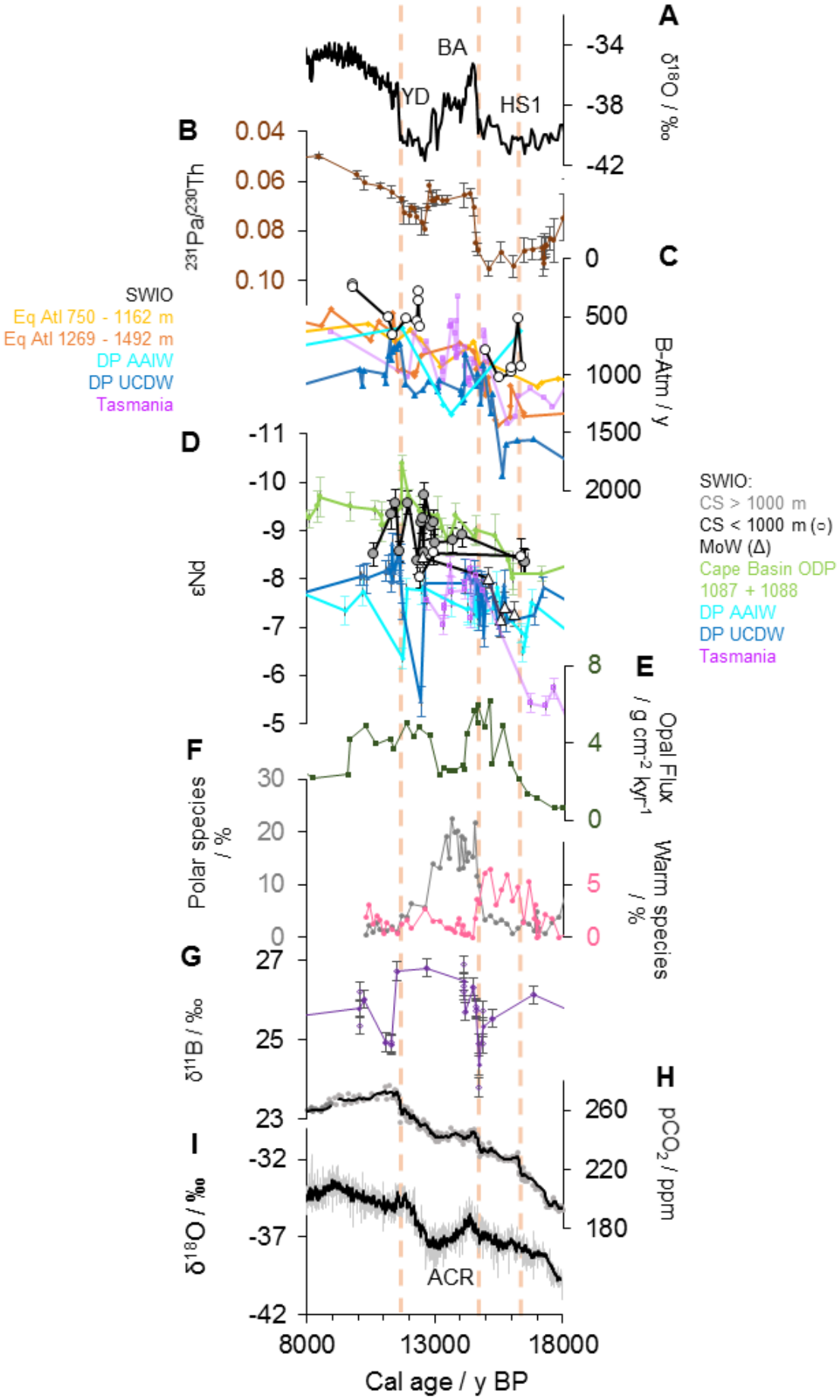
A
BA
YD
HS1
-34
-38
-42
δ18O / ‰
B
0.04
0.06
0.08
0.10
231Pa/230Th
C
0
500
1000
1500
2000
B-Atm / y
SWIO
Eq Atl 750 - 1162 m
Eq Atl 1269 - 1492 m
DP AAIW
DP UCDW
Tasmania
D
-11
-10
-9
-8
-7
-6
-5
εNd
SWIO:
CS > 1000 m
CS < 1000 m (○)
MoW (Δ)
Cape Basin ODP
1087 + 1088
DP AAIW
DP UCDW
Tasmania
E
8
4
0
Opal Flux / g cm-2 kyr-1
F
30
20
10
0
Polar species / %
5
0
Warm species / %
G
27
25
23
δ11B / ‰
H
260
220
180
pCO2 / ppm
I
-32
-37
-42
δ18O / ‰
ACR
8000
13000
18000
Cal age / y BP

Figure 5.9: Deglacial ocean ventilation, water mass structure and frontal position records from the Atlantic and Southern Oceans, plus ice core records. **A)** Greenland oxygen isotope record from GISP2 (Stuiver et al., 1995); **B)** sedimentary Pa/Th from the Bermuda Rise (McManus et al., 2004); **C)** cold-water coral B-atm ages (refer to Figure 5.5 caption for details and references); **D)** cold-water coral ε_{Nd} from Coral Seamount > 1000 m (grey circles), < 1000 m (white circles) and Middle of What Seamount (white triangles) in the southwest Indian Ocean (this study), sedimentary ε_{Nd} from cores 1087 (1372 m) and 1088 (2082 m) in the Cape Basin (Hu et al,. 2016), cold-water coral ε_{Nd} from Antarctic Intermediate Water and Upper Circumpolar Deep Water depths in the Drake Passage (Wilson and Struve, pers. comm.), and from south of Tasmania (Struve, 2016); **E)** opal flux from core TN057-13-4PC in the Atlantic sector of the Southern Ocean (Anderson et al., 2009); **F)** percentage abundance of 'polar' (grey) and 'warm' (pink) foraminiferal species from core TN057-21 in the Southeast Atlantic (note different scales; Barker et al., 2009); **G)** Upper cell cold-water coral $\delta^{11}B$ data from the Drake Passage with individual measurements (averages) in open (filled) diamonds (Rae et al., 2018); **H)** WAIS Divide Core atmospheric CO_2 record (Marcott et al., 2014) and **I)** oxygen isotope record (WAIS Divide Project Members, 2015). Dashed lines represent periods of centennial-scale atmospheric CO_2 increase. Timings of Heinrich Stadial 1 (HS1), the Bølling-Allerød (BA), the Antarctic Cold Reversal (ACR) and the Younger Dryas (YD) are indicated.

5.5.1.3 'Gradient' between Pacific and Atlantic sectors

If we consider all samples from the SWIO to be bathed in AAIW during HS1, adding the Nd data somewhat clarifies the perceived Indian / Pacific gradient in radiocarbon. The most radiogenic ε_{Nd} values in the mid-depth Southern Ocean are found in the SW Pacific (Struve, 2016; Hu et al., 2016), followed by the Drake Passage (Wilson and Struve, pers. comm) and finally SWIO and the Cape Basin (Hu et al., 2016; Fig. 5.9). This provides further evidence that the old ventilation ages are likely sourced from the Pacific and carried to the circumpolar

ocean by PDW, a signal which is diluted slightly by the ACC before the water reaches UCDW in the Drake Passage.

If we do not consider all samples to be from AAIW, the 'UCDW-depth' sample at Coral Seamount is much younger in ventilation age and is more unradiogenic than UCDW samples from HS1 in the Drake Passage. This could potentially have arisen if the flow of the ACC was weaker during the early part of the stadial and strengthened at the end, when the ventilation ages at the Southern Ocean sites converge. Records of flow speed from sediment cores in the Drake Passage do indicate that the SAF may have been in a more northerly position, truncated by the South American continent, until about 15 ka (Lamy et al., 2015; Roberts et al., 2017). This could have reduced communication between the Indian/Atlantic and Pacific regions of the Southern Ocean. Alternatively, shallow topography downstream of the Drake Passage and around the SWIO may have increased mixing and ventilation of UCDW before it reached Coral Seamount (Tamsitt et al., 2017).

5.5.1.4 16.2 ka enrichment

The 16.2 ka enrichment in radiocarbon is recorded by one sample at Coral Seamount with an ε_{Nd} of -8.0. The finding that the ^{14}C excursion is not accompanied by a shift in Nd isotopic composition implies that, rather being due to incursion of a different water mass, a local or regional enrichment of AAIW could be responsible. This is supported by the lack of evidence for AMOC resumption (McManus et al 2004) at this time (Fig. 5.9). The excursion is timed almost simultaneously with the first centennial-scale CO_2 increase of the deglaciation (Marcott et al., 2014; Fig. 5.4).

The presence of a deep current, such as the ARC, over Coral Seamount at 16.2 ka could have mixed well-ventilated waters down to AAIW depths, a feature seen in the modern ocean (Stuiver and Östlund, 1983; Figs. 5.1, 5.2). It is possible that the ARC could have been

positioned further south than the modern day, given the evidence that HS1 was a particularly warm period in the region (Barker et al., 2009; Fig. 5.9).

However, the almost simultaneous drop in atmospheric radiocarbon, and the presence of a low B-atm age coral sample in the Drake Passage, suggest a more widespread ventilation event occurred. Further evidence that the event was caused by release of old carbon from intermediate waters comes from a $\delta^{13}C$ enrichment observed in the southwest Pacific (Bostock et al., 2004; Sikes et al., 2016).

Such an event could be caused by retreat of the sea ice edge, enabling air-sea carbon exchange further south in the ACC, and/or a more vigorous ACC and increase in upwelling, driven by a more southerly position of the southern hemisphere westerlies (see Toggweiler et al., 2006). Evidence of these processes occurring around the time of the enrichment includes low ssNa concentrations in Antarctic ice, indicating less presence of sea ice (WAIS Divide Project Members, 2013); a peak in SST at 41°S in the South Atlantic (Barker and Diz, 2014); an increase in opal flux recorded across the Southern Ocean (Anderson et al., 2009; Fig. 5.9); and a peak in northern ACC flow speed (Lamy et al., 2015). This finding supports the proposal of Marcott et al. (2014) that the concomitant atmospheric carbon increase at the same time was due to ocean ventilation caused by atmospheric circulation shifts. It is worth noting that the radiocarbon enrichment is not seen in UCDW–depth records, which may be an indication that sea ice retreat around Antarctica was not extensive enough for air-sea exchange to occur south of the Polar Front (Nair et al., 2019; Shemesh et al., 2002; WAIS Divide Project Members, 2013).

5.5.1.5 Late HS1 ^{14}C enrichment

A single sample from Middle of What Seamount records both an enrichment in ^{14}C and a decrease in ε_{Nd} towards the end of HS1 (~ 15 ka). This radiocarbon enrichment is also seen

in records from the deep Southern Ocean (Burke and Robinson, 2012; Skinner et al., 2010) and Atlantic (Chen et al., 2015; Fig. 5.6). This event could be caused by a greater proportion of (enriched, unradiogenic) Atlantic-sourced waters entering the Southern Ocean, and/or release of carbon from the deep ocean, enriching the waters that supply AAIW. Atlantic overturning strength begins to increase at this time (McManus et al., 2004; Fig. 5.9), which could explain why the magnitude of ventilation change is greater in the deep than the intermediate ocean. A dramatic unradiogenic shift in ε_{Nd} in the Tasman record also occurs sometime between mid-HS1 and the end of HS1 (Struve, 2016; Fig. 5.9), suggesting that the incursion of PDW towards the Southern Ocean was reduced. This could also have played a role in the changing Nd isotope signature and the ventilation age of circumpolar water masses. The decrease in the ε_{Nd} and increase in ^{14}C of the SWIO coral, and of the ventilation of Drake Passage and Tasman UCDW seem to precede the pronounced increase in AMOC strength at ~ 14.7 ka; this may be worth investigating further in future.

5.5.2 Younger Dryas

5.5.2.1 High ventilation with periodic unradiogenic excursions

Following the gap in data during the ACR, samples from Middle of What and Coral Seamounts appear to converge in terms of ventilation and Nd isotope composition in the YD (Figs. 5.4, 5.9). Younger ventilation ages and ε_{Nd} values around -8 in intermediate waters at both seamounts suggest a modern-like oceanography, although there still does appear to be a gradient in Nd isotopes between the Atlantic / SWIO (-8 to -9) and Drake Passage / south of Tasmania (~ -7.4; Fig. 5.9). The deepest samples at Coral Seamount have fluctuating ε_{Nd} between ~ -9 and -8 which appears to be decoupled from radiocarbon age; the most enriched and depleted samples during the Younger Dryas both have Nd isotope values towards the unradiogenic end of the modern seawater range for this region.

5.5.2.2 12.4 ka enrichment

The fact that the youngest B-atm age of the deglacial is found in one of the deepest samples, with a relatively unradiogenic Nd isotopic composition (ε_{Nd} = -8.7), sheds some doubt on the interpretation that it represents an intermediate water ventilation event like that at 16.2 ka. During the Younger Dryas, generally younger B-atm ages are recorded at the Drake Passage and Tasmanian sites, but none reach the enrichment of the SWIO sample.

An alternative explanation could be that it represents a brief incursion of younger, unradiogenic NADW waters to Coral Seamount, at shallower depths than the modern day. There is no evidence of a simultaneous unradiogenic shift in other Southern Ocean mid-depth records; indeed, a prominent radiogenic ε_{Nd} peak is recorded in the Drake Passage (Wilson and Struve, pers. comm.; Fig. 5.9). In addition, an intermediate-depth sample dated to 12.4 ka from the SWIO also records a slightly radiogenic value of -7.5. This scenario would potentially only result in anomalously unradiogenic, enriched waters deeper at Coral Seamount, and is supported by the within-error Nd isotope compositions in Cape Basin upper deep waters (Hu et al., 2016; Fig. 5.9). However, corals from NADW depths upstream are more depleted than those in the Southern Ocean (Chen et al., 2015), so it does not seem to be a viable source of young waters during HS1. In addition, NADW transport was most likely lower than the modern day during the YD (McManus et al., 2004; Piotrowksi et al., 2012; Pahnke et al., 2008).

Records from the Southern Ocean region indicate similar conditions to HS1, with upwelling at a secondary deglacial peak (Anderson et al., 2009) and the SAF at a similar position to the modern day, with warm foraminiferal species recorded in the subtropical South Atlantic (Barker et al., 2009; Fig. 5.9). Unlike the HS1 enrichment, however, it seems less likely that the positioning of the ARC could result in ventilation of the waters directly around the sample at Coral Seamount: it is almost 300 m deeper in the water column than the 16.2 ka sample, and sea level was only ~ 60 m shallower than the modern day (Carlson and Clark,

2012). That being said, the lack of evidence in the atmospheric record for a large scale oceanic carbon ventilation event (Marcott et al., 2014) suggests it represents a local signal. Therefore, the most likely explanation is in fact a similar mechanism to the 16.2 ka event, with deep mixing either in the close vicinity of Coral Seamount by the ARC, or in the region of UCDW outcropping directly upstream in the South Atlantic or Indian sectors of the Southern Ocean.

5.5.2.3 Decrease in ventilation to 11.4 ka

Ventilation age at UCDW depths in the SWIO increases between 12.4 and 11.4 ka, to a maximum B-atm at the end of the YD recorded in a sample with an ε_{Nd} of -9.1 ± 0.2. This unradiogenic Nd isotope composition suggests that the old carbon may have been released from deeper waters at the same time as waters with a greater NADW component than the modern day were being delivered to the seamount. This may have occurred due to greater inflow directly to the SWIO south of South Africa, or an increase in export of NADW to the whole mid-depth circumpolar ocean (i.e. mixing between upper and lower cells). There is widespread evidence in support of the latter scenario. Northern Hemisphere temperature rose dramatically at ~11.7 ka (Stuiver et al., 1995) and sedimentary Pa/Th, a proxy for overturning strength of the AMOC, increased from a YD minimum (McManus et al., 2004; Fig. 5.9). Anomalously unradiogenic values in UCDW were also seen in the Cape Basin (Hu et al., 2016), and downstream in the Drake Passage (Wilson and Struve, pers. comm.; Fig. 5.9).

If this event represents a flushing out of the remaining reservoir of aged carbon from the lower cell of the overturning circulation, as is suggested by a pH minimum in the upper cell in the Southern Ocean (Rae et al., 2018; Fig. 5.9), one would expect to see a simultaneous ^{14}C enrichment in deep records. This has indeed been observed in the equatorial Atlantic (Chen et al, 2015) and the deep South Atlantic (Skinner et al., 2010), where in both locations B-atm ages drop to within error of the 'depleted' sample in the SWIO (Fig. 5.5). There is also an enrichment at UCDW depths in the Drake Passage (Burke and Robinson, 2012), which may suggest that

the old carbon was released from both deep and abyssal waters in the Atlantic sector, and upper deep waters in the Pacific, at the same time (Fig. 5.5). Sea salt sodium records suggest sea ice may have been less extensive than during HS1 (WAIS Divide Project Members, 2013), allowing ventilation directly from UCDW.

5.5.3 Early Holocene ventilation

Unfortunately, there is no corresponding Nd isotope data for the ^{14}C-enriched AAIW sample dated to the early Holocene temperature optimum (Masson et al., 2000), so it is difficult to draw any further conclusions about the nature of the ventilation. If it was due to the positioning of the ARC over Middle of What Seamount we may have expected a relatively unradiogenic ε_{Nd} (Fig. 5.8).

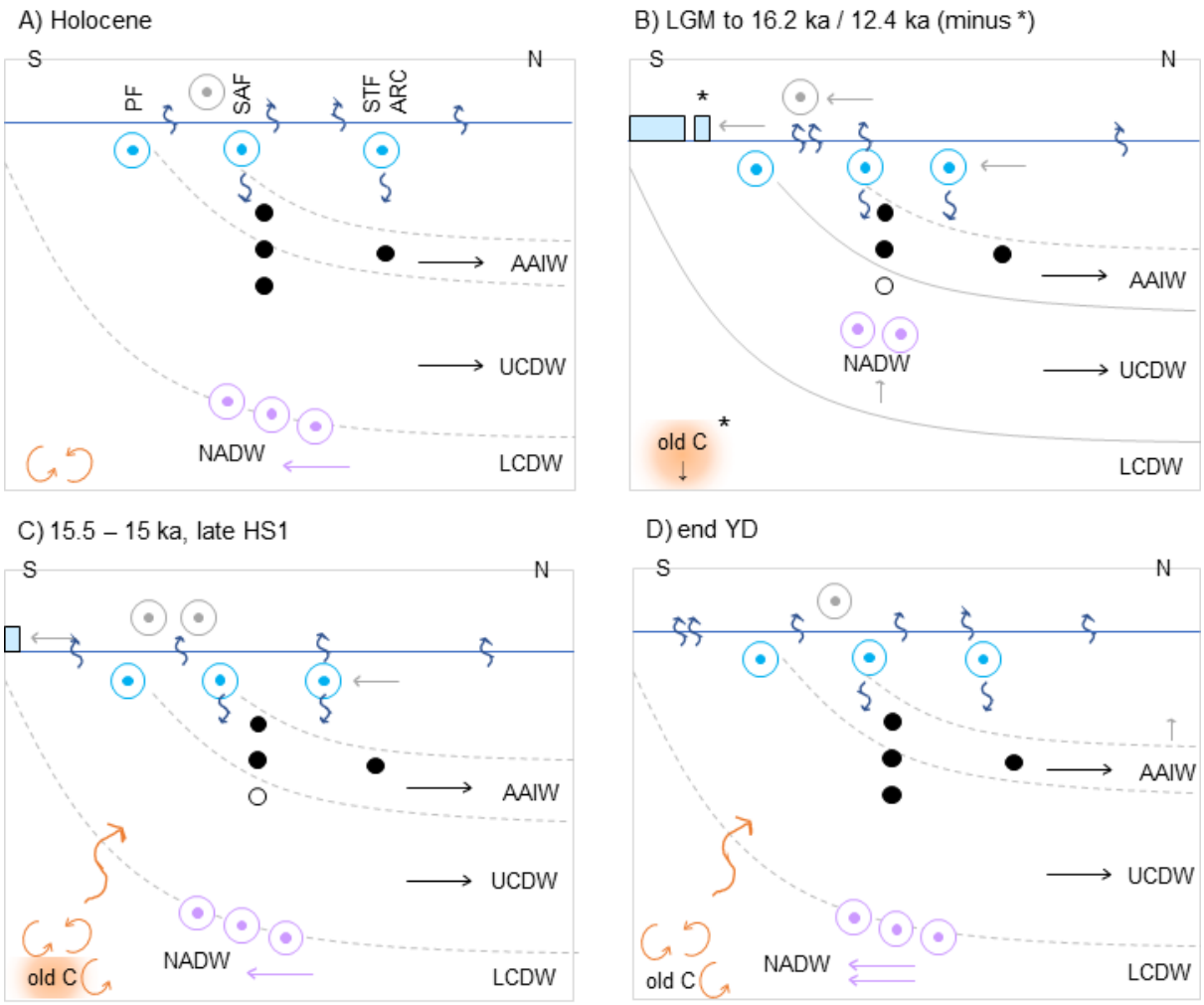

Figure 5.10: Schematic illustrating deglacial water mass and ventilation changes in the SWIO. Locations of cold-water coral samples measured for ^{14}C are indicated by black dots, and approximate positions of water mass boundaries by grey lines. **A)** The Holocene scenario: at Coral Seamount on the left, samples are from modern AAIW and UCDW depths, and at Middle of What Seamount on the right samples are located within modern AAIW. Surface currents are shown by blue dotted circles, with the Subtropical Front / Agulhas Return Current positioned over Middle of What Seamount, the Subantarctic Front south of Coral Seamount, and the Polar Front marking the boundary between the formation region of AAIW and the outcrop of UCDW. NADW incursion near the UCDW/LCDW boundary is shown by purple dotted circles. The position of the southern hemisphere westerlies, roughly over the Subantarctic Zone, is marked by a grey dotted circle, and in the bottom left corner mixing between the upper and lower overturning cells is shown by curved orange arrows. Air-sea exchange of CO_2 takes place across

the subantarctic and subtropical surface ocean and particularly at the SAF and ARC. This scenario, potentially with enhanced subtropical air-sea exchange, also existed in the early Holocene. **B)** Over the glacial period old carbon built up in the lower overturning cell (orange area), and the Southern Ocean was more stratified (grey isopycnals). At ~ 16.2 ka, southern hemisphere westerlies and the sea ice edge (blue boxes) shifted polewards, increasing ventilation of the intermediate ocean, possibly aided locally by strengthened ACC and ARC. NADW incursion was in a shoaled position, mixing more unradiogenic Nd to Coral Seamount samples at the same time as the ventilation event. Lower sea level causes more samples at Coral Seamount to be bathed in AAIW, there are no samples from a depth of > 1200 m from this period. The enrichment at 12.4 ka can be visualised in a similar way, albeit with reduced sea ice coverage, less old carbon stored in the deep ocean (*), and higher sea level. **C)** Towards the end of HS1, between 15.5 - 15.5 ka, strengthened southern westerlies, further retreat of sea ice, and resumption of modern-like NADW flux (purple arrow) increases mixing and release of old carbon from the deep and upper deep circumpolar ocean (orange arrows), causing AAIW in the SWIO to decrease in ε_{Nd} and ventilation age. **D)** The Younger Dryas is a period of relatively high ventilation in the mid-depth SWIO, with unradiogenic ε_{Nd} possibly supplied periodically at shallower depths by shoaled NADW (similar to B). At the end of the YD, increased NADW flux to the Southern Ocean released stored carbon once again from the deep ocean, causing a depletion and low-pH excursion at the same time as unradiogenic Nd values at UCDW depths. Samples close to and below the AAIW boundary at Coral Seamount record fluctuations in ε_{Nd} between -8 and -9. This mechanism can also be applied to the 14.7 ka 'flushing' event, which was not recorded by any samples in this study (Chen et al., 2015; Rae et al., 2018).

5.6 Conclusions

This study presents and explores the first deglacial radiocarbon measurements from the Southwest Indian Ocean. Fifteen cold-water coral samples were successfully measured from two seamounts positioned either side of the Subtropical Front in the modern day, and from depths equating to AAIW and UCDW. Paired Nd isotope measurements exist for 14 of the 15

samples and are utilised to constrain the causes of ^{14}C fluctuations. Much like ε_{Nd}, the B-atm ages of the deglacial samples, which are primarily dated to HS1 and the YD, remain roughly within the range of modern mid-depth waters in the SWIO. The region appears to have been relatively well ventilated, although B-atm ages are notably older during HS1. Three notable 'enrichment' events are recorded, at 16.2, 12.4 and 9 ka, and a 'depletion' event occurs between 12.4 and 11.4 ka. During HS1, in addition to increased stratification between the lower and upper overturning cells, a gradient exists in mid-depth ^{14}C age between Tasmania (Hines et al., 2015), the Drake Passage (Burke and Robinson, 2012; Chen et al., 2015), and the SWIO. More radiogenic ε_{Nd} values at the Pacific sites (Struve, 2016; Wilson and Struve, pers. comm.) suggest that the 'gradient' may result from a greater influence of PDW south of Tasmania, and of NADW in the Cape Basin (Hu et al., 2016) and Coral Seamount. Antarctic Intermediate Water is the most well-ventilated water mass during this period, more so than NADW (Chen et al., 2015), which may be the result of an optimal poleward position of Southern Hemisphere westerlies and the isolation of the upper overturning cell from old, deep waters. The enrichment at 16.2 ka most likely is the result of a widespread AAIW ventilation event, as it corresponds to a centennial-scale atmospheric CO_2 increase (Marcott et al., 2014) and is also recorded in the intermediate Drake Passage (Burke and Robinson, 2012) and downstream on the Chile margin (De Pol-Holz et al., 2010). This ventilation may have been caused by a more southerly position of the fronts of the Southern Ocean and increased upwelling, while the region where deeper waters intersect the surface ocean may have been covered by sea ice. Mid-depth waters were generally more radiogenic than the modern ocean due to reduced inflow of NADW (Wilson and Struve, pers. comm.), whilst Coral Seamount appears to have still received some unradiogenic Nd from the South Atlantic. A widespread radiocarbon enrichment during late HS1 between 15.5 and 15 ka is recorded across the Southern Ocean, and most likely is the result of an increase in NADW delivery (McManus et al., 2004) and gradual ventilation of old

carbon stored in deeper waters (Skinner et al., 2010). The particularly low B-atm age at 12.4 ka seems record a local deep mixing event, as it is not accompanied by an atmospheric CO_2 increase. It does, however, occur at the same time as more radiogenic ε_{Nd} values in the Drake Passage and at shallower depths in the SWIO; a correlation which is yet to be explained. The depletion recorded at UCDW depths to 11.4 ka coincides with another centennial atmospheric CO_2 increase, and is likely to be the result of a final release of old carbon from the deep ocean associated with renewed export of NADW after the YD. During the early Holocene thermal maximum, the lowest ventilation ages are recorded at Middle of What Seamount, which could be due to a deeper mixed layer in the subtropical gyre.

Statement of contribution

Radiocarbon measurements were carried out by Dr. Timothy Knowles at the Bristol Radiocarbon AMS facility (BRAMS). I undertook all sample preparation and data interpretation. Radiocarbon data processing was carried out utilising MATLAB code provided by Dr. Tianyu Chen. Tina van de Flierdt, David Wilson and Susan Little contributed to discussions of data interpretation.

Table 5.1: Calendar age, radiocarbon and Nd isotope data of cold-water corals from the Southwest Indian Ocean. Samples with anomalously high $\Delta^{14}C$ values are in grey italics.

BRAMS Sample #	Sample ID	Cal age / y BP	2σ	Depth / m	^{14}C age / y BP	2σ	Fraction modern (blank corrected)	1σ	$\Delta^{14}C$ / ‰	$\Delta\Delta^{14}C$ / ‰	B-atm / y	ε_{Nd}	2σ
Atlantis Bank (32°42'01" S, 57°17'26" E)													
BRAMS-2644.1.1	JC066_3705	493	81	870	986	42	0.88452	0.00235	-61	-67	539	-8.65	0.31
Middle of What Seamount (37°56'76" S, 50°22'16" E)													
BRAMS-2646.1.1	JC066_3507	9805	204	1014	9011	52	0.32571	0.00105	67	-29	220		
BRAMS-2663.1.1	JC066_3507_dup	9805	204	1014	9035	52	0.32475	0.00105	65	-32	241		
BRAMS-2652.1.1	JC066_3508	12423	117	1014	11051	56	0.25267	0.00087	136	-87	588	-7.90	0.21
BRAMS-2657.1.1	JC066_2590	14969	271	1014	13383	60	0.189	0.00071	156	-120	783	-7.46	0.21
BRAMS-2658.1.1	JC066_3506a	15493	506	1014	13988	62	0.17529	0.00068	143	-156	1028	-6.64	0.33
BRAMS-2659.1.1	JC066_3510	15997	368	1014	14284	64	0.16895	0.00067	170	-152	980	-6.77	0.25
BRAMS-2666.1.1	JC066_3510_dup	15997	368	1014	14253	64	0.1696	0.00067	176	-146	943	-6.77	0.25
Coral Seamount (41°21'23" S, 42°50'31" E)													
BRAMS-2643.1.1	JC066_2795	417	128	702	1126	42	0.86925	0.00232	-86	-93	770	-8.47	0.21
BRAMS-2645.1.1	JC066_117	1713	48	1207.2	2723	44	0.71252	0.00196	-123	-108	933	-8.18	0.31
BRAMS-2647.1.1	JC066_157	11193	242	1395	10273	54	0.27834	0.00093	78	-71	510	-8.81	0.25
BRAMS-2648.1.1	JC066_127	11381	79	1207.2	10634	54	0.26613	0.00091	54	-89	654	-9.01	0.23
BRAMS-2649.1.1	JC066_124	11872	320	1207.2	10709	54	0.26365	0.00089	110	-74	519	-9.08	0.26
BRAMS-2650.1.1	JC066_1002	12304	213	952	10950	56	0.25586	0.00088	134	-79	542	-7.56	0.31
BRAMS-2651.1.1	JC066_1155	12366	134	1207.2	10704	54	0.26382	0.0009	177	-43	277	-8.68	0.17

BRAMS-2664.1.1	JC066_1155_dup	12366	134	1207.2	10796	54	0.26082	0.00089	164	-56	368	-8.68	0.17
BRAMS-2653.1.1	*JC066_1046*	*12864*	*202*	*922.5*	*11020*	*56*	*0.25363*	*0.00087*				*-8.02*	*0.33*
BRAMS-2654.1.1	*JC066_128*	*12898*	*68*	*1207.2*	*11151*	*56*	*0.24954*	*0.00086*					
BRAMS-2655.1.1	*JC066_107*	*12898*	*218*	*1097.2*	*10927*	*56*	*0.25658*	*0.00088*				*-8.26*	*0.26*
BRAMS-2656.1.1	*JC066_1144*	*13628*	*88*	*1097.2*	*10904*	*56*	*0.25733*	*0.0009*				*-8.31*	*0.27*
BRAMS-2665.1.1	*JC066_1144_dup*	*13628*	*88*	*1097.2*	*11012*	*56*	*0.25389*	*0.00088*				*-8.31*	*0.27*
BRAMS-2660.1.1	JC066_1040	16241	253	922.5	14012	62	0.17476	0.00068	246	-83	520	-8.00	0.31
BRAMS-2661.1.1	JC066_1143a	16378	295	1097.2	14521	64	0.16404	0.00065	190	-144	924	-7.86	0.26

Chapter 6: Summary and conclusions

This thesis provides new insights into the deglacial history of the mid-depth Southern Ocean by utilising combined neodymium isotope and radiocarbon measurements on the first collection of cold-water corals from the Indian Ocean sector. Following species identification, a new rapid U-series dating technique was used to establish the temporal spread, before samples were cleaned, precisely dated and measured for Nd and ^{14}C.

Taxonomic analysis revealed a particularly large range of species at Coral Seamount, the most southerly site, possibly a result of higher food availability and its location between two biogeographic zones. Striking similarities were observed in the temporal distribution of CWC abundance with collections in the Drake Passage (Margolin et al., 2014) and south of Tasmania (Thiagarajan et al., 2013), suggesting that large scale changes in ocean chemistry (Yu et al., 2010; Durand et al., 2018; Jaccard et al., 2016), temperature (Roberts et al., 2016) and food supply (Anderson et al., 2009) were major controls on habitat suitability through the deglacial.

Evidence that NADW delivery to intermediate waters was maintained during the deglacial, as has been suggested in previous studies (Howe et al., 2016a; Huang et al., 2014; Noble et al., 2013; Wilson and Struve, pers. comm.), comes from the relatively stable ε_{Nd} record for the southwest Indian Ocean; although radiogenic values during HS1 indicate a smaller contribution of Atlantic relative to Pacific waters than the modern day. This finding is supported by more ^{14}C-depleted mid-depth radiocarbon values. For both water mass composition and ventilation the SWIO appears to be buffered by proximity to the Atlantic in comparison to sampling locations downstream in the ACC (Hines et al., 2015; Burke and Robinson, 2012; Wilson and Struve; pers. comm; Struve, 2016). Direct NADW incursions

appear to influence the Nd isotope compositions at Coral Seamount both during HS1 and periodically during the YD.

A short-lived excursion to similarly young B-atm values in the SWIO and Drake Passage around 16.2 ka appears to indicate that the first centennial-scale atmospheric CO_2 increase resulted from ventilation of intermediate waters in the Southern Ocean. This may reflect a poleward shift in westerly winds from a maximum northerly glacial extent (Barker, 2009), increasing air-sea exchange of carbon near to the region of AAIW formation. Towards the end of HS1, a concomitant increase in ventilation age and decrease in ε_{Nd} provides evidence that the NADW flux to the Southern Ocean had begun to increase, along with a gradual release of old carbon from deeper waters.

A depletion in radiocarbon recorded in upper cell waters in the SWIO at ~ 11.4 ka, combined with an unradiogenic ε_{Nd} signature, contributes to existing evidence for the transfer of old carbon from deep waters in the Southern Ocean at the end of the YD (Burke and Robinson, 2012; Chen et al., 2015), when the NADW flux is thought to have rapidly increased (McManus et al., 2004). Evidence of deep mixing, possibly local to the SWIO and due to proximity of the ARC or a deeper mixed layer, comes from very young B-atm ages at 12.4 and 9 ka.

Overall this study highlights the utility of combined Nd isotope and ^{14}C analyses and cold-water corals as a high resolution archive. It also sheds more light on the variation of deglacial conditions between different regions of the Southern Ocean, and the importance of Atlantic influence on the Indian sector in particular. Further exploration of these ideas would benefit from systematic sampling of cold-water corals in the Indian Ocean in addition to studies of temperature, front positions and flow speed. There is also still work to be done on understanding the deglacial stability of Atlantic and Pacific Ocean end-member ε_{Nd} as well as

better characterising water masses from the Indian Ocean such as RSW. Finally, it would be interesting to explore further the history of the relationships between NADW incursion to the Indian Ocean south of South Africa, Agulhas Current strength and the release of Agulhas rings.

Bibliography

Abouchami, W., Goldstein, S.L., Galer, S.J.G., Eisenhauer, A., Mangini, A., 1997. Secular changes of lead and neodymium in central Pacific seawater recorded by a Fe-Mn crust. Geochim. Cosmochim. Acta 61, 3957–3974. https://doi.org/10.1016/S0016-7037(97)00218-4

Addamo, A.M., Martínez-Baraldés, I., Vertino, A., López-González, P.J., Taviani, M., Machordom, A., 2015. Morphological polymorphism of *Desmophyllum dianthus* (Anthozoa: Hexacorallia) over a wide ecological and biogeographic range: Stability in deep habitats? Zool. Anz. 259, 113–130. https://doi.org/10.1016/j.jcz.2015.10.004

Adkins, J.F., Cheng, H., Boyle, E.A., Druffel, E.R.M., Edwards, R.L., 1998. Deep-Sea coral evidence for rapid change in ventilation of the deep North Atlantic 15,400 years ago. Science 280, 725–728. https://doi.org/10.1016/j.cognition.2008.05.007

Adkins, J.F., Griffin, S., Kashgarian, M., Cheng, H., Druffel, E.R.M., Boyle, E.A., Edwards, R.L., Shen, C.C., 2002a. Radiocarbon dating of deep-sea corals. Radiocarbon 44, 567–580.

Adkins, J.F., McIntyre, K., Schrag, D.P., 2002b. The salinity, temperature, and $\delta^{18}O$ of the glacial deep ocean. Science 298, 1769–1773.

Adkins, J.F., Boyle, E.A., Curry, W.B., Lutringer, A., 2003. Stable isotopes in deep-sea corals and a new mechanism for "vital effects." Geochim. Cosmochim. Acta 67, 1129–1143. https://doi.org/10.1016/S0016-7037(00)01203-6

Alcock, A., 1902. Report on the deep-sea Madreporaria of the Siboga-Expedition. E. J. Brill, Leiden.

Allen, K.A., Sikes, E.L., Hönisch, B., Elmore, A.C., Guilderson, T.P., Rosenthal, Y., Anderson, R.F., 2015. Southwest Pacific deep water carbonate chemistry linked to high southern latitude climate and atmospheric CO_2 during the Last Glacial Termination. Quat. Sci. Rev. 122, 180–191. https://doi.org/10.1016/j.quascirev.2015.05.007

Amakawa, H., Yu, T.L., Tazoe, H., Obata, H., Gamo, T., Sano, Y., Shen, C.C., Suzuki, K., 2019. Neodymium concentration and isotopic composition distributions in the southwestern Indian Ocean and the Indian sector of the Southern Ocean. Chem. Geol. 0–1. https://doi.org/10.1016/j.chemgeo.2019.01.007

Andersen, K.K., Azuma, N., Barnola, J.-M., Bigler, M., Biscaye, P., Caillon, N., Chappellaz, J., Clausen, H.B., Dahl-Jensen, D., Fischer, H., Flückiger, J., Fritzsche, D., Fujii, Y., Goto-Azuma, K., Grønvold, K., Gundestrup, N.S., Hansson, M., Huber, C., Hvidberg, C.S., Johnsen, S.J., Jonsell, U., Jouzel, J., Kipfstuhl, S., Landais, A., Leuenberger, M., Lorrain, R., Masson-Delmotte, V., Miller, H., Motoyama, H., Narita, H., Popp, T., Rasmussen, S.O., Raynaud, D., Rothlisberger, R., Ruth, U., Samyn, D., Schwander, J., Shoji, H., Siggard-Andersen, M.-L., Steffensen, J.P., Stocker, T., Sveinbjörnsdóttir, a E., Svensson, A., Takata, M., Tison, J.-L., Thorsteinsson, T., Watanabe, O., Wilhelms, F., White, J.W.C., 2004. High-resolution record of Northern Hemisphere climate extending into the last interglacial period. Nature 431, 147–151. https://doi.org/10.1038/nature02805

Anderson, B.E., Ali, S., Bradtmiller, L.I., Nielsen, S.H.H., Fleisher, M.Q., Anderson, B.E., Burckle, L.H., 2009. Wind-driven upwelling in the Southern Ocean and the deglacial rise in atmospheric CO_2. Science 323, 1443–1448.

Baco, A.R., Morgan, N., Roark, E.B., Silva, M., Shamberger, K.E.F., Miller, K., 2017. Defying dissolution: Discovery of deep-sea scleractinian coral reefs in the North Pacific. Sci. Rep. 7, 5436. https://doi.org/10.1038/s41598-017-05492-w

Bard, E., Rickaby, R.E.M., 2009. Migration of the subtropical front as a modulator of glacial climate. Nature 460, 380–383. https://doi.org/10.1038/nature08189

Barker, S., Diz, P., Vautravers, M.J., Pike, J., Knorr, G., Hall, I.R., Broecker, W.S., Diz, P., Knorr, G., 2009. Interhemispheric Atlantic seesaw response during the last deglaciation. Nature 457, 1097–1102. https://doi.org/10.1038/nature07770

Barker, S., Knorr, G., Vautravers, M.J., Diz, P., Skinner, L.C., 2010. Extreme deepening of the Atlantic overturning circulation during deglaciation. Nat. Geosci. 3, 567–571. https://doi.org/10.1038/ngeo921

Barker, S., Diz, P., 2014. Timing of the descent into the last Ice Age determined by the bipolar seesaw. Paleoceanography 29, 489–507. https://doi.org/10.1002/2014PA002623

Bauska, T.K., Baggenstos, D., Brook, E.J., Mix, A.C., Marcott, S.A., Petrenko, V. V., Schaefer, H., Severinghaus, J.P., Lee, J.E., 2016. Carbon isotopes characterize rapid changes in atmospheric carbon dioxide during the last deglaciation. Proc. Natl. Acad. Sci. 113, 3465–3470. https://doi.org/10.1073/pnas.1513868113

Beal, L.M., De Ruijter, W.P.M., Biastoch, A., Zahn, R., Cronin, M., Hermes, J., Lutjeharms, J., Quartly, G., Tozuka, T., Baker-Yeboah, S., Bornman, T., Cipollini, P., Dijkstra, H., Hall, I., Park, W., Peeters, F., Penven, P., Ridderinkhof, H., Zinke, J., 2011. On the role of the Agulhas system in ocean circulation and climate. Nature 472, 429–436. https://doi.org/10.1038/nature09983

Beal, L.M., Ffield, A., Gordon, A.L., 2000. Spreading of Red Sea overflow waters in the Indian Ocean. J. Geophys. Res. Ocean. 105, 8549–8564. https://doi.org/10.1029/1999jc900306

Belkin, I.M., Gordon, A.L., 1996. Southern Ocean fronts from the Greenwich meridian to Tasmania. J. Geophys. Res. 101, 3675–3696. https://doi.org/10.1029/95JC02750

Bertram, C.J., Elderfield, H., 1993. The geochemical balance of the rare earth elements and neodymium isotopes in the oceans. Geochim. Cosmochim. Acta 57, 1957–1986. https://doi.org/10.1016/0016-7037(93)90087-D

Blunier, T., Chappellaz, J., Schwander, J., Dällenbach, A., Stauffer, B., Stocker, T.F., Raynaudt, D., Jouzel, J., Clausen, H.B., Hammer, C.U., Johnsen, S.J., 1998. Asynchrony of Antarctic and Greenland climate change during the last glacial period. Nature 394, 739–743. https://doi.org/10.1038/29447

Bosch, D., Blichert-Toft, J., Moynier, F., Nelson, B.K., Telouk, P., Gillot, P.Y., Albarède, F., 2008. Pb, Hf and Nd isotope compositions of the two Réunion volcanoes (Indian Ocean): A tale of two small-scale mantle "blobs"? Earth Planet. Sci. Lett. 265, 748–765. https://doi.org/10.1016/j.epsl.2007.11.018

Bostock, H.C., Opdyke, B.N., Gagan, M.K., Fifield, L.K., 2004. Carbon isotope evidence for changes in Antarctic Intermediate Water circulation and ocean ventilation in the southwest Pacific during the last deglaciation. Paleoceanography 19, 1–15. https://doi.org/10.1029/2004PA001047

Boswell, S.M., Smythe-Wright, D., Holley, S.E., Kirkwood, D., 2002. The tracer signature of Antarctic Bottom Water and its spread in the Southwest Indian Ocean: Part II - Dissolution fluxes of dissolved silicate and their impact on its use as a chemical tracer. Deep. Res. Part I Oceanogr. Res. Pap. 49, 575–590. https://doi.org/10.1016/S0967-0637(01)00067-X

Bourne, G.C., 1905. Report on the solitary corals collected by Professor Herdman, at Ceylon, in 1902. Rep. to Gov. Ceylon Pearl Oyster Fish. Gulf Manaar 4, 187–211.

Bradtmiller, L.I., McManus, J.F., Robinson, L.F., 2014. 231Pa/230Th evidence for a weakened but persistent Atlantic meridional overturning circulation during Heinrich Stadial 1. Nat. Commun. 5, 1–8. https://doi.org/10.1038/ncomms6817

Broecker, W., Barker, S., 2007. A 190‰ drop in atmosphere's Δ14C during the "Mystery Interval" (17.5 to 14.5 kyr). Earth Planet. Sci. Lett. 256, 90–99. https://doi.org/10.1016/j.epsl.2007.01.015

Broecker, W.S., 1998. Paleocean circulation during the lst deglaciation: A bipolar seasaw? Paleoceanography 13, 119–121.

Broecker, W.S., Gerard, R., Ewing, M., Heezen, B.C., 1960. Natural radiocarbon in the Atlantic Ocean. J. Geophys. Res. 65.

Bryan, S.P., Marchitto, T.M., Lehman, S.J., 2010. The release of ^{14}C-depleted carbon from the deep ocean during the last deglaciation: Evidence from the Arabian Sea. Earth Planet. Sci. Lett. 298, 244–254. https://doi.org/10.1016/j.epsl.2010.08.025

Bryden, H., Longworth, H., Cunningham, S., 2005. Slowing of the Atlantic meridional overturning circulation at 25 degrees N. Nature 438, 655–7. https://doi.org/10.1038/nature04385

Buizert, C., Gkinis, V., Severinghaus, J.P., He, F., Lecavalier, B.S., Kindler, P., Leuenberger, M., Carlson, A.E., Vinther, B., Masson-Delmotte, V., White, J.W.C., Liu, Z., Otto-Bliesner, B., Brook, E.J., 2014. Greenland temperature response to climate forcing during the last deglaciation. Science 345, 1177–80. https://doi.org/10.1126/science.1254961

Burke, A., Robinson, L.F., McNichol, A.P., Jenkins, W.J., Scanlon, K.M., Gerlach, D.S., 2010. Reconnaissance dating: A new radiocarbon method applied to assessing the temporal distribution of Southern Ocean deep-sea corals. Deep. Res. Part I Oceanogr. Res. Pap. 57, 1510–1520. https://doi.org/10.1016/j.dsr.2010.07.010

Burke, A., Robinson, L.F., 2012. The Southern Ocean's role in carbon exchange during the last deglaciation. Science 335, 557–561. https://doi.org/10.1126/science.1208163

Burke, A., Stewart, A.L., Adkins, J.F., Ferrari, 2015. The glacial mid-depth radiocarbon bulge and its implications for the overturning circulation. Palaeoceanography 1021–1039. https://doi.org/10.1002/2015PA002778

Büscher, J. V., Form, A.U., Riebesell, U., 2017. Interactive effects of ocean acidification and warming on growth, fitness and survival of the cold-water coral Lophelia pertusa under different food availabilities. Front. Mar. Sci. 4, 1–14. https://doi.org/10.3389/fmars.2017.00101

Cairns, S.D., 1982. Antarctic and Subantarctic Scleractinia. Biol. Antarct. Seas XI Antarct. Res. Ser. 34, 1–74.

Cairns, S.D., Keller, N.B., 1993. New taxa distributional records of azooxanthellate Scleractinia (Cnidaria, Anthozoa) from the tropical southwest Indian Ocean, with comments on their zoogeography and ecology. Ann. South African Museum 103, 213–292.

Cairns, S.D., 1995. The marine fauna of New Zealand: Scleractinia (Cnidaria Anthozoa). New Zeal. Oceanogr. Inst. Mem. 103, 210. https://doi.org/10.1017/CBO9781107415324.004

Cairns, S.D., Zibrowius, H., 1997. Cnidaria Anthozoa : azooxanthellate Scleractinia from the Philippine and Indonesian regions. Mem. du Museum Natl. d'Histoire Nat. 172, 27–243.

Cairns, S.D., 2000. A revision of the shallow-water azooxanthellate Scleractinia of the western Atlantic. Stud. Nat. Hist. Carribean Reg. 75, 1–215.

Cairns, S.D., 2007. Deep water corals : an overview with special reference to diversity and distribution of deep-water scleractininan corals. Bull. Mar. Sci. 81, 311–322.

Cairns, S.D., Polonio, V., 2013. New records of deep-water Scleractinia off Argentina and the Falkland Islands. Zootaxa 3691, 58–86. https://doi.org/10.11646/zootaxa.3691.1.2

Carlson, A.E., Clark, P.U., 2012. Ice sheet sources of sea level rise and freshwater discharge during the last deglaciation. Rev. Geophys. 50, 1–72. https://doi.org/10.1029/2011RG000371

Carter, P., Vance, D., Hillenbrand, C.D., Smith, J.A., Shoosmith, D.R., 2012. The neodymium isotopic composition of waters masses in the eastern Pacific sector of the Southern Ocean. Geochim. Cosmochim. Acta 79, 41–59. https://doi.org/10.1016/j.gca.2011.11.034

Chen, T., Robinson, L.F., Burke, A., Southon, J., Spooner, P., Morris, P.J., Ng, H.C., 2015. Synchronous centennial abrupt events in the ocean and atmosphere during the last deglaciation. Science 349, 1537–1542. https://doi.org/10.1126/science.aac6159

Cheng, H., Adkins, J., Edwards, R.L., Boyle, E.A., 2000. U-Th dating of deep-sea corals. Geochim. Cosmochim. Acta 64, 2401–2416. https://doi.org/10.1016/S0016-7037(99)00422-6

Clark, P.U., Shakun, J.D., Baker, P.A., Bartlein, P.J., Brewer, S., Brook, E.J., Carlson, A.E., Cheng, H., Kaufman, D.S., Lui, Z., Marchitto, T.M., Mix, A.C., Morrill, C., Otto-Bliesner, B.L., Pahnke, K., Russell, J.M., Whitlock, C., Adkins, J.F., Blois, J.L., Clark, J., Colman, S.M., Curry, W.B., Flower, B.P., He, F., Johnson, T.C., Lynch-Stieglitz, J., Markgraf, V., McManus, J.F., Mitrovica, J.X., Moreno, P.I., Williams, J.W., 2012. Global climate evolution during the last deglaciation. Proc. Natl. Acad. Sci. U. S. A. 109, 1134–1142. https://doi.org/10.1073/pnas.1116619109/-

/DCSupplemental.www.pnas.org/cgi/doi/10.1073/pnas.1116619109

Colin, C., Frank, N., Copard, K., Douville, E., 2010. Neodymium isotopic composition of deep-sea corals from the NE Atlantic: Implications for past hydrological changes during the Holocene. Quat. Sci. Rev. 29, 2509–2517. https://doi.org/10.1016/j.quascirev.2010.05.012

Colin, C., Tisnérat-Laborde, N., Mienis, F., Collart, T., Pons-Branchu, E., Dubois-Dauphin, Q., Frank, N., Dapoigny, A., Ayache, M., Swingedouw, D., Dutay, J.C., Eynaud, F., Debret, M., Blamart, D., Douville, E., 2019. Millennial-scale variations of the Holocene North Atlantic mid-depth gyre inferred from radiocarbon and neodymium isotopes in cold water corals. Quat. Sci. Rev. 211, 93–106. https://doi.org/10.1016/j.quascirev.2019.03.011

Cook, M.S., Keigwin, L.D., 2015. Radiocarbon profiles of the NW Pacific from the LGM and deglaciation: Evaluating ventilation metrics and the effect of uncertain surface reservoir ages. Paleoceanography 30, 174–195. https://doi.org/10.1002/2014PA002649

Copard, K., Colin, C., Douville, E., Freiwald, A., Gudmundsson, G., De Mol, B., Frank, N., 2010. Nd isotopes in deep-sea corals in the North-eastern Atlantic. Quat. Sci. Rev. 29, 2499–2508. https://doi.org/10.1016/j.quascirev.2010.05.025

Crocket, K.C., Lambelet, M., van de Flierdt, T., Rehkämper, M., Robinson, L.F., 2014. Measurement of fossil deep-sea coral Nd isotopic compositions and concentrations by TIMS as NdO+, with evaluation of cleaning protocols. Chem. Geol. 374–375, 128–140. https://doi.org/10.1016/j.chemgeo.2014.03.011

Curry, W.B., Oppo, D.W., 2005. Glacial water mass geometry and the distribution of δ13C of ΣCO_2 in the western Atlantic Ocean. Paleoceanography 20, 1–12. https://doi.org/10.1029/2004PA001021

Dana, J.D., 1846. Structure and Classification of Zoophytes. Lea and Blanchard, Philadelphia.

Davies, A.J., Guinotte, J.M., 2011. Global habitat suitability for framework-forming cold-water corals. PLoS One 6, e18483. https://doi.org/10.1371/journal.pone.0018483

De Deckker, P., Moros, M., Perner, K., Jansen, E., 2012. Influence of the tropics and southern westerlies on glacial interhemispheric asymmetry. Nat. Geosci. 5, 266–269. https://doi.org/10.1038/ngeo1431

De Pol-Holz, R., Keigwin, L., Southon, J., Hebbeln, D., Mohtadi, M., 2010. No signature of abyssal carbon in intermediate waters off Chile during deglaciation. Nat. Geosci. 3, 192–195. https://doi.org/10.1038/ngeo745

de Pourtalès, L.F., 1871. Deep-sea corals, in: Illustrated Catalogue of the Museum of Comparative Zoology. p. 93.

de Pourtalès, L.F., 1878. Reports on the results of dredging, under the supervision of Alexander Agassiz, in the Gulf of Mexico, by the United States Coast Survey Steamer "Blake": Corals. Bull. Museum Comp. Zool. 5, 197–212.

Deacon, G.E.R., 1982. Physical and biological zonation in the Southern Ocean. Deep. Res. Part a-Oceanographic Res. Pap. 29, 1–15.

Denton, G.H., Anderson, R.F., Toggweiler, J.R., Edwards, R.L., Schaefer, J.M., Putnam, A.E., 2010. The Last Glacial Termination. Science 328, 1652–1656. https://doi.org/10.1126/science.1184119

Dezileau, L., Reyss, J.L., Lemoine, F., 2003. Late Quaternary changes in biogenic opal fluxes in the Southern Indian Ocean. Mar. Geol. 202, 143–158. https://doi.org/10.1016/S0025-3227(03)00283-4

Djurhuus, A., Boersch-Supan, P.H., Mikalsen, S.O., Rogers, A.D., 2017a. Microbe biogeography tracks water masses in a dynamic oceanic frontal system. R. Soc. Open Sci. 4, 170033. https://doi.org/10.1098/rsos.170033

Djurhuus, A., Read, J.F., Rogers, A.. D., 2017b. The spatial distribution of particulate organic carbon and microorganisms on seamounts of the South West Indian Ridge. Deep. Res. Part II Top. Stud. Oceanogr. 136, 73–84. https://doi.org/10.1016/j.dsr2.2015.11.015

Dodds, L.A., Roberts, J.M., Taylor, A.C., Marubini, F., 2007. Metabolic tolerance of the cold-water coral *Lophelia pertusa* (Scleractinia) to temperature and dissolved oxygen change. J. Exp. Mar. Bio. Ecol. 349, 205–214. https://doi.org/10.1016/j.jembe.2007.05.013

Donohue, K.A., Toole, J.M., 2003. A near-synoptic survey of the Southwest Indian Ocean. Deep. Res. Part II Top. Stud. Oceanogr. 50, 1893–1931. https://doi.org/10.1016/S0967-0645(03)00039-0

Douville, E., Sallé, E., Frank, N., Eisele, M., Pons-Branchu, E., Ayrault, S., 2010. Rapid and accurate U-Th dating of ancient carbonates using inductively coupled plasma-quadrupole mass spectrometry. Chem. Geol. 272, 1–11. https://doi.org/10.1016/j.chemgeo.2010.01.007

Dueñas, L.F., Tracey, D.M., Crawford, A.J., Wilke, T., Alderslade, P., Sánchez, J.A., 2016. The Antarctic Circumpolar Current as a diversification trigger for deep-sea octocorals. BMC Evol. Biol. 16, 2. https://doi.org/10.1186/s12862-015-0574-z

Duineveld, G.C.A., Lavaleye, M.S.S., Bergman, M.J.N., De Stigter, H., Mienis, F., 2007. Trophic structure of a cold-water coral mound community (Rockall Bank, NE Atlantic) in relation to the near-bottom particle supply and current regime. Bull. Mar. Sci. 81, 449–467.

Dullo, W.C., Flögel, S., Rüggeberg, A., 2008. Cold-water coral growth in relation to the hydrography of the Celtic and Nordic European continental margin. Mar. Ecol. Prog. Ser. 371, 165–176. https://doi.org/10.3354/meps07623

Duncan, P.M., 1873. A description of the Madreporaria dredged up during the expeditions of H.M.S. “Porcupine” in 1869 and 1870. Part I. Trans. Zool. Soc. London 8, 303–344. https://doi.org/10.1111/j.1096-3642.1873.tb00560.x

Durand, A., Chase, Z., Noble, T.L., Bostock, H., Jaccard, S.L., Townsend, A.T., Bindoff, N.L., Neil, H., Jacobsen, G., 2018. Reduced oxygenation at intermediate depths of the southwest Pacific during the last glacial maximum. Earth Planet. Sci. Lett. 491, 48–57. https://doi.org/10.1016/j.epsl.2018.03.036

Elderfield, H., Upstill-Goddard, R., Sholkovitz, E.R., 1990. The rare earth elements in rivers,

estuaries, and coastal seas and their significance to the composition of ocean waters. Geochim. Cosmochim. Acta 54, 971–991. https://doi.org/10.1016/0016-7037(90)90432-K

Elmore, A.C., McClymont, E.L., Elderfield, H., Kender, S., Cook, M.R., Leng, M.J., Greaves, M., Misra, S., 2015. Antarctic Intermediate Water properties since 400 ka recorded in infaunal (Uvigerina peregrina) and epifaunal (Planulina wuellerstorfi) benthic foraminifera. Earth Planet. Sci. Lett. 428, 193–203. https://doi.org/10.1016/j.epsl.2015.07.013

Esper, E.J.C., 1794. Die Pflanzenthiere in Abbildungen nach der Natur mit Farben erleuchtet nebst Beschreibungen. Raspeschen Buchhandlung, Nürnberg.

Ferrari, R., Jansen, M.F., Adkins, J.F., Burke, A., Stewart, A.L., Thompson, A.F., 2014. Antarctic sea ice control on ocean circulation in present and glacial climates. Proc. Natl. Acad. Sci. U. S. A. 111, 8753–8758. https://doi.org/10.1073/pnas.1323922111

Fine, R.A., 1993. Circulation of Antarctic intermediate water in the South Indian Ocean. Deep. Res. Part I 40, 2021–2042. https://doi.org/10.1016/0967-0637(93)90043-3

Fink, H.G., Wienberg, C., Hebbeln, D., McGregor, H. V., Schmiedl, G., Taviani, M., Freiwald, A., 2012. Oxygen control on Holocene cold-water coral development in the eastern Mediterranean Sea. Deep. Res. Part I Oceanogr. Res. Pap. 62, 89–96. https://doi.org/10.1016/j.dsr.2011.12.013

Flores, J.A., Gersonde, R., Sierro, F.J., 1999. Pleistocene fluctuations in the Agulhas Current Retroflection based on the calcareous plankton record. Mar. Micropaleontol. 37, 1–22. https://doi.org/10.1016/S0377-8398(99)00012-2

Foster, G.L., Vance, D., Prytulak, J., 2007. No change in the neodymium isotope composition of deep water exported from the North Atlantic on glacial-interglacial time scales. Geology 35, 37–40. https://doi.org/10.1130/G23204A.1

Francois, R., Altabet, M.A., Yu, E.-F., Sigman, D.M., Bacon, M.P., Frank, M., Bohrmann, G., Bareille, G., Labeyrie, L.D., 1997. Contribution of Southern Ocean surface-water stratification to low atmospheric CO_2 concentrations during the last glacial period. Nature 389, 929–935. https://doi.org/10.1038/40073

Frank, M., 2002. Radiogenic isotopes: Tracers of past ocean circulation and erosional input. Rev. Geophys. 40, 1001. https://doi.org/10.1029/2000RG000094

Franzese, A.M., Hemming, S.R., Goldstein, S.L., Anderson, R.F., 2006. Reduced Agulhas Leakage during the Last Glacial Maximum inferred from an integrated provenance and flux study. Earth Planet. Sci. Lett. 250, 72–88. https://doi.org/10.1016/j.epsl.2006.07.002

Freiwald, A., Fossa, J.H., Grehan, A., Koslow, T., Roberts, J.M., 2004. Cold-water coral reefs, NEP-WCMC. Cambridge, UK.

Garcia-Solsona, E., Jeandel, C., Labatut, M., Lacan, F., Vance, D., Chavagnac, V., Pradoux, C., 2014. Rare earth elements and Nd isotopes tracing water mass mixing and particle-seawater interactions in the SE Atlantic. Geochim. Cosmochim. Acta 125, 351–372. https://doi.org/10.1016/j.gca.2013.10.009

Gersonde, R., Crosta, X., Abelmann, A., Armand, L., 2005. Sea-surface temperature and sea ice distribution of the Southern Ocean at the EPILOG Last Glacial Maximum - A circum-Antarctic view based on siliceous microfossil records. Quat. Sci. Rev. 24, 869–896. https://doi.org/10.1016/j.quascirev.2004.07.015

Goldstein, S., Hemming, S., 2003. Long-lived isotopic tracers in oceanography, paleoceanography, and ice-sheet dynamics, in: Treatise on Geochemistry, Col. 6. Elsevier, pp. 453–489.

Gordon, A.L., Lutjeharms, J.R.E., Gründlingh, M.L., 1987. Stratification and circulation at the Agulhas Retroflection. Deep Sea Res. Part A, Oceanogr. Res. Pap. 34, 565–599. https://doi.org/10.1016/0198-0149(87)90006-9

Gordon, A.L., Weiss, R.F., Smethie Jr., W.M., Warner, M.J., 1992. Thermocline and intermediate water communication between the South Atlantic and Indian Oceans. J. Geophys. … 97, 7223–7240.

Gori, A., Ferrier-Pagès, C., Hennige, S.J., Murray, F., Rottier, C., Wicks, L.C., Roberts, J.M., 2016. Physiological response of the cold-water coral *Desmophyllum dianthus* to thermal stress and ocean acidification. PeerJ 2016, e1606. https://doi.org/10.7717/peerj.1606

Gravier, C., 1914. Sur une espèce nouvelle de Madréporaire (Desmophyllum antarcticum). Bull. Muséum Hist. Nat. Paris 20, 236–238.

Gray, J.E., 1847. An outline of an arrangement of stony corals. Ann. Mag. Nat. Hist. Ser. 1 19, 120–128.

Grousset, F.E., Biscaye, P.E., Revel, M., Petit, J.R., Pye, K., Joussaume, S., Jouzel, J., 1992. Antarctic (Dome C) ice-core dust at 18 k.y. B.P.: Isotopic constraints on origins. Earth Planet. Sci. Lett. 111, 175–182. https://doi.org/10.1016/0012-821X(92)90177-W

Gu, S., Liu, Z., Jahn, A., Rempfer, J., Zhang, J., Joos, F., 2019. Modeling Neodymium Isotopes in the Ocean Component of the Community Earth System Model (CESM1). J. Adv. Model. Earth Syst. 11, 624–640. https://doi.org/10.1029/2018MS001538

Guinotte, J.M., Orr, J., Cairns, S., Freiwald, A., Morgan, L., George, R., 2006. Will human-induced changes in seawater chemistry alter the distribution of deep-sea scleractinian corals? Front. Ecol. Environ. 4, 141–146.

Gutjahr, M., Frank, M., Stirling, C.H., Keigwin, L.D., Halliday, A.N., 2008. Tracing the Nd isotope evolution of North Atlantic Deep and Intermediate Waters in the western North Atlantic since the Last Glacial Maximum from Blake Ridge sediments. Earth Planet. Sci. Lett. 266, 61–77. https://doi.org/10.1016/j.epsl.2007.10.037

Hall-Spencer, J., Allain, V., Fosså, J.H., 2002. Trawling damage to Northeast Atlantic ancient coral reefs. Proc. R. Soc. B Biol. Sci. 269, 507–511. https://doi.org/10.1098/rspb.2001.1910

Henry, L.A., Frank, N., Hebbeln, D., Wienberg, C., Robinson, L.F., van de Flierdt, T., Dahl, M., Douarin, M., Morrison, C.L., Correa, M.L., Rogers, A.D., Ruckelshausen, M., Roberts, J.M., 2014. Global ocean conveyor lowers extinction risk in the deep sea. Deep. Res. Part I Oceanogr. Res. Pap. 88, 8–16. https://doi.org/10.1016/j.dsr.2014.03.004

Hines, S.K. V, Southon, J.R., Adkins, J.F., 2015. A high-resolution record of Southern Ocean

intermediate water radiocarbon over the past 30,000 years. Earth Planet. Sci. Lett. 432, 46–58. https://doi.org/10.1016/j.epsl.2015.09.038

Howe, Jacob N. W., Piotrowski, A.M., Noble, T.L., Mulitza, S., Chiessi, C.M., Bayon, G., 2016a. North Atlantic Deep Water Production during the Last Glacial Maximum. Nat. Commun. 7, 11765. https://doi.org/10.1038/ncomms11765

Howe, Jacob N. W., Piotrowski, A.M., Oppo, D.W., Huang, K.F., Mulitza, S., Chiessi, C.M., Blusztajn, J., 2016b. Antarctic intermediate water circulation in the South Atlantic over the past 25,000 years. Paleoceanography 31, 1302–1314. https://doi.org/10.1002/2016PA002975

Hu, R., Noble, T.L., Piotrowski, A.M., McCave, I.N., Bostock, H.C., Neil, H.L., 2016. Neodymium isotopic evidence for linked changes in Southeast Atlantic and Southwest Pacific circulation over the last 200 kyr. Earth Planet. Sci. Lett. 455, 106–114. https://doi.org/10.1016/j.epsl.2016.09.027

Huang, K.F., Oppo, D.W., Curry, W.B., 2014. Decreased influence of Antarctic intermediate water in the tropical Atlantic during North Atlantic cold events. Earth Planet. Sci. Lett. 389, 200–208. https://doi.org/10.1016/j.epsl.2013.12.037

Jaccard, S.L., Galbraith, E.D., 2012. Large climate-driven changes of oceanic oxygen concentrations during the last deglaciation. Nat. Geosci. 5, 151–156. https://doi.org/10.1038/ngeo1352

Jaccard, S.L., Galbraith, E.D., Martínez-García, A., Anderson, R.F., 2016. Covariation of deep Southern Ocean oxygenation and atmospheric CO_2 through the last ice age. Nature 530, 207–10. https://doi.org/10.1038/nature16514

Jeandel, C., Thouron, D., Fieux, M., 1998. Concentrations and isotopic compositions of neodymium in the eastern Indian Ocean and Indonesian straits. Geochim. Cosmochim. Acta 62, 2597–2607. https://doi.org/10.1016/S0016-7037(98)00169-0

Kaufman, A., Broecker, W., 1965. Comparison of ^{230}Th and ^{14}C ages for carbonate materials from lakes Lahontan and Bonneville. J. Geophys. Res. 70, 4039–4054.

Keller, N.B., 1976. The deep-sea madreporarian corals of the genus Fungiacyathus from the Kurile-Kamchatka, Aleutian Trenches and other regions of the world oceans. Tr. Inst. Okeanol. 99, 31–44.

Kitahara, M. V., Cairns, S.D., Miller, D.J., 2010. Monophyletic origin of Caryophyllia (Scleractinia, Caryophylliidae), with descriptions of six new species. Syst. Biodivers. 8, 91–118. https://doi.org/10.1080/14772000903571088

Kohfeld, K.E., Chase, Z., 2017. Temporal evolution of mechanisms controlling ocean carbon uptake during the last glacial cycle. Earth Planet. Sci. Lett. 472, 206–215. https://doi.org/10.1016/j.epsl.2017.05.015

Kohfeld, K.E., Graham, R.M., de Boer, A.M., Sime, L.C., Wolff, E.W., Le Quéré, C., Bopp, L., 2013. Southern Hemisphere westerly wind changes during the Last Glacial Maximum: Paleo-data synthesis. Quat. Sci. Rev. 68, 76–95. https://doi.org/10.1016/j.quascirev.2013.01.017

Kohfeld, K.E., Harrison, S.P., Que, C. Le, Anderson, R.F., 2005. Role of marine biology in

glacial-interglacial CO_2 cycles. Science 308, 74–78. https://doi.org/10.1126/science.1105375

Kroner, A., Hegner, E., Collins, A.S., Windley, B.F., Brewer, T.S., Razakamanana, T., Pigeon, R.T., 2000. Age and magmatic history of the Antananarivo Block, central Madagascar, as derived from zircon geochronology and Nd isotopic systematics. Am. J. Sci. 300, 251–288.

Kuhlbrodt, T., Griesel, A., Montoya, M., Levermann, A., Hofmann, M., Rahmstorf, S., 2007. On the driving processes of the Atlantic meridional overturning circulation. Atlantic 45, RG2001. https://doi.org/10.1029/2004RG000166.1.INTRODUCTION

Kumar, N., Anderson, R.F., Mortlock, R.A., Froelich, P.N., Kubik, P., Dittrich-Hannen, B., Suter, M., 1995. Increased biological productivity and export production in the glacial southern Ocean. Nature 378, 675–680. https://doi.org/10.1038/378675a0

Labracherie, M., Labeyrie, L.D., Duprat, J., Bard, E., Arnold, M., Pichon, J.-J., Duplessy, J.C., 1989. The last deglaciation in the Southern Ocean. Paleoceanography 4, 629–638. https://doi.org/10.1029/PA004i006p00629

Lacan, F., Jeandel, C., 2005. Neodymium isotopes as a new tool for quantifying exchange fluxes at the continent-ocean interface. Earth Planet. Sci. Lett. 232, 245–257. https://doi.org/10.1016/j.epsl.2005.01.004

Lambelet, M., van de Flierdt, T., Crocket, K., Rehkämper, M., Kreissig, K., Coles, B., Rijkenberg, M.J.A., Gerringa, L.J.A., de Baar, H.J.W., Steinfeldt, R., 2016. Neodymium isotopic composition and concentration in the western North Atlantic Ocean: Results from the GEOTRACES GA02 section. Geochim. Cosmochim. Acta 177, 1–29. https://doi.org/10.1016/j.gca.2015.12.019

Lambelet, M., van de Flierdt, T., Butler, E.C.V., Bowie, A.R., Rintoul, S.R., Watson, R.J., Remenyi, T., Lannuzel, D., Warner, M., Robinson, L.F., Bostock, H.C., Bradtmiller, L.I., 2018. The Neodymium Isotope Fingerprint of Adélie Coast Bottom Water. Geophys. Res. Lett. 45, 11,247-11,256. https://doi.org/10.1029/2018GL080074

Lamy, F., Kilian, R., Arz, H.W., Francois, J.P., Kaiser, J., Prange, M., Steinke, T., 2010. Holocene changes in the position and intensity of the southern westerly wind belt. Nat. Geosci. 3, 695–699. https://doi.org/10.1038/ngeo959

Lamy, F., Arz, H.W., Kilian, R., Lange, C.B., Lembke-Jene, L., Wengler, M., Kaiser, J., Baeza-Urrea, O., Hall, I.R., Harada, N., Tiedemann, R., 2015. Glacial reduction and millennial-scale variations in Drake Passage throughflow. Proc. Natl. Acad. Sci. U. S. A. 112, 13496–13501. https://doi.org/10.1073/pnas.1509203112

Lee, J.M., Boyle, E.A., Gamo, T., Obata, H., Norisuye, K., Echegoyen, Y., 2015. Impact of anthropogenic Pb and ocean circulation on the recent distribution of Pb isotopes in the Indian Ocean. Geochim. Cosmochim. Acta 170, 126–144. https://doi.org/10.1016/j.gca.2015.08.013

Li, F., Ginoux, P., Ramaswamy, V., 2008. Distribution, transport, and deposition of mineral dust in the Southern Ocean and Antarctica: Contribution of major sources. J. Geophys. Res. Atmos. 113, 1–15. https://doi.org/10.1029/2007JD009190

Linnaeus, C., 1758. Systema naturæ per regna tria naturæ, secundum classes, ordines, genera, species, cum characteribus, differentiis, synonymis, locis. Tomus I. Laurentii Salvii, Holmiæ.

Lomitschka, M., Mangini, A., 1999. Precise Th/U-dating of small and heavily coated samples of deep sea corals. Earth Planet. Sci. Lett. 170, 391–401. https://doi.org/10.1016/S0012-821X(99)00117-X

Lowry, D.P., Golledge, N.R., Menviel, L., Bertler, N.A.N., 2019. Deglacial evolution of regional Antarctic climate and Southern Ocean conditions in transient climate simulations. Clim. Past 15, 189–215. https://doi.org/10.5194/cp-15-189-2019

Lüthi, D., Le Floch, M., Bereiter, B., Blunier, T., Barnola, J.-M., Siegenthaler, U., Raynaud, D., Jouzel, J., Fischer, H., Kawamura, K., Stocker, T.F., 2008. High-resolution carbon dioxide concentration record 650,000-800,000 years before present. Nature 453, 379–382. https://doi.org/10.1038/nature06949

Lutjeharms, J.R.E., Valentine, H.R., 1984. Southern ocean thermal fronts south of Africa. Deep Sea Res. Part A. Oceanogr. Res. Pap. 31, 1461–1475. https://doi.org/10.1016/0198-0149(84)90082-7

Lutjeharms, J.R.E., Van Ballegooyen, R.C., 1988. The retroflection of the Aghulas Current. J. Phys. Oceanogr. 18, 1570–1583.

Lynch-Stieglitz, J., Fairbanks, R.G., Charles, C.D., 1994. Glacial-interglacial history of Antarctic Intermediate Water: Relative strengths of Antarctic versus Indian Ocean sources. Paleoceanography 9, 7–29. https://doi.org/10.1029/93PA02446

Mangini, A., Godoy, J.M., Godoy, M.L., Kowsmann, R., Santos, G.M., Ruckelshausen, M., Schroeder-Ritzrau, A., Wacker, L., 2010. Deep sea corals off Brazil verify a poorly ventilated Southern Pacific Ocean during H2, H1 and the Younger Dryas. Earth Planet. Sci. Lett. 293, 269–276. https://doi.org/10.1016/j.epsl.2010.02.041

Marchitto, T.M., Lehman, S.J., Ortiz, J.D., Flückiger, J., van Geen, A., 2007. Marine radiocarbon evidence for the mechanism of deglacial atmospheric CO2 rise. Science (80-.). 316, 1456–1459. https://doi.org/10.1126/science.1138679

Marcott, S.A., Bauska, T.K., Buizert, C., Steig, E.J., Rosen, J.L., Cuffey, K.M., Fudge, T.J., Severinghaus, J.P., Ahn, J., Kalk, M.L., McConnell, J.R., Sowers, T., Taylor, K.C., White, J.W.C., Brook, E.J., 2014. Centennial-scale changes in the global carbon cycle during the last deglaciation. Nature 514, 616–9. https://doi.org/10.1038/nature13799

Marenzeller, E.V., 1904. Reports on dredging operations of the west coast of central America and Galapagos by the U.S. Fish Commission Steamer 'Albatross' during 1891: Steinkorallen und Hydro-Korallen. Bull. Museum Comp. Zool. 43, 75–87.

Margolin, A.R., Robinson, L.F., Burke, A., Waller, R.G., Scanlon, K.M., Roberts, M.L., Auro, M.E., van de Flierdt, T., 2014. Temporal and spatial distributions of cold-water corals in the Drake Passage: Insights from the last 35,000 years. Deep Sea Res. Part II Top. Stud. Oceanogr. 99, 237–248. https://doi.org/10.1016/j.dsr2.2013.06.008

Marshall, J., Speer, K., 2012. Closure of the meridional overturning circulation through Southern Ocean upwelling. Nat. Geosci. 5, 171–180. https://doi.org/10.1038/ngeo1391

Martin, E.E., MacLeod, K.G., Jiménez Berrocoso, A., Bourbon, E., 2012. Water mass circulation on Demerara Rise during the Late Cretaceous based on Nd isotopes. Earth Planet. Sci. Lett. 327–328, 111–120. https://doi.org/10.1016/j.epsl.2012.01.037

Martin, F., 2002. Radiogenic isotopes: tracers of past ocean circulation and erosional input. Rev. Geophys. 40, 1–38. https://doi.org/10.1029/2000RG000094

Martin, J.H., 1990. Glacial-interglacial CO_2 change: the iron hypothesis. Paleoceanography 5, 1–13.

Martínez-Botí, M.A., Marino, G., Foster, G.L., Ziveri, P., Henehan, M.J., Rae, J.W.B., Mortyn, P.G., Vance, D., Marino, G., Ziveri, P., Henehan, M.J., Foster, G.L., Vance, D., Martínez-Botí, M.A., Rae, J.W.B., 2015. Boron isotope evidence for oceanic carbon dioxide leakage during the last deglaciation. Nature 518, 219–222. https://doi.org/10.1038/nature14155

Martínez-García, A., Sigman, D.M., Ren, H., Anderson, R.F., Straub, M., Hodell, D.A., Jaccard, S.L., Eglinton, T.I., Haug, G.H., 2014. Iron fertilization of the Subantarctic ocean during the last ice age. Science 343, 1347–50. https://doi.org/10.1126/science.1246848

Martinez-Mendez, G., Zahn, R., Hall, I.R., Peeters, F.J.C., Pena, L.D., Cacho, I., Negre, C.C., 2010. Contrasting multiproxy reconstructions of surface ocean hydrography in the Agulhas Corridor and implications for the Agulhas Leakage during the last 345,000 years. Paleoceanography 25, 1–12. https://doi.org/10.1029/2009PA001879

Masson, V., Vimeux, F., Jouzel, J., Morgan, V., Delmotte, M., Ciais, P., Hammer, C., Johnsen, S., Lipenkov, V.Y., Mosley-Thompson, E., Petit, J.R., Steig, E.J., Stievenard, M., Vaikmae, R., 2000. Holocene climate variability in Antartica based on 11 ice-core isotopic records. Quat. Res. 54, 348–358. https://doi.org/10.1006/qres.2000.2172

Mastumoto, K., Lynch-Stieglitz, J., Anderson, R.F., 2001. Similar glacial and Holocene Southern Ocean hydrography. Paleoceanography 16, 445–454.

McCave, I.N., Kiefer, T., Thornalley, D.J.R., Elderfield, H., 2005. Deep flow in the Madagascar-Mascarene Basin over the last 150 000 years. Philos. Trans. R. Soc. A Math. Phys. Eng. Sci. 363, 81–99. https://doi.org/10.1098/rsta.2004.1480

McCave, I.N., Crowhurst, S.J., Kuhn, G., Hillenbrand, C.D., Meredith, M.P., 2014. Minimal change in Antarctic Circumpolar Current flow speed between the last glacial and Holocene. Nat. Geosci. 7, 113–116. https://doi.org/10.1038/ngeo2037

McDonagh, E.L., Bryden, H.L., King, B.A., Sanders, R.J., 2008. The circulation of the Indian Ocean at 32°S. Prog. Oceanogr. 79, 20–36. https://doi.org/10.1016/j.pocean.2008.07.001

McManus, J.F., Francois, R., Gherardi, J.-M., Keigwin, L.D., Brown-Leger, S., 2004. Collapse and rapid resumption of Atlantic meridional circulation linked to deglacial climate changes. Nature 428, 834–837. https://doi.org/10.1038/nature02494

Menviel, L., Spence, P., Yu, J., Chamberlain, M.A., Matear, R.J., Meissner, K.J., England, M.H., 2018. Southern Hemisphere westerlies as a driver of the early deglacial atmospheric CO2 rise. Nat. Commun. 9, 1–12. https://doi.org/10.1038/s41467-018-04876-4

Miller, K.J., Rowden, A.A., Williams, A., Haussermann, V., 2011. Out of their depth? isolated deep populations of the cosmopolitan coral *Desmophyllum dianthus* may be highly vulnerable to environmental change. PLoS One 6. https://doi.org/10.1371/journal.pone.0019004

Milne Edwards, H., Haime, J., 1848. Recherches sur les polypiers. Deuxième mémoire. Monographie des turbinolides. Ann. des Sci. Nat. série 3, Zool. 9, 211–344, pl. 7–10.

Monnin, E., Indermühle, A., Dällenbach, A., Flückiger, J., Stauffer, B., Stocker, T.F., Raynaud, D., Barnola, J.-M., 2001. Atmospheric CO_2 concentrations over the Last Glacial Termination. Science 291, 112–114. https://doi.org/10.1126/science.291.5501.112

Montero-Serrano, J.-C., Frank, N., Tisnérat-Laborde, N., Colin, C., Wu, C.-C., Lin, K., Shen, C.-C., Copard, K., Orejas, C., Gori, A., De Mol, L., Van Rooij, D., Reverdin, G., Douville, E., 2013. Decadal changes in the mid-depth water mass dynamic of the Northeastern Atlantic margin (Bay of Biscay). Earth Planet. Sci. Lett. 364, 134–144. https://doi.org/10.1016/j.epsl.2013.01.012

Moseley, H.N., 1881. Report on Certain Hydroid, Alcyonarian, and Madreporarian Corals Procured during the Voyage of H. M. S. Challenger, in the Years 1873-1876. Zoology 2, 1–248.

Muller, L.A., Watts, A.B., JC066 shipboard scientific party, 2012. The Morphology, Structure and Origin of Seamounts on the South-West Indian Ocean Ridge. Geophys. Res. Abstr. 14.

Nair, A., Mohan, R., Crosta, X., Manoj, M.C., Thamban, M., Marieu, V., 2019. Southern Ocean sea ice and frontal changes during the Late Quaternary and their linkages to Asian summer monsoon. Quat. Sci. Rev. 213, 93–104. https://doi.org/10.1016/j.quascirev.2019.04.007

Naumann, M.S., Orejas, C., Wild, C., Ferrier-Pages, C., 2011. First evidence for zooplankton feeding sustaining key physiological processes in a scleractinian cold-water coral. J. Exp. Biol. 214, 3570–3576. https://doi.org/10.1242/jeb.061390

Ninnemann, U.S., Charles, C.D., 2002. Changes in the mode of Southern Ocean circulation over the last glacial cycle revealed by foraminiferal stable isotopic variability. Earth Planet. Sci. Lett. 201, 383–396. https://doi.org/10.1016/S0012-821X(02)00708-2

NOAA, 2017. Exploring the Deep Coral Gardens of Channel Islands National Marine Sanctuary [WWW Document]. URL https://sanctuaries.noaa.gov/news/apr17/exploring-deep-coral-gardens-of-cinms.html (accessed 9.26.19).

Noble, T.L., Piotrowski, A.M., Robinson, L.F., McManus, J.F., Hillenbrand, C.D., Bory, A.J.M., 2012. Greater supply of Patagonian-sourced detritus and transport by the ACC to the Atlantic sector of the Southern Ocean during the last glacial period. Earth Planet. Sci. Lett. 317–318, 374–385. https://doi.org/10.1016/j.epsl.2011.10.007

Noble, T.L., Piotrowski, A.M., McCave, I.N., 2013. Neodymium isotopic composition of intermediate and deep waters in the glacial southwest Pacific. Earth Planet. Sci. Lett. 384, 27–36. https://doi.org/10.1016/j.epsl.2013.10.010

Okazaki, Y., Timmermann, A., Menviel, L., Harada, N., Abe-Ouchi, A., Chikamoto, M.O., Mouchet, A., Asahi, H., 2010. Deepwater formation in the North Pacific during the last glacial termination. Science (80-.). 329, 200–204.

Orsi, A.H., Whitworth, T., Nowlin, W.D., 1995. On the meridional extent and fronts of the Antarctic Circumpolar Current. Deep. Res. Part I 42, 641–673. https://doi.org/10.1016/0967-0637(95)00021-W

Östlund, H.G., Stuiver, M., 1980. GEOSECS Pacific Radiocarbon. Radiocarbon 22, 25–53. https://doi.org/10.1017/s0033822200004707

Pahnke, K., Goldstein, S.L., Hemming, S.R., 2008. Abrupt changes in Antarctic Intermediate Water circulation over the past 25,000 years. Nat. Geosci. 1, 870–874. https://doi.org/10.1038/ngeo360

Paquette, J.-L., Nédélec, A., Moine, B., Rakotondrazafy, M., 1994. U-Pb, single zircon Pb-evaporation, and Sm-Nd isotopic study of a granulite domain in SE Madagascar. J. Geol. 102, 523–538.

Parrenin, F., Masson-Delmotte, V., Köhler, P., Raynaud, D., Paillard, D., Schwander, J., Barbante, C., Landais, A., Wegner, A., Jouzel, J., Kohler, P., Raynaud, D., Paillard, D., Schwander, J., Barbante, C., Landais, A., Wegner, A., Jouzel, J., 2013. Synchronous change of atmospheric CO_2 and Antarctic temperature during the last deglacial warming. Science 339, 1060–1063. https://doi.org/10.1126/science.1226368

Peeters, F.J.C., Ganssen, G.M., Ufkes, E., Kroon, D., Brummer, G.-J.A., Acheson, R., De Ruijter, W.P.M., Schneider, R.R., 2004. Vigorous exchange between the Indian and Atlantic oceans at the end of the past five glacial periods. Nature 430, 661–665. https://doi.org/10.1038/nature02785

Piepgras, D.J., Wasserburg, G.J., 1987. Rare earth element transport in the western North Atlantic inferred from Nd isotopic observations. Geochim. Cosmochim. Acta 51, 1257–1271. https://doi.org/10.1016/0016-7037(87)90217-1

Piepgras, D.J., Jacobsen, S.B., 1988. The isotopic composition of neodymium in the North Pacific. Geochim. Cosmochim. Acta 52, 1373–1381.

Piotrowski, A.M., Goldstein, S.L., Hemming, S.R., Fairbanks, R.G., 2005. Temporal relationships of carbon cycling and ocean circulation at glacial boundaries. Science 307, 1933–1938. https://doi.org/10.1126/science.1104883

Piotrowski, A.M., Banakar, V.K., Scrivner, A.E., Elderfield, H., Galy, A., Dennis, A., 2009. Indian Ocean circulation and productivity during the last glacial cycle. Earth Planet. Sci. Lett. 285, 179–189. https://doi.org/10.1016/j.epsl.2009.06.007

Piotrowski, A.M., Galy, A., Nicholl, J.A.L., Roberts, N., Wilson, D.J., Clegg, J.A., Yu, J., 2012. Reconstructing deglacial North and South Atlantic deep water sourcing using foraminiferal Nd isotopes. Earth Planet. Sci. Lett. 357–358, 289–297. https://doi.org/10.1016/j.epsl.2012.09.036

Plancherel, Y., 2012. A study of the ocean's water masses using data and models. Princeton University.

Pollard, R.T., Read, J.F., 2001. Circulation pathways and transports of the Southern Ocean in

the vicinity of the Southwest Indian Ridge. J. Geophys. Res. 106, 2881–2898. https://doi.org/10.1029/2000JC900090

Pollard, R.T., Venables, H.J., Read, J.F., Allen, J.T., 2007. Large-scale circulation around the Crozet Plateau controls an annual phytoplankton bloom in the Crozet Basin. Deep. Res. Part II Top. Stud. Oceanogr. 54, 1915–1929. https://doi.org/10.1016/j.dsr2.2007.06.012

Pollard, R., Read, J.F., 2017. Circulation, stratification and seamounts in the Southwest Indian Ocean. Deep. Res. Part II Top. Stud. Oceanogr. 136, 36–43. https://doi.org/10.1016/j.dsr2.2015.02.018

Prospero, J.M., Ginoux, P., Torres, O., Nicholson, S.E., Gill, T.E., 2002. Environmental characterization of global sources of atmospheric soil dust identified with the Nimbus 7 Total Ozone Mapping Spectrometer (TOMS) absorbing aerosol product. Rev. Geophys. 40, 1–31. https://doi.org/10.1029/2000RG000095

Rae, J.W., Burke, A., Robinson, L.F., Adkins, J.F., Chen, T., Cole, C., Greenop, R., Li, T., Littley, E., Nita, D.C., Stewart, J.A., Taylor, B., 2018. CO2 storage and release in the deep Southern Ocean on millennial to centennial timescales. Nature 562, 569–573. https://doi.org/10.1038/s41586-018-0614-0

Read, J.F., Lucas, M.I., Holley, S.E., Pollard, R.T., 2000. Phytoplankton, nutrients and hydrography in the frontal zone between the Southwest Indian Subtropical gyre and the Southern Ocean. Deep. Res. Part I Oceanogr. Res. Pap. 47, 2341–2368. https://doi.org/10.1016/S0967-0637(00)00021-2

Read, J.F., Pollard, R.T., 1993. Structure and transport of the Antarctic Circumpolar Current and Agulhas Return Current at 40°E. J. Geophys. Res. 98, 12281. https://doi.org/10.1029/93JC00436

Read, J., Pollard, R., 2017. An introduction to the physical oceanography of six seamounts in the southwest Indian Ocean. Deep Sea Res. Part II Top. Stud. Oceanogr. 136, 44–58. https://doi.org/10.1016/j.dsr2.2015.06.022

Reimer, P.J., Baille, M.G.L., Bard, E., Bayliss, A., Beck, J.W., Blackwell, P.G., Bronk Ramsey, C., Buck, C.E., Burr, G.S., 2009. INTCAL09 and MARINE09 radiocarbon age calibration curves, 0-50,000 years cal BP. Radiocarbon 51, 1111–1150.

Reimer, P.J., Bard, E., Bayliss, A., Beck, J.W., Blackwell, P.G., Ramsey, C.B., Buck, C.E., Cheng, H., Edwards, R.L., Friedrich, M., Grootes, P.M., Guilderson, T.P., Haflidason, H., Hajdas, I., Hatté, C., Heaton, T.J., Hoffmann, D.L., Hogg, A.G., Hughen, K.A., Kaiser, K.F., Kromer, B., Manning, S.W., Niu, M., Reimer, R.W., Richards, D.A., Scott, E.M., Southon, J.R., Staff, R.A., Turney, C.S.M., van der Plicht, J., 2013. IntCal13 and Marine13 radiocarbon age calibration curves 0-50,000 years cal BP 55, 1869–1887. https://doi.org/10.2458/azu_js_rc.55.16947

Rempfer, J., Stocker, T.F., Joos, F., Dutay, J.C., Siddall, M., 2011. Modelling Nd-isotopes with a coarse resolution ocean circulation model: Sensitivities to model parameters and source/sink distributions. Geochim. Cosmochim. Acta 75, 5927–5950. https://doi.org/10.1016/j.gca.2011.07.044

Rhodes, R.H., Brook, E.J., Chiang, J.C.H., Blunier, T., Maselli, O.J., McConnell, J.R., Romanini, D., Severinghaus, J.P., 2015. Enhanced tropical methane production in

response to iceberg discharge in the North Atlantic. Science (80-.). 348, 1016–1019. https://doi.org/10.1126/science.1262005

Rintoul, S.R., Hughes, C., Olbers, D., 2001. The Antarctic Circumpolar Current System, Ocean Circulation and Climate. https://doi.org/10.1002/ajp.20122

Roberts, J., Gottschalk, J., Skinner, L.C., Peck, V.L., Kender, S., Elderfield, H., Waelbroeck, C., Vázquez Riveiros, N., Hodell, D.A., 2016. Evolution of South Atlantic density and chemical stratification across the last deglaciation. Proc. Natl. Acad. Sci. 113, 514–519. https://doi.org/10.1073/pnas.1511252113

Roberts, J., McCave, I.N., McClymont, E.L., Kender, S., Hillenbrand, C.D., Matano, R., Hodell, D.A., Peck, V.L., 2017. Deglacial changes in flow and frontal structure through the Drake Passage. Earth Planet. Sci. Lett. 474, 397–408. https://doi.org/10.1016/j.epsl.2017.07.004

Roberts, J.M., Wheeler, A.J., Freiwald, A., 2006. Reefs of the deep: the biology and geology of cold-water coral ecosystems. Science 312, 543–7. https://doi.org/DOI 10.1126/science.1119861

Roberts, N.L., Piotrowski, A.M., McManus, J.F., Keigwin, L.D., 2010. Synchronous deglacial overturning and water mass source changes. Science 327, 75–78. https://doi.org/10.1126/science.1178068

Robinson, L.F., Adkins, J.F., Frank, N., Gagnon, A.C., Prouty, N.G., Brendan Roark, E., van de Flierdt, T., 2014. The geochemistry of deep-sea coral skeletons: A review of vital effects and applications for palaeoceanography. Deep. Res. Part II Top. Stud. Oceanogr. 99, 184–198. https://doi.org/10.1016/j.dsr2.2013.06.005

Robinson, L.F., Adkins, J.F., Keigwin, L.D., Southon, J., Fernandez, D.P., Wang, S.L., Scheirer, D.S., 2005. Ocean science: Radiocarbon variability in the western North Atlantic during the last deglaciation. Science 310, 1469–1473. https://doi.org/10.1126/science.1114832

Rogers, A.D., Taylor, M.L., 2011. Benthic biodiversity of seamounts in the southwest Indian Ocean: Cruise Report – R/V James Cook 066 Southwest Indian Ocean Seamounts expedition.

Rollion-Bard, C., Chaussidon, M., France-Lanord, C., 2003. pH control on oxygen isotopic composition of symbiotic corals. Earth Planet. Sci. Lett. 215, 275–288. https://doi.org/10.1016/S0012-821X(03)00391-1

Romahn, S., MacKensen, A., Groeneveld, J., Pätzold, J., 2014. Deglacial intermediate water reorganization: New evidence from the Indian Ocean. Clim. Past 10, 293–303. https://doi.org/10.5194/cp-10-293-2014

Rousseau, T.C.C., Sonke, J.E., Chmeleff, J., Van Beek, P., Souhaut, M., Boaventura, G., Seyler, P., Jeandel, C., 2015. Rapid neodymium release to marine waters from lithogenic sediments in the Amazon estuary. Nat. Commun. 6. https://doi.org/10.1038/ncomms8592

Rutberg, R.L., Goldstein, S.L., Hemming, S.R., Anderson, R.F., 2005. Sr isotope evidence for sources of terrigenous sediment in the southeast Atlantic Ocean: Is there increased

available Fe for enhanced glacial productivity? Paleoceanography 20, 1–10. https://doi.org/10.1029/2003PA000999

Sabine, C.L., Key, R.M., Feely, R.A., Greeley, D., 2002. Inorganic carbon in the Indian Ocean: Distribution and dissolution processes. Global Biogeochem. Cycles 16, 15-1-15–18. https://doi.org/10.1029/2002GB001869

Sarmiento, J.L., Gruber, N., Brzezinski, M.A., Dunne, J.P., 2004. High-latitude controls of thermocline nutrients and low latitude biological productivity 427. https://doi.org/10.1038/nature02204.1.

Sauter, D., Parson, L., Mendel, V., Rommevaux-Jestin, C., Gomez, O., Briais, A., M??vel, C., Tamaki, K., 2002. TOBI sidescan sonar imagery of the very slow-spreading Southwest Indian Ridge: Evidence for along-axis magma distribution. Earth Planet. Sci. Lett. 199, 81–95. https://doi.org/10.1016/S0012-821X(02)00543-5

Schilt, A., Baumgartner, M., Schwander, J., Buiron, D., Capron, E., Chappellaz, J., Loulergue, L., Sch??pbach, S., Spahni, R., Fischer, H., Stocker, T.F., 2010. Atmospheric nitrous oxide during the last 140,000years. Earth Planet. Sci. Lett. 300, 33–43. https://doi.org/10.1016/j.epsl.2010.09.027

Schlitzer, R., 2017. Ocean Data View [WWW Document]. URL odv.awi.de

Schmitt, J., Schneider, R., Elsig, J., Leuenberger, D., Lourantou, a., Chappellaz, J., Kohler, P., Joos, F., Stocker, T.F., Leuenberger, M., Fischer, H., 2012. Carbon Isotope Constraints on the Deglacial CO2 Rise from Ice Cores. Science (80-.). 336, 711–714. https://doi.org/10.1126/science.1217161

Schneider Von Deimling, T., Ganopolski, A., Held, H., Rahmstorf, S., 2006. How cold was the last Glacial maximum? Geophys. Res. Lett. 33, 1–5. https://doi.org/10.1029/2006GL026484

Scott, E.M., 2003. Part 2: The Third International Radiocarbon Intercomparison (Tiri). Radiocarbon 45, 293–328. https://doi.org/10.1017/s0033822200032677

Shakun, J.D., Clark, P.U., He, F., Marcott, S. a., Mix, A.C., Liu, Z., Otto-Bliesner, B., Schmittner, A., Bard, E., 2012. Global warming preceded by increasing carbon dioxide concentrations during the last deglaciation. Nature 484, 49–54. https://doi.org/10.1038/nature10915

Shemesh, A., Hodell, D., Crosta, X., Kanfoush, S., Charles, C., Guilderson, T., 2002. Sequence of events during the last deglaciation in Southern Ocean sediments and Antarctic ice cores. Paleoceanography 17, 8-1-8–7. https://doi.org/10.1029/2000pa000599

Shen, G.T., Boyle, E.A., 1988. Determination of lead, cadmium and other trace metals in annually-banded corals. Chem. Geol. 67, 47–62. https://doi.org/10.1016/0009-2541(88)90005-8

Shen, C.-C., Li, K.-S., Sieh, K., Natawidjaja, D., Cheng, H., Wang, X., Edwards, R.L., Lam, D.D., Hsieh, Y.-T., Fan, T.-Y., Meltzner, A.J., Taylor, F.W., Quinn, T.M., Chiang, H.-W., Kilbourne, K.H., 2008. Variation of initial $^{230}Th/^{232}Th$ and limits of high precision U–Th dating of shallow-water corals. Geochim. Cosmochim. Acta 72, 4201–4223.

https://doi.org/10.1016/j.gca.2008.06.011

Shen, C.-C., Wu, C.-C., Cheng, H., Lawrence Edwards, R., Hsieh, Y.-T., Gallet, S., Chang, C.-C., Li, T.-Y., Lam, D.D., Kano, A., Hori, M., Spötl, C., 2012. High-precision and high-resolution carbonate ^{230}Th dating by MC-ICP-MS with SEM protocols. Geochim. Cosmochim. Acta 99, 71–86. https://doi.org/10.1016/j.gca.2012.09.018

Siani, G., Michel, E., De Pol-Holz, R., DeVries, T., Lamy, F., Carel, M., Isguder, G., Dewilde, F., Lourantou, A., 2013. Carbon isotope records reveal precise timing of enhanced Southern Ocean upwelling during the last deglaciation. Nat. Commun. 4, 1–9. https://doi.org/10.1038/ncomms3758

Sigman, D.M., Boyle, E.A., 2000. Glacial/Interglacial variations in atmospheric carbon dioxide. Nature 407, 859–869. https://doi.org/10.1038/35038000

Sigman, D.M., Hain, M.P., Haug, G.H., 2010. The polar ocean and glacial cycles in atmospheric CO_2 concentration. Nature 466, 47–55. https://doi.org/10.1038/nature09149

Sikes, E.L., Elmore, A.C., Allen, K.A., Cook, M.S., Guilderson, T.P., 2016. Glacial water mass structure and rapid δ^{18}O and δ^{13}C changes during the last glacial termination in the Southwest Pacific. Earth Planet. Sci. Lett. 456, 87–97. https://doi.org/10.1016/j.epsl.2016.09.043

Sikes, E.L., Howard, W.R., Samson, C.R., Mahan, T.S., Robertson, L.G., Volkman, J.K., 2009. Southern Ocean seasonal temperature and Subtropical Front movement on the South Tasman Rise in the late Quaternary. Paleoceanography 24, 1–13. https://doi.org/10.1029/2008PA001659

Skinner, L.C., Fallon, S., Waelbroeck, C., Michel, E., Barker, S., 2010. Ventilation of the deep Southern Ocean and deglacial CO_2 rise. Science 328, 1147–1151. https://doi.org/10.1126/science.1183627

Skinner, L., McCave, I.N., Carter, L., Fallon, S., Scrivner, A.E., Primeau, F., 2015. Reduced ventilation and enhanced magnitude of the deep Pacific carbon pool during the last glacial period. Earth Planet. Sci. Lett. 411, 45–52. https://doi.org/10.1016/j.epsl.2014.11.024

Skinner, L.C., Scrivner, A.E., Vance, D., Barker, S., Fallon, S., Waelbroeck, C., 2013. North Atlantic versus Southern Ocean contributions to a deglacial surge in deep ocean ventilation. Geology 41, 667–670. https://doi.org/10.1130/G34133.1

Smith, J.E., Schwarcz, H.P., Risk, M.J., McConnaughey, T.A., Keller, N., 2000. Paleotemperatures from deep-sea corals: overcoming "vital effects." Palaios 15, 25–32.

Sokolov, S., Rintoul, S.R., 2009. Circumpolar structure and distribution of the antarctic circumpolar current fronts: 1. Mean circumpolar paths. J. Geophys. Res. Ocean. 114, 1–19. https://doi.org/10.1029/2008JC005108

Spooner, P.T., Chen, T., Robinson, L.F., Coath, C.D., 2016. Rapid uranium-series age screening of carbonates by laser ablation mass spectrometry. Quat. Geochronol. 31, 28–39. https://doi.org/10.1016/j.quageo.2015.10.004

Squires, D.F., 1961. Deep Sea Corals Collected by the Lamont Geological Observatory: Scotia Sea Corals. American Museum of Natural History.

Stanley, G.D., Cairns, S.D., 1988. Constructional azooxanthellate coral communities: An overview with implications for the fossil record. Palaios 3, 233. https://doi.org/10.2307/3514534

Stenni, B., Buiron, D., Frezzotti, M., Albani, S., Barbante, C., Bard, E., Barnola, J.M.M., Baroni, M., Baumgartner, M., Bonazza, M., Capron, E., Castellano, E., Chappellaz, J., Delmonte, B., Falourd, S., Genoni, L., Iacumin, P., Jouzel, J., Kipfstuhl, S., Landais, A., Lemieux-Dudon, B., Maggi, V., Masson-Delmotte, V., Mazzola, C., Minster, B., Montagnat, M., Mulvaney, R., Narcisi, B., Oerter, H., Parrenin, F., Petit, J.R.R., Ritz, C., Scarchilli, C., Schilt, A., Schüpbach, S., Schwander, J., Selmo, E., Severi, M., Stocker, T.F.F., Udisti, R., 2011. Expression of the bipolar see-saw in Antarctic climate records during the last deglaciation. Nat. Geosci. 4, 46–49. https://doi.org/10.1038/ngeo1026

Stenni, B., Masson-Delmotte, V., Johnsen, S., Jouzel, J., Longinelli, A., Monnin, E., Röthlisberger, R., Selmo, E., 2001. An oceanic cold reversal during the last deglaciation. Science 293, 2074–2077. https://doi.org/10.1126/science.1059702

Stephens, B.B., Keeling, R.F., 2000. The influence of Antarctic sea ice on glacial-interglacial CO2 variations. Nature 404, 171–174. https://doi.org/10.1038/35004556

Stern, J. V., Lisiecki, L.E., 2013. North Atlantic circulation and reservoir age changes over the past 41,000 years. Geophys. Res. Lett. 40, 3693–3697. https://doi.org/10.1002/grl.50679

Stichel, T., Frank, M., Rickli, J., Haley, B.A., 2012. The hafnium and neodymium isotope composition of seawater in the Atlantic sector of the Southern Ocean. Earth Planet. Sci. Lett. 317–318, 282–294. https://doi.org/10.1016/j.epsl.2011.11.025

Struve, T., 2016. Deciphering glacial-interglacial Southern Ocean dynamics with deep-sea corals. Imperial College London.

Struve, T., van de Flierdt, T., Burke, A., Robinson, L.F., Hammond, S.J., Crocket, K.C., Bradtmiller, L.I., Auro, M.E., Mohamed, K.J., White, N.J., 2017. Neodymium isotopes and concentrations in aragonitic scleractinian cold-water coral skeletons - Modern calibration and evaluation of palaeo-applications. Chem. Geol. 453, 146–168. https://doi.org/10.1016/j.chemgeo.2017.01.022

Struve, T., van de Flierdt, T., Robinson, L.F., Bradtmiller, L.I., Hines, S.K., Adkins, J.F., Lambelet, M., Crocket, K.C., Kreissig, K., Coles, B., Auro, M.E., 2016. Neodymium isotope analyses after combined extraction of actinide and lanthanide elements fromseawater and deep-sea coral aragonite. Geochemistry, Geophys. Geosystems 17, 232–240. https://doi.org/10.1002/2015GC006130.Received

Stuiver, M., Grootes, P.M., Braziunas, T.F., 1995. The GISP2 $\delta^{18}O$ climate record of the past 16,500 years and the role of the sun, ocean and volcanoes. Quat. Res. 44, 341–354.

Stuiver, M., Östlund, H.G., 1980. GEOSECS Atlantic radiocarbon. Radiocarbon 22, 1–24.

Stuiver, M., Östlund, H.G., 1983. GEOSECS Indian Ocean and Mediterranean Radiocarbon. Radiocarbon 25, 1–29. https://doi.org/10.1017/s0033822200005270

Sultan, E., Mercier, H., Pollard, R.T., 2007. An inverse model of the large scale circulation in the South Indian Ocean. Prog. Oceanogr. 74, 71–94.

https://doi.org/10.1016/j.pocean.2007.02.001

Synal, H.A., Stocker, M., Suter, M., 2007. MICADAS: A new compact radiocarbon AMS system. Nucl. Instruments Methods Phys. Res. Sect. B 259, 7–13. https://doi.org/10.1016/j.nimb.2007.01.138

Tachikawa, K., Athias, V., Jeandel, C., 2003. Neodymium budget in the modern ocean and paleo-oceanographic implications. J. Geophys. Res. 108, 3254. https://doi.org/10.1029/1999JC000285

Talley, L.D., 1996. Antarctic Intermediate Water in the South Atlantic, in: Wefer, G., Berger, W.H., Seidler, G., Webb, D.J. (Eds.), The South Atlantic: Present and Past Circulation. Springer-Verlag, Berlin Heidelberg, pp. 219–238. https://doi.org/10.1007/978-3-642-80353-6_11

Talley, L.D., 2013. Closure of the global overturning circulation through the Indian, Pacific and Southern Oceans: schematics and transports. Oceanography 1–21.

Talley, L.D., Pickard, G.L., Emery, W.J., Swift, J.H., 2011. Descriptive Physical Oceanography: An Introduction, 6th ed.

Tamsitt, V., Drake, H.F., Morrison, A.K., Talley, L.D., Dufour, C.O., Gray, A.R., Griffies, S.M., Mazloff, M.R., Sarmiento, J.L., Wang, J., Weijer, W., 2017. Spiraling pathways of global deep waters to the surface of the Southern Ocean. Nat. Commun. 8, 172. https://doi.org/10.1038/s41467-017-00197-0

Tanaka, T., Togashi, S., Kamioka, H., Amakawa, H., Kagami, H., Hamamoto, T., Yuhara, M., Orihashi, Y., Yoneda, S., Shimizu, H., Kunimaru, T., Takahashi, K., Yanagi, T., Nakano, T., Fujimaki, H., Shinjo, R., Asahara, Y., Tanimizu, M., Dragusanu, C., 2000. JNdi-1: A neodymium isotopic reference in consistency with LaJolla neodymium. Chem. Geol. 168, 279–281. https://doi.org/10.1016/S0009-2541(00)00198-4

Tao, C., Lin, J., Guo, S., Chen, Y.J., Wu, G., Han, X., German, C.R., Yoerger, D.R., Zhu, J., Zhou, N., Su, X., Baker, E.T., Party, S., 2004. First discovery and investigation of a high-temperature hydrothermal vent field on the ultra-slow spreading Southwest Indian Ridge. AGU Fall Meet. Abstr. 1.

Thiagarajan, N., Gerlach, D., Roberts, M.L., Burke, A., McNichol, A., Jenkins, W.J., Subhas, A. V., Thresher, R.E., Adkins, J.F., 2013. Movement of deep-sea coral populations on climatic timescales. Paleoceanography 28, 227–236. https://doi.org/10.1002/palo.20023

Thomas, A.L., Henderson, G.M., Robinson, L.F., 2006. Interpretation of the ^{231}Pa/^{230}Th paleocirculation proxy: New water-column measurements from the southwest Indian Ocean. Earth Planet. Sci. Lett. 241, 493–504. https://doi.org/10.1016/j.epsl.2005.11.031

Thresher, R.E., Tilbrook, B., Fallon, S., Wilson, N.C., Adkins, J., 2011. Effects of chronic low carbonate saturation levels on the distribution, growth and skeletal chemistry of deep-sea corals and other seamount megabenthos. Mar. Ecol. Prog. Ser. 442, 87–96. https://doi.org/10.3354/meps09400

Tittensor, D.P., Baco, A.R., Brewin, P.E., Clark, M.R., Consalvey, M., Hall-Spencer, J., Rowden, A.A., Schlacher, T., Stocks, K.I., Rogers, A.D., 2009. Predicting global habitat suitability for stony corals on seamounts. J. Biogeogr. 36, 1111–1128.

https://doi.org/10.1111/j.1365-2699.2008.02062.x

Tittensor, D.P., Baco, A.R., Hall-Spencer, J.M., Orr, J.C., Rogers, A.D., 2010. Seamounts as refugia from ocean acidification for cold-water stony corals. Mar. Ecol. 31, 212–225. https://doi.org/10.1111/j.1439-0485.2010.00393.x

Toggweiler, J.R., 2009. Shifting westerlies. Science 323, 1434–1435. https://doi.org/10.1126/science.1169823

Toggweiler, J.R., Russell, J.L., Carson, S.R., 2006. Midlatitude westerlies, atmospheric CO_2, and climate change during the ice ages. Paleoceanography 21, 1–15. https://doi.org/10.1029/2005PA001154

Tomczak, M., Godfrey, J.S., 2003. The Indian Ocean, in: Regional Oceanography: An Introduction.

Toole, J.M., Warren, B.A., 1993. A hydrographic section across the subtropical South Indian Ocean. Deep. Res. Part I 40, 1973–2019.

van Aken, H.M., Ridderinkhof, H., de Ruijter, W.P.M., 2004. North Atlantic deep water in the south-western Indian Ocean. Deep Sea Res. Part I Oceanogr. Res. Pap. 51, 755–776. https://doi.org/10.1016/j.dsr.2004.01.008

van de Flierdt, T., Griffiths, A.M., Lambelet, M., Little, S.H., Stichel, T., Wilson, D.J., Lambelet, M., Stichel, T., van de Flierdt, T., Griffiths, A.M., Wilson, D.J., 2016. Neodymium in the oceans: a global database, a regional comparison and implications for palaeoceanographic research. Philos. Trans. R. Soc. A Math. Phys. Eng. Sci. 374, 20150293. https://doi.org/10.1098/rsta.2015.0293

van de Flierdt, T., Robinson, L.F., Adkins, J.F., 2010. Deep-sea coral aragonite as a recorder for the neodymium isotopic composition of seawater. Geochim. Cosmochim. Acta 74, 6014–6032. https://doi.org/10.1016/j.gca.2010.08.001

van de Flierdt, T., Robinson, L.F., Adkins, J.F., Hemming, S.R., Goldstein, S.L., 2006. Temporal stability of the neodymium isotope signature of the Holocene to glacial North Atlantic. Paleoceanography 21, 1–6. https://doi.org/10.1029/2006PA001294

van Sebille, E., Johns, W.E., Beal, L.M., 2012. Does the vorticity flux from Agulhas rings control the zonal pathway of NADW across the South Atlantic? J. Geophys. Res. Ocean. 117, 1–12. https://doi.org/10.1029/2011JC007684

Wacker, L., Bonani, G., Friedrich, M., Hajdas, I., Kromer, B., Němec, M., Ruff, M., Suter, M., Synal, H.A., Vockenhuber, C., 2010a. Micadas: Routine and high-precision radiocarbon dating. Radiocarbon 52, 252–262. https://doi.org/10.1017/S0033822200045288

Wacker, L., Christl, M., Synal, H.A., 2010b. Bats: A new tool for AMS data reduction. Nucl. Instruments Methods Phys. Res. Sect. B Beam Interact. with Mater. Atoms 268, 976–979. https://doi.org/10.1016/j.nimb.2009.10.078

Wacker, L., Fülöp, R.-H., Hajdas, I., Molnár, M., Rethemeyer, J., 2013. A novel approach to process carbonate samples for radiocarbon measurements with helium carrier gas. Nucl. Instruments Methods Phys. Res. Sect. B Beam Interact. with Mater. Atoms 294, 214–217. https://doi.org/10.1016/j.nimb.2012.08.030

WAIS Divide Project Members, 2013. Onset of deglacial warming in West Antarctica driven by local orbital forcing. Nature 500, 440–4. https://doi.org/10.1038/nature12376

WAIS Divide Project Members, 2015. Precise interpolar phasing of abrupt climate change during the last ice age. Nature 520, 661–665. https://doi.org/10.1038/nature14401

Wang, X.T., Sigman, D.M., Prokopenko, M.G., Adkins, J.F., Robinson, L.F., Hines, S.K., Chai, J., Studer, A.S., Martínez-García, A., Chen, T., Haug, G.H., 2017. Deep-sea coral evidence for lower Southern Ocean surface nitrate concentrations during the last ice age. Proc. Natl. Acad. Sci. 114, 3352–3357. https://doi.org/10.1073/pnas.1615718114

Wasserburg, G.J., Jacousen, S.B., DePaolo, D.J., McCulloch, M.T., Wen, T., 1981. Precise determination of Sm Nd ratios, Sm and Nd isotopic abundances in standard solutions. Geochim. Cosmochim. Acta 45, 2311–2323. https://doi.org/10.1016/0016-7037(81)90085-5

Watling, L., Guinotte, J., Clark, M.R., Smith, C.R., 2013. A proposed biogeography of the deep ocean floor. Prog. Oceanogr. 111, 91–112. https://doi.org/10.1016/j.pocean.2012.11.003

Watson, A.J., Bakker, D.C., Ridgwell, A.J., Boyd, P.W., Law, C.S., 2000. Effect of iron supply on Southern Ocean CO_2 uptake and implications for glacial atmospheric CO2. Nature 407, 730–733. https://doi.org/10.1038/35037561

Watson, A.J., Vallis, G.K., Nikurashin, M., 2015. Southern Ocean buoyancy forcing of ocean ventilation and glacial atmospheric CO_2. Nat. Geosci. 8, 861–864. https://doi.org/10.1038/ngeo2538

Weber, M.E., Clark, P.U., Kuhn, G., Timmermann, A., Sprenk, D., Gladstone, R., Zhang, X., Lohmann, G., Menviel, L., Chikamoto, M.O., Friedrich, T., Ohlwein, C., 2014. Millennial-scale variability in Antarctic ice-sheet discharge during the last deglaciation. Nature 510, 134–8. https://doi.org/10.1038/nature13397

Weijer, W., De Ruijter, W.P.M., Sterl, A., Drijfhout, S.S., 2002. Response of the Atlantic overturning circulation to South Atlantic sources of buoyancy. Glob. Planet. Change 34, 293–311. https://doi.org/10.1016/S0921-8181(02)00121-2

Weis, D., Kieffer, B., Maerschalk, C., Barling, J., De Jong, J., Williams, G.A., Hanano, D., Pretorius, W., Mattielli, N., Scoates, J.S., Goolaerts, A., Friedman, R.M., Mahoney, J.B., 2006. High-precision isotopic characterization of USGS reference materials by TIMS and MC-ICP-MS. Geochemistry, Geophys. Geosystems 7. https://doi.org/10.1029/2006GC001283

White, W.M., Cheatham, M.M., Duncan, R.A., 1990. Isotope Geochemistry of Leg 115 Basalts and Inferences on the History of the Reunion Mantle Plume 1. Proc. Ocean Drill. Prgram, Sci. Results 115, 53–61.

Wilson, D.J., Crocket, K.C., Van De Flierdt, T., Robinson, L.F., Adkins, J.F., 2014. Dynamic intermediate ocean circulation in the North Atlantic during Heinrich Stadial 1: A radiocarbon and neodymium isotope perspective. Paleoceanography 29, 1072–1093. https://doi.org/10.1002/2014PA002674

Wilson, D.J., Piotrowski, A.M., Galy, A., Clegg, J.A., 2013. Reactivity of neodymium

carriers in deep sea sediments: Implications for boundary exchange and paleoceanography. Geochim. Cosmochim. Acta 109, 197–221. https://doi.org/10.1016/j.gca.2013.01.042

Wilson, D.J., Piotrowski, A.M., Galy, A., McCave, I.N., 2012. A boundary exchange influence on deglacial neodymium isotope records from the deep western Indian Ocean. Earth Planet. Sci. Lett. 341–344, 35–47. https://doi.org/10.1016/j.epsl.2012.06.009

Wong, A.P.S., 2005. Subantarctic Mode Water and Antarctic Intermediate Water in the South Indian Ocean based on profiling float data 2000–2004. J. Mar. Res. 63, 789–812. https://doi.org/10.1357/0022240054663196

Wyrtki, K., 1971. Oceanographic Atlas of the International Indian Ocean Expedition. National Science Foundation, Washington, D. C.

Xie, R.C., Marcantonio, F., Schmidt, M.W., 2012. Deglacial variability of Antarctic Intermediate Water penetration into the North Atlantic from authigenic neodymium isotope ratios. Paleoceanography 27, 1–12. https://doi.org/10.1029/2012PA002337

Xie, R.C., Marcantonio, F., Schmidt, M.W., 2014. Reconstruction of intermediate water circulation in the tropical North Atlantic during the past 22,000 years. Geochim. Cosmochim. Acta 140, 455–467. https://doi.org/10.1016/j.gca.2014.05.041

You, Y., 2000. Implications of the deep circulation and ventilation of the Indian Ocean on the renewal mechanism of North Atlantic Deep Water. J. Geophys. Res. Ocean. 105, 23895–23926. https://doi.org/10.1029/2000jc900105

You, Y., 2002. Quantitative estimate of Antarctic Intermediate Water contributions from the Drake Passage and the southwest Indian Ocean to the South Atlantic. J. Geophys. Res. 107. https://doi.org/10.1029/2001jc000880

Yu, J., Broecker, W.S., Elderfield, H., Jin, Z., McManus, J.F., Zhang, F., 2010. Loss of carbon from the deep sea since the Last Glacial Maximum. Science 330, 1084–1087.

Yu, Z., Colin, C., Ma, R., Meynadier, L., Wan, S., Wu, Q., Kallel, N., Sepulcre, S., Dapoigny, A., Bassinot, F., 2018. Antarctic Intermediate Water penetration into the Northern Indian Ocean during the last deglaciation. Earth Planet. Sci. Lett. 500, 67–75. https://doi.org/10.1016/j.epsl.2018.08.006

Zibrowius, H., 1980. Les scléractiniaires de la Méditerranée et de l'Atlantique nord-oriental. Mémoires de l'Institut Océanographique, Monaco 11, 1–284.

Zieringer, M., Frank, M., Stumpf, R., Hathorne, E.C., 2019. The distribution of neodymium isotopes and concentrations in the eastern tropical North Atlantic. Chem. Geol. 1–14. https://doi.org/10.1016/j.chemgeo.2018.11.024

Appendices

A1. Equatorial Atlantic cold-water coral Nd isotope data

A1.1 Introduction and methods

Neodymium isotope values of ten cold-water coral samples from the equatorial Atlantic were measured in order to explore possible water mass-source changes associated with deglacial low-pH events (Stewart, pers. comm.). As lower seawater pH values most likely arise from a greater dissolved inorganic carbon content of the water, it has been suggested that negative excursions recorded at intermediate water depths by boron isotopes result from transfer of glacially stored carbon from deep waters (Rae et al., 2018). In the Drake Passage, a close relationship has been inferred between such excursions and abrupt increases in atmospheric CO_2 during the last deglaciation (Marcott et al., 2014; Rae et al., 2018).

The samples were collected in October-November 2013 during the RRS *James Cook* Cruise JC094 from Carter Seamount (EBA, eastern basin, 5.6°N, 26.9°W, n = 2), Vema Fracture Zone (VEM, western basin, 10.7°N, 44.6°W, n = 6), Vayda Seamount (VAY, western basin, 14.9°N, 48.2°W, n = 1) and Gramberg Seamount (GRM, western basin, 15.4°N, 51.1°W, n = 1). Samples were supplied as physically cleaned aragonite by Dr. Joe Stewart and Prof. Laura Robinson at the University of Bristol. Prior to this, samples from the same coral specimens underwent U-Th dating and radiocarbon measurement by Chen and colleagues (2015), and boron isotope analysis by Stewart and colleagues (pers. comm.). All samples belong to the colonial genus *Enallopsammia*, and were collected from water depths between 1544 – 1657 m, roughly the same depth as, or slightly deeper than, the salinity minimum of NADW in both the eastern and western basins of the modern equatorial Atlantic (Chen et al., 2015). One sample is dated to the late Holocene (692 ± 17 y BP), and the others between 10.5 and 15.5 kyrs BP (Table A1). Cleaning and Nd isotope measurement was carried out using the

procedure described in Chapter 2 (Methods). Neodymium isotope data was collected on JIM/NP2 over two sessions in the MAGIC labs at Imperial College London in November-December 2018.

Table A1: Neodymium isotope data from equatorial Atlantic cold-water corals

JC094 ID	Sample ID	Imperial ID	Site	Age / y BP	2σ	Depth / m	Sample mass / g	Coral [Nd] / ppb	$^{143}Nd/^{144}Nd$	2σ	εNd	2σ*
f0218enansml001	F218-001	J1	VAY	692	17	1612	0.75	24.5	0.511989	0.000005	-12.66	0.21
f0160enapsm001b	F160-001b	J3	VEM	10499	44	1657	0.20	179.9	0.511879	0.000006	-14.80	0.23
f0161enacsm001c	F161-001c	J4	VEM	10813	50	1648	0.72	55.9	0.511925	0.000005	-13.91	0.21
f0160enapsm001d	F160-p001d	J5	VEM	11358	68	1657	0.45	42.8	0.511937	0.000005	-13.67	0.26
f0160enansm001d	F160-n001d	J6	VEM	11742	53	1657	0.42	38.9	0.512006	0.000006	-12.33	0.26
f0160enansm001a	F160-001a	J7	VEM	12238	57	1657	0.28	59.3	0.511974	0.000007	-12.96	0.29
f0160enansm001e	F160-001e	J8	VEM	12291	150	1657	0.74	105.1	0.512040	0.000006	-11.67	0.26
f0255enansm001	F255-001	J9	GRM	13972	93	1544	0.66	130.8	0.512016	0.000006	-12.13	0.22
f0021enacm001a†	F21-001a	J10	EBA	15378	107	1545	0.31	134.2	0.511997	0.000006	-12.50	0.26
f0021enacm001b†	f0021enacm001b	J11	EBA	15451	103	1545	0.22	234.2	0.511970	0.000007	-13.03	0.27

* 2σ is the higher value between a) the average standard error of JNdi standards measured around the samples or b) the internal standard error of the measurement
† Sample also records a 'low-pH event'

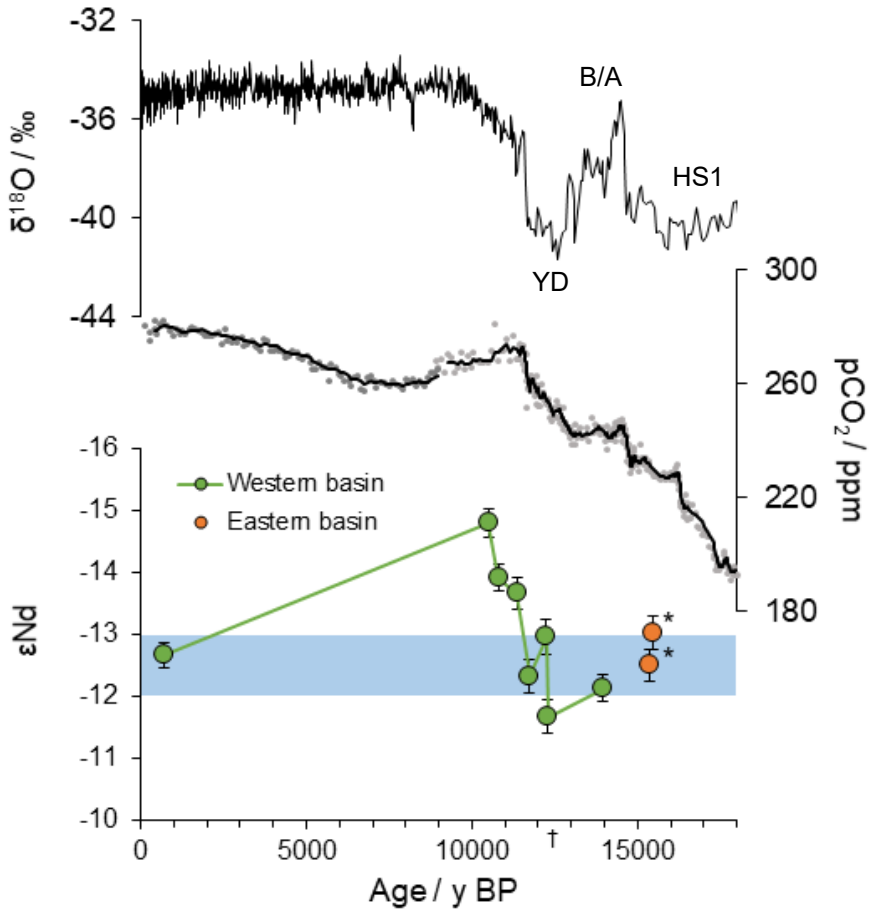

Figure A1: GISP2 ice core $\delta^{18}O$ (top panel; Stuiver et al., 1995), WAIS Divide Core atmospheric CO2 record (Marcott et al., 2014), and cold-water coral Nd isotope data from the western (green circles) and eastern (orange circles) basins of the equatorial Atlantic (bottom panel). The modern ε_{Nd} range of NADW-depth (1250 - 1979 m) seawater of the combined eastern (Zieringer et al., 2019) and western (Lambelet et al., 2016) basins is indicated by the blue bar. Asterisks indicate the coral samples which also record 'low pH events' (boron isotope minima) and the dagger indicates the age of a coral recording a second low pH event which was not measured for Nd isotopes (Stewart, pers. comm.). Timings of the Heinrich Stadial 1 (HS1), the Bolling-Allerod (B/A) and the Younger Dryas (YD) are highlighted in the top panel.

A1.2 Results and discussion

The youngest sample, dated to the late Holocene, records an ε_{Nd} of -12.7 ± 0.21, which is within modern seawater range at these depths (-12 to -13; Fig. A1; Lambelet et al., 2016; Zieringer et al., 2019), as are the six oldest samples dating to between 15.5 and 11.7 kyrs BP.

The ε_{Nd} of the AAIW core in the north Atlantic has been measured to between -11.0 and -11.3 (Lambelet et al., 2016; Zieringer et al., 2019), which could suggest that the slightly radiogenic 12.3 kyr BP sample contemporaneous with the YD 'low pH event' was influenced by AAIW (Fig. A1). Besides this sample, however, there is no evidence of enhanced AAIW influence at the depths of these corals. For the two samples which also recorded low-pH events, but have a clear NADW signature we suggest the following explanations to be explored in future work:

1. The low-pH signal is the result of old carbon being transferred by AAIW from the Southern Ocean, but the more radiogenic Nd signature of this water mass was not recorded. As the concentration of Nd in coral aragonite is much lower than boron, if the low-pH event was very rapid, this could result from a) a different part of the coral aragonite being sampled or b) the southern-sourced Nd-isotope signal being buffered by the sampled part of the coral being bathed in NADW for the majority of the time the aragonite was forming.
2. The low-pH signal is a result of a release of old carbon, however it did not originate from southern-sourced intermediate waters. Evidence in favour of this hypothesis includes the older B-atm ages recorded by these samples than those at AAIW depths in the Drake Passage (Burke and Robinson, 2012) and the Southwest Indian Ocean (Chapter 5).
3. The low-pH excursion is a local productivity signal.

4. The Nd-isotope samples were diagenetically overprinted with modern seawater. We find this unlikely, as the samples were extensively physically and chemically cleaned and contained no visible impurities.

Three samples dating to between 11.4 and 10.5 kyrs BP exhibit ε_{Nd} values outside the modern NADW range (Fig. A1). The only seawater values as unradiogenic as these in the modern ocean are found in Labrador Sea Water (LSW; Lambelet et al., 2016). This feature has also been observed in the deep western North Atlantic (Roberts et al., 2010) and may be evidence of increased LSW contribution to NADW in the late deglacial / early Holocene.